SYNTHESIS OF METALLIC NANOPARTICLES USING DEFENSIVE SECRETION OF THE BEETLE *LUPROPS TRISTIS* AND ITS BIOLOGICAL ACTIVITIES

Thesis submitted to
the University of Calicut in partial fulfillment of
the requirements for the degree of

DOCTOR OF PHILOSOPHY IN ZOOLOGY

By

SABIRA O.

Under the guidance of

Dr. AJAYKUMAR A. P.

Research and Post Graduate Department of Zoology
Sree Neelakanta Government Sanskrit College, Pattambi
(Affiliated to the University of Calicut, Kerala, India)

June 2025

Sree Neelakanta Govt. Sanskrit College
Pattambi, Palakkad Dt, Kerala - 679 306
(Accredited by NAAC with A^+ Grade)
Ph: 0466-2212223
e-mail: sngscollege@gmail.com
website: www.sngscollege.org

Dr. Ajaykumar A. P.
Assistant Professor
Research supervisor,
Department of Zoology, SNGS College, Pattambi
E-mail: ajaykumar@sngscollege.org
Mob: +91 9446433104

CERTIFICATE

This is to certify that the thesis entitled **"SYNTHESIS OF METALLIC NANOPARTICLES USING DEFENSIVE SECRETION OF THE BEETLE *LUPROPS TRISTIS* AND ITS BIOLOGICAL ACTIVITIES"** submitted by **SABIRA O.** in partial fulfillment of the requirements for the degree of **Doctor of Philosophy** in Zoology of the **University of Calicut**, is a bona fide record of the research work undertaken by her in this department under my supervision and guidance during the period 2019-2025 and no part thereof has been submitted for the award of any other degree.

S.N.G.S College, Pattambi **Dr. Ajaykumar A. P.**

Sree Neelakanta Govt. Sanskrit College
Pattambi, Palakkad Dt, Kerala - 679 306
(Accredited by NAAC with A^+ Grade)
Ph: 0466-2212223
e-mail: sngscollege@gmail.com
Website: www.sngscollege.org

Dr. Ajaykumar A. P.
Assistant Professor
Research supervisor,
Department of Zoology, SNGS College, Pattambi
E-mail: ajaykumar@sngscollege.org
Mob: +91 9446433104

CERTIFICATE

This is to certify that all the corrections mentioned by the adjudicators in the thesis entitled **"SYNTHESIS OF METALLIC NANOPARTICLES USING DEFENSIVE SECRETION OF THE BEETLE *LUPROPS TRISTIS* AND ITS BIOLOGICAL ACTIVITIES"** submitted by **SABIRA O.** have been incorporated as per the adjudication report. It is also certified that the contents in the thesis and the CD submitted are the same.

Pattambi
Date:

Dr. Ajaykumar A. P.

DECLARATION

I, **SABIRA O.** hereby declare that the work presented in the thesis entitled **"SYNTHESIS OF METALLIC NANOPARTICLES USING DEFENSIVE SECRETION OF THE BEETLE *LUPROPS TRISTIS* AND ITS BIOLOGICAL ACTIVITIES"** is based on the original work done by me under the guidance of **Dr. AJAYKUMAR AP.,** and has not been included in any other thesis submitted previously for the award of any degree. The contents of the thesis have undergone a plagiarism check using iThenticate software at C.H.M.K. Library, University of Calicut, and the similarity index was found within the permissible limit. I also declare that the thesis is free from AI-generated content.

S.N.G.S. College Pattambi **SABIRA O.**

Dr. Ajaykumar A. P.
Assistant Professor
Research supervisor,
Department of Zoology, SNGS College, Pattambi

ACKNOWLEDGEMENT

With profound gratitude and humility, I first and foremost thank God, the Almighty, for granting me the opportunity to explore the extraordinary world of science. His boundless grace has been my source of strength, inspiration, and resilience throughout this journey. It is through His guiding hand that I have undertaken and completed this research.

I extend my heartfelt gratitude to my guide and supervisor, ***Dr. Ajaykumar A. P.****, Assistant Professor, Department of Zoology, SNGS College, Pattambi. His unwavering support, insightful guidance, and encouragement have been the cornerstone of my research journey. His belief in my potential has inspired me to strive for excellence and discover new horizons.*

I am deeply indebted to our esteemed ***Principal*** *for his exemplary leadership and for providing the essential facilities required for the successful completion of my work. I also express my sincere appreciation to* ***Dr. Zeena K.V.****, Head of the Department of Zoology, for her steadfast support and guidance. Her leadership has been instrumental in fostering an environment conducive to academic growth.*

I am profoundly grateful to my dedicated teachers: ***Mr. Prasant C.M., Dr. Abdul Rasheed, Mr. Shihabudheen, Mr. Janish, Dr. Sheena, Dr. CV Sri Ranjith kumar, Dr. Anjali, Dr. Usha, Dr. Resmi, and Dr. Manoj.*** *Their mentorship has enriched my academic journey, and their dedication continues to inspire me.*

A special mention goes to my exceptional labmates: ***Ms. Veena, Ms. Priyanka, and Ms. Aswathi.*** *Their camaraderie, tireless dedication, and collaborative spirit have created a dynamic and uplifting research environment. Together, we have navigated challenges, celebrated victories, and forged an inspiring community that has enriched both our scientific pursuits and personal growth.*

I also extend my gratitude to the facilities that supported my research, including the ***CSIR for funding, Central Sophisticated Instrumentation Facility (CSIF), University of Calicut; Sophisticated Test and Instrumentation Centre (STIC), SAIF MG University, and IIT Bombay****, for providing the advanced instrumentation (SEM-EDX, TEM, GC-MS, LC-MS, and XRD) that was crucial for my work.*

No acknowledgment would be complete without honoring my greatest source of strength: my family. I am forever grateful to God for blessing me with their unwavering love, prayers, and support. To my husband, ***Mr. Abdul Rasheed****, you are my steadfast pillar, my cheerleader, and my greatest ally. Your belief in me, your encouragement, and your boundless support have been the driving force behind my aspirations and accomplishments. This work stands as a tribute to your love and faith in me. To my precious daughter,* ***Ayrin Rasheed****, the cornerstone of my academic pursuits. You are the unsung heroine of this journey, and my heart overflows with gratitude and pride for you.*

I express my heartfelt thanks to my parents, ***Muhammed*** *and* ***Fathimakutty****, and my siblings,* ***Nusaiba, Salma, and Abdulla.*** *Their unwavering support and belief in my abilities have been my guiding light. To my nieces and nephews* ***Mr. Shanid, Mr. Shibil, Ms. Salma Shirin****, and my brother-in-law,* ***Mr. Muhammed Ali****, your presence has been a source of joy and positivity throughout my journey.*

I pay tribute to my late mother-in-law, ***Mrs. Iyyathu,*** *whose unwavering support and love remain a cherished memory. I also extend my deepest gratitude to my in-laws for their encouragement, camaraderie, and positive influence on my academic endeavors.*

Finally, I express my sincere appreciation to everyone who supported me, whether mentioned here or not. Each of you holds a special place in my journey. With heartfelt humility, I once again thank the Supreme Power for guiding me to the realization of this work.

Sabira O.

"To

My Family"

ABSTRACT

The present study highlights the potential of the defensive secretion of the tenebrionid beetle *Luprops tristis* as an innovative and sustainable source for the green synthesis of metal nanoparticles. This chemically diverse secretion offers a robust platform for nanoparticle synthesis, with its inherent reducing and stabilizing agents playing vital roles in nanoparticle formation and stabilization. By using this unique biological resource, the study emphasises the synthesis of four distinct types of nanoparticles: nickel (LNiNPs), copper oxide (LCuONPs), zinc oxide (LZnONPs), and gold (LAuNPs). These nanoparticles exhibit unique physicochemical properties that make them suitable for diverse applications, ranging from biosensing to therapeutics.

Among the synthesized nanoparticles, LAuNPs demonstrated exceptional potential in biosensing applications, particularly for glucose monitoring. Their detection limit of 0.75 establishes their utility for non-invasive glucose monitoring, especially in neonatal care. UV-Visible spectroscopy validated the well-defined optical properties of all the synthesized nanoparticles, further confirming their applicability in diagnostic technologies. The unique characteristics of each nanoparticle type reflect the complex interactions between the beetle's defensive secretion metabolites and the synthesis process, showcasing the versatility of this eco-friendly methodology.

The antioxidant activity of four nanoparticles, LNiNPs, LCuONPs, LAuNPs, and LZnONPs, synthesized using defensive secretions, was analyzed. This method not only facilitates nanoparticle synthesis but also creates a stabilizing environment that prevents aggregation, ensuring uniform size and shape, as confirmed by SEM and TEM analyses. The presence of 3-dehydro-L-gulonate, a derivative of ascorbic acid, enhances antioxidant activity through effective free radical scavenging, evidenced by the IC_{50} value of 26µg/mL for LZnONPs, which demonstrated the highest antioxidant efficacy among the tested nanoparticles. Additionally, uric acid, a natural antioxidant and metabolic byproduct, plays a crucial role in redox reactions during nanoparticle synthesis, further enhancing their antioxidative potential.

Biological assays revealed the broad-spectrum efficacy of these nanoparticles, particularly in antimicrobial applications. LAuNPs displayed the highest antibacterial activity against *Staphylococcus aureus* and *Klebsiella pneumoniae*, attributed to their smaller size and higher surface area. The heightened efficacy against *S. aureus* was linked to structural vulnerabilities in its cell wall, positioning these nanoparticles as promising candidates to combat antibiotic-resistant pathogens. These findings support the potential of such bio-synthesized nanoparticles as next-generation antimicrobial agents in healthcare.

Genotoxicity assessments conducted using the *Allium cepa* root tip model demonstrated the environmentally benign nature of these nanoparticles. While LNiNPs exhibited the strongest genotoxic effects at higher concentrations, these

remained below 50%, ensuring minimal environmental impact when applied judiciously. This environmentally friendly profile highlights their suitability for agricultural applications, particularly as biomaterials for controlled genetic modulation in plants, contributing to sustainable agricultural practices.

The anticancer potential of the synthesized nanoparticles was a significant aspect of the study. Among them, LCuONPs showed the highest cytotoxic activity against Dalton's Lymphoma Ascites (DLA) cells, primarily through the induction of oxidative stress. Additionally, the antiangiogenic properties of LNiNPs and LCuONPs emphasized their therapeutic potential in inhibiting tumor vascularization, a critical factor in cancer progression. These findings illustrate the promise of these nanoparticles in cancer therapy, offering novel approaches to target and disrupt tumor growth.

The comprehensive metabolomic analysis of the defensive secretion using LC-MS identified key compounds such as D-Gluconic acid, 3-Dehydro-L-gulonate, Uric acid, Citric acid, and 2-Pyrrolidone-5-carboxylic acid. Each of these metabolites played a pivotal role in the nanoparticle synthesis process. D-Gluconic acid acted as both a reducing and stabilizing agent, ensuring uniform morphology and size distribution of the nanoparticles. 3-Dehydro-L-gulonate contributed to the antioxidant activities, while Uric acid further enhanced these properties through redox reactions. Citric acid stabilized the nanoparticles via its carboxy and hydroxyl groups, as confirmed by FTIR and zeta potential analyses, particularly for LCuONPs. The role of 2-Pyrrolidone-5-carboxylic acid was equally significant, enhancing the structural integrity of the nanoparticles and broadening their biological applicability.

In conclusion, the study establishes the defensive secretion of *L. tristis* as a transformative resource for green nanotechnology. The metabolites identified within this secretion not only drive the synthesis of nanoparticles but also augment their biological activities, including antioxidant, antimicrobial, and anticancer properties. By converting a pest species into a valuable resource, this research exemplifies sustainable innovation, paving the way for cost-effective and eco-friendly solutions to pressing challenges in healthcare, agriculture, and industrial applications. The integration of biological richness with advanced nanotechnology heralds a new era of multifunctional nanomaterial design, rooted in environmental sustainability and scientific ingenuity.

Key words: *Nanoparticles, Luprops tristis, antioxidant activity, antibacterial effect, chromosomal aberrations.*

സംഗ്രഹം

ഈ പഠനം ലൂപ്രോപ്സ് ട്രിസ്റ്റിസ് എന്ന ടെനെബ്രിയോണിഡ് വർഗത്തിൽപ്പെട്ട പ്രാണിയുടെ പ്രതിരോധ സ്രവത്തെ ലോഹ നാനോസംശ്ലേഷണത്തിനായുള്ള പുതിയ ജൈവിക സാങ്കേതിക സ്രോതസായി പരിശോധിക്കുന്നു. ഈ സ്രവം നാനോകണങ്ങളുടെ രൂപീകരണത്തിലും പ്രവർത്തനക്ഷമതയിലും നിർണായകമായ പങ്കുവഹിക്കുന്ന വൈവിധ്യമാർന്ന രണ്ടാം നിര മെറ്റബൊലൈറ്റുകൾ അടങ്ങിയ രാസപദാർത്ഥങ്ങളാൽ സമ്പന്നമായ അന്തരീക്ഷം വാഗാനം ചെയ്യുന്നു. LC-MS, GC-MS സാങ്കേതിക വിദ്യകൾ ഉപയോഗിച്ച് നടത്തിയ സമഗ്രമായ വിശകലനത്തിൽ D-ഗ്ലൂക്കോണിക് ആസിഡ്, 3-ഡീഹൈഡ്രോ-എൽ-ഗുലൊനേറ്റ്, യൂറിക് ആസിഡ്, സിട്രിക് ആസിഡ്, 2-പൈറോളിഡോൺ-5-കാർബോക്സിലിക് ആസിഡ് എന്നിവ ഉൾപ്പെടെ പ്രധാന മെറ്റബൊലൈറ്റുകൾ തിരിച്ചറിഞ്ഞു, ഇവ സംയോജിത നാനോകണങ്ങളുടെ ഘടനാപരവും ജൈവസജീവവുമായ ഗുണങ്ങൾ മെച്ചപ്പെടുത്തുന്നു.

ഓരോ മെറ്റബൊലൈറ്റും സംശ്ലേഷണ പ്രക്രിയയിൽ അതാത് രീതിയിൽ പങ്കുചേരുന്നു. D-ഗ്ലൂക്കോണിക് ആസിഡ് ലോഹ അയോണുകളെ കുറയ്ക്കുകയും നാനോകണങ്ങളുടെ ഏകീകൃത രൂപീകരണം പ്രോത്സാഹിപ്പിക്കുകയും ചെയ്യുന്ന, സ്ഥിരത നൽകുന്ന ഏജന്റായി പ്രവർത്തിക്കുന്നു. ശക്തമായ ഫ്രീ-റാഡിക്കൽ സ്കാവഞ്ചിംഗ് സ്വഭാവമുള്ള 3-ഡീഹൈഡ്രോ-എൽ-ഗുലൊനേറ്റ് ആന്റി-ഓക്സിഡൻറ് പ്രവർത്തനക്ഷമത വർദ്ധിപ്പിക്കുന്നു, സ്വർണ നാനോകണങ്ങൾക്ക് 40 എന്ന IC_{50} മൂല്യത്താൽ ഇത് തെളിയിച്ചിരിക്കുന്നു. യൂറിക് ആസിഡ് റെഡോക്സ് പ്രതികരണങ്ങളിൽ പങ്കുചേരുകയും ആന്റി-ഓക്സിഡൻറ് പ്രവർത്തനം വർദ്ധിപ്പിക്കുകയും ചെയ്യുന്നു. കാർബോക്സി, ഹൈഡ്രോക്സിൽ ഗ്രൂപ്പുകൾ അടങ്ങിയ സിട്രിക് ആസിഡ് നാനോകണങ്ങളെ സ്റ്റാബിലൈസ് ചെയ്യുകയും ക്യാപ് ചെയ്യുകയും ചെയ്യുന്നു, ഇത് FTIR, സീറ്റാ പൊട്ടൻഷ്യൽ വിശകലനങ്ങളിൽ സ്ഥിരീകരിക്കുന്നു, പ്രത്യേകിച്ച് കോപ്പർ ഓക്സൈഡ് നാനോകണങ്ങൾ ഉയർന്ന സ്ഥിരതയിൽ കാണപ്പെടുന്നു. അവസാനമായി, 2-പൈറോളിഡോൺ-5-കാർബോക്സിലിക് ആസിഡ് ഘടനാ സമഗ്രത ശക്തിപ്പെടുത്തുകയും ജൈവ സംവേദനങ്ങൾ എളുപ്പമാക്കുകയും ചെയ്യുന്നു, ഇത് നാനോകണങ്ങളെ ബയോസെൻസിങ്, ആന്റിമൈക്രോബയൽ ചികിത്സകൾ പോലുള്ള പ്രവർത്തനങ്ങൾക്ക് അനുയോജ്യമാക്കുന്നു.

ലോഹ നാനോകണങ്ങൾ; നിക്കൽ (LNiNPs), കോപ്പർ ഓക്സൈഡ് (LCuONPs), സിങ്ക് ഓക്സൈഡ് (LZnONPs), ഗോൾഡ് (LAuNPs) സംശ്ലേഷണം നടത്തിയതിൽ ഓരോന്നും വ്യത്യസ്ത ജൈവശാസ്ത്രപരവും ഭൗതികരാസപരവുമായ ഗുണങ്ങളാണ് കാണിച്ചിരിക്കുന്നത്. UV-Vis ആബ്സോർപ്ഷൻ പീക്കുകൾ നന്നായി നിർവചിക്കപ്പെട്ട ഓപ്റ്റിക്കൽ ഗുണങ്ങളെ സൂചിപ്പിക്കുന്നു, പ്രത്യേകിച്ച് ബയോസെൻസിംഗിന് ആവശ്യമായവ. ഗോൾഡ് നാനോകണങ്ങൾ മികച്ച ഗ്ലൂക്കോസ് സെൻസിംഗ് കഴിവുകൾ (LOD = 0.75) പ്രകടിപ്പിച്ചു, പ്രത്യേകിച്ച് നവജാത ശിശുക്ഷേമത്തിന് സഹായകരമായ അതിക്രമമില്ലാത്ത ഗ്ലൂക്കോസ് നിരീക്ഷണത്തിനായുള്ള പ്രബലമായ സ്ഥാനാർത്ഥിയായി മാറുന്നു.

ആന്റിബാക്ടീരിയൽ പരീക്ഷണങ്ങൾ *സ്റ്റാഫിലോകോക്കസ് ഔറിയസ്*, *ക്ലെബ്സിയല്ല ന്യുമോണിയ* എന്നീ ബാക്ടീരിയകളിൽ ഡോസ്-ഡിപെൻഡന്റ് പ്രവർത്തനക്ഷമത കാണിച്ചു, ഗോൾഡ് നാനോകണങ്ങൾ ഏറ്റവും ഉയർന്ന ഫലപ്രാപ്തി പ്രകടിപ്പിച്ചത് ചെറുതായ ഗുണനിലവാരം, ഉയർന്ന ഉപരിതല പ്രദേശം എന്നിവയുടെ ഫലമായി. *സ്റ്റാഫിലോകോക്കസ് ഔറിയസ്* -നോടുള്ള പ്രവർത്തനം കൂടുതൽ മുകളിൽ നിന്നു, അതിന്റെ കോശഭിത്തിയുടെ ഘടനാപരമായ അനന്തരങ്ങൾ കാരണമാകുന്നു. *Allium cepa* മൂല കോശങ്ങൾ ഉപയോഗിച്ചുള്ള ജനിതക വിഷപരിശോധനയിൽ ഉയർന്ന നാനോകണങ്ങളുടെ അളവിൽക്രോമോസോമൽ അപവ്യവസ്ഥകൾ തെളിഞ്ഞു, എന്നാൽ ഇത് നിയന്ത്രിത ഉപയോഗത്തിൽ പരിസ്ഥിതി ആഘാതം ഇല്ലാത്തതായും തെളിയിച്ചു. ഡാൾട്ടൺസ് ലിംഫോമ ആസൈറ്റ്സ് (DLA) കോശങ്ങളിലെത്തിയുള്ള പരീക്ഷണങ്ങളിൽ, കോപ്പർ ഓക്സൈഡ് നാനോകണങ്ങൾ ഏറ്റവും ഉയർന്ന ആന്റികാൻസർ പ്രവർത്തനക്ഷമത പ്രകടിപ്പിച്ചു. ഈ പഠനം, ലൂപ്രോപ്സ് ട്രിസ്റ്റിസ് പ്രതിരോധ സ്രവത്തിൽ നിന്ന് ഉത്പാദിപ്പിച്ച നാനോകണങ്ങളുടെ വൈവിധ്യമാർന്ന ഉപയോഗശേഷി തിരിച്ചറിയുന്നു.

Key words: നാനോകണങ്ങൾ, ലൂപ്രോപ്സ് ട്രിസ്റ്റിസ്, ആന്റി-ഓക്സിഡൻറ് പ്രവർത്തനം, ആന്റിബാക്ടീരിയൽ പരീക്ഷണങ്ങൾ, അളവിൽക്രോമോസോമൽ അപവ്യവസ്ഥകൾ.

CONTENTS

LIST OF TABLES

LIST OF FIGURES

ABBREVIATIONS

L. tristis	–	*Luprops tristis*
NPs	–	Nanoparticles
LNiNPs	–	Nickel Nanoparticles synthesized using *Luprops tristis*
LCuONPs	–	Copper Oxide Nanoparticles synthesized using *Luprops tristis*
LZnONPs	–	Zinc Oxide Nanoparticles synthesized using *Luprops tristis*
LAuNPs	–	Gold Nanoparticles synthesized using *Luprops tristis*
LC-MS	–	Liquid Chromatography-Mass Spectrometry
GC-MS	–	Gas Chromatography-Mass Spectrometry
2-P-5-CA	–	2-Pyrrolidone-5-carboxylic acid
DGA	–	D-Gluconic Acid
3-D-L-G	–	3-Dehydro-L-gulonate
UA	–	Uric Acid
CA	–	Citric Acid
FTIR	–	Fourier Transform Infrared Spectroscopy
LOD	–	Limit of Detection
S. aureus	–	*Staphylococcus aureus*
K. pneumoniae	–	*Klebsiella pneumoniae*
DLA	–	Dalton's Lymphoma Ascites
IC_{50}	–	Half Maximal Inhibitory Concentration

CHAPTER I

INTRODUCTION

1.1. *Luprops tristis* – EXPERIMENTAL ORGANISM

The species *Luprops tristis*, described by Fabricius in 1801, finds its place within the vast Kingdom Animalia, signifying its status as an animal. It belongs to the Phylum Arthropoda, a diverse group of invertebrates recognized for their exoskeletons, segmented bodies, and jointed appendages. Within Arthropoda, *L. tristis* is further classified in the Class Insecta, marking it among the insects. It is part of the Order Coleoptera, the beetles, which are distinguished by their hardened forewings. In this order, it falls under the Family Tenebrionidae, known as darkling beetles, a diverse and resilient group. The genus *Luprops* unites beetles with shared morphological characteristics, while the species designation *L. tristis* identifies this beetle's distinct place within its genus (Watt, 1974).

L. tristis Fabricius, a detritivorous beetle, is found mostly in leaf litter habitats. It has a distribution ranging from tropical Asia and the East Indies to Papua New Guinea, and into tropical Africa as well. In India, specifically in the western slopes of the southern Western Ghats in rubber plantation areas, *L. tristis* populations have been known to congregate in exceptionally massive numbers between about 0.5 and more than 4 million individuals per residential building, after the beginning of summer monsoon rains. The collective congregation is mostly due to their long duration of dormancy, with emergence and invasion habits often induced by the first heavy rains of the season (Sabu *et al.,* 2008). While not harmful, these beetles emit a phenolic secretion, causing skin irritation when startled, prompting some residents to evacuate. Designations like "Ola Prani" and "Oadu" are prevalent in northern Kerala, while in central and southern regions, they are referred to as "Mupli vandu," tracing back to congregations in rubber estates during the 1970s. Their life cycle includes larval, pupal, and adult stages, with their abundance in rubber tree plantations attributed to the availability of early-falling rubber tree leaves as a food source (Sabu & Vinod, 2009). Investigating their life cycle and seasonal patterns reveals enormous population growth due to predation absence (Abhitha *et al.,* 2010). Defensive glands in both larvae and adults secrete compounds triggered by haemolymph pressure (Tschinkel, 1975), offering defense

against predators (Kendall, 1974). In agricultural fields and woodland areas of the South Western Ghats, these darkling beetles are observed, with *L. tristis* being the predominant species (Arunraj *et al.,* 2017). Our research aims to utilize the defensive secretion of *L. tristis* for biosynthesis of metallic NPs, examining their characteristics through various assays, including electrochemical sensing, antibacterial, antioxidant, environmental hazard analysis, cytotoxicity assays, and antiangiogenesis by CAM assay.

1.2. NANOPARTICLES

In the last century, there has been remarkable acknowledgment and progress in nanotechnology studies. The word "nanotechnology" was coined by Richard P. Feynman's powerful 1959 lecture, "There is Plenty of Room at the Bottom" (Feynman, 1960). Early work by pioneers such as Paul Ehrlich, Ursula Scheffel, and Professor Peter Speiser's group at ETH Zurich during the late 1960s and early 1970s has laid the groundwork for the development of Nanoparticles (NPs) (Kreuter, 2007). NPs, officially known as zero-dimensional nanomaterials, have special properties that make them distinct from materials at larger scales. Size, energy absorption, and chemical reactivity distinguish NPs from their bulk materials (Murthy, 2007). Nanotechnology consists of working at the level of molecules in manipulating materials so as to tap into their specific characteristics. Nanotechnology includes nanoscale designing, characterization, producing, and applying structures, devices, and systems (Brock, 2004). NPs generally range from a dimension of 10 nm up to 100 nm and can consist of metals, metal oxides, organic materials, and carbon (Hasan, 2015). They display remarkable physical, chemical, and biological characteristics at the nanoscale due to their high surface area to volume ratio, mechanical stability, and reactivity. Their unique features render NPs ideal for various applications in many areas (Salata, 2004; Machado *et al.,* 2015).

1.3. GROUPING OF NPS

1.3.1. Organic NPs

There are three types of NPs (organic, inorganic, and carbon-based). Organic NPs include natural nanomaterials like liposomes, ferritin, dendrimers, and micelles

that tend to reside under the category of polymers. They are defined by the fact that they are non-toxic and biodegradable. As seen, specific ones like micelles and liposomes, popularly referred to as nanocapsules, have an empty center and are sensitive to electromagnetic and thermal radiation, e.g., light and heat. These special features render them especially suitable for pharmaceutical drug delivery applications (Tiwari *et al.,* 2008).

1.3.2. Inorganic NPs

Those particles that are not made of carbon are inorganic NPs. Inorganic NPs are generally composed of metal and metal oxides. They are safe to handle. They are hydrophilic and biocompatible. In comparison with organic NPs, inorganic NPs are far more stable.

1.3.2.1. Metal NPs

Metals are converted into metallic NPs either by constructive or destructive processes and reach nanoscale sizes. Almost any metal is suitable for generating NPs. Zinc (Zn), iron (Fe), lead (Pb), aluminum (Al), cadmium (Cd), cobalt (Co), copper (Cu), gold (Au), and silver (Ag) are some of the metals that are frequently used to generate NPs. These NPs generally vary in size from 10 nm to 100 nm and are identified based on their high surface area-to-volume ratio, adjustable pore sizes, surface charge, and surface charge density. They may have spherical or cylindrical shapes and exhibit crystalline and amorphous structures. Their characteristics include color, reactivity, and sensitivity to heat, moisture, sunlight, and air (Salavati-Niasari *et al.,* 2008).

1.3.2.2. Metal oxide NPs

The intention of metal oxide nanoparticles fabrication is to change the characteristics of the initial metal nanoparticles. For instance, oxidizing iron nanoparticles produces iron oxide nanoparticles. Iron oxide nanoparticles are more reactive than their iron equivalents. This heightened reactivity and efficiency in producing metal oxide nanoparticles are reflected in different compounds, including zinc oxide (ZnO), iron oxide (Fe_2O_3), aluminum oxide (Al_2O_3), cerium oxide (CeO_2), and titanium oxide (TiO_2) (Tai *et al.,* 2007).

1.3.3. Carbon-based

This group of NPs is made up primarily of carbon due to their elemental composition, carbon-based NPs are specially characterized by their sole carbon composition. This group comprises a number of subgroups, including carbon black, carbon nanofibers (CNFs), fullerenes, graphene, and carbon nanotubes (CNTs). Activated carbon is also, on occasion, classified under this group at nanoscale size (Bhaviripudi *et al.,* 2007).

1.3.3.1. Fullerenes

Fullerenes are nanomaterials formed as empty cages. For commercial purposes, their very good electrical conductivity, electron affinity, resistance to breakdown, and ability to do anything have raised major interest. Fullerenes consist of pentagon and hexagon-shaped units of carbon atoms that are held together by sp2 hybridization. Precisely, fullerenes such as C60 or C70 possess diameters of 7.114 nm and 7.648 nm, respectively. The structure of fullerene is divisible into two classes: single-layer and multilayer (Astefanei *et al.,* 2015)

1.3.3.2. Graphene

Graphene, a carbon allotrope, displays a honeycomb lattice structure made up of carbon atoms arranged hexagonally. This arrangement results in a flat surface with two-dimensional properties. Graphene's thickness is typically around 1 nm (Geim, 2009).

1.3.3.3. Carbon Nanofibers (CNFs)

CNFs are derived from the same graphene nanofoils utilized in the production of Carbon Nanotubes (CNTs). However, instead of forming cylindrical tubes, these graphene nanofoils are arranged into a conical or cup-shaped structure (Chatterjee & Deopura, 2002).

1.3.3.4. Carbon nanotubes (CNTs)

CNTs are elongated tubular structures with diameters ranging from 1-2 nm. The inherent properties of carbon nanotubes suggest that they can exhibit either

metallic or semiconducting characteristics, depending on their diameter. Structurally, CNTs resemble a graphite sheet rolled upon itself. CNTs are categorised into three groups based on their rolling method: single-walled (SWNTs), double-walled (DWNTs), and multi-walled (MWNTs) (Saeed & Khan, 2013) .

1.3.3.5. Carbon Black

This is a carbonaceous amorphous material known for its diameters ranging from 20 to 70 nm, commonly presenting a spherical shape. These particles display significant interactivity, resulting in their aggregation into larger structures called agglomerates, typically sized around 500 nm (Gómez-Hernández *et al.,* 2019).

1.4. METHODS OF SYNTHESIS OF METAL NPs

Different techniques exist for synthesizing NPs, and these techniques are classified into two primary types,

1.4.1. Top-down synthesis

The approach employed in this scenario follows a deconstructive method. The larger-scale material is broken down into smaller molecules, which further disintegrate into smaller particles. Examples of processes for top-down synthesis include physical vapor deposition, grinding, milling, and other destructive techniques (Iravani, 2011).

1.4.1.1. Mechanical milling

Mechanical milling stands as the most prevalent top-down method for generating various NPs. It finds extensive application in post-annealing and milling procedures for nanoparticle creation, where different components are ground in an inert atmosphere. The subsequent stages in mechanical milling involve plastic deformation, altering the particle's shape, reducing the particle's size, and cold-welding, increasing the particle's size (Yadav *et al.,* 2012).

1.4.1.2. Nanolithography

Nanolithography involves the scientific exploration of constructing structures on the nanoscale, typically with dimensions ranging between 1nm and 100

nm. This field employs various nanolithographic techniques such as optical, electron-beam, multiphoton, nanoimprint, and scanning probe lithography. Essentially, lithography selectively removes material to create a desired configuration while imprinting a defined shape or structure onto a photosensitive substance (Pimpin & Srituravanich, 2012). Nanolithography offers the advantage of creating structures of diverse sizes and shapes, from individual NPs to clusters. However, it comes with certain drawbacks, including the requirement for expensive equipment and associated expenses (Hulteen *et al.,* 1999). In addition to nanolithography, many more methods are available, such as Laser ablation (Amendola & Meneghetti, 2009), Sputtering (Lugscheider *et al.,* 1998; Shah & Gavrin, 2006), Thermal decomposition (Salavati-Niasari *et al.,* 2008) etc.

1.4.2. Bottom-up method

Bottom-up methods, also known as constructive approaches, operate distinctively from top-down methods by converting simpler materials into NPs. Examples of bottom-up techniques 1as follows;

1.4.2.1. Chemical Vapor Deposition (CVD)

Chemical Vapor Deposition (CVD) involves depositing a thin layer of gaseous reactant onto a substrate inside a reaction chamber. When the heated substrate comes into contact with the gas, it initiates a chemical reaction, resulting in the formation of a thin layer of the product on the substrate surface (Bhaviripudi *et al.,* 2007). The advantages of the CVD process include the production of extremely pure, homogeneous, robust, and hard NPs. However, drawbacks include the necessity for specialized equipment and the generation of highly hazardous gaseous byproducts (Adachi *et al.,* 2003).

1.4.2.2. Sol-gel method

The Sol-gel method, derived from "sol" and "gel", entails dissolving a solid macromolecule (gel) in a solvent to form a colloid (sol) of solid particles suspended in a continuous liquid (Sivasamy, 2013). In addition to this bottom-up method includes Pyrolysis (Kammler *et al.,* 2001), Spinning (Tai *et al.,* 2007, Mohammadi *et al.,* 2014), etc.

1.4.3. BIOLOGICAL SYNTHESIS

NPs are commonly synthesized using a blend of chemical and physical methods. However, the chemicals employed in this process pose environmental risks due to their hazardous nature. Additionally, physical approaches are less cost-effective as they require substantial energy consumption (Iravani *et al.,* 2014; Wageh *et al.,* 2015). Consequently, biological synthesis of nanomaterials emerges as a superior choice, being more cost-efficient, environmentally friendly, and devoid of energy consumption or hazardous chemicals. This method finds particular relevance in clinical and biomedical applications. Various plants and microorganisms, including bacteria, fungi, yeast, and algae, have been utilized to create silver, gold, copper, palladium, and iron nanostructures (Saxena *et al.,* 2012). One advantage of biological nanoparticle synthesis is the avoidance of harsh processing conditions, leading to cost savings by enabling synthesis at physiological pH, temperature, and pressure. A wide array of microbes has demonstrated the ability to produce inorganic nanoparticle composites, either internally or externally. To overcome the negative aspects of the chemical and physical methods of NPs synthesis, the biological approaches were used recently, using bacteria, fungi, protists, and plant extracts (Li *et al.,* 1999).

1.4.3.1. Nanoparticles from Bacteria

Bacteria react with the metallic particles through the reduction of metallic ions as well as the production of nanoparticles outside the cell. It is an efficient, greener methodology in NPs synthesis (Saratale *et al.,* 2018). A wide variety of bacteria were used for the reduction purpose, such as *Cupria vidus* for AgNPs synthesis (Ameen *et al.,* 2020). Bacteria-produced metabolites also take part in the reduction role, as in the case of lignin peroxidase enzyme from *Acinetobacter sp.* Mediated AuNPs synthesis (Elmegdar *et al.,* 2024). *Pseudomonas fluorescens* produces the AuNPs by extracellular activity (Rajasree & Suman, 2012). Recent research shows the use of a bacterial mix solution for the NPs synthesis (Siva Kumar *et al.,* 2014). *Pseudomonas putida* culture used for the synthesis of ZnONPs, the study shows the tolerance of microorganisms to the metals in effluents (Jayabalan *et*

al., 2019). Many species of bacteria were used for this NPs synthesis as AgNPs from *Bacillus cereus* and *Lactobacillus casei* (Sunkar & Nachiyar, 2012; Korbekandi *et al.,* 2012), AuNPs synthesis from *E. coli* and *B. subtilis* (Southam & Beveridge, 1994; Du *et al.,* 2007). CoNPs synthesis from *Pyrobaculum islandicum* (Li *et al.,* 2011).

1.4.3.2. Nanoparticles from Fungus

Fungi are potent biological tools in nanoparticle synthesis owing to the presence of intercellular enzymes (Mohanpuria *et al.,* 2008). Silver nanocrystals were synthesized through the biological synthesis process using lignolytic fungi, *Trametes trogii*, as evident from previous studies (Kobashigawa *et al.,* 2019). Wanarska and Maliszewska observed the ability of *Penicillium cyclopium* to synthesize metallic silver NPs. Metabolites produced by the fungal cells also take part in the reduction of metal NPs formation (Wanarska & Maliszewska, 2019; Naimi-Shamel *et al.,* 2019). CuONPs were synthesized using fungi that develop naturally by employing an aqueous extract prepared from the mycelium of *Trichoderma asperellum* (Saravanakumar *et al.,* 2019). A fungus, *Periconium sp.,* from the leaves of *Balanites aegyptiaca*, stimulated the biosynthesis of ZnNPs (Ganesan *et al.,* 2020). Two more fungus species, *Verticillium sp.* and *F. oxysporum*, have been screened to obtain NPs with the addition of metal ion solutions such as Ag^{+} and $AuCl_4$-. Experiments conducted by Mukherjee and coworkers (Mukherjee *et al.,* 2001) and Ahmad *et al.,* (2002) identified that it could be done within cells as well as outside cells (Ahmad *et al.,* 2002). *F. solani* (USM-3799), a pathogenic fungus, synthesized polydispersed NPs having an average size of 16.23 nm with 1mM $AgNO_3$ (Ingle *et al.,* 2008). Binupriya and coworkers successfully employed the cell filtrate of the stationary biomass of filamentous fungus *Rhizopus stolonifer* (KCCM 35486). This was the first such report where equivalent-sized and shaped NPs of (Au) and (Ag) were prepared at room temperature (Binupriya *et al.,* 2010).

1.4.3.3. Nanoparticle synthesis using Algae

Synthesis of nanoparticles from algae offers a promising platform for synthesizing NPs with new properties. Algae with their dense species diversity and

high biomass are superior sources for the synthesis of nanoparticles in an eco-friendly and economical way. Various species of algae, including red, brown, and green algae, have been employed for NPs production, like gold, zinc oxide, and silver. These microorganisms possess inherent biological processes that enable the process of forming NPs, typically within their cell structures or extracellularly. NPs synthesis using algae not only provides a green process alternative to traditional chemical processes but also promises designed NPs properties using control of algal species and growth conditions. In addition, algae application for NPs synthesis is in accordance with green chemistry, cutting down on environmental traces and favoring sustainable material use in nanotechnology. AuNPs are intracellularly synthesized through the *Tetraselmis kochinensis* cell wall (Senapati *et al.,* 2012). *Cystoceria baccatta* is employed in AuNPs synthesis against the treatment of colon and rectal cancer. The extract rapidly generates the NPs, with further analysis verifying that polycrystalline NPs comprise the majority of the composition of the extract. This suggests that, as indicated by González-Ballesteros and team in 2017, the formation and nucleation processes occur in the extract (González-Ballesteros *et al.,* 2017). Recently, several NPs were synthesised from different species of algae, especially *Egregia sp* (Yılmaz Öztürk *et al.,* 2020; Colin *et al.,* 2018).

1.4.3.4. Nanoparticles from Yeast

Yeast is used instead of bacteria for NPs synthesis because it can be easily cultivated and controlled under laboratory conditions despite its limited food requirements for high growth and enzyme synthesis (Soliman *et al.,* 2018). NPs synthesis was more affected by the yeast's greater cytosolic volume than by bacterial production (Sandana Mala & Rose, 2014). *Yarrowia lipolytica* facilitated AuNPs were reported to control the process as well as metal ions and biomass concentration (Pimprikar *et al.,* 2009). Nitrate reductase, a protein that is enzymatically synthesized from epiphytic yeasts *Rhodotorula glutinis* and *Cryptococcus laurentii,* facilitates efficient synthesis of NPs through silver metal ion reduction to silver NPs (Ananthi *et al.,* 2018; Fernández *et al.,* 2016).

1.4.3.5. Nanoparticles from plants

Green synthesis of nanomaterials adopts an eco-friendly strategy across their life cycle, using organic substances such as plant extracts and low-toxicity solvents to incur minimal harm on the environment (Hischier & Walser, 2012; Salieri *et al.,* 2018). Bioactive molecules in plant extracts, including flavonoids, carotenoids, and polysaccharides, are important for decreasing precursor ions to atoms, determining the biological properties and cytotoxicity of the generated nanomaterials (Bansal *et al.,* 2014; Behzad *et al.,* 2021; Santos *et al.,* 2023; Jadoun *et al.,* 2021; Parveen *et al.,* 2016). Gold NPs (AuNPs) were recently synthesized in an eco-friendly way using the extracts of both leaves and fruit of *Pistacia atlantica*. These spherical AuNPs with a size ranging from 40-60 nm showed antibacterial activity (Carvalho *et al.,* 2021; Hamelian *et al.,* 2018). In the same way, scientists investigated the fabrication of bioactive NiNPs using the water extract of *Medicago sativa*. The green synthesis process resulted in the reduction of reducing sugars, proteins, and polysaccharides, such as flavonoids, indicating a possible correlation with these bioactivities and nickel bioreduction (Chen *et al.,* 2014). Plant-mediated NPs show several activities such as antimicrobial, genetic aberrations, etc (Król *et al.,* 2019; Akintelu *et al.,* 2020).

1.4.3.6. NPs from other organisms

NPs were also synthesised from many higher-level organisms other than bacteria and fungi, such as insects and snakes such as defensive gland secretion of the beetle *L. tristis* Fabricius, popularly referred to as the mupli beetle, is applied in microwave-mediated AgNPs synthesis. The gland extract serves as the reducing and capping agent (Ajaykumar *et al.,* 2023). AuNPs were also synthesised from jellyfish nematocysts. These AuNPs are screened for their anticancer potential against breast cancer cells via *in vitro* experiments (Amreen Nisa *et al.,* 2023). Biogenic synthesis of AuNPs using jellyfish *Acromitus flagellatus* (*A. flagellatus*) nematocyst venom reveals their anti-proliferative properties (Nisa *et al.,* 2023). A

very interesting area includes the development of stable AuNPs from the sponge *Acanthella elongata*, collected from the Gulf of Mannar, Tamil Nadu, India (Inbakandan *et al.,* 2010). These instances demonstrate the ways in which NPs can be biosynthesized from higher organisms, providing environmentally friendly and potentially influential solutions in fields such as medicine and environmental science. Snakes' biosynthesis of NPs is an interesting direction for environmentally friendly and sustainable NPs production. Some snake venoms consist of a vast array of bioactive molecules, such as enzymes and proteins, that have distinct properties that can be utilized in nanoparticle synthesis. Scientists have investigated the use of snake venom proteins to make different NPs, such as silver and AuNPs. The venom proteins are responsible for mediating the NPs forming reactions while maintaining their stability as well as biocompatibility. The method not only provides a sustainable means of replacing classical chemical synthesis pathways but also promises to be useful in the future of medicine. Additionally, the investigation of snake venom as a nanoparticle synthesis medium highlights the immense capability of nature's resources to contribute to the development of nanotechnology for a variety of useful purposes (Mohammadpourdounighi *et al.,* 2010). Such bio-based strategies not only provide eco-friendly alternatives to traditional chemical approaches but also produce NPs with designed properties for different applications, such as medicine, catalysis, and environmental remediation. Additional investigation of nanoparticle biosynthesis from higher organisms is likely to reveal novel synthesis routes and widen the palette of sustainable nanotechnological solutions.

1.5. HYPOTHESIS

Hypothesis: The defensive secretion of *Luprops tristis* can be utilized as a starting material for the synthesis of metallic NPs, with potential applications across diverse biological domains.

1.6. OBJECTIVES

1. Evaluation of the chemical composition and multifunctional biological activities (antimitotic, antioxidant, antibacterial, and cytotoxic) of the defensive gland extract of *Luprops tristis* Fabricius.
2. Biosynthesis of nickel nanoparticles using beetle defensive gland extract for electrochemical and biological applications.
3. Biosynthesis of copper oxide nanoparticles using beetle defensive gland extract for electrochemical and biological applications.
4. Biosynthesis of gold nanoparticles using beetle defensive gland extract for electrochemical and biological applications.
5. Biosynthesis of zinc oxide nanoparticles using beetle defensive gland extract for electrochemical and biological applications.

1.6. RELEVANCE OF THE STUDY

The importance of research in nanoparticle biosynthesis has been well-established, covering various organisms like bacteria, fungi, protists, viruses, algae, and plants. However, the synthesis of metal NPs (nickel, copper oxide, gold, and zinc) from insects remains largely unexplored. Recent studies highlight the extensive use of metal NPs in medicine, agriculture, and water treatment. This investigation aims to address the limitations of conventional physical and chemical synthesis methods by focusing on eukaryotic organisms without killing them for nanoparticle synthesis, potentially offering innovative methodologies for producing these NPs. Additionally, the study will assess the biological activities, including antimicrobial, antiangiogenic, and anticancer properties of these NPs, suggesting potential applications as biosensors, effective antimicrobials, anticancer, and anti-angiogenesis properties. Biosynthesized NPs are advantageous over physically or chemically synthesized ones, presenting diverse applications in medicine, technology, and scientific research. In this study, the focus will be on synthesizing four types of metal NPs, such as Ni, CuO, Au, and ZnO, from the defensive gland secretion of the beetle *L. tristis*. The research aims to analyze the various biological properties of these NPs, offering a greener and economically viable approach to creating nanomaterials.

CHAPTER II

REVIEW OF LITERATURE

Nanoparicles having a wide variety of application in every field. Present chapter deals with a review on metal NPs, mainly discussing nickel, copper oxide, gold, and zinc oxide.

2.1. Biological Application of Nickel Nanoparticles (NiNPs)

NiNPs have drawn significant attention as a result of their high-quality physical, chemical, and magnetic properties that support a wide array of applications in catalysis, electronics, and biomedicine (Abdel Fattah *et al.,* 2016; Barsan *et al.,* 2019; Bibi *et al.,* 2017; Cheng *et al.,* 2020; Jiao *et al.,* 2019; Kiran *et al.,* 2020; Ni *et al.,* 2019). In organic synthesis, NiNPs catalyze reactions like the hydrogenation of olefin and the reduction of aldehydes or ketones (Alonso *et al.,* 2008, 2009; Dhakshinamoorthy & Pitchumani, 2008), and inorganically, they catalyze reactions like ammonia degradation (Li *et al.,* 2005). They also play a major role in carbon nanotube synthesis (Li *et al.,* 2006). Nickel, having good prevalence and economic viability, NiNPs are useful additives in coatings, polymers, and fibers (Bian *et al.,* 2017; Hill *et al.,* 2019). Green synthesis pathways provide eco-friendly methods to NiNPs, which provide uniform nanoparticles with increased antibacterial and antioxidant activity with low cytotoxicity Chen *et al.,* 2014; Jeyaraj Pandian *et al.,* 2016; Sudhasree *et al.,* 2014). NiNPs suppress pathogens such as *E. coli* and *S. aureus* (Helen *et al.,* 2016), inhibit rice blast disease in agriculture (Parthasarathy *et al.,* 2023), and show antioxidant, antibacterial, and anticancer activities (Ali *et al.,* 2021; Hussain *et al.,* 2023; Kareem *et al.,* 2022). Their magnetic and catalytic characteristics render NiNPs extremely versatile for renewable biomedical and technological advances (Roselina & Azizan, 2012).

2.1.1. Antimicrobial Activity

NiNPs show strong antibacterial activity against drug-resistant species. NiNPs reduce microbial growth and, therefore, find applications as antimicrobial devices and coatings (Pal *et al.,* 2019). Green synthesis gives them efficacy against methicillin-resistant *Staphylococcus aureus* (MRSA), conferring greater therapy value (Zarenezhad *et al.,* 2022). The antibacterial effectiveness of NiO/NiO NPs biosynthesized using *Lactuca serriola* seeds is very effective (Ali *et al.,* 2021).

NiNPs are also inhibit the biofilms by *Staphylococcus epidermidis* (Vahedi *et al.,* 2017) and prove effective against human pathogens in dental use (Argueta-Figueroa *et al.,* 2014). Sonication based NiNPs also improve antimicrobial effectiveness (Gomaji Chaudhary *et al.,* 2015). Overall, these results affirm NiNPs as potential antimicrobial agents in the biomedical field.

2.1.2. Anticancer Potential

NiNPs show cytotoxicity towards cancer cells. NiNPs extracted from *Azadirachta indica* and *Psidium guajava* leaves exhibit cytotoxicity against colon cancer cells (HT29) due to their nanoscale shape (Mariam *et al.,* 2014). Their capacity to increase membrane permeability allows targeted delivery into leukemia cells (Guo *et al.,* 2008). NiNPs from Cressa leaves also reduced SKOV3 ovarian cancer cell viability through MTT assays (Wei *et al.,* 2023). Likewise, NiNPs prepared from *Penicillium chrysogenum* exhibited significant anticancer and antioxidant activities (Hashem *et al.,* 2022). In lung cancer cell lines (A549, NCIH-460), NiNPs triggered apoptosis and protein expression modifications, nickel fine particles shows genotoxicity and carcinogenic activity (Magaye *et al.,* 2016; Pietruska *et al.,* 2011). These results highlight the therapeutic value of NiNPs in cancer studies.

2.1.3. Drug Delivery

NiNPs are becoming multifunctional drug delivery system agents due to their chemical stability, high binding ability, and magnetic responsiveness. They can be used in MRI, biomedical analysis, and targeted gene and drug delivery (Jaji *et al.,* 2020; Ban *et al.,* 2018). Their ability to enable functionalization and targeted transport increases their utility in diagnostics and therapeutics (Adhikary *et al.,* 2015). These properties make NiNPs good candidates for next-generation biomedical delivery platforms. Table II. 1 gives a broad overview of the extensive biological applications of NiNPs prepared from different sources. It points out the universality of NiNPs in various areas of biology, highlighting their prospects in drug delivery, antimicrobial therapy, cancer treatment, and biosensing. The table also indicates the impact of the source material on the properties and activity of the

NiNPs, emphasizing the need to select proper synthesis routes for particular biomedical applications.

Table II. 1: Biological application of NiNPs.

No	Method/Source of synthesis	Biological activity	Form of metal NPs.	Reference
1	*Ocimum sanctum* leaf extract	Antibacterial	NiNPs	(Jeyaraj Pandian *et al.,* 2016)
2	*Euphorbia heterophylla* (L.) leaves extract	Antibacterial	NiONPs	(Lingaraju *et al.,* 2020)
3	*Prosopis fracta* extract	Anticancer	NiO & NiO composite	(Alsamhary *et al.,* 2024)
4	*Azadirachta indica* and *Psidium guajava.*	Anticancer	NiO & NiNPs	(Mariam *et al.,* 2014)
5	*Shewanella* spp	Azo dye degradation and industrial wastewater treatment	(NiO-NPs)	(Mustafa *et al.,* 2023)
6	*Salvia rosmarinus* extract	Antibacterial properties, manufacture of dental amalgam.	(NiO)	(Nazaripour *et al.,* 2022)
7	*Penicillium chrysogenum*	Cytotoxicity & anticancer activity	(NiNPs)	(Hashem *et al.,* 2022)
9	Chemical synthesis	Anticancer activity	Ni composite	(Gorgizadeh *et al.,* 2019)
10	Chemical synthesis	Integrated biomedical applications	Ni composite	(Ivanov *et al.,* 2018)
11	*Azadirachta indica leaves*	Antibacterial activity	NiO	(Helan *et al.,* 2016)
12	Chemical synthesis	Absorbent of safranin-O	NiS	(Ghaedi *et al.,* 2014)
13	Chemical synthesis	Hydrodeoxygenation of microalgae	NiNPs	(Song *et al.,* 2013)
14	Polyol method	Biomedical	NiNPs	(Roselina & Azizan, 2012)
15	Co-precipitation method,	Thermo-therapeutic	$NiFe_2O_4$	(Hoque *et al.,* 2016)
16	Polyol method.	Electrochemical sensor	NiNPs	(Neiva *et al.,* 2014)
17	Homogeneous precipitation method	Bio-remediation by microalgae *Chlorella Vulgaris*	NiO	(Gong *et al.,* 2011)
18	*Ocimum sanctum* leaf extract	Anticancer activity	Quercetin conjugated NiNPs.	(Rameshthangam & Chitra, 2018)

2.2. Biological Use of Copper Oxide Nanoparticles (CuONPs)

Copper oxide nanoparticles (CuONPs) are active nanomaterials used in different fields of science. Their antimicrobial potential to act against a wide range of bacteria, fungi, viruses, and drug-resistant strains attests to their therapeutic use (Azam *et al.,* 2012; Ijaz *et al.,* 2017). CuONPs show preferential cytotoxicity to cancer cells but spare normal cells, indicating their potential for application in targeted anticancer treatments (Seigneuric *et al.,* 2010). They are also drug carriers and show antioxidant and anti-inflammatory activity, which indicates other applications in treating oxidative stress-related diseases (Liu *et al.,* 2010). CuONPs are used as nano-pesticides and fertilizers, which improve crop yield and pathogen protection when used as foliar sprays or soil amendments (Kasana *et al.,* 2016; Seregina *et al.,* 2020). In the environment, CuONPs allow for pollutant removal and are used as nanosensors for contaminant detection (Gautam *et al.,* 2016). In industry, CuONPs are used in catalysis, sensor development, and material synthesis. Their nanoscale sizes enable effective interaction with biomolecules, contributing to applications in drug delivery, bioimaging, and anti-tumor activities (Kim & Nie, 2005; Szymański *et al.,* 2012). Such multifunctional capabilities make CuONPs good candidates for innovation in biomedicine, agriculture, and environmental remediation.

2.2.1. Antibacterial Activity

CuONPs have strong antibacterial activity against a broad spectrum of pathogenic bacteria. Biogenic synthesis employing *Magnolia kobus* and *Punica granatum* extracts led to the preparation of nanoparticles with greater activity compared to traditional antibiotics (Lee *et al.,* 2013; Kaur *et al.,* 2016; T. de B. Machado *et al.,* 2002; Naz *et al.,* 2007). Similar effectiveness was reported with *Millettia pinnata* and *Gum karaya*-derived CuONPs, where efficacy depended on nanoparticle size and bacterial cell wall morphology (Thiruvengadam *et al.,* 2019; Azam *et al.,* 2012; Khani *et al.,* 2018). CuONPs prepared from *Bifurcaria bifurcata, Eichhornia crassipes,* and *Tribulus terrestris* also exhibited tremendous bactericidal activity (Abboud *et al.,* 2014; Vanathi *et al.,* 2016; Gopinath *et al.,* 2016), similarly,

the activity shown by those prepared from *Gloriosa superba* also (Regier *et al.,* 2015). Nevertheless, their aquatic toxicity in the aquatic organism *Daphnia magna* indicates caution in ecological evaluation (Saif *et al.,* 2016). These results further support the antibacterial application of CuONPs in biomedicine and environmental science.

2.2.2. Anticancer Potential

The antitumor activity of CuONPs is primarily attributed to copper's capacity to modulate intracellular redox homeostasis, leading to oxidative stress and subsequent cancer cell apoptosis. Cellular chaperones such as ATOX1 and CCS are responsible for selective protection in normal cells towards higher copper levels (Yang *et al.,* 2017). CuONPs have proven to be effective in treating various cancer forms, such as renal (Xue *et al.,* 2018), lung, brain (Joshi *et al.,* 2016), liver (Siddiqui *et al.,* 2013), breast (Jeronsia *et al.,* 2016), ocular (Song *et al.,* 2015), and prostate cancer tumors (Wang *et al.,* 2017). The above-presented research indicates their potential for further research in targeted cancer treatments.

2.2.3. Drug Delivery Applications

The low price and functional diversity of CuONPs facilitate their use in drug delivery and imaging. Luminescent transferrin-templated copper nanoclusters (Tf-CuNCs) were shown to be effective in tumor targeting and life-span extension in animal models (Goswami *et al.,* 2018). Curcumin-capped CuNPs were shown to possess anti-angiogenic and anticancer activities (Kamble *et al.,* 2016), whereas mupirocin-functionalized CuNPs displayed high rates of release and excellent antibacterial effects, being active against drug-resistant *S. aureus* (Verma & Kaushik, 2020). These findings indicate CuONPs to be promising platforms for next-generation therapeutic delivery systems. Further investigation into their synthesis and functionalization is essential to optimize biomedical performance. Table II. 2 shows the different biomedical applications of CuONPs prepared from different sources.

Table II. 2: Biological application of CuONPs

No	Source/method	Biomedical application	Reference
1	*Syzygium alternifolium*	Antibacterial activity, Antifungal activity.	(Yugandhar *et al.,* 2017)
2	*Phaseolus vulgaris*	Anticancer activity	(Nagajyothi *et al.,* 2017)
3	*Trichoderma asperellum*	Anticancer activity	(Saravanakumar *et al.,* 2019)
4	*Lactobacillus casei subsp. Casei*	Anticancer activity	(Kouhkan *et al.,* 2020)
5	*Anabaena cylindrica.*	Anticancer activity	(Bhattacharya *et al.,* 2019)
6	*Sargassum polycystum.*	Anticancer activity	(Ramaswamy *et al.,* 2016)
7	*Citrus medica* Linn.	Antifungal activity	(Shende *et al.,* 2015)
8	*Penicillium chrysogenum*	Antifungal activity	(El-Batal *et al.,* 2020)
9	*Oxalis corniculata* L	Antifungal activity	(Hassan *et al.,* 2019)
10	*Saccharum officinarum*	Antibacterial activity	(Angeline Mary *et al.,* 2019)
11	*Syzygium aromaticum*	Antibacterial activity	(Rajesh *et al.,* 2018)
12	*solanum lycopersicum*	Antibacterial activity	(Vaidehi *et al.,* 2018)
13	*Proteus mirabilis*	Antibacterial activity	(Eltarahony *et al.,* 2018)
14	*Bifurcaria bifurcata*	Antibacterial activity	(Abboud *et al.,* 2014)
15	*Aloe vera*	Antibacterial activity	(Kumar *et al.,* 2015)

2.3. Biological Applications of Gold Nanoparticles (AuNPs)

Gold nanoparticles (AuNPs) have become major nanomaterials because they possess distinct physicochemical characteristics, high biocompatibility, and surface functionalities. Their optical and electronic characteristics, particularly surface plasmon resonance, allow applications in biosensing, imaging, drug and gene delivery, and theranostics (Cai & Chen, 2007; Mohanpuria *et al.,* 2008; Yu *et al.,* 1997). Their stability, simplicity of synthesis, and similar size to biomolecules facilitate their application as diagnostic probes, targeted delivery vehicles for drugs,

and imaging contrast agents (Wang *et al.,* 2012; Dhar *et al.,* 2009; Doubrovsky *et al.,* 2011; Seigneuric *et al.,* 2010; Sperling *et al.,* 2008). The intersection of AuNPs and nanomedicine has the potential to revolutionize personalized diagnostics and therapy.

2.3.1. Antimicrobial Potential

Biogenic AuNPs have shown broad-spectrum antimicrobial activity. AuNPs prepared from *Abelmoschus esculentus* seeds are antifungal active (Jayaseelan *et al.,* 2013), whereas banana peel-based AuNPs inhibit *Shigella, E. coli,* and *Candida albicans* (Bankar *et al.,* 2010). *Trichoderma spp., Camellia japonica*, and *Camellia sinensis,* and other plant and fungal extracts also provided AuNPs with broad antibacterial action (Das *et al.,* 2009; Bindhu *et al.,* 2014; Dimitrov, 2006; Mishra *et al.,* 2014; Oh *et al.,* 2018; Sharma *et al.,* 2019; Singh *et al.,* 2018), highlighting their uses for the generation of eco-friendly antimicrobial compounds.

2.3.2. Anticancer Potential

AuNPs have been promising in oncology for drug delivery, imaging, and targeted therapy. Methods such as SERS and antibody-functionalized AuNPs allow for specific cancer cell detection (Grubisha *et al.,* 2003; Huang *et al.,* 2007; Kneipp *et al.,* 2002; Neng *et al.,* 2010). AuNPs prepared from *Punica granatum* have been found to be cytotoxic toward cancerous breast cells (Ganeshkumar *et al.,* 2013), whereas magnetic AuNPs have been suggested to be used for the prevention of metastasis (Yadav *et al.,* 2011). Targeted AuNPs are also directed toward cardiovascular diseases and leukemia (Kah *et al.,* 2007; R. Bhattacharya *et al.,* 2007; Zent *et al.,* 2006; Rahman *et al.,* 2005). Plant-based AuNPs synthesis has proven potent anticancer activity: *Glycyrrhiza uralensis* and *Mangifera indica* extracts were cytotoxic against MCF-7 and gastric cancer cells (Huo *et al.,* 2018; Vimalraj *et al.,* 2018), *Crocus sativus* and *Hylocereus sabdariffa* extracts inhibited breast and glioblastoma cells respectively (Hoshyar *et al.,* 2016; Mishra *et al.,* 2016), and AuNPs from *Cystoseira baccata* exhibited potential against colon cancer (González-Ballesteros *et al.,* 2017). These results validate the potential of AuNPs in targeted, green therapeutics for cancer treatment.

2.3.3. Applications in Drug Delivery

AuNPs are extensively researched for applications in drug delivery because of their surface, stability, and ability to deliver various therapeutic agents. AuNPs triggered release of drugs can be prompted by pH or light (Paciotti *et al.,* 2004; Bao *et al.,* 2013; Cheng *et al.,* 2014; Madhusudhan *et al.,* 2014).

Table II. 3: Biological application of AuNPs

No	Source of AuNPs	Biological property	Reference
1	*Croton Caudatus* (Euphorbiaceae)	Anticancer, antimicrobial, antifungal agent.	(Vijaya Kumar *et al.,* 2019)
2	*Syzygium jambos (Myrtaceae)*	Anticancer, Antimalarial	(Dutta *et al.,* 2017)
3	*Anacardium occidentale* (Anacardiaceae)	Antibacterial agent	(Sunderam *et al.,* 2019)
4	*Andrographis paniculata* (Acanthaceae)	Anticancer	(Kumari *et al.,* 2019)
5	*Clonorchis sinensis* (Theaceae)	antimicrobial,	(Onitsuka *et al.,* 2019)
6	*Pistacia atlantica* (Anacardiaceae)	Antibacterial agent. Antioxidant	(Hamelian *et al.,* 2018)
7	*Fusarium oxysporum* (Nectriaceae)	Antibacterial agent	(Naimi-Shamel *et al.,* 2019)
8	*Cornus mas* (Cornaceae)	Antioxidant, anticancer agent	(Filip *et al.,* 2019)
9	*Hylocereus undatus* (Cactaceae)	Anticancer agent	(Divakaran *et al.,* 2019)
10	*Garcinia indica (*Clusiaceae)	Antioxidant,	(Desai *et al.,* 2018)
11	*Punica granatum* (Lythraceae)	Antioxidant,	(Gubitosa *et al.,* 2018)
12	*Terminalia chebula* (Combretaceae)	Antimicrobial agent	(Mohan Kumar *et al.,* 2012)
13	*Camellia sinensis* (Rosaceae)	Antioxidant, Antimicrobial, Anticancer	(Oh *et al.,* 2018)
14	*Cibotium barometz (Dicksoniaceae)*	Antioxidant, Antimicrobial, Anticancer	(Wang *et al.,* 2017)
15	*Aquilegia pubescens* (Apiaceae)	Anticancer	(Markus *et al.,* 2017)
16	*Plectranthus barbatus* (Lamiaceae)	Anticancer	(Dhayalan *et al.,* 2018)
17	*Benincasa hispida* (Cucurbitaceae)	Anti-helminthic, Antioxidant.	(Aromal & Philip, 2012)

Functionalization approaches enable targeting of tumor and phagocytic cells (Hu *et al.,* 2019). Chitosan-coated AuNPs have been investigated for insulin delivery (Bhumkar *et al.,* 2007), whereas albumin and ApoE-conjugated AuNPs enhance targeting specificity (Schäffler *et al.,* 2014). New applications also include vaccine platforms, e.g., for tick-borne encephalitis (Demenev *et al.,* 1996). These advances make AuNPs a promising and versatile nanoplatform in sophisticated drug delivery. Table II. 3 emphasizes the wide range of biological applications of AuNPs prepared using different sources.

2.4. Biological application of Zinc Oxide Nanoparticles (ZnONPs)

The unique optical, electrical, and physicochemical properties of ZnONPs, along with their highly advantageous surface chemistry, make them universal probes for an abundance of applications in biomedical science. Among the most notable attributes of ZnONPs is their ability to fight microbial attacks based on their intrinsic antibacterial activity. By production of reactive oxygen species (ROS) and photocatalytic activity, ZnONPs have strong antimicrobial activity, as discussed by Sirelkhatim and coworkers (Sirelkhatim *et al.,* 2015). The antimicrobial activity has practical uses in various industries, such as dental composite, mouthwash, diapers, and shampoos, as proven by (Aydin Sevinç & Hanley, 2010; Hernández-Sierra *et al.,* 2008). Aside from antimicrobial control, ZnONPs provide promising prospects in the treatment of cancer. Work by Hanley and Ancona emphasizes their selective toxicity against cancer cells, indicating their suitability as potent anticancer agents. In addition, Ancona and co-workers., lipid-coated ZnONPs represent an interesting method of photodynamic cancer therapy, highlighting their utility in targeted treatment protocols (Ancona *et al.,* 2018; Hanley *et al.,* 2008).

ZnONPs are gaining recognition due to their wide range of biomedical applications, owing to their beneficial surface chemistry, positive charge under physiological conditions, and high biocompatibility. All these characteristics allow them to interact with biological systems, making them better candidates for drug delivery (Wu *et al.,* 2008; Xu *et al.,* 2013). Coating techniques, including chitosan-modified ZnONPs, have also been found promising in targeted anticancer therapies

(Yuan *et al.,* 2010), while other nanocarrier designs have promoted their application in controlled drug release (Muhammad *et al.,* 2011). ZnONPs are also found to have good sensing capabilities, thereby proving to be good biosensors for analytes like glucose, dopamine, xanthine, urea, and acetylcholinesterase (Devi *et al.,* 2012; Fang *et al.,* 2014; Hwa & Subramani, 2014; Wang *et al.,* 2014). Their biomedical property encompasses wound healing, reduction of inflammation, neuroregeneration, and dermatological applications, such as sunscreens and dental materials. Interestingly, Seil & Webster (2008), illustrated their ability to stimulate neuronal activity and inhibit astrocyte adhesion, pertinent to nerve regeneration (Seil & Webster, 2008). Additionally, ZnONPs have been investigated for analgesia and antidepressant activity through the opioidergic pathway, with improved results compared with bulk formulations (Torabi *et al.,* 2013; Kesmati & Torabi, 2014).

2.4.1. Antimicrobial Activity of ZnONPs

ZnONPs have broad-spectrum antimicrobial activity and are capable of targeting both Gram-positive and Gram-negative bacteria, including drug-resistant strains. Their antimicrobial activity is size-dependent, with smaller particles having greater activity (Ohira & Yamamoto, 2012; Limbach *et al.,* 2007). Their action has been proven against a range of pathogens like *E. coli, S. aureus, P. aeruginosa, B. subtilis, Proteus vulgaris,* and *E. faecalis* (Chatterjee *et al.,* 2010; Dutta *et al.,* 2013; Ishwarya *et al.,* 2018; Premanathan *et al.,* 2011; Reddy *et al.,* 2007).

Their combined potential with antibiotics was proven against *A. baumannii* (Ghasemi & Jalal, 2016), and their bactericidal activity against *Vibrio cholerae* confirms their use in waterborne disease management (Sarwar *et al.,* 2016). Additionally, ZnO/Ag hybrid nanoparticles have exhibited strong efficacy against *Mycobacterium tuberculosis* without host cytotoxicity (Jafari *et al.,* 2016), highlighting their utility in the fight against drug-resistant pathogens.

2.4.2. Anticancer Potential of ZnONPs

ZnONPs have been found to be effective anticancer agents because of their selective cytotoxicity, biocompatibility, and capacity to trigger oxidative stress in

cancer cells. ZnONPs target cancer cells preferentially by ROS generation and caspase activation, without affecting normal cells (Martínez-Carmona *et al.,* 2018 ; Premanathan *et al.,* 2011; Chandrasekaran & Pandurangan, 2016). Lipid-coated ZnONPs applied in photodynamic therapy have demonstrated improved ROS generation and cellular uptake under UV light exposure, enhancing therapeutic efficacy (Ancona *et al.,* 2018). Anticancer activity of ZnONPs covers different cancers, such as gliomas, hepatic, and breast carcinomas (Han *et al.,* 2015; Sharma *et al.,* 2012; Wahab *et al.,* 2013). Green-synthesized ZnONPs also prevent cell cycle progression and control apoptotic genes in breast cancer cells (Boroumand Moghaddam *et al.,* 2017). Besides, ZnONPs are able to induce non-autophagic cell death in EGFR-mutated lung adenocarcinoma (Bai *et al.,* 2017), and induce apoptosis and autophagy in ovarian and leukemia cells (Namvar *et al.,* 2016).

2.4.3. ZnONPs in Drug Delivery

ZnONPs are potent drug delivery carriers for chemotherapeutic and genetic loads. Chitosan-coated ZnONPs were used effectively to deliver doxorubicin to cancer cells, promoting therapeutic specificity (Yuan *et al.,* 2010). They have also been shown to bypass P-glycoprotein efflux pumps to combat multidrug resistance (Liu *et al.,* 2016). Moreover, ZnO quantum dots with surface functionalization of polycations facilitated effective DNA delivery into COS-7 cells, in conjunction with real-time imaging (Zhang & Liu, 2010). This evidence shows that ZnONPs possess multifunctional efficiancy in therapeutic drug delivery systems.

Literature under review highlights the extensive applicability and biological significance of metal nanoparticles (NiNPs, CuONPs, AuNPs, ZnONPs), inspired by their distinctive physicochemical properties. Nanomaterials show great promise in a wide range of applications, ranging from catalysis to energy systems, antimicrobial treatment, oncology, and drug delivery. Biosynthesized nanoparticles are particularly shown to have improved bioactivity over chemically synthesized equivalents, which underlines the importance of green synthesis pathways using microbial and plant-based extracts. Even though they hold promise, critical challenges exist. Protocol variability for synthesis, non-uniform nanoparticle

characterization, and a lack of standardized toxicity testing hamper reproducibility and scalability. Additionally, long-term stability, biodegradability, and ecological consequences are underdeveloped and need to be investigated further prior to clinical or industrial translation. Closing these gaps with interdisciplinary research will be critical to maximizing synthesis parameters, enhancing nanoparticle effectiveness, and making them safe and sustainable.

Table II. 4: Biological application of ZnONPs

No	Source	Activity	Reference
1	*Cassia fistula*	Antibacterial activity	(Suresh *et al.,* 2015)
2	*Phyllanthus niruri*	Antibacterial activity	(Anbuvannan *et al.,* 2015)
3	*Solanum nigrum*	Antibacterial activity	(Ramesh *et al.,* 2015)
4	*Staphylococcus aureus*	Antibacterial activity	(Ahmar Rauf *et al.,* 2017)
5	*Aeromonas hydrophila*	Antibacterial activity	(Sadhasivam *et al.,* 2021)
6	*Sargassum muticum*	Anticancer activity	(Namvar *et al.,* 2016)
7	*Eclipta prostrata*	Anticancer activity	(Chung *et al.,* 2015)
8	*Ziziphus nummularia*	Anticancer activity	(Padalia & Chanda, 2017)
9	*Rhodococcus pyridinivorans*	Anticancer activity	(Kundu *et al.,* 2014)
10	*Hyssops officinalis*	Anti-inflammatory	(Rahimi Kalateh Shah Mohammad *et al.,* 2021)
11	*Polygala tenuifolia*	Anti-inflammatory	(Nagajyothi *et al.,* 2015)

In general, the current findings of this review of literature highlight that there is more to be investigated in terms of bio-inspired synthesis of nanoparticles, especially from insect-derived metabolites. The convergence of biological variability with nanotechnology may contribute to improving nanoparticle performance while fostering sustainability. Future research must aim to fine-tune biosynthetic routes, perform detailed toxicity assessments, and discover unique

applications to fully exploit the promise of metal nanoparticles in health, agriculture, and environmental sustainability. The present research extends this platform by using the defensive secretion of *L. tristis* as a new and renewable source for NPs biosynthesis. The chemically rich metabolites of this secretion serve as natural reducing and stabilizing agents to enable the synthesis of LNiNPs, LCuONPs, LZnONPs, and LAuNPs. These NPs exhibit promising biological activities such as antioxidant, antimicrobial, and anticancer activity, further validating the prospect of insect-derived metabolites in green nanotechnology. By combining biological diversity with nanotechnology, the present work shows a novel green strategy for the synthesis of NPs, opening avenues for eco-friendly biomedical, agricultural, and environmental applications. For the full exploitation of metal nanoparticles' potential for innovative and sustainable applications, future studies must aim at optimizing biosynthetic routes, performing thorough toxicological evaluations, and discovering new applications.

CHAPTER III

MATERIALS AND METHODS

The metal NPs employed in this research were synthesized from the defense secretion of the insect *Luprops tristis*. Insects were manually gathered and moved in perforated bottles to provide them maximum safety and comfort. Some of the insects were dissected by forceps and needles at the time of collection for morphological gland research, while the rest of the insects were gently disturbed to release gland secretions without dissecting or damaging them. Secretions were stored in microtubes (300 µL) for NPs preparation. These secretions were then blended with different metal solutions and exposed to microwave radiation, leading to the formation of respective nanoparticles (NPs). Obtained NPs were separated by centrifugation, and moisture was removed, followed by lyophilization to maintain stability, thereby making them amenable to subsequent biological assays. This section gives a step-by-step account of the research methodology, including each step taken and materials used in the experimental process.

3.1. Experimental insect- *Luprops tristis* Fabricius

The beetle, *L. tristis* (Family: Tenebrionidae, Order: Coleoptera), is a darkling beetle and an unobtrusive detritivore inhabiting leaf litter of rubber plantation regions on the western slopes of the southern Western Ghats. The species follows a univoltine life cycle consisting of five stages, and its abundance is correlated with the availability of early-falling rubber tree leaves as a food source. Distributed throughout India, it feeds on plant debris. Adult beetles measure approximately 8 mm in length and are black. Typically, they pose no threat to humans, though they release a defensive phenolic fluid that can cause skin irritation when provoked. This defensive secretion contains phenol, flavonoids, alkaloids, and other bioactive chemicals with significant potential as reducing and capping agents. These beetles are notorious for complicating living conditions when large groups enter farmhouses, roofs of houses are shown in Fig. III. 2.

Systematic position	
Kingdom	**Animalia**
Phylum	**Arthropoda**
Class	**Insecta**
Order	**Coleoptera**
Family	**Tenebrionidae**
Genus	***Luprops***
Species	***tristis***
Binomial name	***Luprops tristis* Fabricius, 1801**

3.2. Collection of beetle *Luprops tristis.*

The experimental insect, *Luprops tristis,* was gathered from Sree Neelakanta Govt. Sanskrit college campus, Pattambi (10.809526,76.199281), Kerala, India (Fig III. 1). The insects were hand-picked and stored in a perforated insect box following collection and then transported to the laboratory for the extraction of the defensive gland (Fig III. 2).

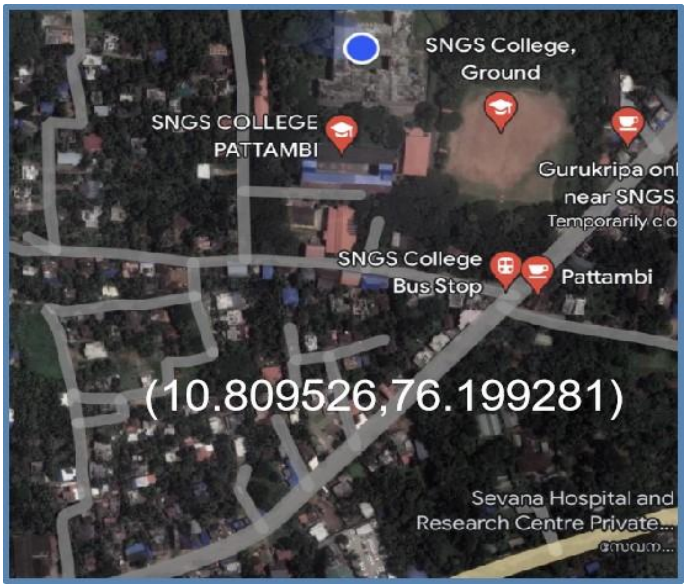

Fig III. 1: GPS Coordinates of the location

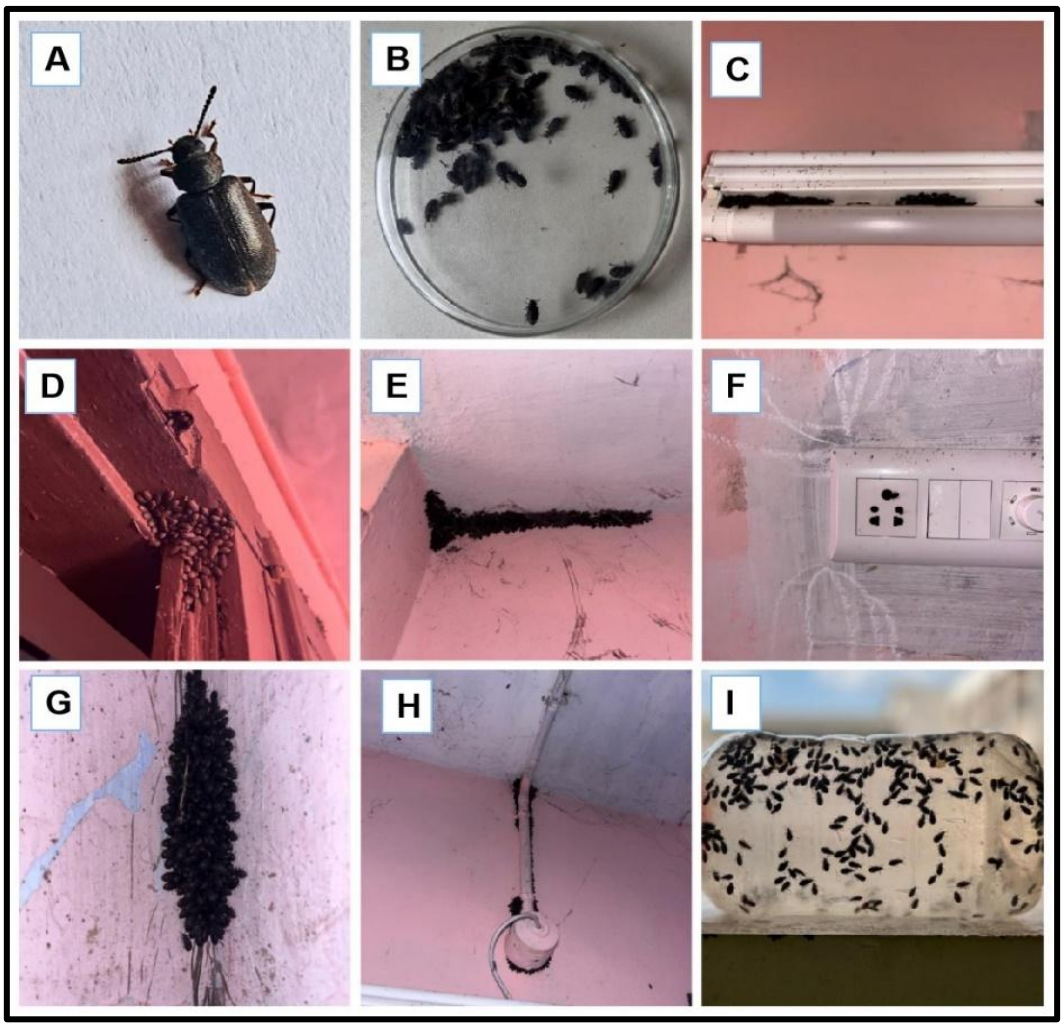

Fig III. 2: Colony of *L. tristis* in different areas (A-H), collected beetles in perforated bottle (I).

3.3. Study the morphology of the defensive gland

The methodology for investigating the morphology of the defensive gland entailed delicately dissecting it using forceps, scissors, and a needle under a dissection microscope (MESWOX DM100, India). The dissected gland was then rinsed in an insect Ringer solution and transferred to a glass slide for further examination. Subsequently, the gland underwent scrutiny using a compound microscope (Leica ICC50E, Germany) equipped with a camera, a fluorescent microscope (ZEISS Axiocam 305 colour, Germany), and a scanning electron microscope (VEGA 3 TESCAN, Czech Republic). The evaluation primarily concentrated on analyzing the surface structures of the gland.

3.4. Tissue sampling for histological study and slide preparation

The defensive gland was carefully dissected in insect Ringer solution and fixed by immersion in Bovin's solution. Each sample was placed in an individual microtube. After a 24-hour fixation period, the gland secretion underwent gradual dehydration using ascending grades of alcohol. The glands were gross-stained in a 70% aqueous eosin solution to aid in orientation during embedding. The tissues were fully dehydrated in acetone and absolute alcohol, cleared with xylene, and embedded in paraffin wax. Sections were cut to a thickness of 6 µm, deparaffinized with progressively concentrated alcohol, stained with hematoxylin, and counterstained with aqueous eosin for microscopic examination. Microphotographs were subsequently captured for documentation (Hewitson *et al.,* 2010; Silva-Zacarin *et al.,* 2012).

3.5. Extraction of defensive gland secretion from *L. tristis*

Defensive glands of the insects extruded out by gentle pressing on the abdomen; the glandular secretion collected to microtube (300 µL capacity) containing deionized water by pressing on the extruded glands without any contamination from fecal matter (Fig III. 3). These glands extract centrifuged and used for the synthesis of metal NPs like nickel (NiNPs), copper oxide (CuONPs), zinc oxide (ZnONPs) and gold (AuNPs).

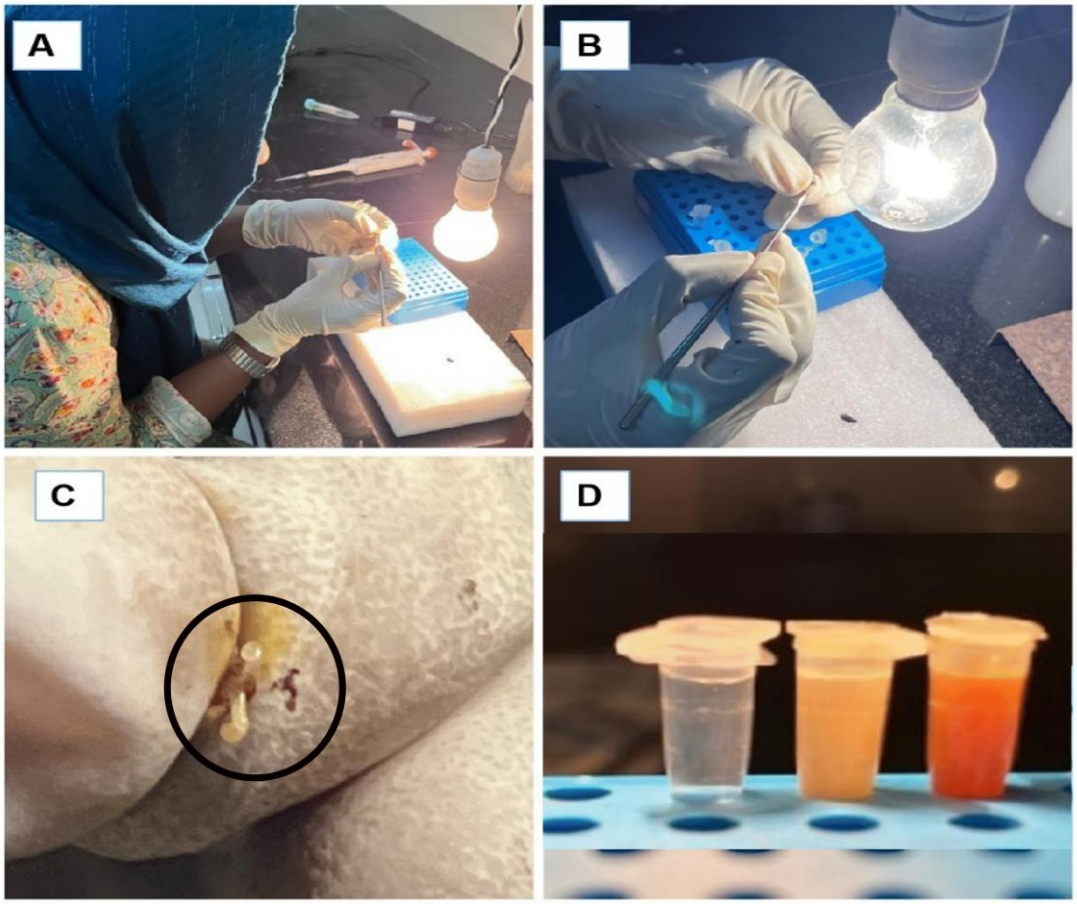

Fig III. 3: Extracting secretion from defensive gland (A-B), Extruded defensive gland (C), Collected secretion stored in eppendorffs tubes (D).

3.6. High-Resolution Liquid Chromatography–Mass Spectrometry (HR-LCMS)

The chemical composition of the beetle's defensive gland secretions was characterized by high-resolution LC-MS-QTOF (Agilent Technologies, USA), which involves the combination of chromatographic separation with exact mass detection to identify compounds in complicated matrices. Methanolic extracts of the secretion were analyzed on an Agilent ZORBAX Eclipse Plus C18 column (150 × 2.1 mm, 5 µm) with a binary solvent system: Solvent A (0.1% formic acid in Milli-Q water) and Solvent B (acetonitrile) under the optimum gradient elution conditions.

Instrument settings were carefully optimized to achieve maximum resolution and sensitivity. Reference standard calibration was used to determine the accurate mass and retention time. Data acquisition was done on Agilent MassHunter software (Qualitative Analysis Version B.06). This method allowed for in-depth profiling and initial identification of bioactive components present in the secretion extract.

3.7. Fabrication of Metal NPs

NiNPs, CuONPs, ZnONPs, and AuNPs were prepared by employing solutions of nickel chloride ($Nicl_2.6H_2O$), copper sulphate ($CuSO_4.6H_2O$), zinc acetate Zn $(CH3CO_2)_2$, and auric chloride ($AuCl_3.H_2O$), respectively, from NICE Chemicals Pvt. Ltd. The preparation of *L. tristis*- mediated metal NPs involved mixing gland extract from 30 beetles with 300 µL of distilled water. A corresponding 0.01 molar (M) metal solution was prepared in deionized water. The reaction mixture was then synthesised by combining 300 µL of the defensive gland extract (equivalent to 30 gland pairs) with 600 µg/mL of the metal solution (0.01 M). The solution was heated in a microwave (LG MS2042DB, South Korea) for 15 minutes at a power level of 350 W, and the change in colour of the solution was noted. Subsequently, the solution was centrifuged and lyophilized for further chemical characterization and applications.

3.8. Characterization of NPs.

3.8.1. Structural characterization

The reduction of metal-to-metal NPs (Ni, CuO, ZnO, Au) by defensive gland secretion of *L. tristis* was characterized by UV-Vis spectroscopy (PerkinElmer UV WinLab, US), compounds bind with the biosynthesized metal NPs for the stabilization were identified by Fourier transform infrared spectroscopy (FTIR) (PerkinElmer IR, USA). The morphology and size details of synthesized NPs were determined using electron microscopy techniques (Scanning electron microscopy-SEM & transmission electron microscopy- TEM) (JEOL JEM-2100, JAPAN). Stability is an important factor in the case of NPs, which was measured by zeta potential analysis (HORIBA SCIENTIFIC SZ 100, FRANCE).

3.8.1.1.UV-Vis spectroscopy

UV-Vis spectroscopy was used to confirm the synthesis of NPs. The optical absorbance of the nanoparticle solutions was recorded using a PerkinElmer UV/Vis spectrometer (Waltham, MA, USA), identifying the characteristic surface plasmon resonance peak indicative of NPs formation. 4 mL of the diluted NPs solution was made to produce the sample after adjusting the wavelength to 300 to 700 nm. The diluted NPs solution was put in an appropriate cuvette and placed into the UV-Vis spectrophotometer as part of the measuring process.

3.8.1.2. Fourier transform infrared spectroscopy (FTIR)

FTIR spectroscopy was used to analyze functional group interactions in the biosynthesized NPs. Comparative FTIR analyses were performed on the defensive secretion and the synthesized NPs. Samples were dried, ground with KBr pellets, and analyzed using a PerkinElmer FTIR spectrometer (Waltham, MA, USA), with spectra recorded as transmittance percentage against wave number in cm^{-1}.

3.8.1.3. Transmission Electron Microscopy (TEM)

The structural and morphological characteristics of NPs synthesized from the secretion were analyzed using a JEOL JEM 2100 High-Resolution Transmission Electron Microscope (Tokyo, Japan). The HRTEM, equipped with a LaB6 electron source, operated at 200 kV and 80 kV, providing a lattice resolution of 0.14 nm and point-to-point resolution of 0.19 nm. Images were captured using a Gatan Orius SC200 CCD camera (2K × 2K resolution, Pleasanton, CA, USA) across various scales (1 μm to 2 nm) to obtain comprehensive structural details. This method enabled high-resolution imaging and detailed analysis of the NPs' morphology.

3.8.1.4. Scanning Electron Microscopy (SEM)

Surface characterization of the NPs was carried out on a JEOL JEM-2100 SEM at 15 kV in high vacuum. The samples were dispersed in ethanol, sonicated for

30 min, and drop-cast on silicon wafers. Following air drying for 24 h, a gold coating was done through sputtering to increase conductivity. SEM imaging gave precise information regarding NPs' morphology.

3.8.1.5. ZETA Potential measurement

The surface charge and stability of the synthesized NPs were evaluated using zeta potential measurements using the HORIBA SZ-100 nanoparticle analyzer (Kyoto, Japan). This analysis provided insights into the surface charge distribution and colloidal stability of the nanoparticles.

3.8.2. Electrochemical studies

An Electrochemical workstation (Instrument Model DY2113 developed by Digi-Ivy) was used to conduct DPV measurements (Fig. III. 4). Using a three-electrode cell setup with a platinum foil counter electrode, an Ag/AgCl reference electrode, and a working electrode coated with LNiNPs in 10 mL of phosphate buffer saline. The potential was applied from +1.000 to -1.000 at the initial and final stages. Measurements of glucose concentration ranging from 10 mM to 70 mM were plotted, and calibration linear relationships between DPV current output and glucose concentration were plotted. Using the equation LOD = (3∗SD)/Slope of the curve, it was possible to determine the limit of detection of the NPs sensor (Abrori *et al.,* 2020).

3.8.2.1. Glucose sensing by DPV study for LNiNPs.

Glucose solutions (10 mM, 20 mM, 30 mM, 40 mM, 50 mM, 60 mM and 70 mM) were added sequentially into the cell setup, the working electrode coated with LNiNPs was used, and DPV was used to measure current responses. Glucose concentration with peak current used for calibration curve as given in section 3.8.2.

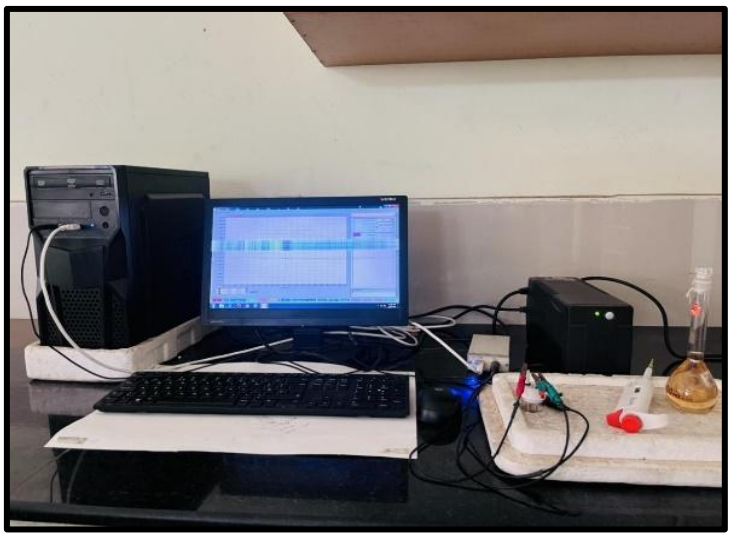

Figure III. 4: Electrochemical sensing- experimental setup.

3.8.2.2. Hydrogen peroxide sensing by DPV study for LCuONPs

Hydrogen peroxide solutions (10 mM, 20 mM, 30 mM, 40 mM, 50 mM, and 60 mM) were added sequentially into the cell setup, the working electrode coated with LCuONPs was used, and DPV was used to measure current responses. Glucose concentration with peak current used for calibration curve as given in section 3.8.2.

3.8.2.3. Glucose sensing by DPV study for LAuNPs

Glucose solutions (10 mM, 20 mM, 30 mM, 40 mM, 50 mM, and 60 mM) were added sequentially into the cell setup, the working electrode coated with LAuNPs was used, and DPV was used to measure current responses. Glucose concentration with peak current used for calibration curve as given in section 3.8.2.

3.8.2.4. Glucose sensing by DPV study for LZnONPs

Glucose solutions (10 mM, 20 mM, 30 mM, 40 mM, 50 mM, 60 mM, and 70 mM) were added sequentially into the cell setup, the working electrode coated with LZnONPs was used, and DPV was used to measure current responses. Glucose concentration with peak current used for calibration curve as given in section 3.8.2.

.

3.8.3. Biological Applications

3.8.3.1. Antibacterial analysis of defensive gland secretion

Dose-dependent antibacterial action of defensive gland extract was checked by disc diffusion assay against the Gram-negative (*Escherichia coli*) and Gram-positive bacteria (*Staphylococcus aureus*) by the standard Kirby-Bauer technique (Bauer *et al.,* 1966). Muller Hinton agar powder (4 gm) in distilled water (100 ml) was added to autoclaved Petri plates. Pure microbial cultures were sub-cultured on nutrient agar and evenly swabbed on separate plates. For the antibacterial assay, there were clear sample concentrations employed (5 µg/mL and 10 µg/mL). Filter paper discs (5 mm) were loaded with secretions, dried, and placed on the culture plate. Tetracycline, an antibiotic, acted as the positive control. The Petri dish was incubated for 16 h at 37 °C. The zone of inhibition was analysed to estimate the antibacterial effect (Buszewski *et al.,* 2018; Chand *et al.,* 2019; Horváth *et al.,* 2016; Kourmouli *et al.,* 2018).

3.8.3.1.1. Antibacterial Activity of LNiNPs

The antibacterial activity of LNiNPs (5 µg/mL, 10 µg/mL, 15 µg/mL, and 20 µg/mL) was tested through agar disc diffusion against *S. aureus* (ATCC 700603) and *K. pneumoniae* (ATCC 33591) according to Section 3.8.3.1

3.8.3.1.2. Antibacterial Activity of LCuONPs

The antibacterial activity of LCuONPs (5 µg/mL, 10 µg/mL, 15 µg/mL, and 20 µg/mL) was tested through agar disc diffusion against *S. aureus* (ATCC 700603) and *K. pneumoniae* (ATCC 33591) according to Section 3.8.3.1

3.8.3.1.3. Antibacterial Property of LAuNPs

The antibacterial activity of LAuNPs (5 µg/mL, 10 µg/mL, 15 µg/mL, and 20 µg/mL) was tested through agar disc diffusion against *S. aureus* (ATCC 700603) and *K. pneumoniae* (ATCC 33591) according to Section 3.8.3.1

3.8.3.1.4. Antibacterial Activity of LZnONPs

The antibacterial activity of LZnONPs (5 µg/mL, 10 µg/mL, 15 µg/mL, and 20 µg/mL) was tested through agar disc diffusion against *S. aureus* (ATCC 700603) and *K. pneumoniae* (ATCC 33591) according to Section 3.8.3.1

3.8.3.2. Antioxidant analysis

Anti-oxidant activity of the defensive gland secretion and NPs synthesized was analysed by standard DPPH assay (Blois, 1958; Becker *et al.,* 2004; Thangaraj, 2016).

3.8.3.2.1. DPPH (2,2-diphenyl-1-picrylhydrazyl) Assay for Defensive secretion:

The DPPH assay, generally regarded as a standard, has been employed to study the ability to scavenge free radicals. DPPH solution (2 mL) was mixed with 5 different concentrations of samples (20 µg/mL, 40 µg/mL, 60 µg/mL, 80 µg/mL, and 100 µg/mL). Ascorbic acid dissolved in distilled water was used as the reference solution. The resulting solution was analysed by UV spectroscopy (PerkinElmer UV-WinLab) after being kept in the dark for 30 min. The Colour change from deep violet to pale yellow is observed; it was recorded at 517 nm. When the concentration of NPs increases, the colour of the DPPH vanishes from deep violet to pale yellow, by scavenging activity noted by UV spectroscopic analysis and calculated by the equation as;

S% = [(Absorbance of control – Absorbance of sample) / Absorbance of control] x 100

The concentration of the sample is essential to produce 50 % scavenging activity (IC_{50} value) obtained from the graph through a linear regression equation (Gulcin & Alwasel, 2023; Kedare & Singh, 2011; Rubab *et al.,* 2022).

3.8.3.2.2. DPPH (2,2-diphenyl-1-picrylhydrazyl) Assay for LNiNPs:

The antioxidant activity of LNiNPs was assessed following the methodology outlined in Section 3.8.3.2.1, with sample concentrations of 20 µg/mL, 40 µg/mL, 60 µg/mL, 80 µg/mL, and 100 µg/mL.

3.8.3.2.3. DPPH (2,2-diphenyl-1-picrylhydrazyl) Assay for LCuONPs:

The antioxidant activity of LCuONPs was conducted by the protocol specified in Section 3.8.3.2.1, with sample concentrations of 20 µg/mL, 40 µg/mL, 60 µg/mL, 80 µg/mL, and 100 µg/mL.

3.8.3.2.4. DPPH (2,2-diphenyl-1-picrylhydrazyl) Assay for LAuNPs:

The antioxidant capacity of LAuNPs was tested according to the procedure outlined in Section 3.8.3.2.1, at sample concentrations of 20 µg/mL, 40 µg/mL, 60 µg/mL, 80 µg/mL, and 100 µg/mL.

3.8.3.2.5. DPPH (2,2-diphenyl-1-picrylhydrazyl) Assay for LZnONPs:

ZnONPs were tested according to the parameters outlined in Section 3.8.3.2.1, at sample concentrations of 20 µg/mL, 40 µg/mL, 60 µg/mL, 80 µg/mL, and 100 µg/mL.

3.8.3.3. Environmental toxicity testing using *Allium* assay

3.8.3.3.1. Environmental toxicity testing assay for gland secretion

Allium test, a classical technique for analyzing the effect of chemicals on plant chromosomes. For analyzing their possible environmental dangers after being released into the environment, their effect on plants was tested by the Allium test (Fiskesjö, 1985). Environmental toxicity was determined by analyzing the rate of chromosomal aberrations. For this experiment, a tip of the root (3-5) from *Allium cepa L.* (2n = 16) was used to examine how biosynthesized NPs influence mitosis. Hydrogen peroxide was used as the positive control, and distilled water was used as the negative control. From a population of common onion bulbs, equal-sized bulbs were selected, and experimental bulbs were incubated in sample solutions at different concentrations (100 µg/mL, 200 µg/mL, 300 µg/mL, 400 µg/mL, and 500 µg/mL), while control bulbs were incubated in distilled water. When the roots reached a length of 2-3 cm, the chromosomal impact studies were carried out by the squash technique. A thin onion cell film after cutting the roots from the disc of the root primordial. The root nodules were stained with acetocarmine and methylene

blue, and 1500 cells from the three best preparations were utilized for analysis. Results were interpreted and represented as (mean ± standard deviation) under a compound microscope (LEICA ICC50E, Germany), and the cells were analyzed to detect chromosomal alterations and compared to the control group (Bonciu *et al.,* 2018; Fiskesjö, 1985; Sabeen *et al.,* 2020).

3.8.3.3.2. Environmental toxicity Testing for LNiNPs

As per the procedure outlined in Section 3.8.3.3.1, various concentrations of LNiNPs (100 µg/mL, 200 µg/mL, 300 µg/mL, 400 µg/mL, and 500 µg/mL) were used for the environmental toxicity analysis.

3.8.3.3.3. Environmental Hazard Testing for LCuONPs

According to the procedure outlined in Section 3.8.3.3.1, various concentrations of LCuONPs (100 µg/mL, 200 µg/mL, 300 µg/mL, 400 µg/mL, and 500 µg/mL) were used for the environmental toxicity analysis.

3.8.3.3.4. Environmental Hazard Test for LAuNPs

As per the procedure outlined in Section 3.8.3.3.1, various concentrations of AuNPs (100 µg/mL, 200 µg/mL, 300 µg/mL, 400 µg/mL, and 500 µg/mL) were used for the environmental toxicity analysis.

3.8.3.3.5. Environmental Hazard Testing for LZnONPs

Environmental toxicity of various concentrations of LZnONPs (100 µg/mL, 200 µg/mL, 300 µg/mL, 400 µg/mL, and 500 µg/mL) was done as per the procedure outlined in Section 3.8.3.3.1

3.8.3.4. Anticancer assay for Defensive gland secretion

3.8.3.4.1. Anticancer assay for Defensive gland secretion by Trypan blue assay (Strober, 1997).

The gland extract of the beetle was studied for short-term *in vitro* cytotoxicity using DLA cells. The tumour cells aspirated from the peritoneal cavity

of tumour-bearing mice were washed thrice with phosphate-buffered saline (PBS) or normal saline. Cell viability was determined using the trypan blue exclusion method. Viable cell suspension (1×10^6 cells in 0.1 mL) was added to tubes containing various concentrations of the gland extract (2.5 µg/mL, 5 µg/mL, 10 µg/mL, 15 µg/mL, 20 µg/mL, and 25 µg/mL), and the volume was made up to 1 mL using PBS. The control tube contained only the cell suspension. The assay mixture was incubated for 3 h at 37 °C. After the incubation, the cell suspension was mixed with 0.1 mL of 1% trypan blue, kept for 2–3 min, and then loaded on a haemocytometer. Dead cells take up the blue colour of trypan blue, while live cells do not take up the dye. The number of stained and unstained cells was counted individually, and the following formula was used to estimate the percentage of cytotoxicity.

Percentage of cytotoxicity = number of dead cells/numbers of live cells + number of dead cells × 100 (Lebeau *et al.,* 2019; Strober, 2015).

3.8.3.4.2. Anticancer assay for LNiNPs

Anticancer effect of LNiNPs was studied according to the methodology described in Section 3.8.3.4.1, using concentrations ranging from 2.5 µg/mL, 5 µg/mL, 10 µg/mL, 15 µg/mL, 20 µg/mL, and 25 µg/mL.

3.8.3.4.3. Anticancer Assay for LCuONPs

The effect of LCuONPs on DLA cells was studied according to the methodology described in Section 3.8.3.4.1, using concentrations ranging from 10 µg/mL, 20 µg/mL, 50 µg/mL, 100 µg/mL, and 200 µg/mL.

3.8.3.4.4. Anticancer Assay of LAuNPs

Anticancer effect of LAuNPs was studied according to the methodology described in Section 3.8.3.4.1, using concentrations ranging from 10 µg/mL, 20 µg/mL, 50 µg/mL, 100 µg/mL, and 200 µg/mL.

3.8.3.4.5. Anticancer Assay of LZnONPs

Anticancer effect of LZnONPs was studied according to the methodology described in Section 3.8.3.4.1, using concentrations ranging from 10 µg/mL, 20 µg/mL, 50 µg/mL, 100 µg/mL, and 200 µg/mL.

3.8.3.5. Anti-angiogenesis by CAM assay (Lokman *et al.*, 2012)

To examine the antiangiogenic property of the nanoparticles, the *in vivo* chorioallantoic membrane CAM assay was used (Lokman *et al.,* 2012).

3.8.3.5.1. Methodology for LNiNPs-mediated Anti-angiogenesis Assay Using 48-hour Chick Embryos:

Freshly fertilized Leghorn chicken eggs were procured from Kerala Veterinary and Animal Husbandry Center, Thrissur, and cleaned thoroughly with 70% ethanol to remove impurities. Then, they were incubated at 37.5°C in a humidified incubator with 60% humidity for 48 hours to allow the initial growth of the chick embryos. After incubation, eggs were gently placed in a sterile setting, and the eggshell was gently cracked at the blunt end using sterile forceps to expose the embryo with minimal disturbance. The chick embryos were immersed in sterile phosphate-buffered saline (PBS) for cleaning. 5-mm-diameter filter paper discs were prepared by punching out circles from standard laboratory filter paper and were impregnated with 2 µg/mL of LNiNPs in a sterile environment, with the control being discs that were soaked in PBS. These discs were placed on top of the exposed embryos close to the forming blood vessels without harming the tissues and the eggs were sealed with sterile parafilm to avoid dehydration and then placed back in the incubator with the same conditions. The embryos were observed and imaged every two hours after treatment for a maximum of eight hours using a Leica microscope (LEICA ICC50E, Germany) equipped with a digital camera attachment to take high-resolution images of the emerging vasculature. The images were analyzed using AngioGen 0.5 software to measure angiogenesis parameters, including vessel area, junctions, and length, by comparing LNiNPs-treated embryos with PBS-treated controls to determine the impact of NPs on vascular development.

3.8.3.5.2. Anti-angiogenesis Assay for LCuONPs (CAM Assay)

Inhibition of the anti-angiogenic effect of LCuONPs (5 µg/mL) towards the formation of blood vessels was determined using the 48-hour chick embryo model, as presented in Section 3.8.3.5.1, under time intervals of 2, 4, 6, and 8 hours.

3.8.4. Statistical analysis and Data representation

All the experimental results were given as mean ± standard deviation (SD) from triplicate assays to ensure reproducibility and minimize variability. Statistical analysis included antimicrobial (zone of inhibition), anticancer (cell death%), antioxidant (radical scavenging%), environmental toxicity (viability/mortality rates), anti-angiogenic (vessel area, length, and junctions), and electrochemical sensing responses. Data analysis assured concordance across biological replicates and enabled comparative analysis. Electrochemical sensing outcomes were presented with peak current values, also given as mean ± SD. To facilitate clarity and interpretation, data were shown both in tabular and graphical representations. Bar charts represented mean ± SD values across all assays, whereas line graphs represented dose-response trends seen in anticancer and antioxidant research. Scatter plots represented IC_{50} values, trends in toxicity, and sensing responses. Representative photographs were provided to visually enhance main findings, for example, those from the chorioallantoic membrane (CAM) assay in anti-angiogenesis, anticancer, and environmental toxicity tests. Error bars on all graphs represented standard deviation, giving a visible impression of variability in the data.

This thorough and methodical approach meant that the findings in the study were clearly represented, openly, and in a way that was facilitating interpretation and comparison.

CHAPTER IV

RESULTS

RESULT 1

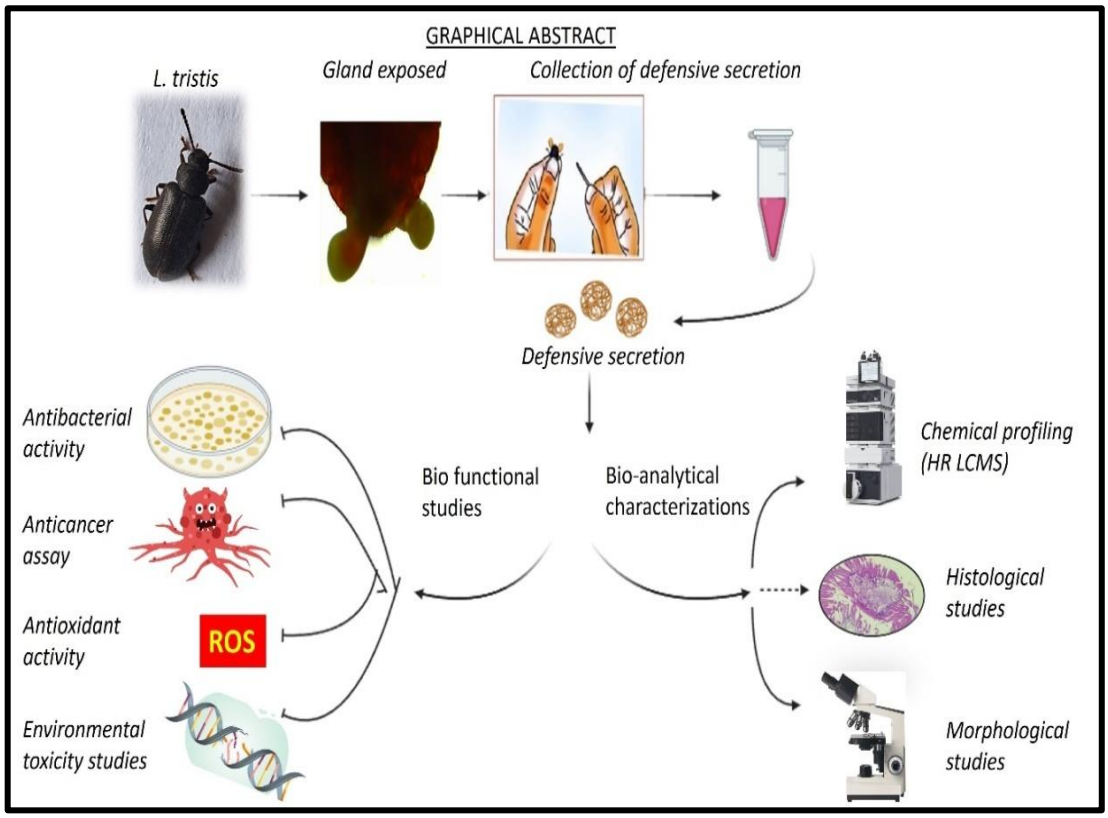
GRAPHICAL ABSTRACT
L. tristis
Gland exposed
Collection of defensive secretion
Defensive secretion
Antibacterial activity
Anticancer assay
Antioxidant activity
ROS
Environmental toxicity studies
Bio functional studies
Bio-analytical characterizations
Chemical profiling (HR LCMS)
Histological studies
Morphological studies

4.1 The Chemical Composition and Antimitotic, Antioxidant, Antibacterial, and Cytotoxic Properties of the Defensive Gland Extract of the Beetle, *Luprops tristis* Fabricius

Coleoptera, the largest order of insects, includes the Tenebrionidae family, known for inhabiting decaying wood and other plant debris. Some of these beetles use chemical secretions as a defense mechanism, with variations across evolutionary lineages. While extensive research has explored defensive compounds in some beetle families, studies on Indian species, particularly the genus *Luprops*, remain limited. *Luprops tristis*, or the Mupli beetle, is notable for its skin-irritating secretion. This study investigates the histological analysis of the defensive gland and the chemical composition of *L. tristis* defensive secretions and evaluates their potential antimitotic, antibacterial, antioxidant, and cytotoxic properties, aiming to uncover bioactive compounds with therapeutic relevance.

4.1.1. Tissue sampling of the defensive gland for histological study

Microscopic and histological analysis of the secretory lobes reveals that the two lobes of the gland, located dorsally, receive secretions from numerous secretory units. These units consist of internally positioned secretory cells, spherical in shape, containing tightly packed spherical secretory vesicles filled with defensive secretion (Fig. IV. I.2). Each glandular system comprises several secretory lobes, reminiscent of the tenebrio type of gland, featuring a pair of conical reservoirs opening into a common discharge area without exit ducts. Scanning electron microscopy investigations and histological studies of the gland indicate that each lobe terminates blindly without any specific cuticular openings. Cross-sectional analysis reveals dimensions of 600 μm in length and 200 μm in width for the gland (Figure IV. I. 1 and Figure IV. I. 2).

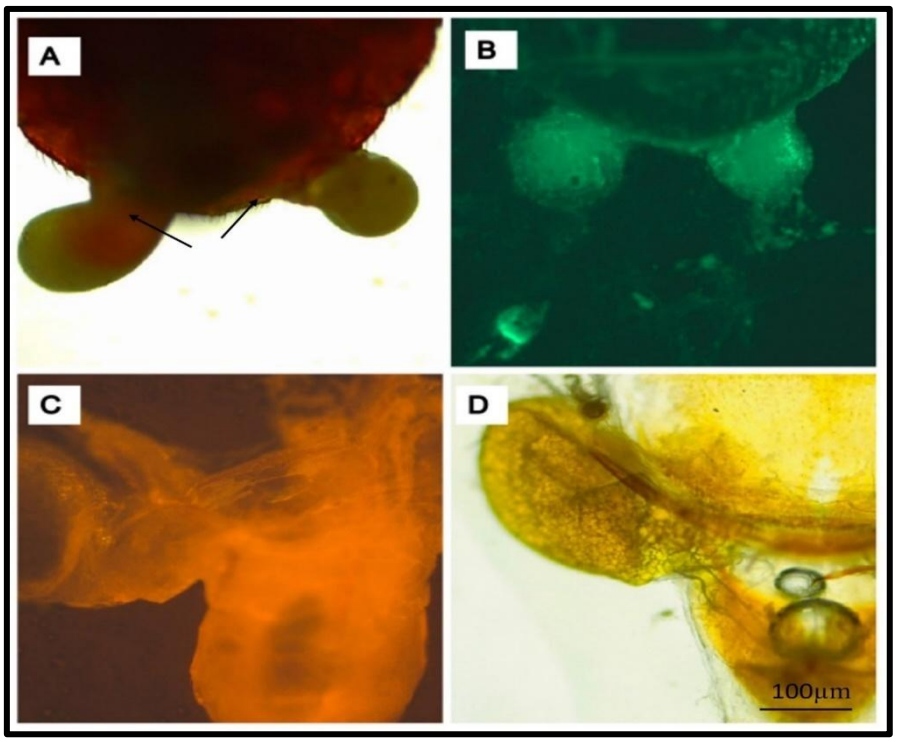

Figure IV. I. 1: Compound Microscopic images of defensive gland (A), Fluorescent microscopic images Cy3 and FITC (B-C), compound microscopic images of single lobe of the gland (D).

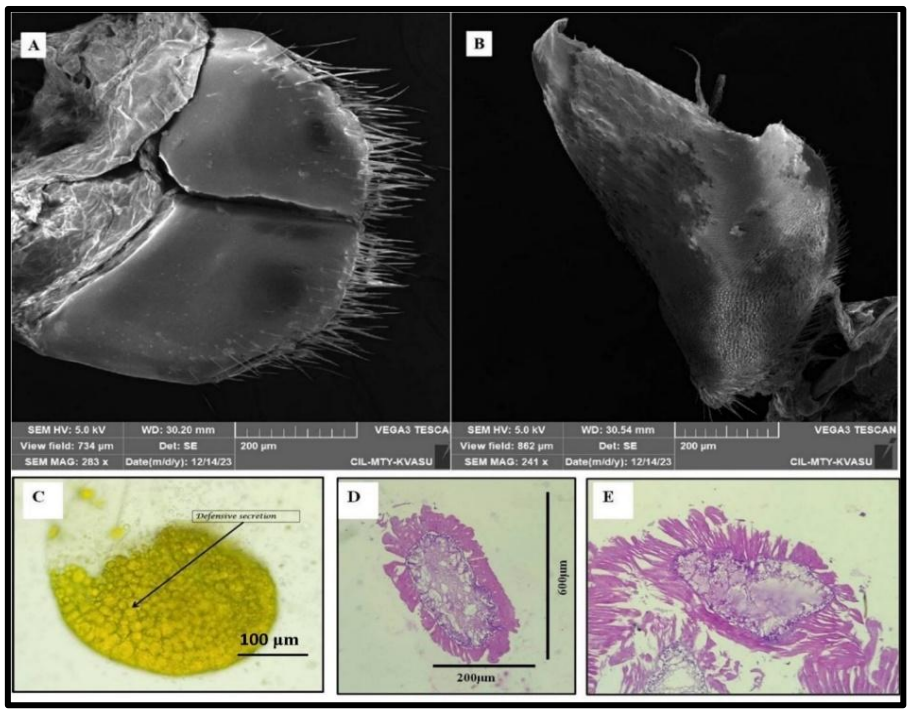

Figure IV. I. 2: Scanning electron microscopy images of gland (A) Non-erected gland pairs, (B) Erected single lobe, (C) Lobe with secretory vesicles, (D) Cross-sectional view of gland, (E).

Figures IV. I. 1 and IV. I. 2 illustrate the detailed structural and microscopic features of the defensive gland under various imaging techniques. Figure IV. I. 1 presents compound and fluorescent microscopic images that reveal the gland's anatomical and cellular organization. Panel A shows a general compound microscopic view of the intact defensive gland, highlighting its overall morphology. Panels B and C provide fluorescent microscopic images using Cy3 and FITC staining, respectively, which emphasize specific structural and possibly functional components within the gland tissue. Panel D focuses on a single lobe of the gland under compound microscopy, offering a more localized view of its internal structure. Figure IV.I.2 includes scanning electron microscopy (SEM) images that offer a higher-resolution perspective of the gland's surface and internal architecture. Panel A displays a pair of non-erected gland lobes, while Panel B shows a single lobe in its erected state, suggesting dynamic structural behavior. Panel C captures the presence of secretory vesicles on the lobe surface, indicating active secretion sites. Panel D gives a cross-sectional image, enabling the observation of internal layers and organization, and Panel E fills in the gap by giving additional information to aid structural interpretation. These two figures collectively give a full morphological and ultrastructural description of the defensive gland, which enables further functional and biological investigation.

4.1.2. Liquid Chromatography-Mass Spectrometry (LC-MS) analysis of the Defensive Gland Extract of the Beetle, *L. tristis* Fabricius

The glands of *L. tristis* secrete a defensive secretion, and LC-MS Q-TOF of the methanolic extract from the glands exhibited a diverse spectrum of secondary metabolites, highlighting the chemical diversity of the extract. The compounds isolated are diverse in their chemical classes, and each contributes to the distinct biochemical profile of the extract and can further enhance its biological activity. Highlighted metabolites identified are D-Gluconic acid ($C_6H_{12}O_7$), 3-Dehydro-L-gulonate ($C_6H_{10}O_7$), Uric Acid ($C_5H_4N_4O_3$), Citric Acid ($C_6H_8O_7$), and 2-Pyrrolidone-5-carboxylic Acid ($C_5H_7NO_3$), listed in Table IV.I. 1, which can be responsible for the bioactivity of the extract.

Table IV. I. 1: Secondary metabolites present in the defensive secretion of *L. tristis.*

Compound Name	Formula	Structure
D-Gluconic acid	$C_6H_{12}O_7$	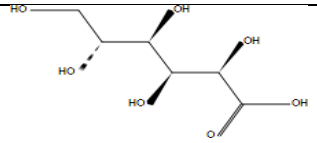
3-Dehydro-L-gulonate	$C_6H_{10}O_7$	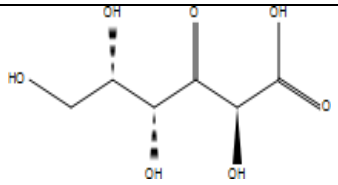
Uric Acid	$C_5H_4N_4O_3$	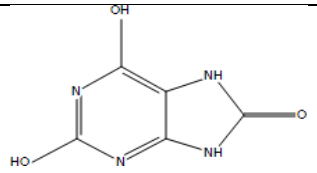
Citric Acid	$C_6H_8O_7$	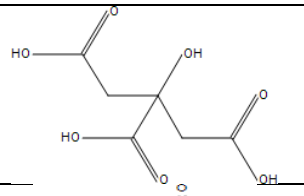
2-Pyrrolidone-5-carboxylic Acid	$C_5H_7NO_3$	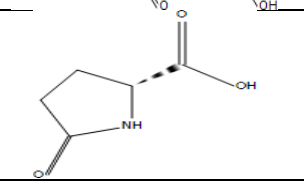

Each of these metabolites has a specific function in determining the overall biochemical nature of the defensive extract. Together, these metabolites could provide synergistic action that amplifies the potential biochemical activity of the extract, such as antioxidant, anti-cancer, anti-bacterial activity, and antiangiogenic activity. The LC-MS Q-TOF Chromatogram is provided below as Figure IV.I. 3.

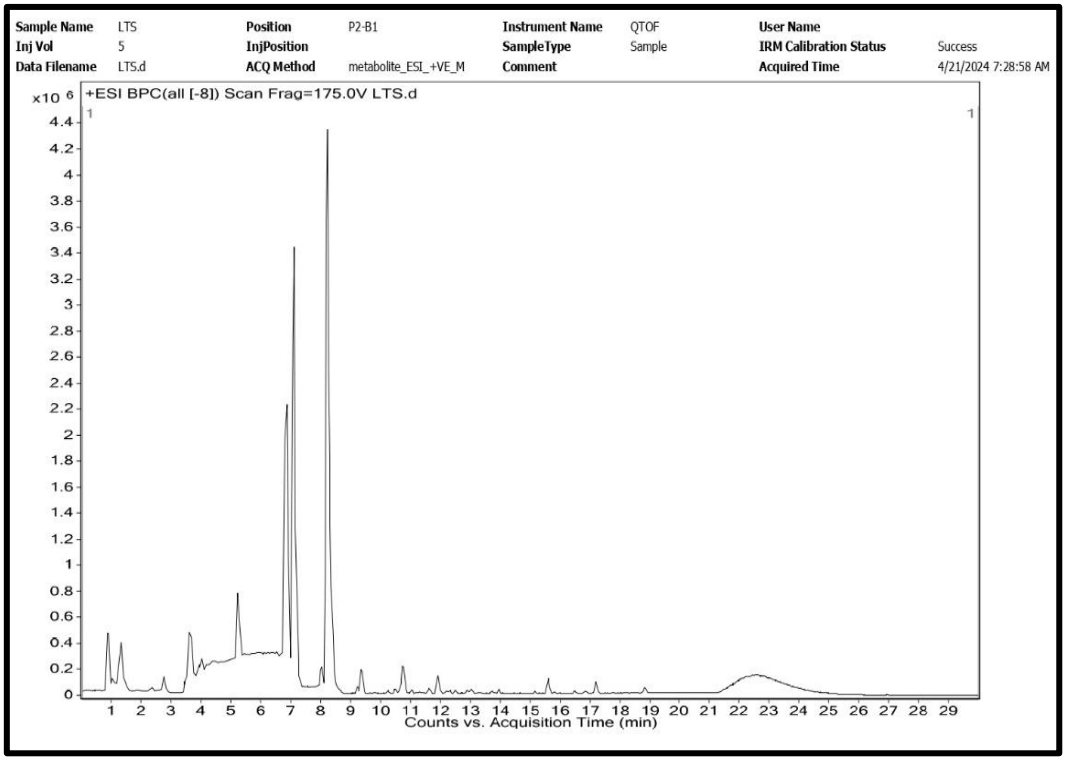

Figure IV. I. 3: HRLC-MS- QTOF chromatogram of *L. tristis* defensive gland extract

4.1.3. Environment hazard testing of defensive gland secretion by *Allium* assay

Toxicity assessment of beetle defensive secretions using the *Allium cepa* assay provides a straightforward and reliable method for evaluating their cytogenotoxic effects. By analyzing parameters such as root growth inhibition, changes in mitotic index, and chromosomal abnormalities in onion root cells, this assay serves as an effective bioindicator of environmental contaminants. Its significance lies in determining the environmental safety of bioactive compounds in secretions, supporting their responsible use in fields such as nanotechnology and biomedicine.

Varying quantities of the defensive secretion of *L. tristis* to the growing root meristematic cells of *A. cepa*, we observed various minor chromosomal abnormalities in the mitotic chromosomes (see Figure IV. I. 4 and Table IV. I. 2). The table compares the effects of varying concentrations of defensive gland extract on *A. cepa* root tip cells, analyzing the Mitotic Index (% of dividing cells) and Chromosomal Aberration (% of abnormal cells). For the control group (distilled

water), the Mitotic Index increases with concentration, ranging from 11.29% ± 0.32 at 100 µg/mL to 15.58% ± 0.30 at 500 µg/mL, with no chromosomal abnormalities observed (NIL). In contrast, the experimental group treated with the defensive gland extract shows a concentration-dependent decline in the Mitotic Index, from 9.50% ± 0.50 at 100 µg/mL to 3.33% ± 0.33 at 500 µg/mL, indicating reduced mitotic activity (cytotoxicity). Simultaneously, Chromosomal Aberration rises from 11.17% ± 0.29 at 100 µg/mL to 16.33% ± 0.33 at 500 µg/mL, suggesting increased genotoxic effects with higher extract concentrations. These results demonstrate that the defensive gland extract inhibits cell division and induces genetic damage in a dose-dependent manner.

The incidence of chromosomal abnormalities in the experimental group grew steadily in tandem with the concentration of defensive gland extract (Table IV. I. 2). Defensive extracts cause disintegrated prophase as depicted in Figure IV. I. 4 (D), aberrant metaphase (E), and disintegrated nuclei (F) by interfering with the regular process of mitotic cell division. In contrast, there were no abnormalities observed in the control group's mitotic cell division process.

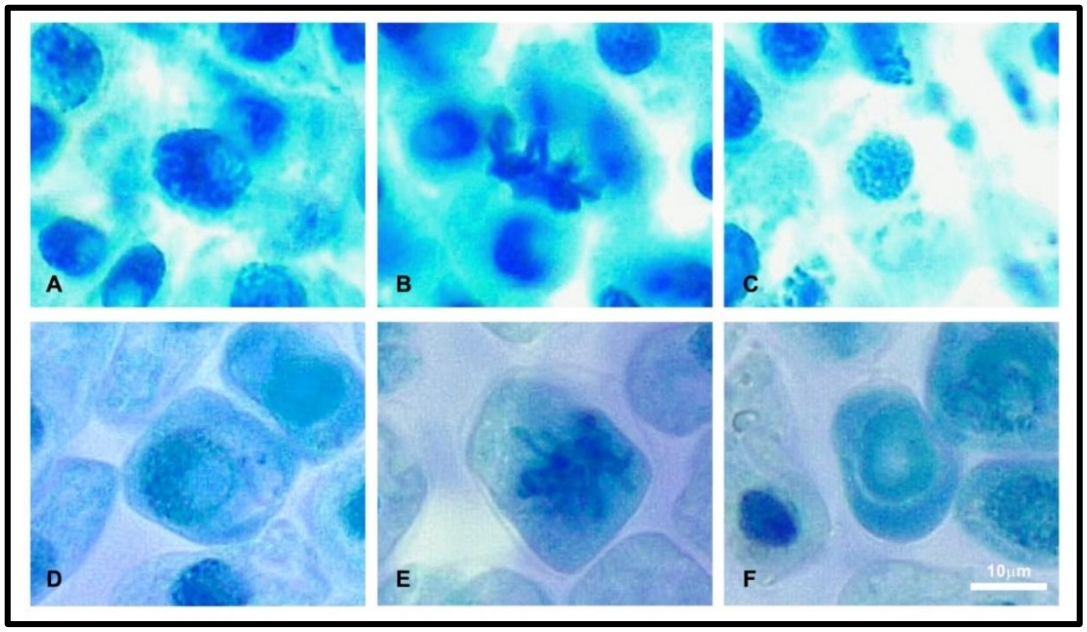

Figure IV. I. 4: The impact of the extract from the defense gland on *A. cepa* cell division. Normal prophase (A), normal metaphase (B), normal nuclei (C), disintegrated prophase (C), aberrant metaphase (E) and disintegrated nuclei are shown in (F) respectively.

Table IV. I. 2. Effect of different concentrations of defensive gland extract on *A. cepa*.

Treatment	Concentration (µg/mL)	Mitotic Index (% ± SD)	Chromosomal Aberration (% ± SD)
Control (distilled water)	100	11.29 ± 0.32	NIL
	200	12.65 ± 0.25	NIL
	300	14.44 ± 0.37	NIL
	400	14.55 ± 0.32	NIL
	500	15.58 ± 0.30	NIL
Experiment	100	9.50 ± 0.50	11.17 ± 0.29
(defensive gland extract)	200	6.57 ± 0.27	13.61 ± 0.27
	300	5.64 ± 0.24	14.46 ± 0.42
	400	3.57 ± 0.36	15.35 ± 0.36
	500	3.33 ± 0.33	16.33 ± 0.33

4.1.4. Antioxidant Activity of defensive gland secretion by DPPH assay

To assess the free radical scavenging potential of the defensive secretion of *L. tristis,* the DPPH assay is widely used. The half-maximal inhibitory concentration (IC_{50}) for the defensive gland extract was determined as 121.35 ± 2.1 µg/mL for the DPPH activity, as shown in Figure IV. I. 5 and Table IV. I. 3. The table presents the effect of varying concentrations (20 µg/mL to 100 µg/mL) of gland extract on the absorbance (optical density) and its corresponding scavenging activity percentage (S%). The control absorbance remains constant at 0.9 across all concentrations. As the concentration increases, the absorbance decreases, indicating higher scavenging activity. Specifically, at 20 µg/mL, the absorbance is 0.77, corresponding to a scavenging activity of 14.44%. With increasing concentrations, the scavenging activity rises progressively: at 40 µg/mL, the absorbance drops to 0.72 with a scavenging percentage (S%) of 20%; at 60 µg/mL, absorbance further declines to 0.66 with an S% of 26.67%; and at 80 µg/mL, it reduces to 0.6 with an S% of 33.33%. The maximum effect is observed at 100 µg/mL, where the absorbance is 0.52, leading to a scavenging activity of 42.22%. The IC_{50} value, determined to be 121.35 µg/mL, represents the concentration required to achieve 50% scavenging activity (Table IV. I. 3). These results highlight a concentration-dependent increase

in scavenging activity, indicating the antioxidant potential of defensive gland extract.

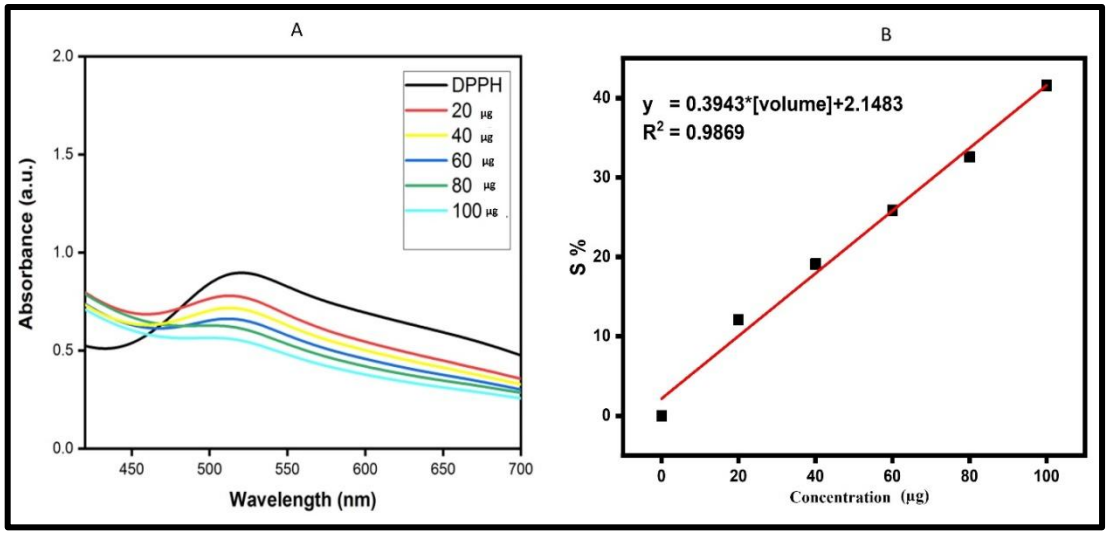

Figure IV. I. 5: Absorbance graph showing DPPH activity & Calibration curve correlating concentration and scavenging activity.

Table IV. I. 3: DPPH activity of defensive gland extract

Concentration (µg/mL)	Control	Absorbance	S%
20	0.9	0.77 ± 0.01	0.1 ±.01
40	0.9	0.72 ± 0.01	0.2 ±.01
60	0.9	0.66 ± 0.01	0.2 ±.01
80	0.9	0.6 ± 0.01	0.3 ±.01
100	0.9	0.52 ± 0.01	0.4 ±.01
IC_{50}			121.35 µg/mL

4.1.5. Antibacterial Activity of defensive gland secretion by Disc diffusion assay

Using two different bacterial strains, the agar disc diffusion assay method was used to evaluate the defensive gland secretion *in vitro* antibacterial effectiveness. The disc diffusion assay results are shown in Figure IV. I. 6. The current study using *L. tristis'* defense secretion demonstrates strong antibacterial efficacy against the selected *E. coli* and *S. aureus* bacteria. The measured values for the zone of inhibition against *E. coli* recorded 9 ± .02 and 11 ± .02 mm for 5 µg/mL

and 10 µg/mL, and *S. aureus* were 7 ±.02 mm and 9 ± .02 mm, respectively (Figure IV. I. 6 & Table IV. I. 4). *E. coli* was more prone to defensive secretion than *S. aureus*.

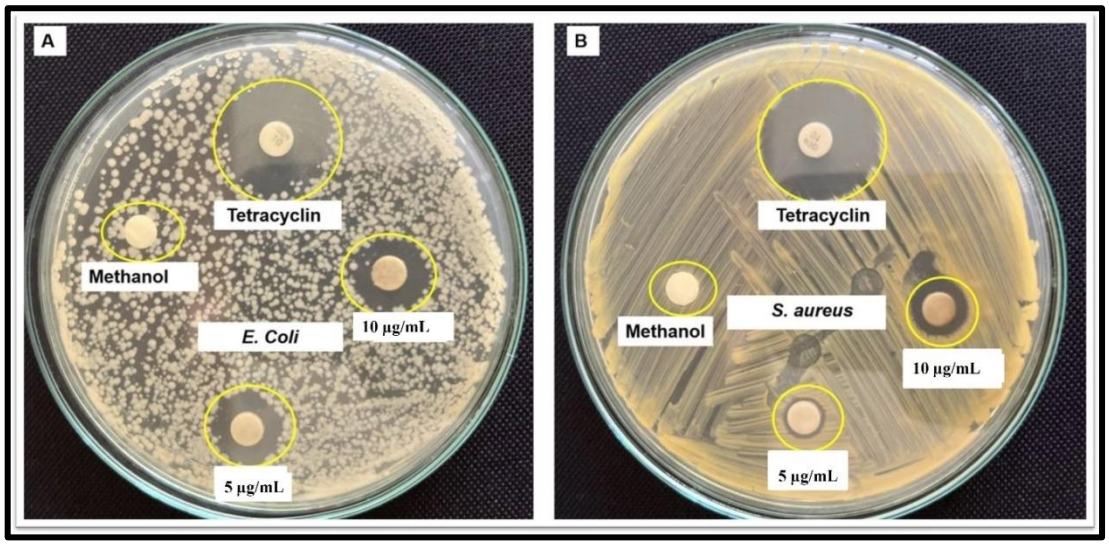

Figure IV. I. 6. Disc diffusion analysis of *L. tristis* defensive secretion on *E. coli* (A) and *S. aureus* (B).

Table IV. I. 4: Disc diffusion analysis of *L. tristis* defensive secretion

Concentration of secretion (µg/mL)	*Zone of inhibition (ZOI)*	
	E. coli	***S. aureus***
5 µg/mL	9 ± .02	7 ± .02
10 µg/mL	11 ± .02	11 ± .02

4.1.6. Anticancer analysis of defensive gland secretion by Trypan blue assay.

The defensive gland extract from the *L. tristis* beetle was evaluated for its potential to fight cancer, and the results are shown in Figure IV. I. 7. The anticancer efficacy of *L. tristis'* defensive secretion was observed by a cytotoxicity experiment using Dalton's lymphoma ascites (DLA) cells. The anticancer activity of the defensive gland extract of *L. tristis* was evaluated against DLA cells, showing a dose-dependent increase in cytotoxicity. Even at the lowest tested concentration (2.5 µg/mL), the extract was very mildly cytotoxic at a level of around 5 ± 0.2%. Increasing the concentration to 5 µg/mL and 10 µg/mL elevated the cytotoxic effect to levels of around 10 ± 0.2% and 15 ± 0.2%, respectively. At 15 µg/mL, there was a

remarkable escalation in cytotoxicity to the level of 17 ± 0.2%. At higher doses of 20 µg/mL and 25 µg/mL, cytotoxicity increased further to 22 ± 0.2% and reached a peak of 44 ± 0.2%, respectively. The trend indicates that the extract is highly dose-dependent cytotoxic on DLA cells, pointing to its anticancer potential. Based on this data, it can be deduced that levels above 25 µg/mL can provide even greater cytotoxicity, possibly reaching saturation points where the highest effect of the extract can be achieved, as in Table IV. I. 5. More studies are required to determine the precise concentration point for maximum efficacy and to investigate the mechanisms behind its anticancer action.

Table IV. I. 5: Cytotoxicity assay of defensive gland secretion

Concentration (µg/mL)	Cell death (%)
2.5	5 ± 0.2
5	10 ± 0.2
10	15 ± 0.2
15	17 ± 0.2
20	22 ± 0.2
25	44 ± 0.2

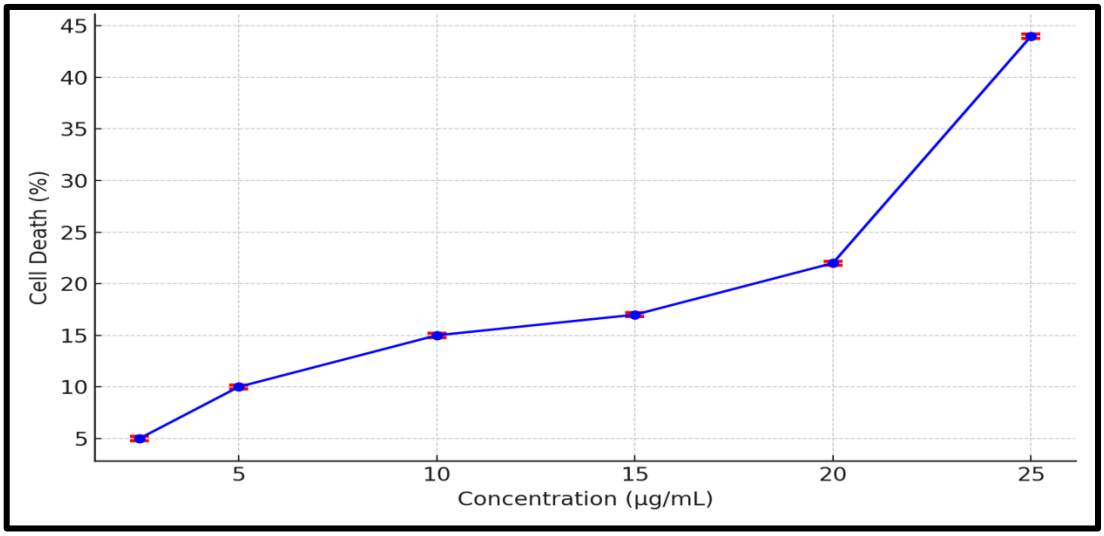

Figure IV. I. 7. Anticancer effect of the defensive gland extract of *L. tristis*.

4.1.7. Cyclic Voltammetry (CV) Analysis Defensive Gland Secretion.

The various compounds present in the gland secretion were oxidized at a potential range from 1 to -1 V as shown in the cycle voltammogram (Figure IV. I. 8) for 0.05 mM standards. The upper scan represents the oxidation of the phenolic groups, giving rise to a positive current (anode), which interprets the reducing capacity of the compounds, substantiates the reducing power of defensive gland secretion in the production of metal NPs.

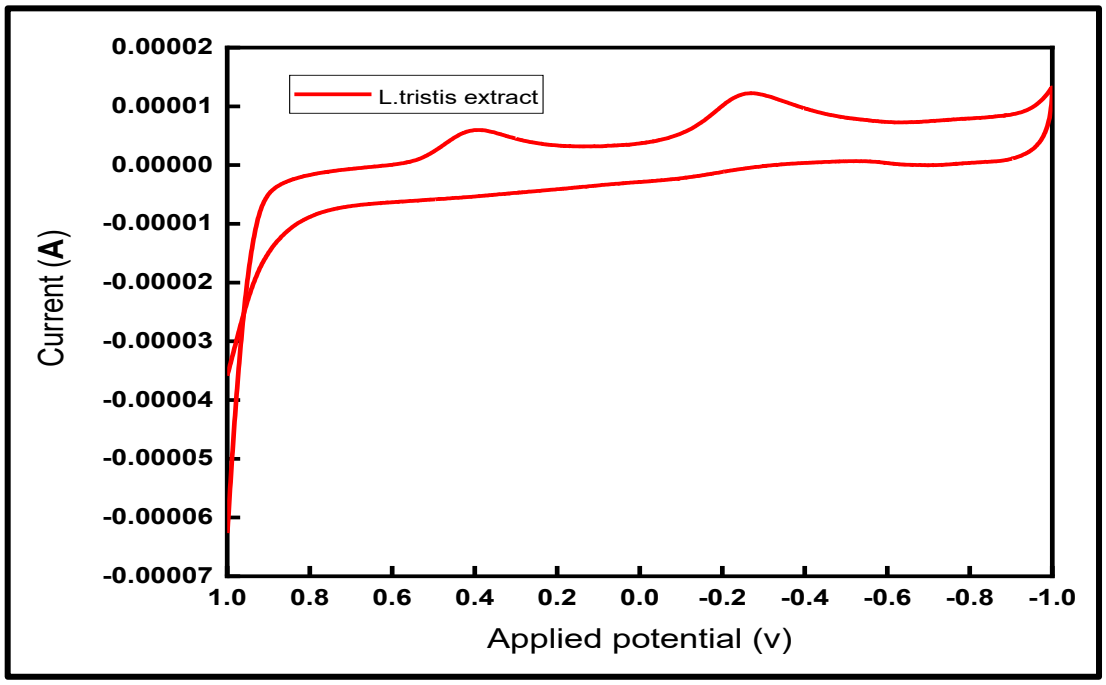

Figure IV. I. 8. Cyclic voltammetry of defensive gland extract of *L. tristis*.

RESULT 2

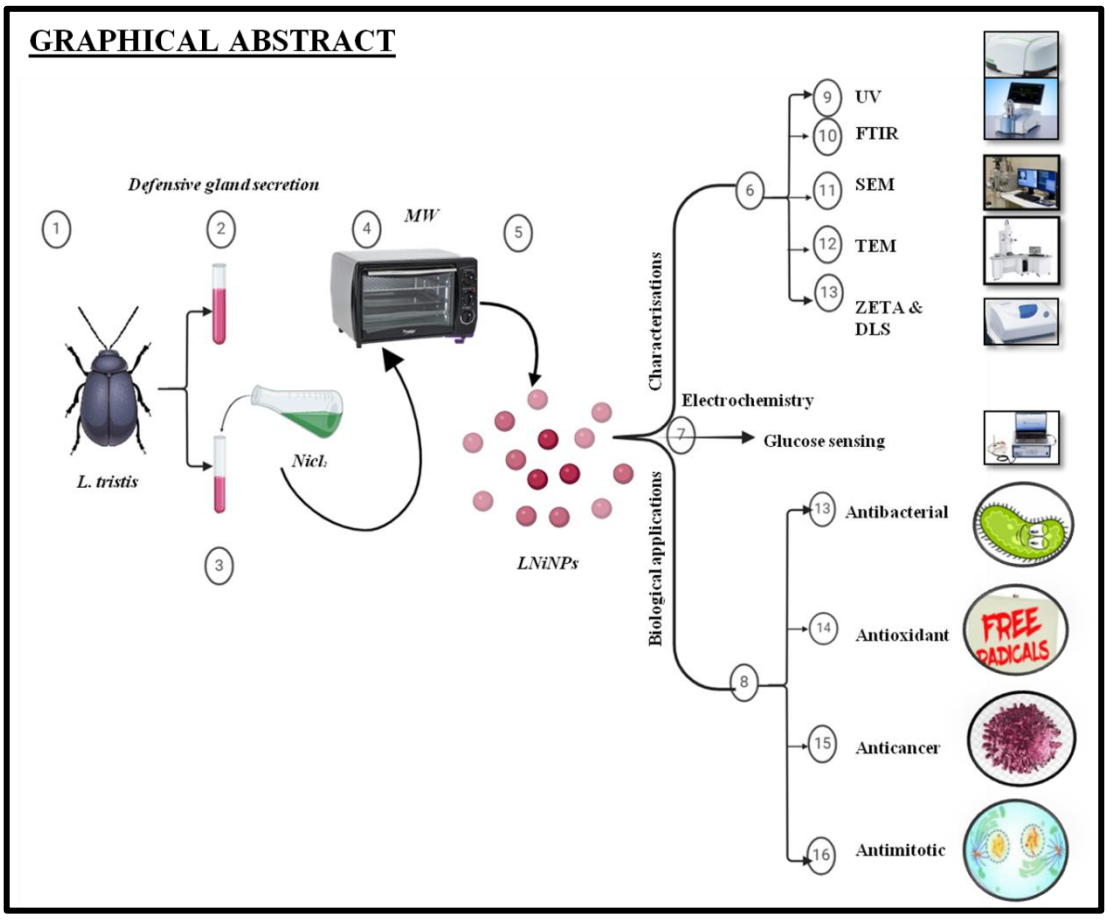
GRAPHICAL ABSTRACT
Defensive gland secretion
MW
L. tristis
NiCl2
LNiNPs
Characterisations
9 UV
10 FTIR
11 SEM
12 TEM
13 ZETA & DLS
Electrochemistry
7
Glucose sensing
Biological applications
8
13 Antibacterial
14 Antioxidant
FREE RADICALS
15 Anticancer
16 Antimitotic

4.2. Biosynthesis of LNiNPs using Beetle Defensive Gland Extract for Multifunctional Applications.

In the present study, LNiNPs were synthesized by reducing a nickel chloride solution using an extract derived from the defensive secretion of the insect *Luprops tristis*. Following synthesis, the nanoparticles were thoroughly characterized using UV–Vis spectroscopy, Fourier-transform infrared spectroscopy (FTIR), scanning electron microscopy (SEM), transmission electron microscopy (TEM), and zeta potential analysis. Subsequently, their biochemical applications were evaluated, including glucose sensing, antibacterial activity, antioxidant potential, antimitotic effects, and anticancer properties.

4.2.1. Chemical characterization of LNiNPs

4.2.1.1. UV- Vis spectroscopy of LNiNPs

The reaction mixture's apparent color shift from purple to reddish brown (Figure IV. II. 1A & B), following microwave irradiation within 15 minutes, was the first indicator of the formation of LNiNPs. This was followed by UV-Vis spectroscopy, the result is shown in Figure IV. II. 1. LNiNPs showed the maximum absorption peak at the wavelength (λ-max) 206 nm, it was caused by the surface plasmon resonance phenomenon, which offers a useful indicator of the LNiNPs formation.

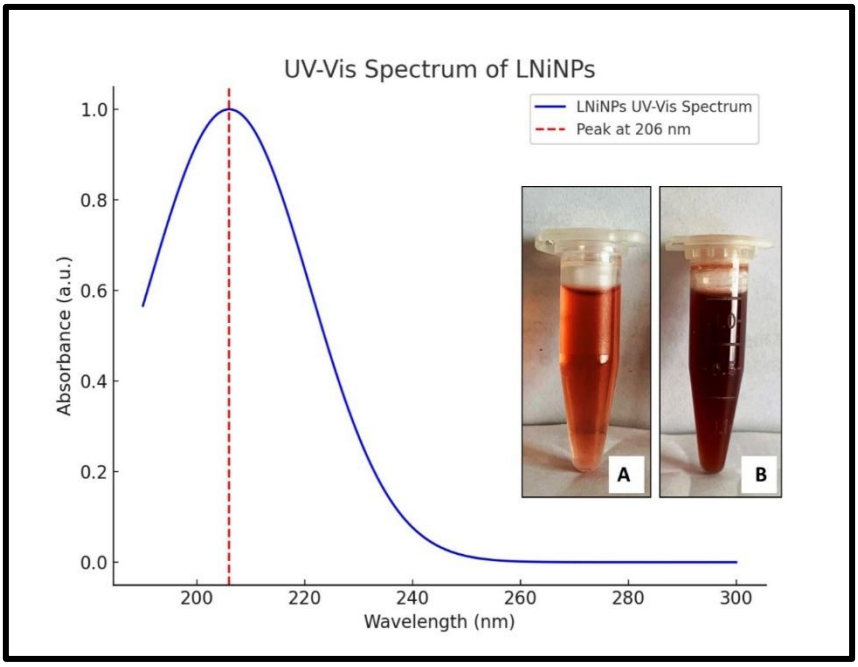

Figure IV. II. 1: UV-Vis spectrum of LNiNPs

4.2.1.2. FTIR analysis of LNiNPs

The functional groups involved in the LNiNPs were identified using FT-IR spectroscopy. The FTIR spectra of LNiNPs were compared with those of the gland secretion, LNiNPs before microwave (M/W) irradiation, and the gland secretion after M/W irradiation. The resulting spectra revealed the corresponding functional groups, and it was observed that there was minimal difference in the functional groups before and after exposure to microwave irradiation. The number of recorded absorption peaks that were associated with the FTIR results (Figure IV. II**.** 2) ranged between 4000-400 cm^{-1}. The spectrum shows peaks at ranges of 3412, 2937, 1633, 1404,1096 and 602 cm^{-1}corresponding to O-H, CH/CH2, C-H, C-O, C-H, C-O, C=C(Adwin Jose *et al.,* 2018; Duan & Li, 2004; Patra & Baek, 2014; Shankar & Rhim, 2015; Tomar *et al.,* 2015; C. Yuan *et al.,* 2022) (Table IV. II. 1). Therefore, it is assumed that metabolites were present around the synthesized NiNPs.

Table IV. II. 1: Functional groups obtained in FTIR

Wave number (cm^{-1})	Functional group
3412	O-H
2937	CH/CH2
1633	C-O
1404	C-H
1096	C-O
602	C=C

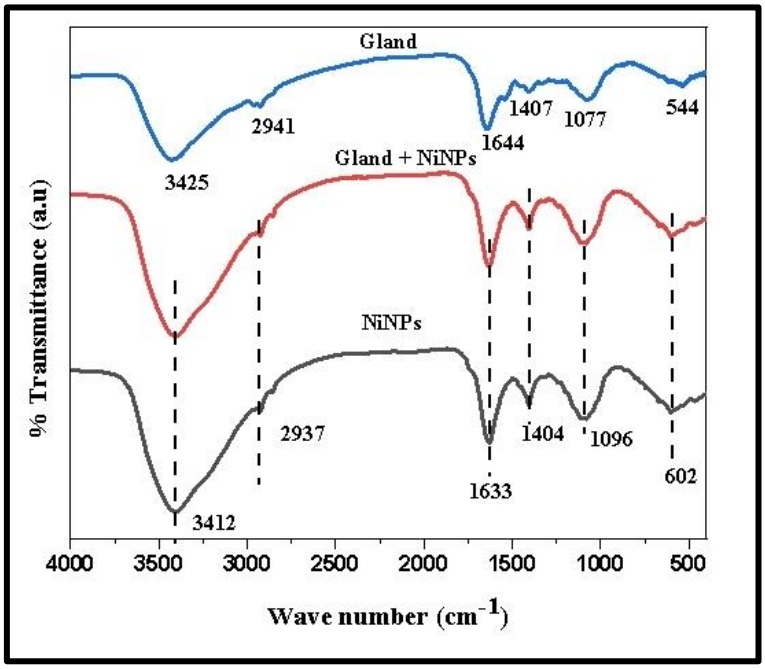

Figure IV. II. 2: FTIR spectra of LNiNPs compared with FTIR of Gland secretion and LNiNPs before microwave irradiation(M/W), and FTIR of gland secretion after M/W irradiation.

4.2.1.3. Scanning electron microscopy (SEM) & Transmission electron microscopy (TEM) of LNiNPs

To examine the morphological characteristics of the synthesized LNiNPs, both Scanning Electron Microscopy (SEM) and Transmission Electron Microscopy (TEM) analyses were carried out. The SEM analysis, as shown in Figure IV.II.3A, provided detailed surface morphology of the LNiNPs. The images revealed that the nickel nanoparticles synthesized using the defensive gland extract of *L. tristis* were predominantly spherical in shape. These nanoparticles exhibited a rough surface

texture, indicative of the biological synthesis process. Moreover, the distribution of the particles appeared fairly uniform across the field of view. However, it was observed that some nanoparticles tended to aggregate, possibly due to van der Waals interactions or partial surface capping by biomolecules from the extract. This aggregation resulted in the formation of larger composite clusters, which is commonly reported in biologically mediated nanoparticle synthesis.

To gain further insight into the internal structure and precise dimensions of the nanoparticles, TEM analysis was conducted, as depicted in Figure IV.II.3B. The TEM images provided high-resolution visualization, confirming the spherical morphology of the individual nanoparticles. The analysis revealed that the average size of the LNiNPs was approximately 18 nm, Figure IV.II.3C. which is consistent with the expected nanoscale dimensions for biologically synthesized nickel nanoparticles. The relatively small size and spherical structure suggest potential for high surface area, which is favorable for applications in catalysis, antimicrobial activity, and biomedical uses. Together, the SEM and TEM results confirm that the synthesized LNiNPs exhibit nanoscale dimensions, spherical morphology, and moderate aggregation, consistent with the characteristics of green-synthesized metallic nanoparticles.

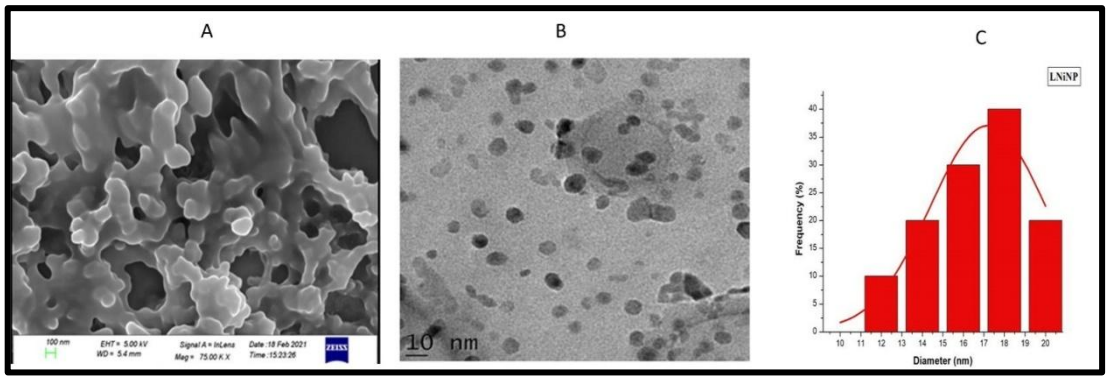

Figure IV. II. 3: Scanning electron microscopy images of LNiNPs (A). Transmission electron microscopy image of LNiNPs (B) Histogram showing average particle size of LNiNPs (C).

4.2.1.4. Zeta Potential of LNiNPs

Using the nanoparticles analyzer (HORIBA SCIENTIFIC SZ 100, Japan), further investigated the Zeta Potential of LNiNPs to assess their stability (Clogston

& Patri, 2011; Doostmohammadi *et al.,* 2011). The outcomes reveal a robust stability of -16.5 meV for LNiNPs, as depicted in Figure IV. II. 4**.** The negative value of the zeta potential is indicative of this stability, facilitating uptake through electrostatic interactions between the cationic NPs and the cationic membrane.

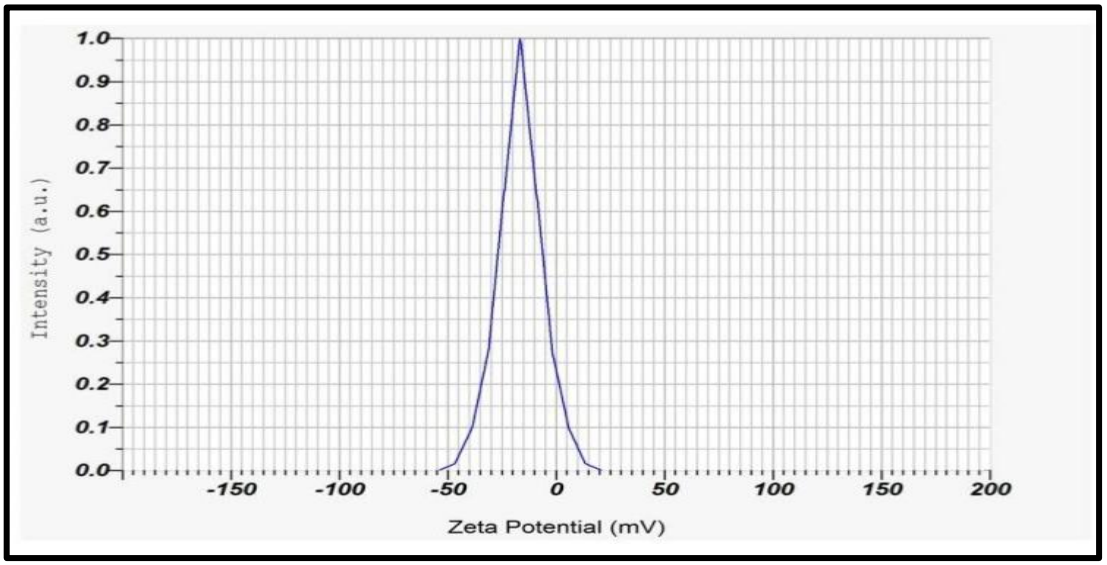

Figure IV. II. 4: Zeta potential of LNiNPs.

4.2.2. Applications of LNiNPs

4.2.2.1. Electrochemical glucose sensing by differential pulse voltammetry (DPV) of LNiNPs

In this investigation, plots of measurements of the glucose (3M) concentration of 10 mM, 20 mM, 30 mM, 40 mM, 50 mM, 60 mM and 70 mM were made (Figure IV. II. 5A), and calibration linear relationships between DPV current output and glucose concentration were plotted (Figure IV. II. 5B) and limit of detection found to be 1.31 µM. LNiNPs produced in this study can be used in electrochemical glucose monitors. The binding of glucose molecules to the functionalized LNiNPs can cause changes in electrical conductivity or redox processes that can be observed and associated with glucose levels. The given graphs illustrate the enzyme-free glucose sensing capability of NiNPs using the DPV method.

In Figure IV. II. 5A, the DPV response was recorded for glucose concentrations ranging from 10 to 70 mM. The current intensity progressively increased with higher glucose concentrations, indicating a clear correlation between glucose concentration and the electrochemical response. The peak currents for glucose concentrations of 10 mM, 20 mM, 30 mM, 40 mM, 50 mM, 60 mM, and 70 mM showed incremental increases, demonstrating the sensitivity of the NiNPs to varying glucose levels.

Figure IV. II. 5B presents the calibration curve derived from the DPV data, plotting the current intensity against glucose concentration. A linear relationship is observed with a regression equation (R^2) indicating a strong correlation and reliable sensor performance. This linearity signifies the ability of the LNiNPs to detect glucose accurately in the tested range.

The results confirm that LNiNPs exhibit excellent enzyme-free glucose-sensing ability, characterized by a clear and linear response across different glucose concentrations. This makes them promising candidates for non-enzymatic glucose detection applications. Further exploration of sensitivity limits and interference from other analytes would be necessary to refine their practical application in glucose monitoring.

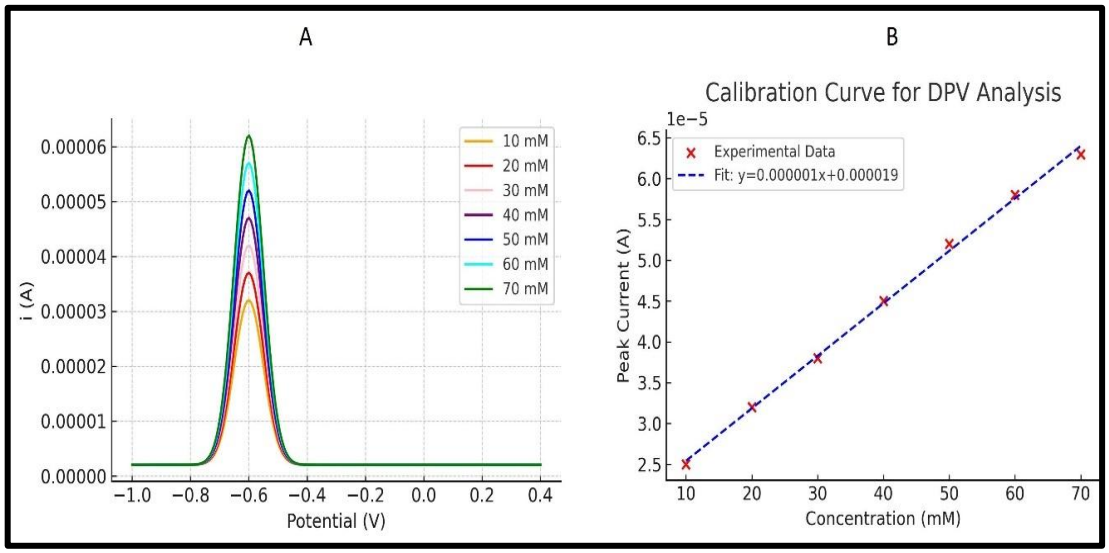

Figure IV. II. 5: Sensing of glucose by DPV method (A), Calibration curve of DPV method (B).

4.2.2.2. Anti-Bacterial Assay of LNiNPs

Disc diffusion assay was used to examine the bactericidal properties of LNiNPs. The effects on the growth of both Gram-negative bacteria (*K. pneumoniae*- ATCC 33591) and Gram-positive bacteria (*S. aureus*- ATCC 700603) were evaluated. Table IV. II. 2 and Figure IV. II. 6. shows the antibacterial activity of LNiNPs against *S. aureus* and *K. pneumoniae* at varying concentrations (5µg/mL,10 µg/mL,15 µg/mL & 20 µg/mL), measured as the diameter of inhibition zones (in mm ± SD). In the experimental group**,** antibacterial efficacy increases with concentration. At 5 µg/mL, the inhibition zones are 12.67 ± 0.58 mm for *S. aureus* and 7.33 ± 0.57 mm for *K. pneumoniae*. This increases to 14.33 ± 0.58 mm and 8.66 ± 0.57 mm at 10 µg/mL, showing a stronger antibacterial effect. At 15 µg/mL, inhibition zones further expand to 16.67 ± 0.58 mm (*S. aureus*) and 10.66 ± 0.57 mm (*K. pneumoniae*). The highest activity is observed at 20 µg/mL, with inhibition zones reaching 19.00 ± 0.58 mm and 12.66 ± 0.57 mm for *S. aureus* and *K. pneumoniae*, respectively. These findings prove the concentration-dependent antibacterial activity of LNiNPs, with *S. aureus* more sensitive than *K. pneumoniae*. This implies that LNiNPs are an effective antimicrobial compound with potential in the treatment of infections caused by such pathogens.

Table IV. II. 2: Effect of LNiNPs on bacteria.

Treatment	**Concentration (µg/mL)**	***S. aureus* (mm ± SD)**	***K. pneumonia* (mm ± SD)**
Experiment	5 µg/mL	12.67 ± 0.58	7.33 ± 0.57
	10 µg/mL	14.33 ± 0.58	8.66 ± 0.57
	15 µg/mL	16.67 ± 0.58	10.66 ± 0.57
	20 µg/mL	19.00 ± 0.58	12.66 ± 0.57

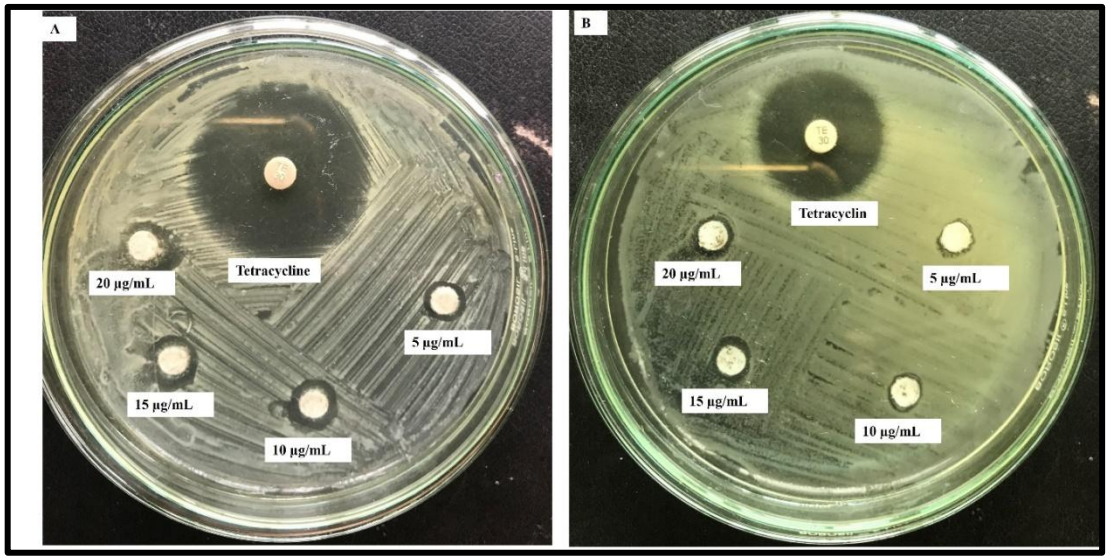

Figure IV. II. 6: Zone of inhibition of *S. aureus* (A) & *K. pneumoniae* by the action of LNiNPs (B) & comparison of the effect of LNiNPs on both strains of bacteria.

4.2.2.3. Anti-Oxidant Activity (DPPH Assay) of LNiNPs.

The DPPH assay, one of the well-established methods used to determine the ability of nanoparticles to scavenge free radicals, has been widely utilized to determine antioxidant activity. Different concentrations of LNiNPs (20 µg/mL, 40 µg/mL, 60 µg/mL, 80 µg/mL, and 100 µg/mL) were utilized in the assay. The highest electron absorption of DPPH- free radicals was observed at 517 nm. Concentration-dependent scavenging activity of LNiNPs was documented in Table IV. II. 3. The EC_{50} value was determined to be 48 µg/mL. With an increase in the concentration of LNiNPs, the colour of the DPPH converted to pale yellow from deep violet. UV spectroscopic analysis verified the heightened antioxidant potency of NiNPs at elevated concentrations, as indicated in Table IV. II. 3 and Figure IV. II. 7. The table presents the DPPH free radical scavenging activity of LNiNPs at varying concentrations (20 – 100 µg/mL). The DPPH assay measures the antioxidant potential of LNiNPs based on the reduction of the DPPH radical, indicated by a decrease in absorbance and an increase in scavenging activity (S%).

At 20 µg/mL, the absorbance of the DPPH solution mixed with LNiNPs is 0.45 ± 0.01, resulting in a scavenging activity of 43%. As the concentration increases to 40 µg/mL, the absorbance decreases to 0.41 ± 0.01, and the scavenging activity rises to 48.4%. At 60 µg/mL, the absorbance drops further to 0.37 ± 0.01,

with a scavenging activity of 53.56%. This trend continues at 80 µg/mL, where the absorbance is 0.33 ± 0.01, and scavenging activity reaches 58.11%. At the highest tested concentration, 100 µg/mL, the absorbance is 0.29 ± 0.01, corresponding to a maximum scavenging activity of 63.7%. The EC_{50} value (effective concentration required to achieve 50% scavenging activity) is determined to be 48 µg/mL. These results demonstrate a concentration-dependent increase in the antioxidant activity of LNiNPs, suggesting their potential as efficient free radical scavengers.

Table IV. II. 3: Concentration-dependent scavenging activity of LNiNPs.

Concentration of LNiNPs(µg/mL).	**Absorbance of control**	**The absorbance of the LNiNPs mixed DPPH solution**	**S%**
20	0.8	0.45± 0.01	43 ± 0.02
40	0.8	0.41± 0.01	48.4 ± 0.02
60	0.8	0.37± 0.01	53.56 ± 0.02
80	0.8	0.33± 0.01	58.11 ± 0.02
100	0.8	0.29± 0.01	63.7 ± 0.02
		EC_{50}	48µg

DPPH anti-oxidant activity (S%) of the sample against concentration was plotted using the equation S% = [($A_{control} - A_{sample}$) / $A_{control}$] x 100. The EC_{50} value, which represents the concentration of the sample needed to achieve 50% scavenging activity, was determined from the graph using a linear regression equation.

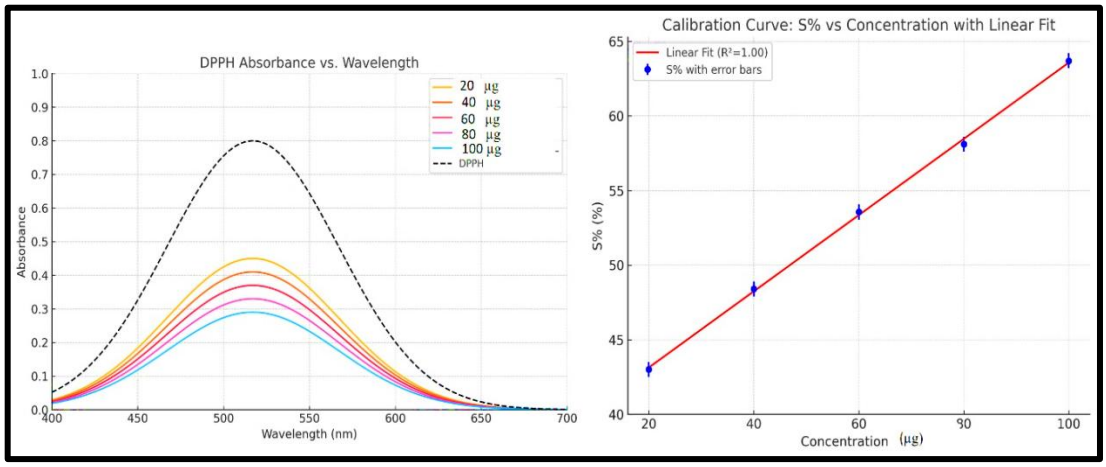

Figure IV. II. 7: DPPH activity of LNiNPs (A) and Calibration curve of LNiNPs (B).

4.2.2.4. Environmental hazard testing of LNiNPs

The biosynthesized LNiNPs exhibited the dose-dependent cytotoxicity and genotoxicity in *Allium cepa* chromosomal aberration studies. The mitotic index (MI) declined progressively with increasing concentrations, from 20% at 100 µg/mL to ~1-2% at 500 µg/mL, indicating inhibition of cell division. Conversely, chromosomal aberrations increased from 2-3% at 100 µg/mL to 25% at 500 µg/mL. The IC_{50} value, representing the concentration at which mitotic activity is reduced by 50%, was estimated to be approximately 250-300 µg/mL. While higher concentrations showed significant genotoxicity, the lower concentrations exhibited relatively mild effects, suggesting that biosynthesized LNiNPs are more biocompatible at lower doses (Figure IV. II. 8 A & B).

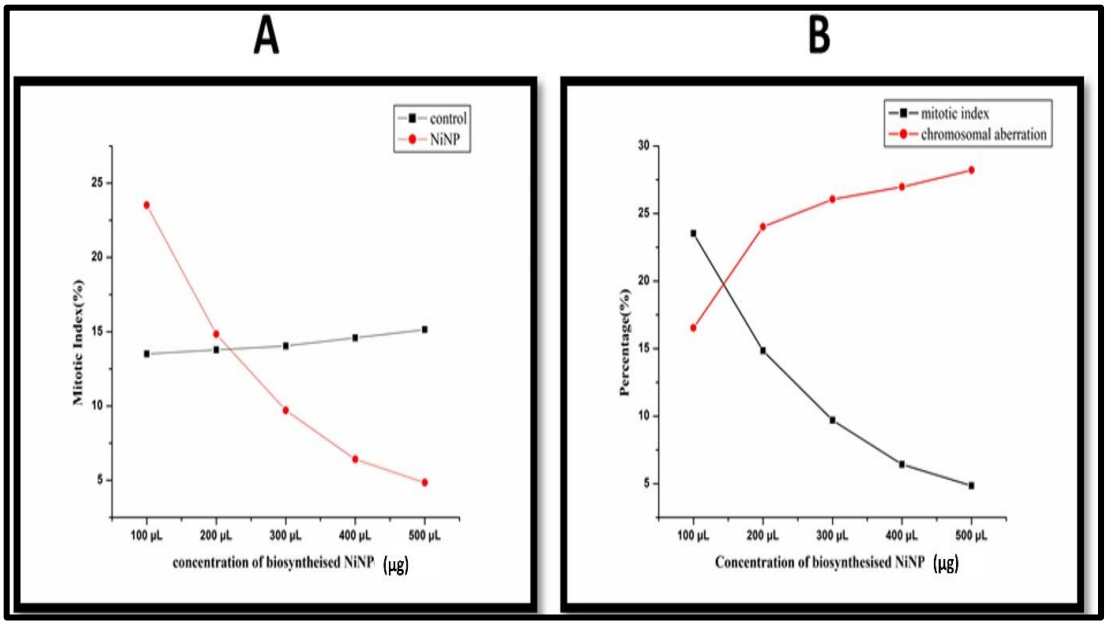

Figure IV. II. 8: Normal mitotic index of control and declined mitotic index of LNiNPs-treated root cells (A). Comparison of the percentage of mitosis and chromosomal aberrations on LNiNPs-treated root cells (B).

4.2.2.5. Anticancer assay of LNiNPs

This study demonstrated the effectiveness of biologically synthesized LNiNPs as a cytotoxic agent using DLA cell lines *in vitro*. The assay showed a gradual increase in cell death according to the concentration of LNiNPs. The anticancer activity of LNiNPs on DLA cells demonstrates a clear concentration-

dependent increase in cytotoxicity, as shown in both the table and graphical data (Figure IV. II. 9, Table IV.II.4). At the lowest concentration of 2.5 µg/mL, cell death is minimal, with cytotoxicity recorded at around 4.9% ± 1.0. This percentage gradually rises as the concentration increases: at 5 µg/mL, cell death reaches 12.3% ± 1.5; at 10 µg/mL, it climbs to 13.8% ± 1.3; and at 15 µg/mL, cytotoxicity increases further to 17.6% ± 1.4. A notable jump occurs at 20 µg/mL, where cell death reaches 23.8% ± 1.6, and at the highest concentration tested, 25 µg/mL, cell death peaks at 44.9% ± 1.5. This progressive increase in cytotoxicity with rising LNiNPs concentrations highlights the potent, dose-dependent anticancer effects of LNiNPs on DLA cells.

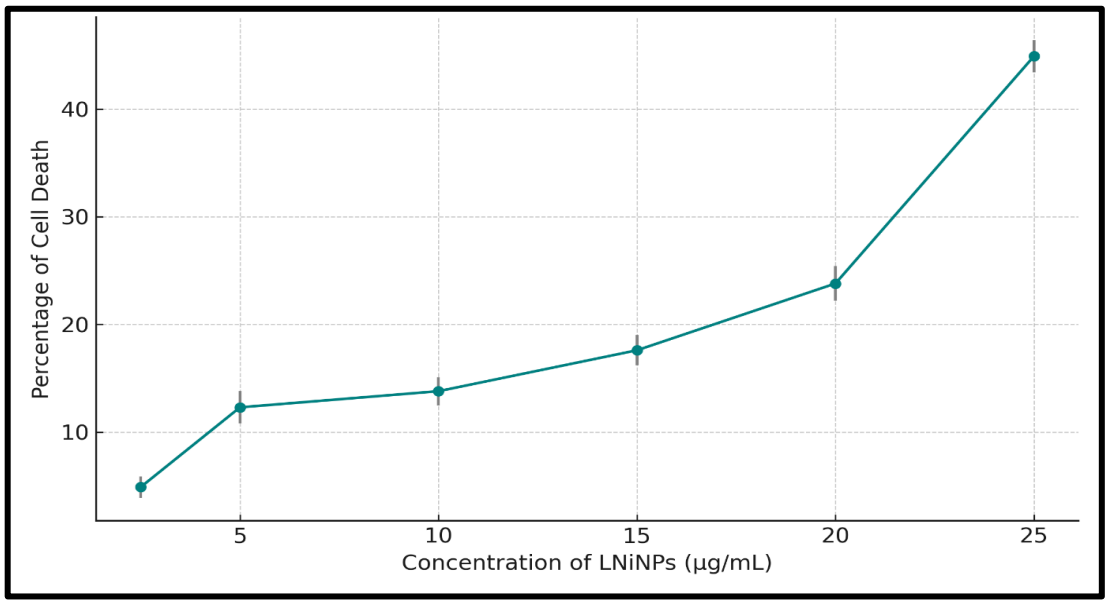

Figure IV. II. 9: Anticancer property of LNiNPs on DLA cells

Table IV. II. 4: Anticancer activity of LNiNPs

Concentration of LNiNPs (µg/mL)	Percentage of cell death
2.5	4.9 ± 1.0
5	12.3 ± 1.5
10	13.8 ±1.3
15	17.6 ±1.4
20	23.8 ± 1.6
25	44.9±1.5

4.2.2.6. Antiangiogenesis by CAM assay of LNiNPs

The angiogenesis assay was successfully performed, demonstrating the impact of LNiNPs on the vascular development of chick embryos. The treated embryos showed significant decreases in vessel growth parameters compared to the PBS control, enabling a thorough evaluation of the nanoparticles' anti-angiogenic effects (Figure IV. II. 10). The three graphs display data related to the effect of LNiNPs on angiogenesis in a 48-hour chick embryo, compared to a control (PBS) over a series of time intervals (Figure IV. II. 11 A, B, C).

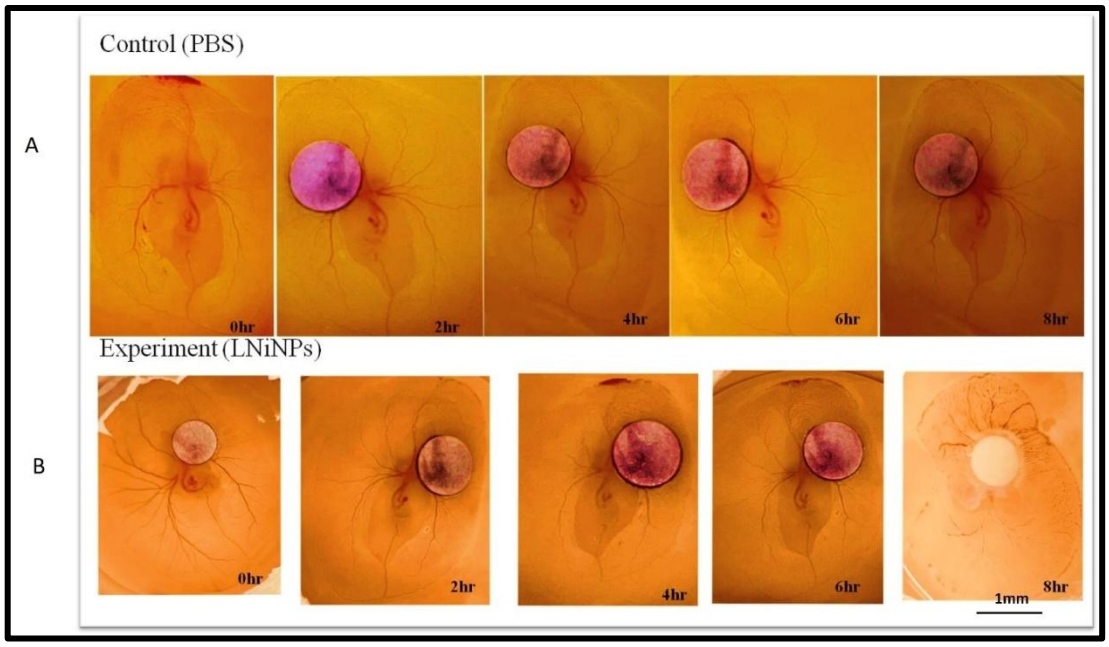

Figure IV. II. 10: Antiangiogenesis property of LNiNPs on chick embryo showing control (A) with normal growth and experiment (B).

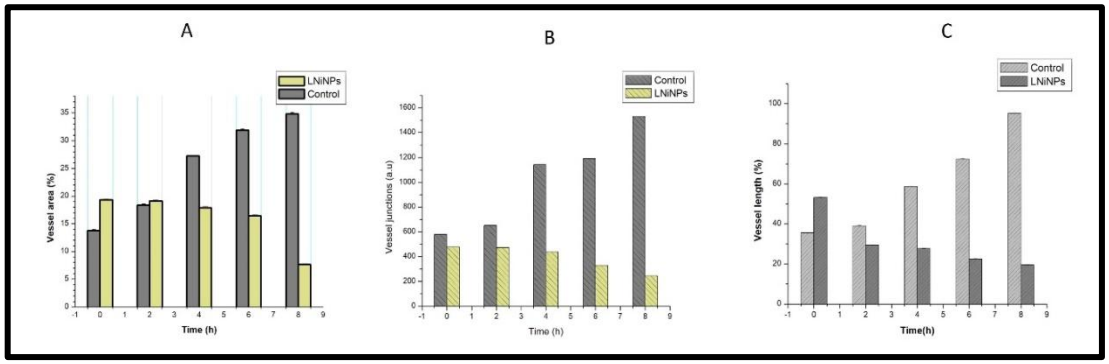

Figure IV. II. 11: A) CAM Assay- vessel area relative to time, B) vessel junctions relative to time, C) CAM Assay- vessel length relative to time

In the PBS control group, the vessel area, junctions, and length showed a progressive increase over time, reaching their peak between 7 to 8 hours. This trend highlights robust angiogenesis, marked by sustained vessel growth, elongation, and the formation of new junctions, indicating stable vascular development in the absence of treatment. In contrast, the group treated with LNiNPs (2 µg/mL) exhibited a distinct inhibitory effect on angiogenesis, with vessel area, junctions, and length consistently lower than the control throughout the observation period. By 4 hours, the vessel area in the LNiNPs-treated group was significantly reduced, with this effect increasing further after 6 hours to reach a dramatic decline by 8 hours. Likewise, vessel junctions in the treated group were initially elevated but were still significantly lower than the control, with a steep drop seen after 4 hours and a significant decline by 8 hours. The length of the vessel also had a similar pattern, with minimal elongation and levelling off at 4 hours before dropping by 8 hours. The results suggest that LNiNPs cause dramatic vessel degeneration, possibly by toxicity or interference with essential cellular processes necessary for angiogenesis. All together, the data show that LNiNPs have potent anti-angiogenic activity in the chick embryo assay, causing vessel destabilization, degeneration and ultimate cell loss with time (Figures IV.II.11 A, B and C).

RESULT 3

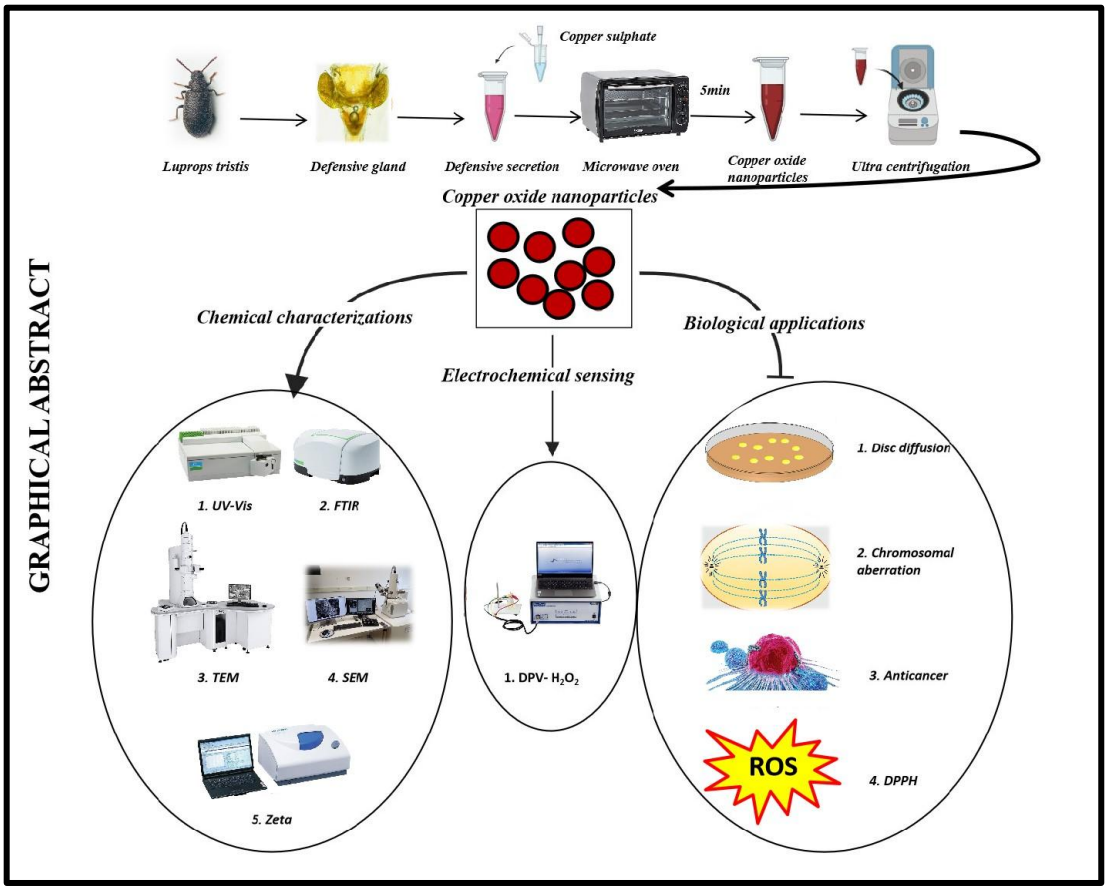
GRAPHICAL ABSTRACT
Copper sulphate
5min
Luprops tristis
Defensive gland
Defensive secretion
Microwave oven
Copper oxide nanoparticles
Ultra centrifugation
Copper oxide nanoparticles
Chemical characterizations
Biological applications
Electrochemical sensing
1. UV-Vis
2. FTIR
3. TEM
4. SEM
5. Zeta
1. DPV- H_2O_2
1. Disc diffusion
2. Chromosomal aberration
3. Anticancer
ROS
4. DPPH

4.3. Bio-synthesis of Copper Oxide Nanoparticles Using Beetle defensive gland Extract: Exploring Diverse Applications.

Biosynthesis of CuONPs is a multi-step process in which copper ions in various forms are oxidized using plant, fungal, algal, bacterial extracts and protista. This method ensures consistency in producing various copper oxide phases such as CuO, Cu_2O, and Cu_4O_3. In this study, we utilize compounds present in the defensive secretion of the insect *Luprops tristis* defensive gland extract, which can reduce Cu^{2+} ions to Cu^0 and then oxidize them to form nanoparticles. These LCuONPs are further characterized by UV, FTIR, SEM, TEM, and ZETA, followed by the investigation focusing on exploring the diverse biological applications of these nanoparticles, including hydrogen peroxide sensing, antibacterial analysis, antioxidant activity, antimitotic effects, and anticancer properties.

4.3.1. UV-Visible Spectroscopy of LCuONPs

The visual colour change of the reaction mixture, transitioning from purple to reddish-brown as illustrated in Fig. IV. III. 1. (a-b), after a 15-min exposure to microwave irradiation, signaled the initial formation of LCuONPs. This observation was further confirmed using UV-visible spectroscopy. The shift in colour of the reactive mixture, attributed to the occurrence of surface plasmon resonance (Fig. IV. III. 1), provided a clear indication of LCuONPs formation. Specifically, the prominent absorption peak at a wavelength (λ_{max}) of 218 nm, associated with the surface plasmon resonance phenomenon, served as a reliable marker for LCuONPs formation.

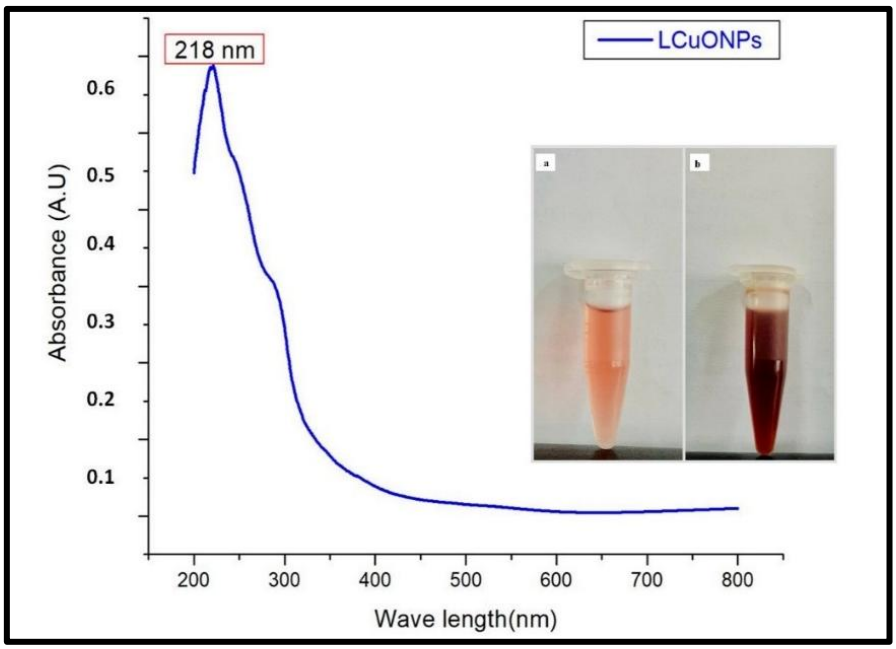

Figure IV. III. 1: UV spectrum of LCuONPs, a, b) colour transitions during microwave irradiation.

4.3.2. FTIR Analysis of LCuONPs

The process of identifying functional groups involved in the bio-synthesized LCuONPs was conducted through FT-IR spectroscopy. The recorded absorption peaks are delineated in Fig IV. III. 2, spanned a range from 4000 cm^{-1} to 400 cm^{-1}. Especially, the spectrum exhibited prominent peaks at 1500 cm^{-1}, indicating the existence of metabolites in the vicinity of copper oxide nanoparticles that were synthesized. The results showed the following peaks at 2906 cm^{-1} (C-H stretch), 2926 cm^{-1} (C-H stretch), 1650 cm-1 (C=O), 1432 cm^{-1} (C-H and O-H), and 1250 cm^{-1} (C-O stretch).

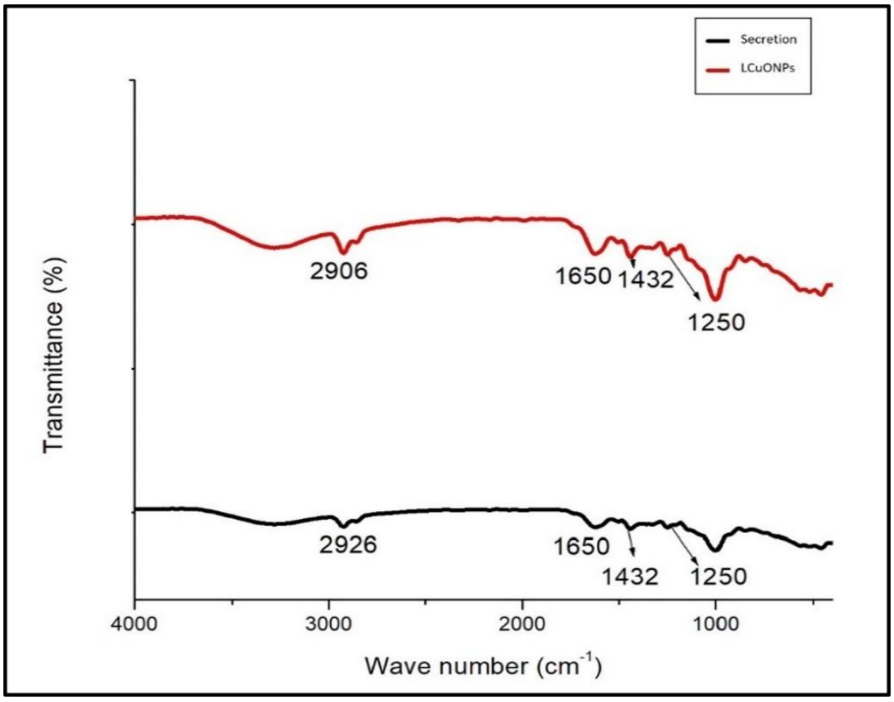

Figure IV. III. 2: Spectroscopic analysis of the LCuONPs: FTIR spectrum of LCuONPs

4.3.3. Scanning Electron Microscopy (SEM) & Transmission Electron Microscopy (TEM) of LCuONPs.

The examination of NPs morphology employed scanning electron microscopy, as shown in IV. III. 3 (A). The SEM images provided a clear depiction of the significant density of LCuONPs produced via the defensive gland extract of *L. tristis.* A detailed analysis of the biosynthesized LCuONPs was done using Transmission Electron Microscopy (TEM), shown in IV. III. 3(B). This was found to yield an average nanoparticle size of approximately 15 nm (Figure IV. III. 3(C)). These LCuONPs were found to have a largely spherical morphology, with a surface texture that was rugged and a uniform dispersion, as identifiable in IV. III. 3(B). There was also a tendency for individual nanoparticles to group together, leading to the formation of larger nanoparticle structures. The LCuONPs were attributed to hydrogen bonding and electrostatic interactions between bio-organic compounds. SEM and TEM images reveal that the particles are uniformly distributed and possess a crystalline structure.

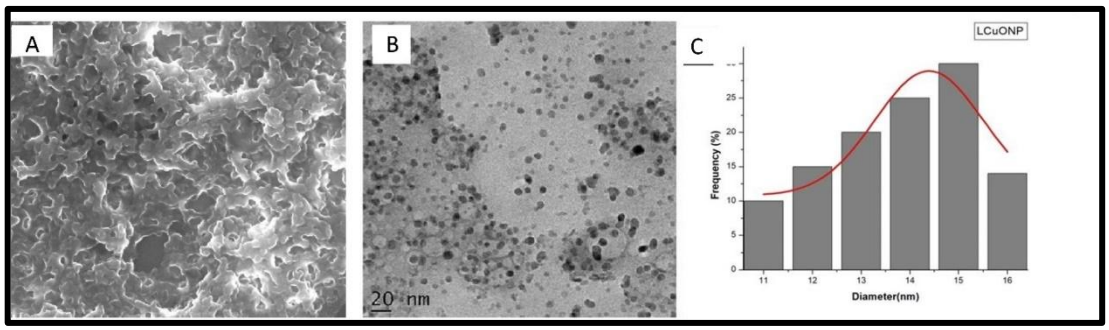

IV. III. 3: A) SEM image of LCuONPs B) TEM image of LCuONPs (C) Average particle size.

4.3.4. Zeta Potential Analysis of LCuONPs

To assess the stability of the biosynthesized LCuONPs, a nanoparticle analyzer (HORIBA SCIENTIFIC SZ 100) was used. The analysis revealed significant stability, with the LCuONPs showing a Zeta Potential of -22 mV, as depicted in Figure. IV. III. 4. This finding highlights the commendable stability of our prepared LCuONPs. The Zeta Potential measurement provides valuable information about the charge and stability of NPs indicating favourable characteristics for potential applications.

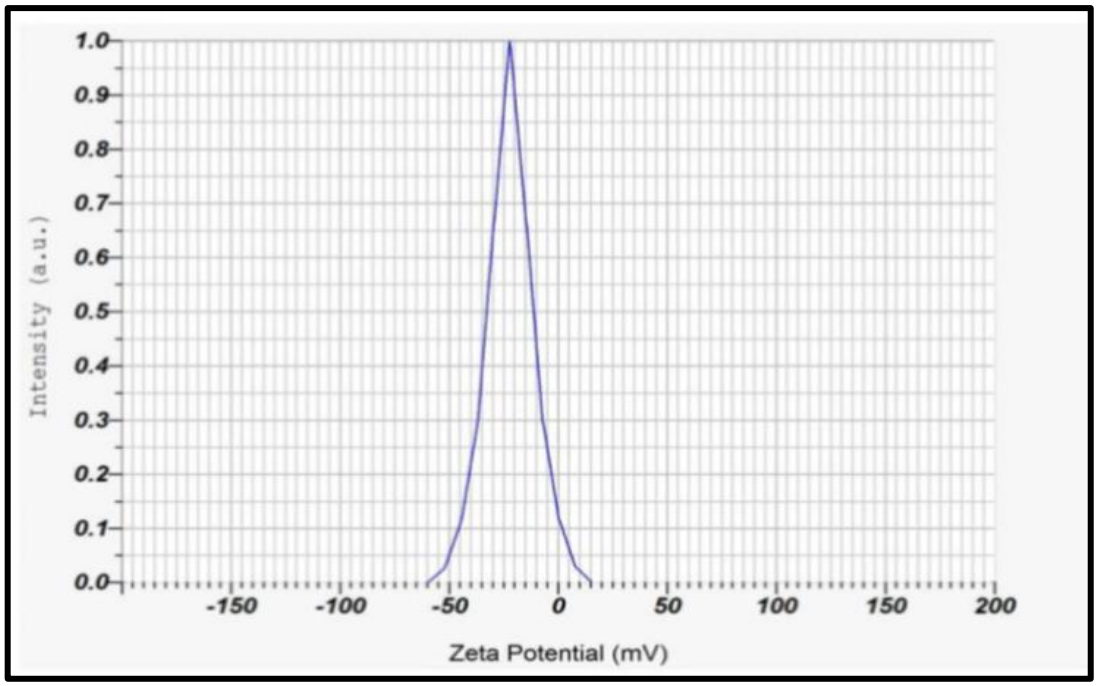

Figure. IV. III. 4: Zeta potential of LCuONPs

4.3.5. Electrochemical hydrogen peroxide sensing by Differential pulse voltammetry of LCuONPs.

In this inquiry, from the differential pulse voltammetry (DPV) graph (Figure IV. III. 5A), the electrochemical response of the LCuONPs-coated electrode was analyzed at various concentrations of H_2O_2. The concentrations tested include 10 mM, 20 mM, 30 mM, 40 mM, 50 mM and 60 mM of H_2O_2. At 10 mM, the peak current was approximately 4.5×10^{-6} A, which increased to 5.3×10^{-6} A at 20 mM. Similarly, for 30 mM, the peak current rose further to 6.1×10^{-6} A, and at 40 mM, it reached 6.8×10^{-6} A, at 50 mM, it reached 7.2 x 10^{-6} A. The highest concentration tested, 60 µg/mL, exhibited the maximum peak current of approximately 7.5×10^{-6} A. These results indicate a clear trend where the peak current increases linearly with the concentration of H_2O_2, as reflected in the calibration curve (Figure IV. III. 5B). The calibration curve shows a strong linear correlation, confirming the sensitivity of the LCuONPs-coated electrode for H_2O_2 detection within the tested range as LOD of 0.9 mM.

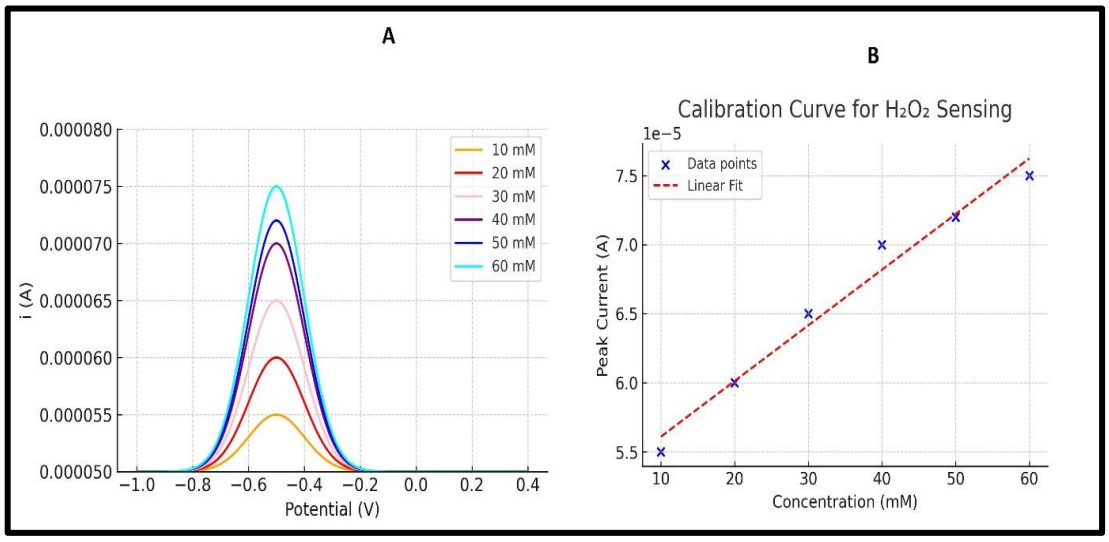

Figure IV. III. 5: (A, B). Hydrogen peroxide sensing by Differential pulse voltammetry DPV measurement of the LCuONPs-coated electrode at different concentrations of H_2O_2 (a) and calibration curve (b).

4.3.6. Antibacterial Assessment of LCuONPs.

Disc diffusion assay was employed to scrutinize the antibacterial attributes. The impact of LCuONPs on the proliferation of both Gram-negative bacteria (*K. pneumoniae*) and Gram-positive bacteria (*S. aureus*) was evaluated. Filter papers with different concentrations of LCuONPs (5 µg/mL, 10 µg/mL, 15 µg/mL, and 20 µg/mL) resulted in inhibition zones ranging from 6.66 ± 0.57 mm, 9.66 ± 0.57 mm, 8.33 ± 0.57 mm, to 11.12 ± 0.57 mm for *K. pneumoniae,* as shown in Fig. IV. III. 6 (a, b). For *S. aureus,* filter papers with 5 µg/mL, 10 µg/mL, 15 µg/mL, and 20 µg/mL of LCuONPs had inhibition zone diameters of 10.33 ± 0.57 mm, 12.66 ± 0.57 mm, 14.66 ± 0.57 mm, and 17.33 ± 0.57 mm, respectively. This pattern signifies a progressive augmentation in the inhibition zone's diameter with an escalating concentration of LCuONPs.

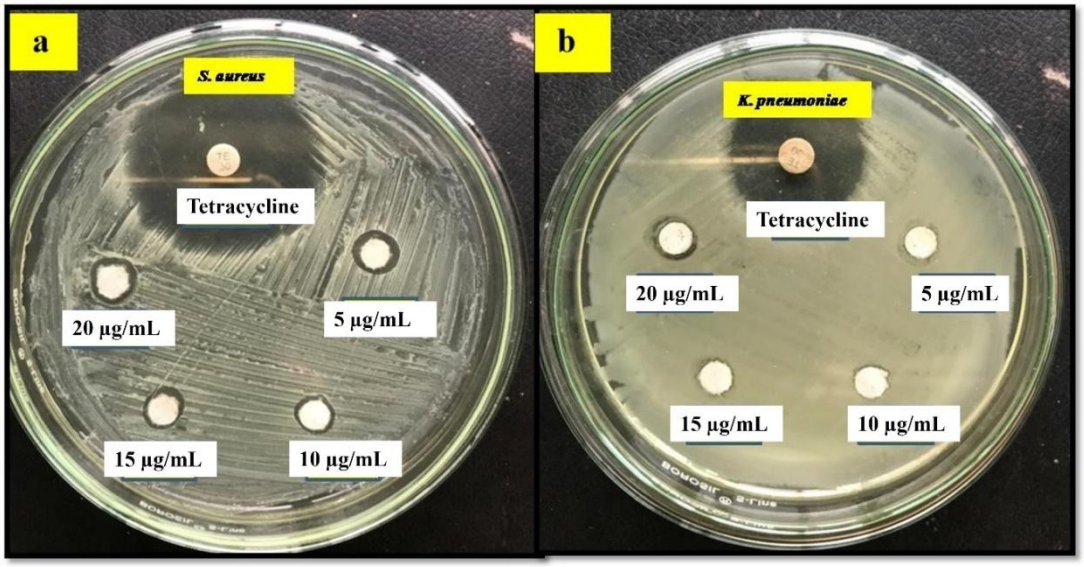

Figure IV. III. 6: Disc diffusion assay of LCuONPs (a, b): action of LCuONPs on *S. aureus* (a) action of LCuONPs on *K. pneumonia* (b).

Table IV. III. 1: Comparison of bactericidal activity of LCuONPs.

Treatment	Concentration (µg/mL)	*S. aureus* (mm ± SD)	*K. pneumoniae* (mm ± SD)
Control	20 µg/mL	10. 23 ± 0.57	6.33 ± 0.57
Experiment (LCuONPs)	5 µg/mL	10. 76 ± 0.57	6.66 ± 0.57
	10 µg/mL	12. 16 ± 0.57	9.66 ± 0.57
	15 µg/mL	14. 23 ± 0.57	8.33 ± 0.57
	20 µg/mL	17. 12 ± 0.57	11.12 ± 0.57

4.3.7 Antioxidant activity of LCuONPs

The DPPH assay, extensively recognized for its efficacy in assessing the capability of NPs to neutralize free radicals, has been widely utilized in the assessment of antioxidant potential. Various concentrations of LCuONPs (20 µg/mL,40 µg/mL, 60 µg/mL, 80 µg/mL, and 100 µg/mL) were used in this research, and every sample was combined with DPPH to yield 2 ml solutions. Ascorbic acid, employed as the standard, was made soluble in purified water as the solvent. After a 30-min incubation period under conditions of darkness, the solution underwent UV spectroscopic examination. At 517 nm, the maximum absorption caused by DPPH free radicals was observed. The concentration-dependent scavenging behaviour of LCuONPs is 57% at 20 µg/mL, 60 % at 40 µg/mL, 63% at 60 µg/mL, 66% at 80 µg/mL and 70% at 100 µg/mL detailed in Fig. IV. III. 7 (A, B). It was found that 74 µg/mL of sample concentration was required to produce 50% scavenging activity (EC_{50} value). Notably, with an escalation in the concentration of LCuONPs, the colour of the DPPH solution transitioned from a deep violet hue to a pale-yellow shade. UV spectroscopic analysis substantiated the amplified antioxidant efficacy of LCuONPs at higher concentrations, as delineated in the graph.

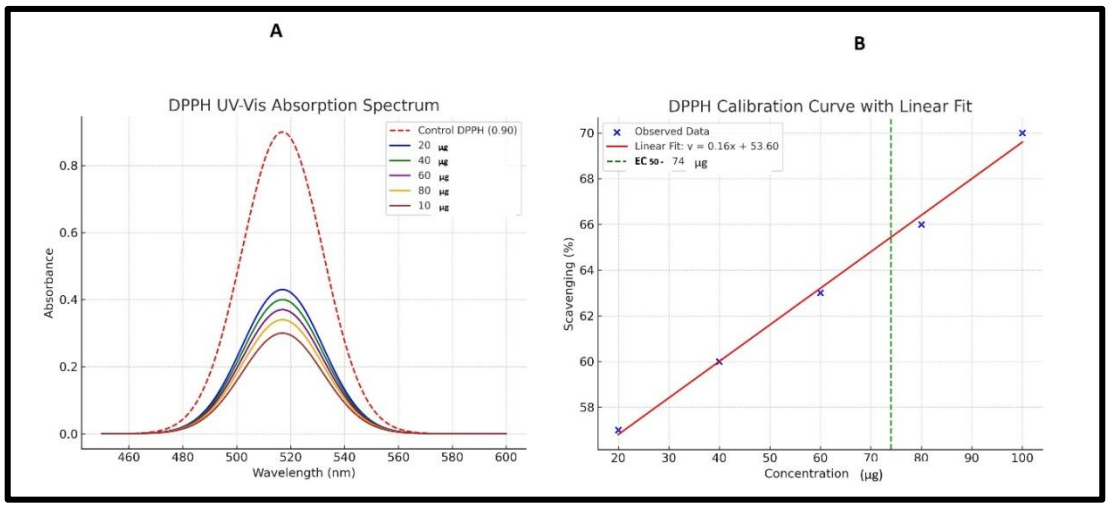

Figure. IV. III. 7: DPPH assay (A, B): activity of LCuONPs at different concentration of LCuONPs (A) & Calibration curve (B).

4.3.8 Environmental hazard testing assay of LCuONPs

Biosynthesized LCuONPs induced dose-dependent chromosomal aberrations in *Allium cepa*, including anaphase stickiness, chromosome bridges, and lag chromosomes. The mitotic index (MI) decreased with increasing concentrations, from 16% at 100 µg/mL to 12% at 500 µg/mL, while chromosomal aberrations rose from 8% to 12%, indicating cytotoxic and genotoxic effects.

However, compared to chemically synthesized nanoparticles, the biosynthesized LCuONPs exhibited relatively higher MI and lower chromosomal aberrations, suggesting greater biocompatibility at lower concentrations. The control group (distilled water) showed no chromosomal abnormalities, confirming the dose-dependent effect of LCuONPs as in Figure. IV. III. 8.

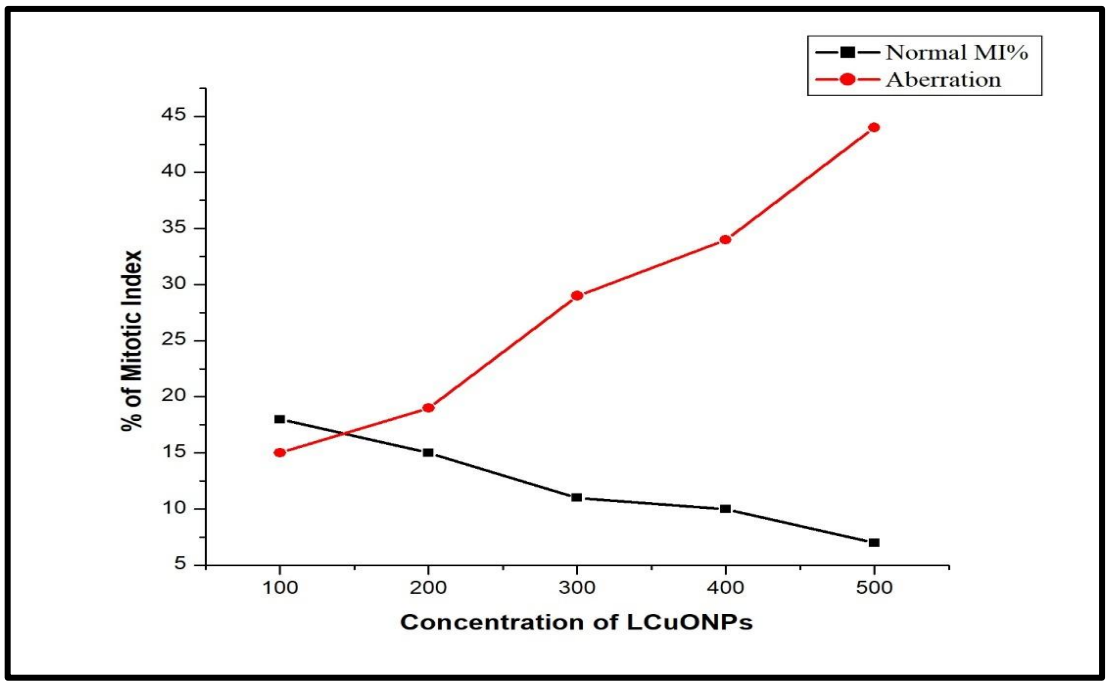

Figure. IV. III. 8: Comparison of increase in Chromosomal aberration and decrease in MI.

Table IV. III. 2: Effect of LCuONPs on *Allium cepa*

Treatment	Concentration (µg/mL)	Mitotic Index (% ± SD)	Chromosomal Aberration (%±SD)
Control (Distilled water)	100 µg/mL	11.41 ± 0 .21	NIL
	200 µg/mL	12.69 ± 0.21	NIL
	300 µg/mL	13.14 ± 0.21	NIL
	400 µg/mL	14.79 ± 0.21	NIL
	500 µg/mL	15.24 ± 0.21	NIL
Experiment (LCuONPs)	100 µg/mL	16 ± 0.03	8 ± 0.03
	200 µg/mL	15 ± 0.03	9 ± 0.03
	300 µg/mL	14.8 ± 0.03	10 ± 0.03
	400 µg/mL	13 ± 0.03	11 ± 0.03
	500 µg/mL	12 ± 0.03	12 ± 0.03

4.3.9 Anticancer study of LCuONPs

The LCuONPs demonstrate dose-dependent cytotoxicity against DLA cells. The assay reveals a progressive escalation in cellular demise commensurate with the concentration of LCuONPs (Figure. IV. III**.** 9 and Table. IV. III. 3). The table shows the anticancer activity of LCuONP at different concentrations as 10 µg/mL, 20 µg/mL, 50 µg/mL, 100 µg/mL, and 200 µg/mL, measured as the percentage of cell death in a cancer cell assay. The results demonstrate a concentration-dependent increase in cytotoxicity, indicating that higher concentrations of LCuONPs lead to greater cell death.

At the lowest concentration of 10 µg/mL, the percentage of cell death is 15.1% ± 1.34, reflecting minimal cytotoxicity. As the concentration increases to 20 µg/mL, the percentage of cell death rises to 20.8% ± 1.33. At 50 µg/mL, a significant increase in cytotoxicity is observed, with 32.0% ± 1.01 of the cells dying. When the concentration reaches 100 µg/mL, the percentage of cell death jumps to 54.9% ± 4.75, indicating strong anticancer activity. At the highest tested concentration of 200 µg/mL, the percentage of cell death is 75.9% ± 1.78, demonstrating the maximum observed cytotoxic effect.

Table IV. III. 3: Anticancer activity of LCuONPs on DLA cells.

Concentration of LCuONPs (µg/mL)	% of cell death
10	15.1 ± 1.34
20	20.8 ± 1.33
50	32.0 ± 1.01
100	54.9 ± 4.75
200	75.9 ± 1.78

These results confirm the potent anticancer potential of LCuONPs, with effectiveness increasing proportionally to the concentration. This concentration-dependent cytotoxicity suggests that LCuONPs could serve as a promising agent in cancer treatment. The present investigation affirms that biologically synthesized LCuONPs possess comprehensive anti-cancer properties.

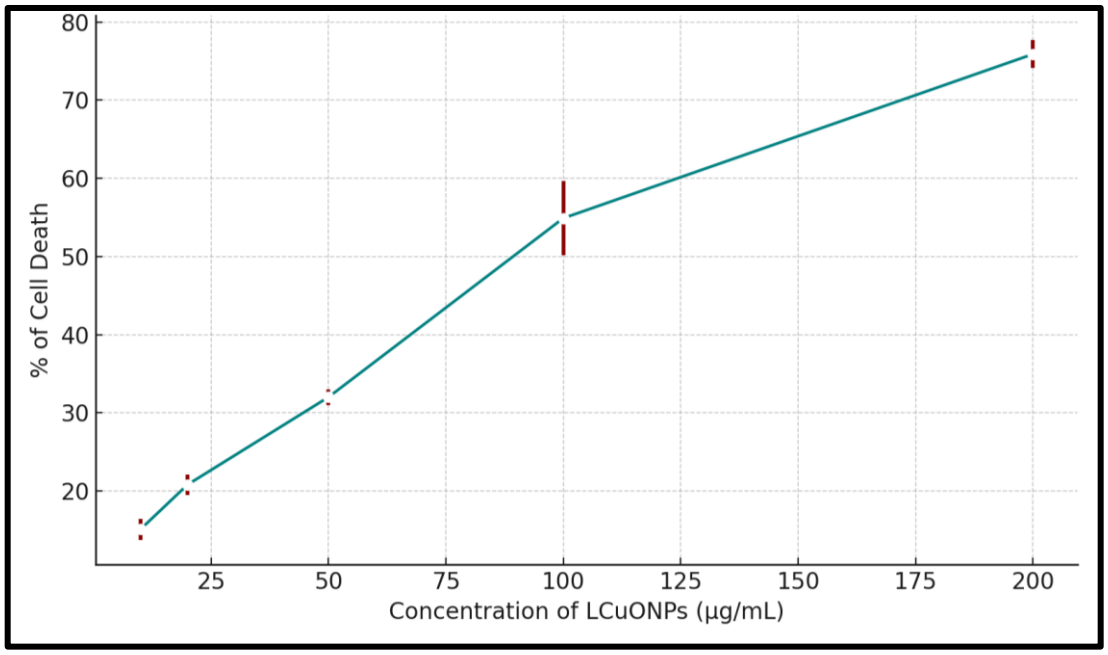

Figure. IV. III. 9: Graph showing effect of LCuONP on DLA cells

4.3.10. CAM assay of LCuONPs

The angiogenesis assay was conducted successfully, providing clear evidence of the effect of *Luprops tristis*-mediated LCuONPs on the vascular development of chick embryos. The treated embryos exhibited significant reductions in vessel growth parameters compared to the PBS control, which allowed for a detailed analysis of the anti-angiogenic properties of the NPs. The study focused on investigating the effect of copper oxide nanoparticles (CuONPs), sourced from beetle defensive gland secretions, on angiogenesis using a 48-hour chick embryo model (Figure. IV. III 10). By applying 5 µg of CuONPs on a filter paper disc, we assessed the inhibitory effect of these nanoparticles on blood vessel formation over time (Figure. IV. III**.** 11 A, B & C).

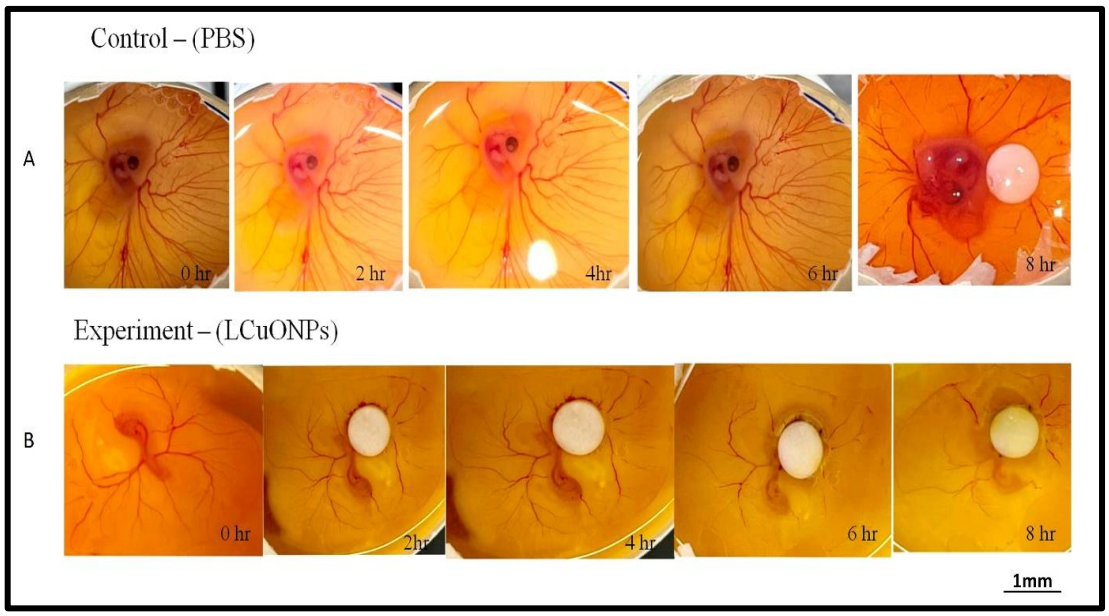

Figure. IV. III. 10: CAM assay showing antiangiogenic activity of LCuONPs with decreased blood vessel growth.

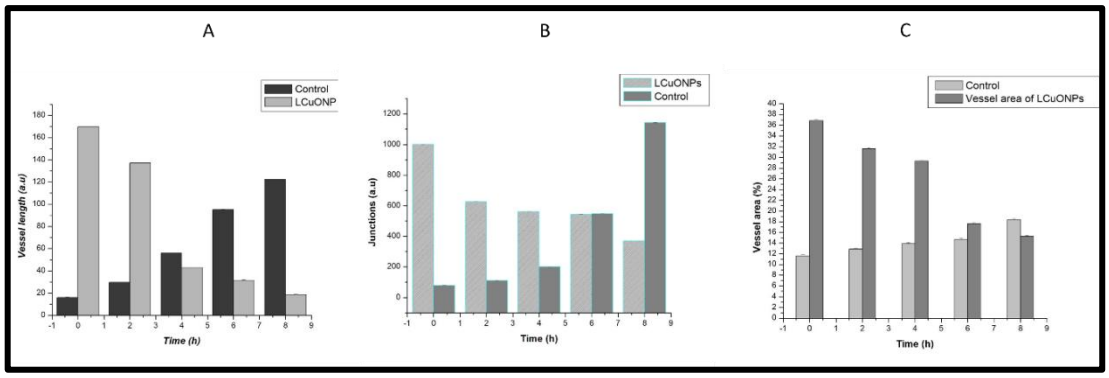

Figure. IV. III. 11: A) CAM assay showing Vessel length relative to time B) CAM assay showing Vessel junctions relative to time C) CAM assay showing Vessel area relative to time

The LCuONPs-treated group exhibited a strong inhibitory effect on angiogenesis in chick embryos, as evidenced by reductions in vessel length, vascular junctions, and vessel area over time. Initially, vessel length in the LCuONPs group was higher during the early hours (0–2 hours) but sharply declined after 3 hours, contrasting with the control group (PBS-treated), which showed steady vessel elongation peaking at 7–8 hours. Similarly, the number of vascular junctions in the LCuONPs-treated embryos was consistently lower than the control throughout the observation period, with the control group displaying a peak at 8 hours. This

reduction in vascular junctions underscores the nanoparticles' impact on limiting the branching and interconnectedness of blood vessels. In terms of vessel area, the LCuONPs-treated group initially exhibited larger areas during the early phase (0–4 hours), likely due to vessel dilation or abnormal growth, but this trend reversed after 4 hours, with the vessel area becoming smaller than the control by 7–8 hours (Figure IV. III 11 A, B and C). These combined effects suggest that LCuONPs disrupt the normal process of blood vessel formation and the development of a functional vascular network, leading to embryo death due to insufficient oxygen and nutrient supply. In contrast, the PBS-treated control group demonstrated robust angiogenesis, characterized by steady vessel formation, branching, and growth throughout the 8 hours, reflecting normal vascular development. The observed anti-angiogenic effects of LCuONPs highlight their potential applications in cancer research, where inhibiting angiogenesis could be a strategy to prevent tumor growth and metastasis.

RESULT 4

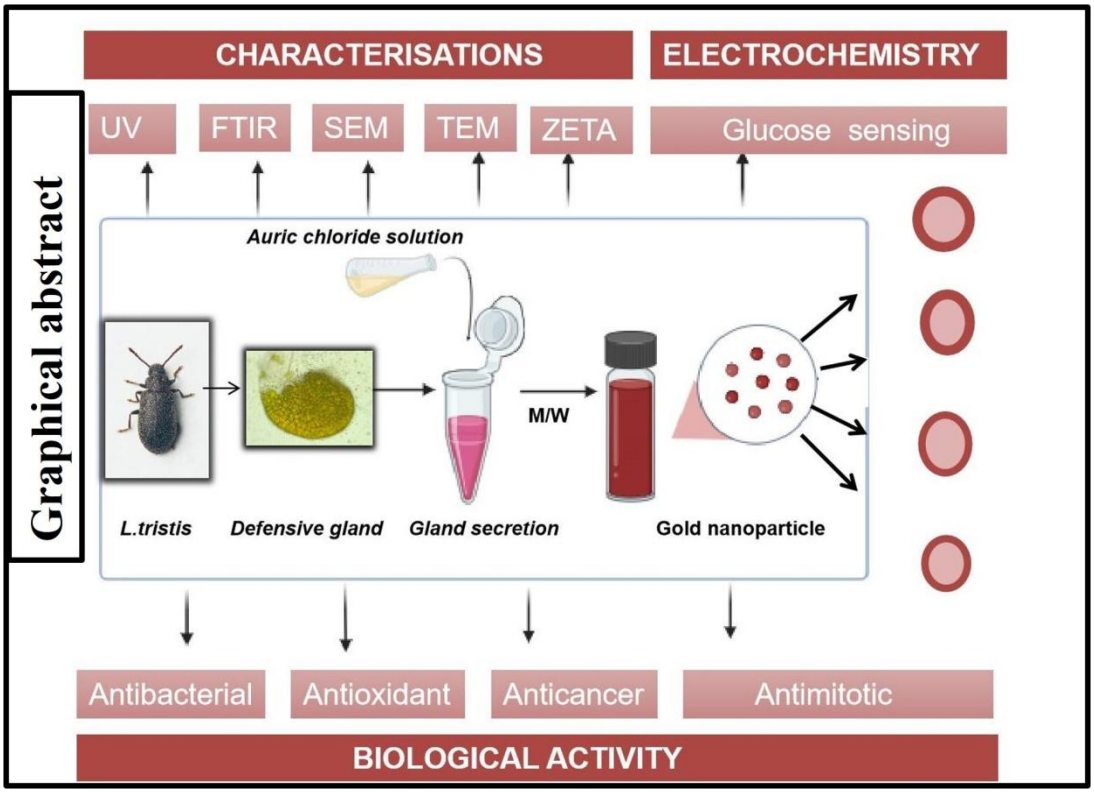
Graphical abstract
CHARACTERISATIONS
ELECTROCHEMISTRY
UV
FTIR
SEM
TEM
ZETA
Glucose sensing
Auric chloride solution
M/W
L.tristis
Defensive gland
Gland secretion
Gold nanoparticle
Antibacterial
Antioxidant
Anticancer
Antimitotic
BIOLOGICAL ACTIVITY

4.4. Harnessing *Luprops tristis* Defensive Secretion for Gold Nanoparticle Synthesis and Its Remarkable Biological Uses

The reduction of auric chloride ($AuCl_4^-$) using an extract from the defensive gland of the insect *Luprops tristis* led to the synthesis of gold nanoparticles, termed LAuNPs. These nanoparticles were thoroughly characterized using advanced techniques such as UV-Vis spectroscopy, FTIR, SEM, TEM, and zeta potential analysis. Following characterization, their potential biomedical applications were explored, including glucose sensing, antibacterial activity, antioxidant properties, antimitotic effects, and anticancer activity. The findings of this study highlight the versatility and efficacy of LAuNPs, underscoring their potential for significant contributions to the biomedical field.

4.4.1. UV- Spectroscopy of LAuNPs

The reaction mixture's obvious colour change from purple to reddish brown (as shown in Figure. IV. IV. 1), which took place after a 15-min. exposure to microwave radiation was the first indication that LAuNPs was formed. Figure. IV. IV. 1, also demonstrates how UV-Visible spectroscopic analysis was utilized to corroborate this observation further. The surface plasmon resonance phenomenon was the cause of the LAuNPs' apparent absorption peak at 563 nm. This occurrence serves as a trustworthy predictor of LAuNPs formation.

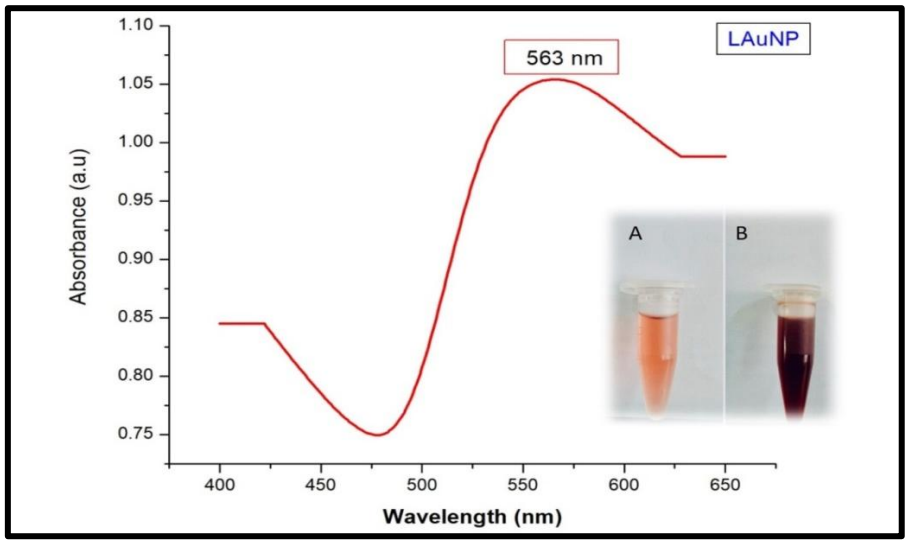

Figure. IV. IV. 1: UV-Vis spectrum of LAuNPs and colour transition during microwave irradiation.

4.4.2. FTIR analysis of LAuNPs

FT-IR spectroscopy was used to identify the functional groups involved in the biosynthesis of LAuNPs. The observed absorption peaks spanned from 4000 cm^{-1} to 400 cm^{-1}, as depicted in Figure. IV. IV. 2. Notably, the spectra exhibited prominent peaks at 3200 cm^{-1}, 1600 cm^{-1}, 1700 cm^{-1} and 1100cm^{-1}, signifying the existence of metabolites near the synthetic gold nanoparticles, including OH, N-H, COOH and C=O groups. FTIR analysis confirmed the significant role of phenolic compounds in stabilizing LAuNPs and their likelihood of interaction with them.

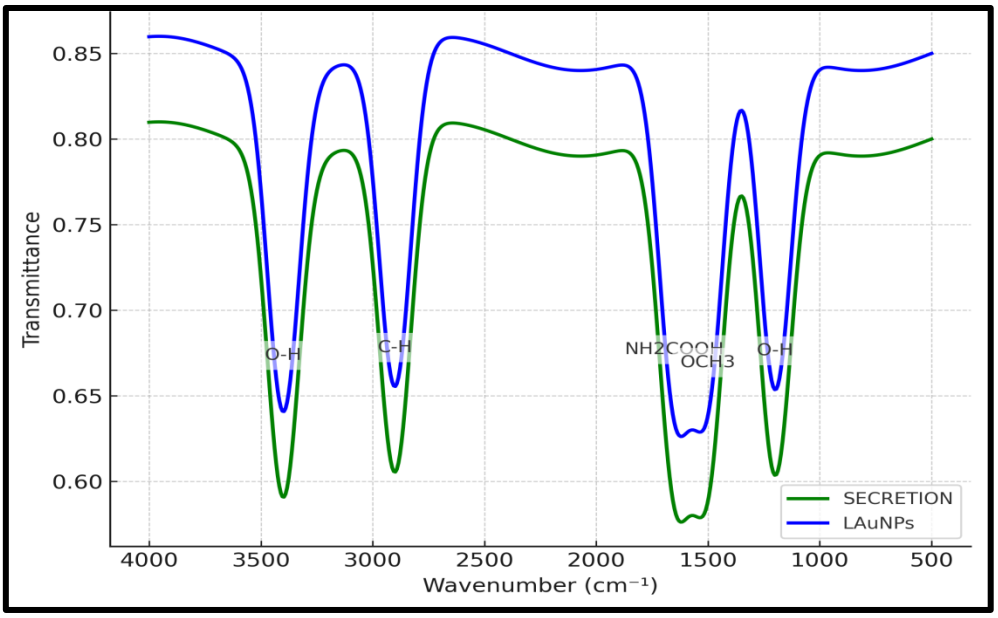

Figure. IV. IV. 2: FTIR specrum of LAuNPs

4.4.3. SEM and TEM analysis of LAuNPs

The SEM image provided a clear representation of the significant density of LAuNPs produced by the *L. tristis* defensive gland extract (Figure. IV. IV. 3A). According to Figure. IV. IV. 3B, these AuNPs had a mostly spherical shape with a rough surface texture and a uniform dispersion and 17 nm size is observed by TEM (Figure. IV. III. 3C). Additionally, individual nanoparticles tended to group and create bigger nanoparticle formations.

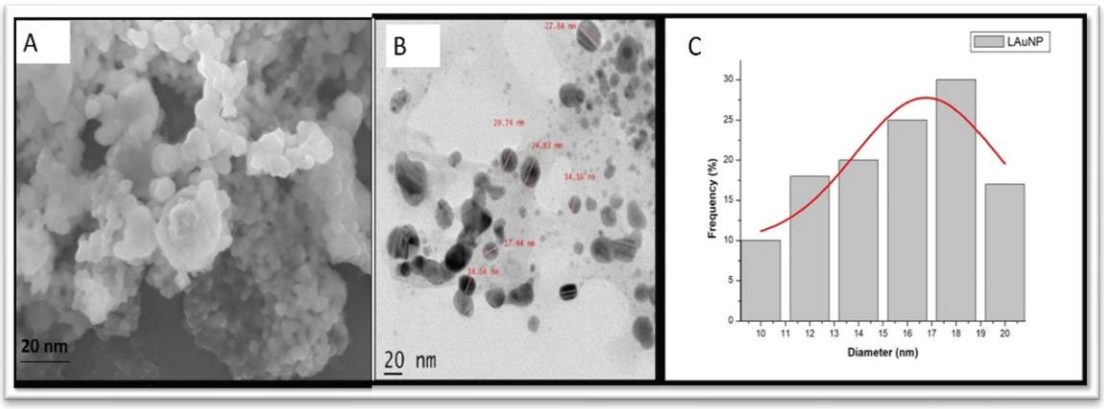

Figure. IV. IV. 3: (A) SEM images of LAuNPs, (B) TEM images of LAuNPs. (C) Average particle size

4.4.4. Zeta Potential Analysis of LAuNPs

The stability of the LAuNPs was employed by a nanoparticle analyzer (HORIBA SCIENTIFIC SZ 100) to assess the stability of the *L. tristis-mediated* LAuNPs. The findings revealed substantial stability, with a Zeta Potential of -21.4 mV for the LAuNPs, as illustrated in Figure. IV. IV. 4.

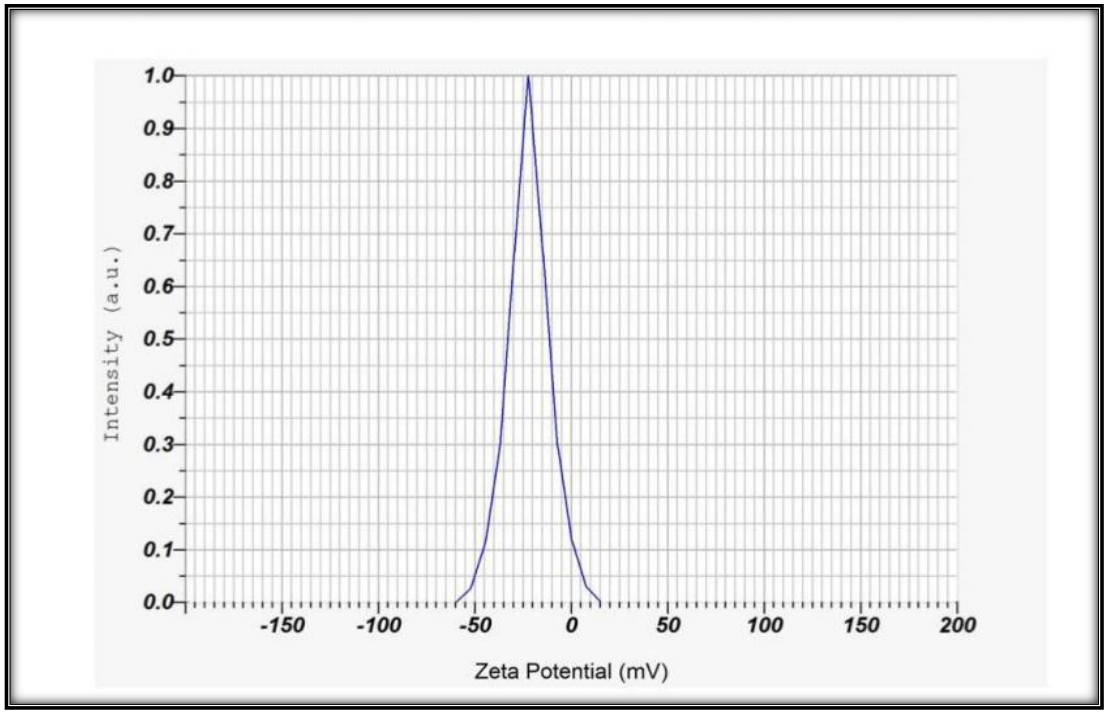

Figure. IV. IV. 4: Zeta potential measurement of LAuNPs

4.4.5. Glucose sensing property of LAuNPs

The study involved electrochemical glucose sensing using Differential Pulse Voltammetry (DPV). Figure. IV. IV. 5A presents the findings from a series of experiments conducted with 3M glucose concentrations ranging from 10 mM to 60 mM. Additionally, as depicted in Figure. IV. IV. 5B, linear calibration curves were established correlating DPV current output with glucose concentration. The lower limit of detection (LOD) was determined to be 7 mM. The LAuNPs synthesized in this study show promise for integration into electrochemical glucose monitoring systems. Functionalized LAuNPs can interact with glucose molecules, leading to detectable changes in electrical conductivity or redox processes that can be correlated with glucose levels.

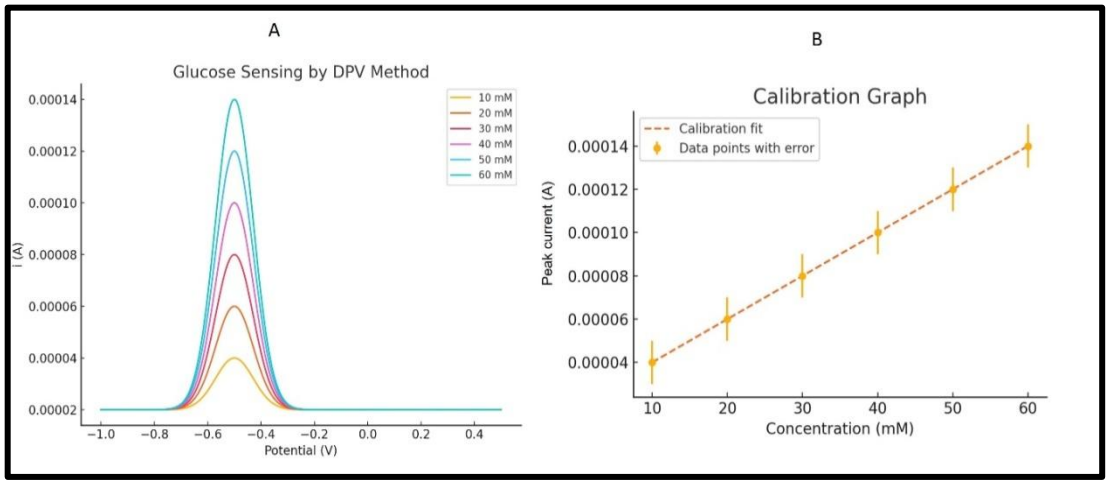

Figure. IV. IV. 5: A) DPV graph of LAuNPs-coated electrode B) Calibration curve of DPV of LAuNPs

4.4.6. Study on antibacterial activity of LAuNPs

The effects of LAuNPs on the growth of the microorganisms *Staphylococcus aureus* and *Klebsiella pneumoniae*, both of which are Gram-positive and negative, were assessed. The diameters of the inhibition zones for *K. pneumoniae*, however, revealed diameter of 7.33 mm, 9.5 mm, 11.16 mm, and 13.33 mm when filter papers impregnated with varied concentrations of LAuNPs (5µg, 10µg, 15µg and 20µg) were used (as shown in Figure. IV. IV. 6). The inhibition zone diameters on filter papers saturated with 5 µg, 10 µg, 15 µg, and 20 µg of LAuNPs were 13.23 mm,

15.76 mm, 17.16 mm, and 19.23 mm, respectively. This pattern indicates a progressive rise in the diameter of the inhibitory zone with an increase in LAuNPs concentration, as seen in Figure. IV. IV. 6 & Table IV. IV. 1. An increase in LAuNPs concentration results in an improved antimicrobial impact, especially when compared to *K. pneumoniae* and *S. aureus*.

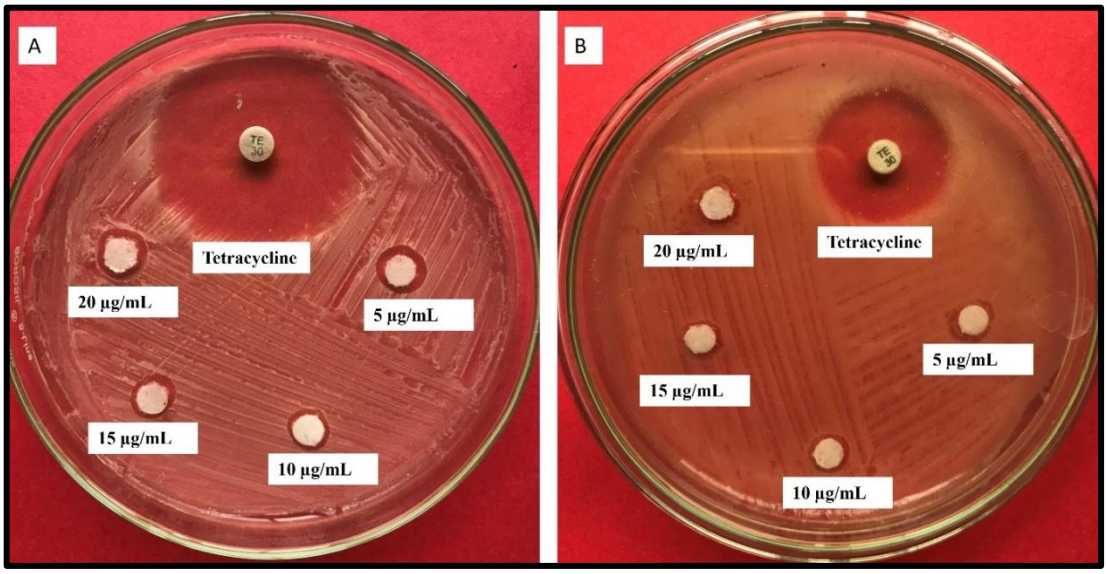

Figure. IV. IV. 6: Disc Diffusion assay of LAuNPs on *S. aureus* (A) and *K. Pneumoniae* (B).

Table IV. IV. 1: Antibacterial activity of LAuNPs

Treatment	Concentration (µg)	*S. aureus* (mm ± SD)	*K. pneumonia* (mm ± SD)
Experiment (LAuNPs)	5 µg	13. 23 ± 0.66	7.33 ± 0.66
	10 µg	15. 76 ± 0.66	9.5 ± 0.66
	15 µg	17. 16 ± 0.66	11.16 ± 0.66
	20 µg	19. 23 ± 0.66	13.33 ± 0.66

4.4.7. Antioxidant activity of LAuNPs

The DPPH assay is widely used to assess antioxidant capacity, particularly in evaluating nanoparticles' antioxidant activity. In this study, various concentrations of LAuNPs (20 µg to 80 µg) were tested. DPPH was added to each sample to make up 2 mL solutions, with ascorbic acid as the reference material and pure water as the

solvent. After incubating in complete darkness for 30 minutes, the solutions were analyzed using UV spectroscopy, detecting the highest absorption of DPPH free radical electrons at 517 nm. Figure. IV. IV. 7A. illustrates the concentration-dependent scavenging activity of LAuNPs. The EC_{50} value was determined to be 39 µg based on the calibration curve (Figure. IV. IV. 7B). Notably, as the concentration of LAuNPs increased, the DPPH solution changed colour from deep violet to light yellow., confirming enhanced antioxidant activity of LAuNPs validated by UV spectroscopic analysis.

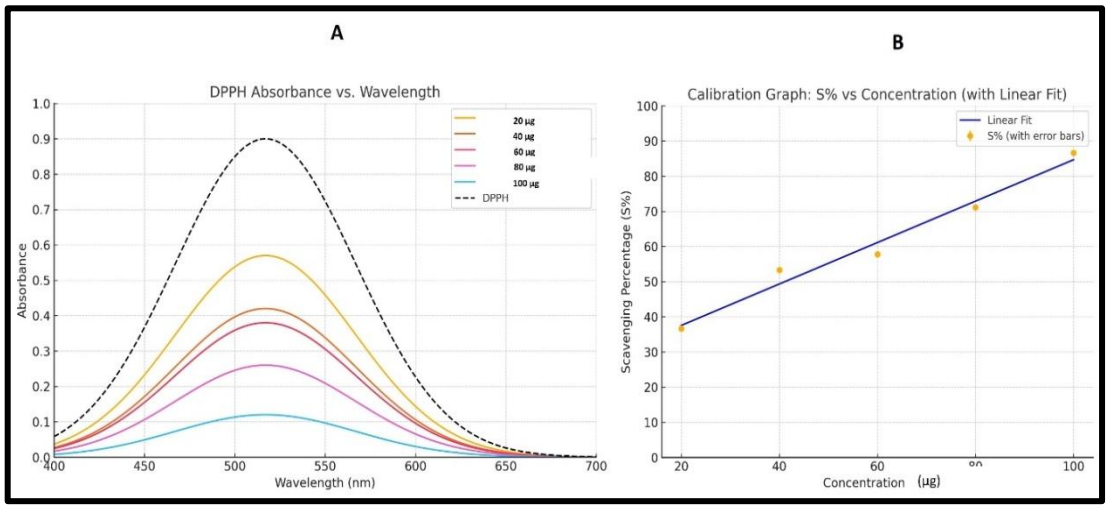

Figure. IV. IV. 7: A) DPPH Assay of LAuNPs. B) Calibration curve of DPPH of LAuNPs.

4.4.8. Environmental hazard testing of LAuNPs

Biosynthesized LAuNPs exhibited a dose-dependent decrease in mitotic index (MI) and an increase in chromosomal aberrations (CA) in *Allium cepa*, indicating mild cytotoxic and genotoxic effects. MI declined from 14% at 100 µg/mL to 10% at 500 µg/mL, while CA increased from 7% to 11%, showing inhibition of cell division and chromosomal anomalies like vagrant chromosomes and anaphase stickiness represented in Figure. IV. IV. 8.

Compared to chemically synthesized nanoparticles, biosynthesized LAuNPs demonstrated lower genotoxicity within safe limits, suggesting higher biocompatibility and minimal environmental risk at controlled concentrations.

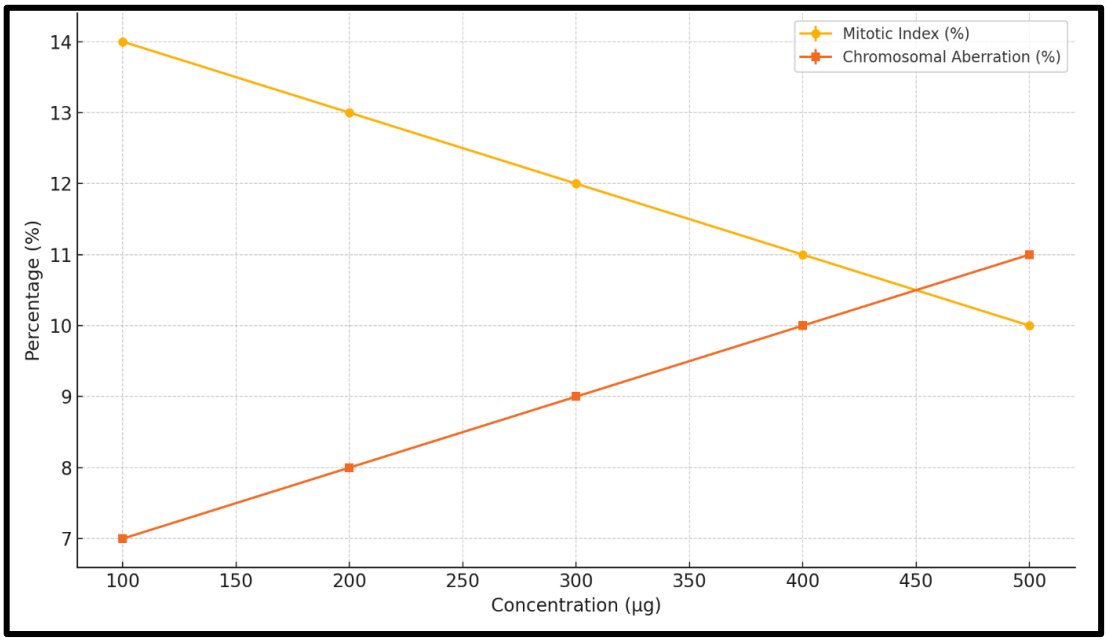

Figure. IV. IV. 8: Comparison of the effect of LAuNPs on mitosis

Table IV. IV. 3: Environmental hazard testing of LAuNPs

Treatment	Concentration (µg/mL)	Mitotic Index (%±SD)	Chromosomal Aberration (%±SD)
Control (Distilled water)	100 µg/mL	10.51 ± 0.25	NIL
	200 µg/mL	11.59 ± 0.25	NIL
	300 µg/mL	12.04 ± 0.25	NIL
	400 µg/mL	13.19 ± 0.25	NIL
	500 µg/mL	14.14 ± 0.25	NIL
Experiment (Biosynthesized LAuNPs)	100 µg/mL	14 ± 0.05	7 ± 0.05
	200 µg/mL	13 ± 0.05	8 ± 0.05
	300 µg/mL	12 ± 0.05	9 ± 0.05
	400 µg/mL	11 ± 0.05	10 ± 0.05
	500 µg/mL	10 ± 0.05	11 ± 0.05

4.4.9. Anticancer assay of LAuNPs

Numerous NPs possess pharmacological and biochemical characteristics, such as antioxidant and anti-inflammatory qualities, which may contribute to their

anticarcinogenic and antimutagenic properties. Several disorders, including cancer, are currently treated with the help of biologically produced nanoparticles. The current study emphasises the potency of biologically produced AuNPs as an anticancer treatment using cell lines of Dalton's lymphoma ascites (DLA) in an *in vitro* setting. The LAuNPs cytotoxicity towards DLA cells is dose-dependent (Figure. IV. IV. 9). The test demonstrates that the rate of cellular death increases over time in direct proportion to the quantity of LAuNPs.

The cytotoxicity assessment of biosynthesized LAuNPs revealed a concentration-dependent increase in the percentage of cell death. At the lowest concentration of 10 µg/mL, the cell death was minimal at 4.67 ± 0.0%, indicating limited toxicity. However, as the concentration increased to 20 µg/mL, cell death rose moderately to 5.92 ± 1.5%, suggesting the onset of cytotoxic effects. A significant increase was observed at 50 µg/mL, with cell death reaching 11.6 ± 1.3%, nearly doubling from the previous concentration. At 100 µg/mL, the cytotoxicity intensified, with cell death recorded at 15.8 ± 1.4%, reflecting a pronounced effect of the nanoparticles. The highest concentration, 200 µg/mL, exhibited the maximum cytotoxicity, with cell death escalating to 24.8 ± 1.8%, which is more than five times the effect observed at the lowest concentration. These results indicate that LAuNPs exhibit dose-dependent cytotoxicity, likely due to the generation of reactive oxygen species or nanoparticle-induced interference with cellular mechanisms. The steep increase in cytotoxicity at higher concentrations underscores their potential as a targeted therapeutic agent, but also highlights the need for careful dose optimization to mitigate adverse effects.

Table IV. IV. 4: Anticancer activity of LAuNPs

Concentration of LAuNPs (µg/mL)	% of cell death
10	4.67 ± 0.
20	5.92 ± 1.5
50	11.6 ± 1.3
100	15.8 ± 1.4
200	24.8 ± 1.8

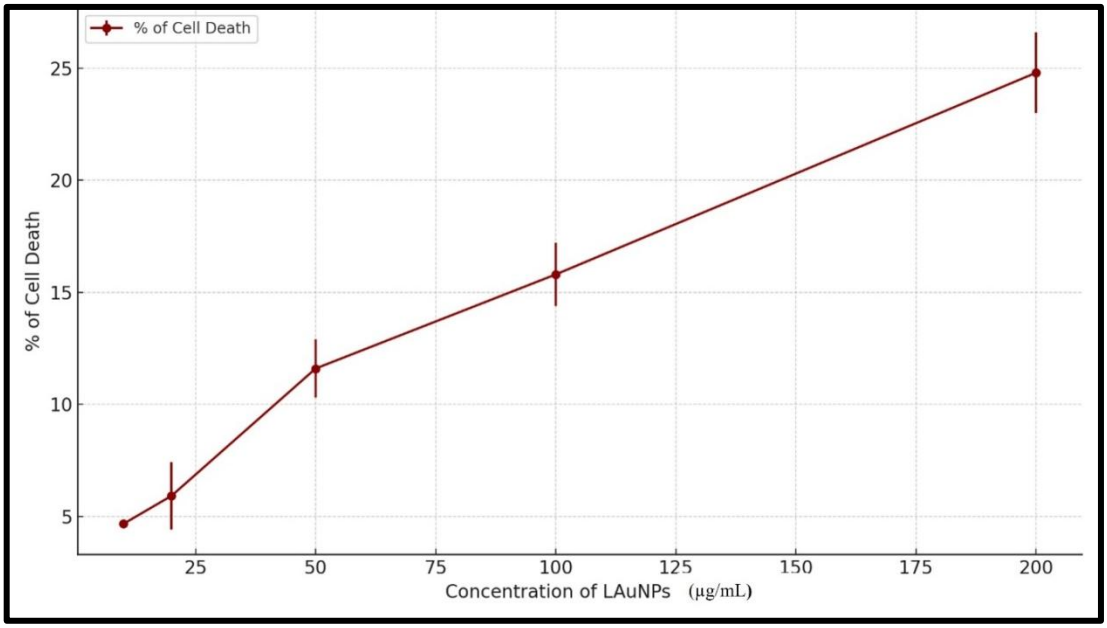

Figure. IV. IV. 9: Anticancer activity analysis

RESULT 5

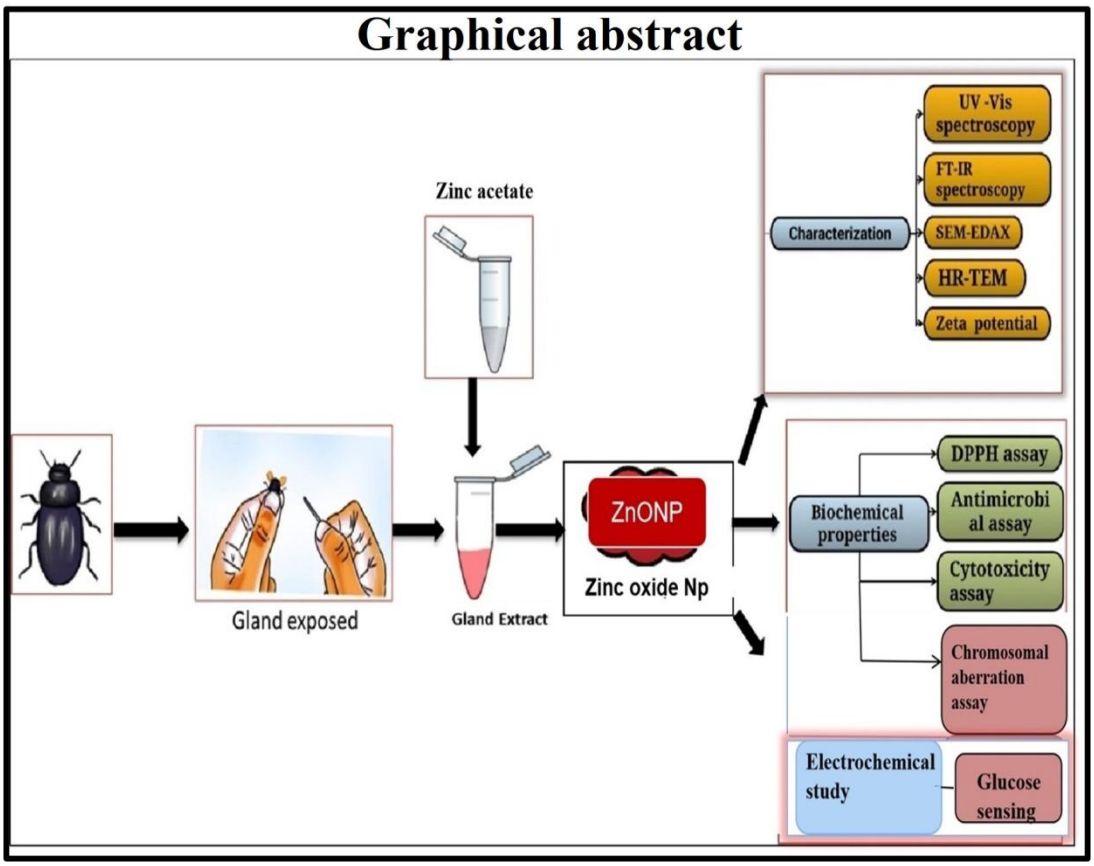
Graphical abstract
Zinc acetate
Gland exposed
Gland Extract
ZnONP
Zinc oxide Np
Characterization
UV -Vis spectroscopy
FT-IR spectroscopy
SEM-EDAX
HR-TEM
Zeta potential
Biochemical properties
DPPH assay
Antimicrobial assay
Cytotoxicity assay
Chromosomal aberration assay
Electrochemical study
Glucose sensing

4.5. Biosynthesis of Zinc Oxide Nanoparticles From *Luprops tristis* and their Diverse Applications

In this study, zinc oxide nanoparticles (referred to as LZnONPs) were produced using the reduction of a zinc acetate solution utilizing an extract derived from the defensive secretion of the *L. tristis* insect. After the chemical characterization employing methodologies such as UV-Vis spectroscopy, Fourier-transform infrared spectroscopy (FTIR), Electron Microscopy (SEM and TEM), and Zeta potential assessment, the investigation proceeded to scrutinize its biological applications, encompassing glucose sensing, antibacterial analysis, antioxidant activity, antimitotic activity, and anticancer activity.

4.5.1. Synthesis of LZnONPs and preliminary characterisation by UV-Visible spectroscopic Analysis

The perceptible shift in the shade of the reaction solution, shifting from violet to reddish-brown (as exemplified in Figure IV. V. 1), after a 15-minute exposure to microwave irradiation constituted the initial indication of LZnONPs formation. This observation was further substantiated through UV-visible spectroscopic analysis, as depicted in Figure IV. V. 1. LZnONPs exhibited a prominent absorption peak at λ_{max} 378 nm, attributed to the surface plasmon resonance phenomenon. This phenomenon serves as a dependable indicator of LZnONPs formation.

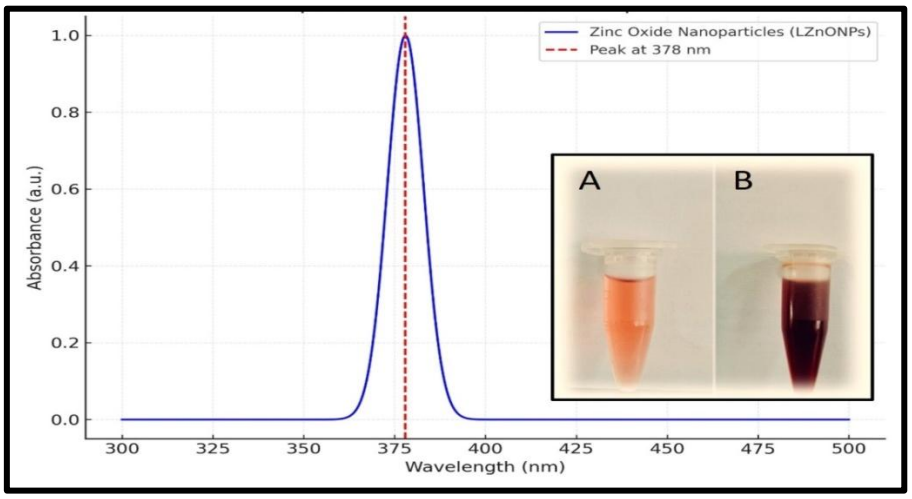

Figure IV. V. 1: UV-Vis spectrum of LZnONPs

4.5.2. Fourier-Transform Infrared Spectroscopic Analysis of LZnONPs

The determination of functional groups in the biosynthetic process of ZnNOPs was conducted using FT-IR spectroscopy, with absorption peaks recorded across a spectrum ranging from 4000 cm^{-1} to 400 cm^{-1}, as depicted in Figure IV.V. 2. Notably, the spectrum exhibited distinct peaks indicative of metabolite presence in the vicinity of the synthesized zinc oxide nanoparticles. Our FTIR analysis confirmed that phenolic compounds play a crucial role in stabilizing zinc nanoparticles and demonstrate a heightened propensity for interaction with them. Figure 3 highlights absorption peaks observed at 3300 cm^{-1}, 2931 cm^{-1}, 1647 cm^{-1}, 1725 cm^{-1}, 1300 cm^{-1}, and 1150 cm^{-1}, suggesting O-H stretching, C-H stretching, N-H bending, CO, C-H, C=O, C=O and O-H, etc.

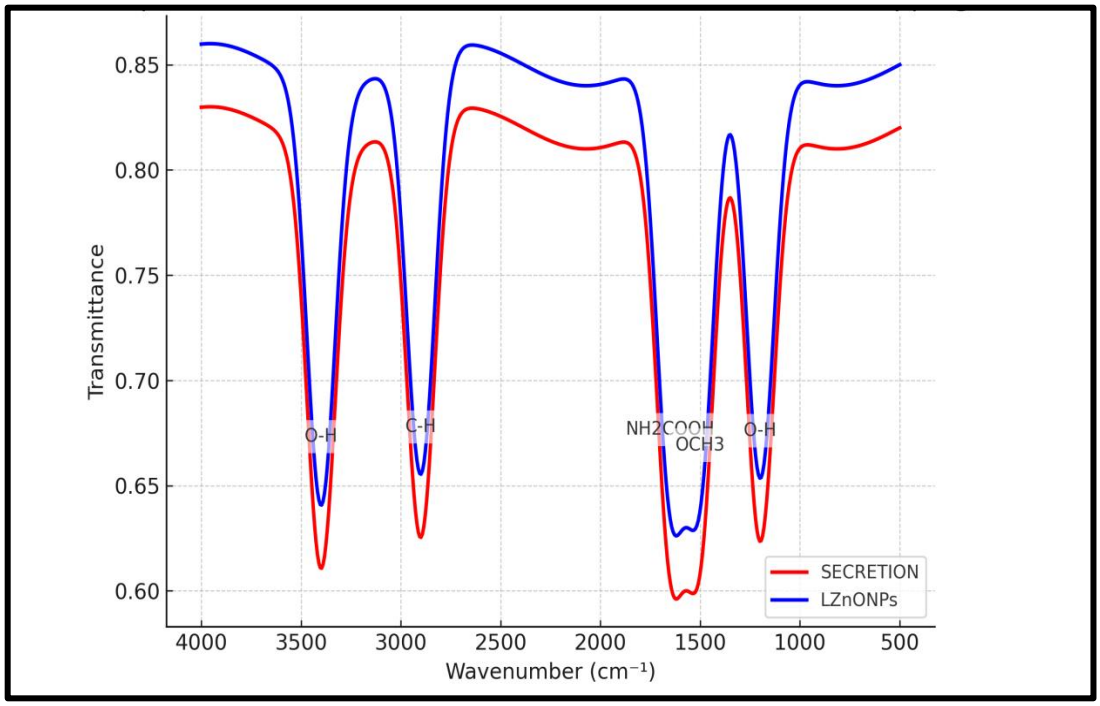

Figure IV.V. 2: FTIR graph of LZnONPs

4.5.3. Scanning Electron Microscopy (SEM) & Transmission Electron Microscopy (TEM) of LZnONPs

The structure of LZnONPs was analyzed through scanning electron microscopy (SEM) utilizing a JEOL JSM-6610 LV device. SEM analysis, utilizing an electron beam for detailed surface investigation, revealed that the particles exhibited predominantly spherical shapes and tended to cluster together, forming a sponge-like configuration. Figure IV.V. 3A. clearly illustrates the spherical morphology of the ZnONPs as observed in the SEM image. Moreover, TEM analysis was conducted to examine the dimensions and morphology of the fabricated ZnONPs. The TEM images revealed an average particle size of 26 ± 2 nm with a clearly evident spherical morphology (Figure IV.V. 3B & 3C).

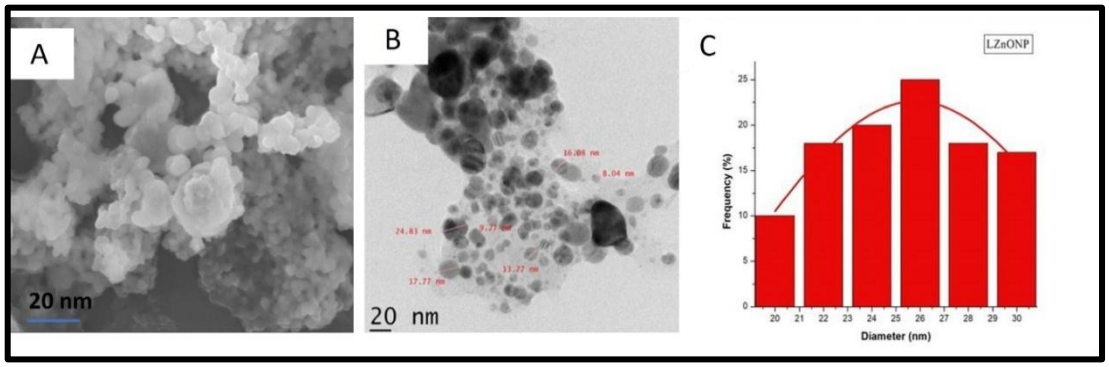

Figure IV. V. 3: A) SEM images at different magnification, (B) TEM images of LZnONPs C) Average particle size.

4.5.4. Zeta Potential Analysis of LZnONPs

To evaluate the durability of the biosynthesized LZnONPs, a nanoparticle analyzer (HORIBA SCIENTIFIC SZ 100) was employed. The findings revealed significant stability, with a Zeta Potential of -11.9 meV for LZnONPs, as depicted in Figure IV. V. 4. The LZnONPs prepared in this study displayed commendable stability.

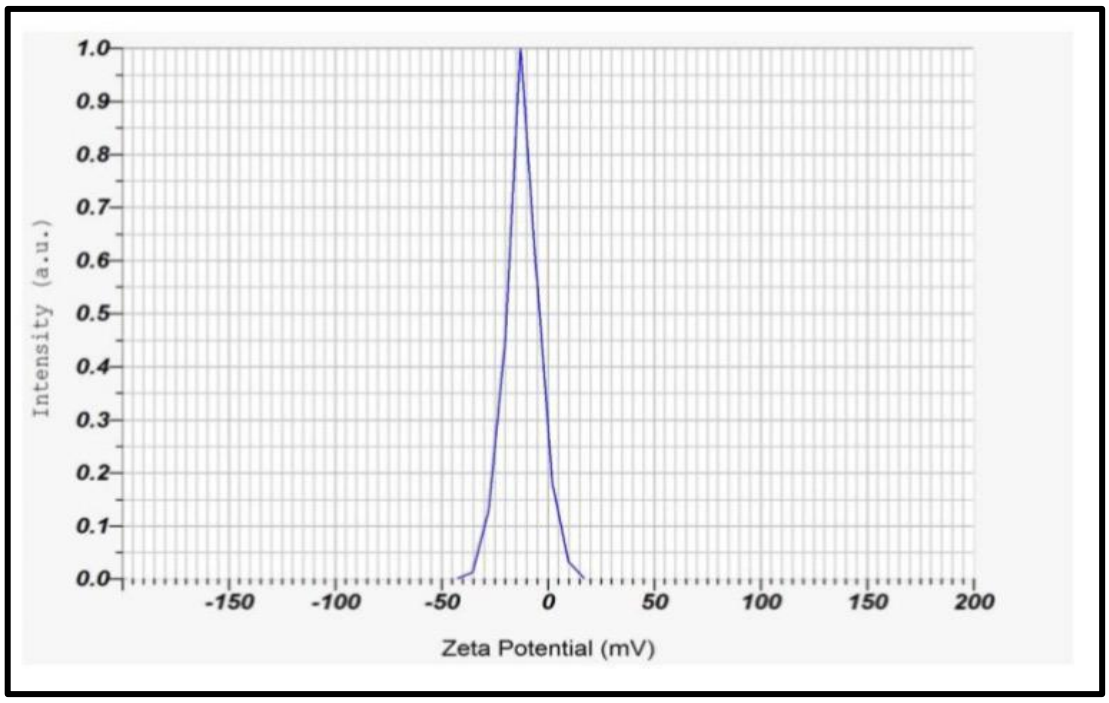

Figure IV.V. 4: Zeta potential measurement of LZnONPs

4.5.5. Differential Pulse Voltammetry (DPV) of LZnONPs

The investigation encompassed electrochemical glucose sensing through the utilisation of Differential Pulse Voltammetry (DPV). A sequence of measurements involving glucose concentrations of 3M, ranging from 10 mM to 70 mM, was conducted and is presented in Figure IV.V. 5A. Furthermore, linear calibration correlations were established between DPV current output and glucose concentration, as depicted in Figure IV.V. 5B. It was discovered that the set detection limit was 15 mM. The LZnONPs synthesised within the framework of the present inquiry exhibit potential for integration into electrochemical glucose monitoring systems.

The differential pulse voltammetry (DPV) graph illustrates the enzyme-free glucose sensing capability of zinc oxide nanoparticles, with clear responses observed at increasing glucose concentrations. At the minimum glucose concentration of 10 mM, the current response begins with a small peak, reflecting

the initiation of the oxidation of glucose. With an increase in glucose concentration to 20 mM, there is a larger peak current, showing that zinc oxide nanoparticles are efficient in catalyzing the oxidation reaction. Likewise, at 30 mM glucose, the peak current still increases, exhibiting a linear trend of increased electrochemical activity with a rising glucose concentration. At 40 mM, the peak current becomes even more defined and prominent, indicating the zinc oxide nanoparticles' strong interaction with glucose molecules. Lastly, at the highest glucose concentration that was tested at 70 mM, the peak current has its highest value in the tested range, which demonstrates a strong catalytic activity and high sensitivity of the modified electrode. The concentration-dependent increase in current confirms a consistent and linear electrochemical behavior, emphasizing the reliability and efficiency of LZnONPs in glucose sensing applications.

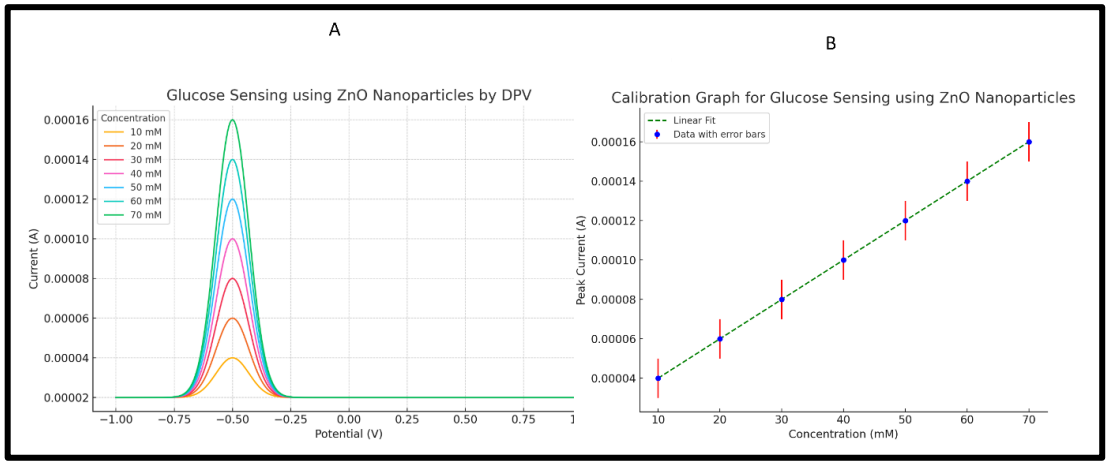

Figure IV.V. 5: A) DPV graph of LZnONPs-coated electrode B) Calibration curve of DPV of LZnONPs.

4.5.6. Antibacterial activity of LZnONPs

In the current study, the antibacterial properties were investigated using the disc diffusion experiment. The impact of LZnONPs on the growth of Gram-positive and Gram-negative bacteria (*S. aureus* and *K. pneumoniae*) was assessed. Filter papers impregnated with varying amounts of LZnONPs (5 µg/mL, 10 µg/mL, 15 µg/mL, and 20 µg/mL), the inhibition zone diameters for *K. pneumoniae* ranged from 7.25 mm, 9.34 mm, 11.26 mm, and 13.25 mm (as shown in Figure IV.V. 6 & Table IV. V. 1). For *S. aureus*, the filter papers with 5 µg/mL, 10 µg/mL, 15 µg/mL,

and 20 µg/mL of LZnONPs showed inhibition zones of 13 mm, 15 ± 05 mm, 17 ± 55 mm, and 19 ± 25 mm. This pattern indicates a steady increase in the inhibition zone diameter with rising concentrations of LZnONPs as depicted in Figure IV. V. 6. The antibacterial effectiveness of LZnONPs has a dose-dependent characteristic; an increase in LZnONPs concentration leads to an enhanced antimicrobial impact, especially when compared to *K. pneumoniae* and *S. aureus.* ZnONPs shows more antibacterial activity.

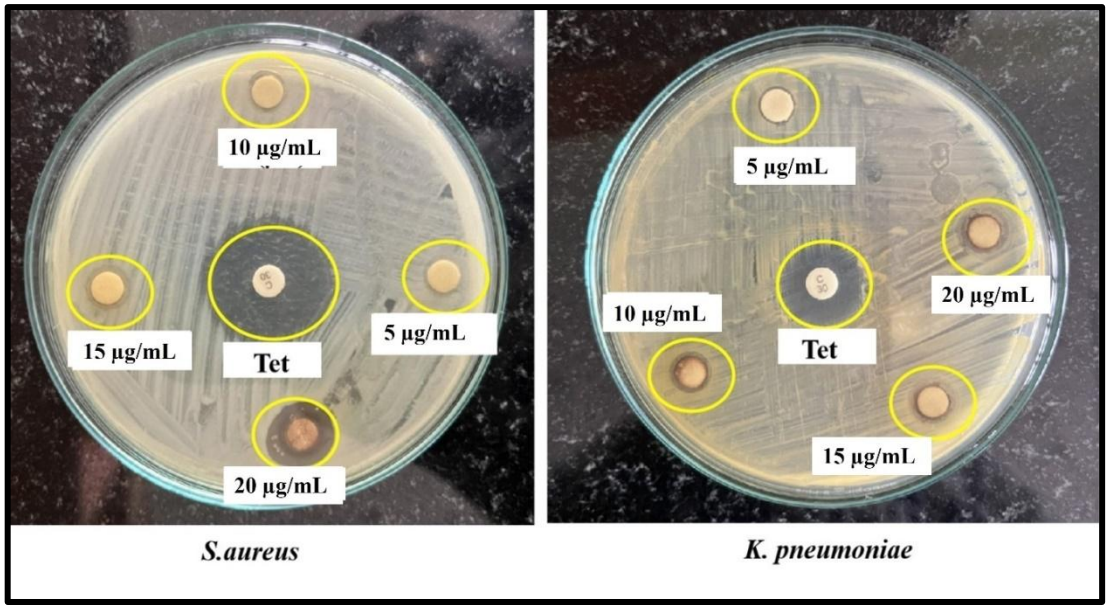

Figure IV.V. 6: Antibacterial activity of LZnONPs

Table IV. V. 1: Antibacterial activity of LZnONPs.

Treatment	Concentration (µg)	*S. aureus* (mm ± SD)	*K. pneumonia* (mm ± SD)
Experiment (LAuNPs)	5 µg	13. 00 ± 0.05	7.25 ± 0.05
	10 µg	15. 05 ± 0.05	9.34 ± 0.05
	15 µg	17. 55 ± 0.05	11.26 ± 0.05
	20 µg	19. 25 ± 0.05	13.25 ± 0.05

4.5.7. Anti-oxidant function of LZnONPs

The DPPH test has been extensively used in the assessment of antioxidant potential since it is well known for its efficacy in determining the ability of nanoparticles to neutralize free radicals. Figure IV.V. 7A, carefully describes the scavenging activity varying with concentration of LZnONPs. The calibration curve indicated an EC_{50} value of 26 µg/mL (Figure IV.V. 7B). Notably, the colour of the DPPH solution changed from a deep violet hue to a pale-yellow tint with an increase in the concentration of LZnONPs. LZnONPs enhanced antioxidant activity at increasing concentrations was confirmed by UV spectroscopic investigation, as shown in Figure IV.V. 7A.

The graph demonstrates the radical scavenging activity of LZnONPs using the DPPH assay, with absorbance values recorded across a wavelength range of 500 to 800 nm. The DPPH control, without LZnONPs (black line), exhibited the highest absorbance of approximately 0.85 at 520 nm, steadily decreasing to around 0.6 at 700 nm. Upon adding 20 µg/mL of ZnONPs (red line), the absorbance decreased slightly, starting at 0.75 at 520 nm and tapering off to about 0.5 at 700 nm, indicating minimal radical scavenging activity. When the concentration was increased to 40 µg/mL (green line), the absorbance further reduced, beginning at approximately 0.7 at 520 nm and declining to 0.4 at 700 nm, demonstrating enhanced activity. At 60 µg/mL of LZnONPs (blue line), the absorbance dropped more significantly, starting at around 0.65 at 520 nm and falling to 0.35 at 700 nm, indicating a considerable increase in scavenging efficiency. Finally, with 80 µg/mL of LZnONPs (cyan line), the absorbance reached its lowest levels, beginning at 0.6 at 520 nm and reducing to 0.3 at 700 nm, showcasing the highest antioxidant activity. This progressive reduction in absorbance with increasing LZnONPs concentration confirms the dose-dependent radical scavenging capacity of ZnONPs across the tested wavelength range

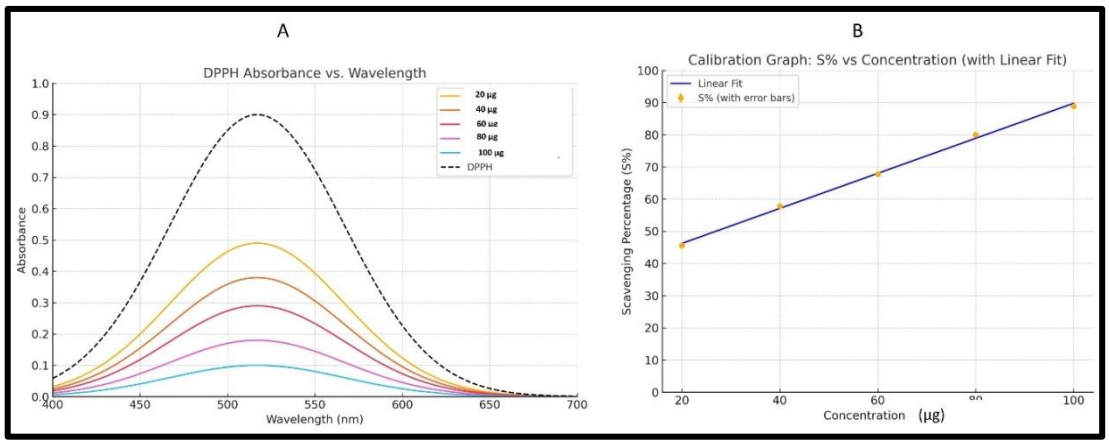

Figure IV.V. 7: A) Radical scavenging activity of LZnONPs by DPPH method. B) Calibration curve of DPPH assay of LZnONPs

4.5.8. Environmental hazard testing assay of LZnONPs

Biosynthesized LZnONPs exhibited dose-dependent chromosomal aberrations in *Allium cepa*, including chromosome bridges, lag chromosomes, and anaphase stickiness. The mitotic index (MI) declined from 15% at 100 µg/mL to 11% at 500 µg/mL**,** while chromosomal aberrations increased from 8% to 12%**,** indicating mild cytotoxic and genotoxic effects (Figure IV.V. 9). However, as MI remained above 50% across all concentrations, LZnONPs demonstrated greater biocompatibility and pose no significant threat to plants, making them an eco-friendlier alternative when released into the environment.

Table IV. V. 2: Environmental hazard testing assay of LZnONPs

Treatment	Concentration (µg/mL)	Mitotic Index (%±SD)	Chromosomal Aberration (%±SD)
Control (Distilled water)	100 µg/mL	10.41 ±0 .20	NIL
	200 µg/mL	11.69 ± 0.20	NIL
	300 µg/mL	12.14 ± 0.20	NIL
	400 µg/mL	13.79 ± 0.20	NIL
	500 µg/mL	14.24 ± 0.20	NIL
Experiment (Biosynthesised ZnONPs)	100 µg/mL	15 ± 0.01	8 ± 0.01
	200 µg/mL	14 ± 0.01	9 ± 0.01
	300 µg/mL	13.5 ± 0.01	10 ± 0.01
	400 µg/mL	12 ± 0.01	11 ± 0.01
	500 µg/mL	11 ± 0.01	12 ± 0.01

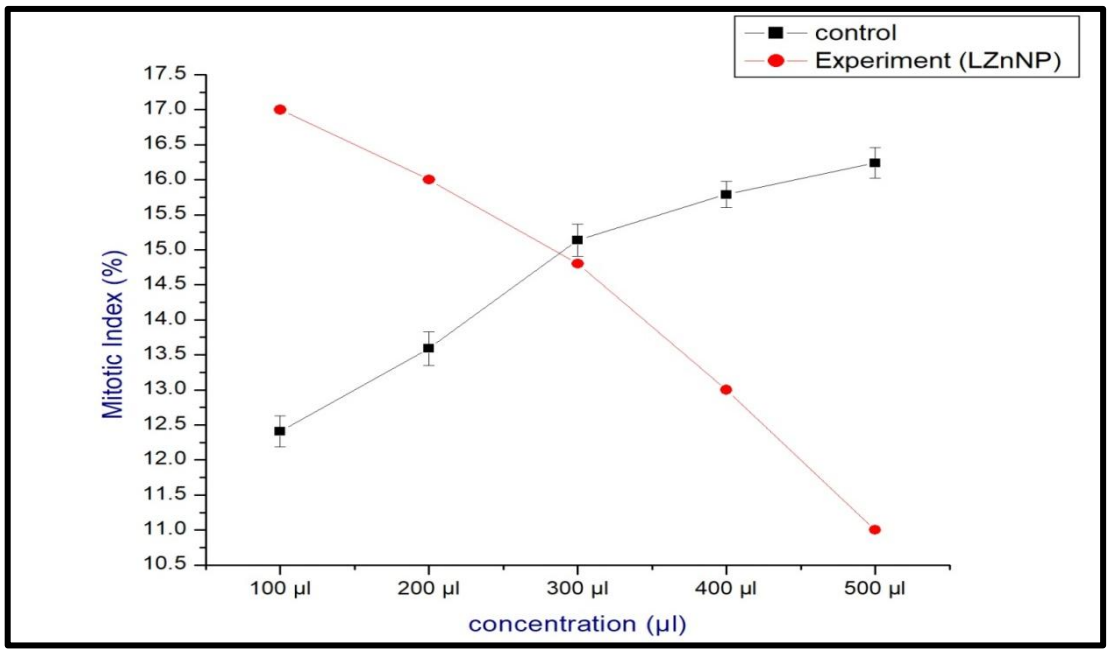

Figure IV.V. 8: Comparison of MI Vs Aberration.

The chromosomal aberration assay using *A. cepa* cells demonstrated distinct differences between the control group (distilled water) and the experimental group (biosynthesized ZnONPs). In the control group, increasing concentrations of distilled water from 100 µg/mL to 500 µg/mL resulted in a gradual rise in the mitotic index (MI) from 10.41% ± 0.20 to 14.24% ± 0.20, with no chromosomal aberrations observed at any concentration. In contrast, the experimental group treated with biosynthesized ZnONPs exhibited a dose-dependent decrease in MI, starting at 15% ± 0.01 at 100 µg/mL and reducing to 11% ± 0.01 at 500 µg/mL. Simultaneously, chromosomal aberrations increased progressively, beginning at 8% ± 0.01 at 100 µg/mL and reaching 12% ± 0.01 at 500 µg/mL. These findings indicate that while distilled water did not induce genotoxic effects, ZnONPs caused significant chromosomal aberrations and reduced mitotic activity in a concentration-dependent manner, suggesting their cytotoxic and genotoxic potential at higher doses as in figure IV.V. 8 & Table IV. V. 2**.**

4.5.9. Anticancer assay of of LZnONPs

This study demonstrates the potential of LZnONPs as an anticancer agent using Dalton's lymphoma ascites (DLA) cell lines in an *in vitro* setting. The

cytotoxicity of the Zinc oxide nanoparticles against DLA cells is dose-dependent (Figure IV.V. 9 & table IV. V. 3). The test shows that cellular death escalates over time in proportion to the concentration of biosynthesized zinc oxide nanoparticles. Therefore, the current study confirms that LZnONPs made through biological synthesis have extensive anti-cancer capabilities.

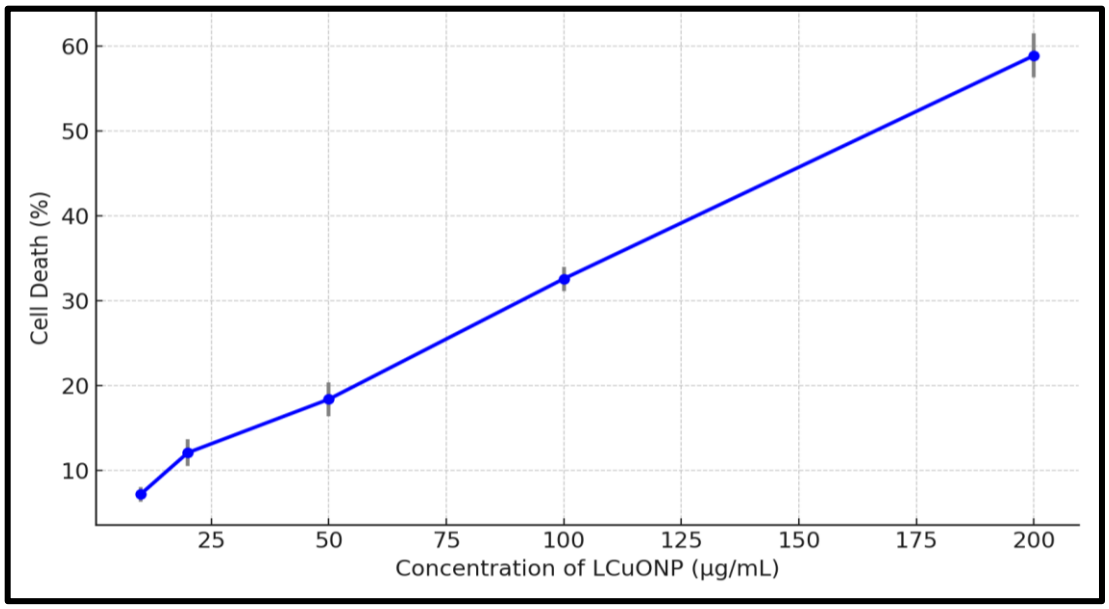

Figure IV.V. 9: Anticancer effect of LZnONPs

Table IV. V. 3: Anticancer activity of LZnONPs

Concentration (µg/mL)	Cell death (%)
10	7.22 ± 0.86
20	12.1 ± 1.6
50	18.4 ±1.98
100	32.6 ±1.43
200	58.9 ± 2.59

The anticancer assay evaluating the effect of ZnONPs on Dalton's Lymphoma Ascites (DLA) cells revealed a concentration-dependent increase in cell death percentages. At the lowest concentration of 10 µg/mL, ZnONPs induced 7.22 ± 0.86% cell death, indicating minimal cytotoxic activity. As the concentration

increased to 20 µg/mL, the percentage of cell death rose to 12.1 ± 1.6%, demonstrating a slight improvement in cytotoxicity. At 50 µg/mL, the cell death percentage significantly increased to 18.4 ± 1.98%, showcasing a more pronounced effect of ZnONPs. When the concentration was further elevated to 100 µg/mL, the cytotoxic activity markedly increased, resulting in 32.6 ± 1.43% cell death, indicating substantial nanoparticle-induced cell toxicity. At the highest tested concentration of 200 µg/mL, ZnONPs exhibited their maximum effect, inducing 58.9 ± 2.59% cell death. This data demonstrates a clear concentration-dependent increase in the anticancer activity of ZnONPs against DLA cells, with higher concentrations leading to significantly greater cell death percentages.

CHAPTER V

DISCUSSIONS

5.1. The Chemical Composition and Antimitotic, Antioxidant, Antibacterial, and Cytotoxic Properties of the Defensive Gland Extract of the Beetle, *Luprops tristis* Fabricius.

High-resolution analysis of methanolic defensive gland extract of *L. tristis* yielded a chemically rich profile of secondary metabolites such as D-gluconic acid ($C_6H_{12}O_7$), 3-dehydro-L-gulonate ($C_6H_{10}O_7$), uric acid ($C_5H_4N_4O_3$), citric acid ($C_6H_8O_7$), and 2-pyrrolidone-5-carboxylic acid ($C_5H_7NO_3$), all of which could be responsible for its bioactivity. Quinonoid compounds, often found in beetle secretions (Blum *et al.,* 1971; Gross *et al.,* 2002; Markarian *et al.,* 1978), are particularly highlighted. Methyl- and ethyl-p-benzoquinones, which are significant constituents of *Blaps mucronata* (Peschke, K, & Eisner, T., 1987), and hydroquinones, reported to have irritant actions in *L. tristis* (Peschke & Eisner, 1987), were also present. Comparative research on *Abax parallelepipedus, Calosoma sycophanta,* and *Carabus ullrichii* documented aliphatic acids, methacrylic, tiglic, and isobutyric acids (Leić *et al.,* 2014), whereas Tenebrionid beetles produced toluquinone, ethylquinone, and benzoquinone (Kanehisa, 1978), as well as new unsaturated and methyl ketones (Zvereva & Kozlov, 2016). Our previous research established important constituents in *L. tristis* secretions through GC-HRMS, such as 2,3-dimethyl-1,4-benzoquinone, polyphenols, long-chain hydrocarbons, fatty acids, and thiols, which also have the potential for nanoparticle biosynthesis (Sabira *et al.,* 2022).

5.1.1. Histological and Microscopic Examination of Beetle Defensive Gland Tissues

Morphological analysis of the gland shows a pair of small wrinkled conical pouches (0.8 to 0.9 mm). These glands are located parallel to the longitudinal axis of the body and extend from the membrane that divides the eighth and seventh sternites (Abhitha *et al.,* 2010). Lying on either side of the hindgut, they are embedded in a rich matrix of fat stores. Histological studies bring out the conical shape with hair-like surface appearance of the gland pairs, as illustrated in Scanning Electron Microscopy (SEM) micrographs presented in Figure IV.I. 2. Microscopic and

histological analysis of the anatomy of the secretory lobes revealed that the two lobes of the gland, located dorsally, receive secretions from numerous secretory units. These units consist of internally positioned secretory cells, spherical in shape, containing tightly packed spherical secretory vesicles filled with defensive secretion. Each glandular system comprises several secretory lobes, resembling the tenebrio type of gland, featuring a pair of conical reservoirs opening into a common discharge area without exit ducts, as shown in Figure IV. I. 1. SEM investigations and histological studies of cleared specimens indicated that each lobe terminates blindly without any specific cuticular openings, aligning with previous research highlighting the behaviour of strongly disturbed beetles rupturing the gland, gently massaging the rear tarsus to expel the fluid. Cross-sectional analysis revealed dimensions of 600 μm in length and 200 μm in width for the gland. These findings exhibit similarities to previous studies on glandular and anatomical structures of certain coleopteran beetles (Di Giulio *et al.,* 2015; Vesović *et al.,* 2017). This study provides crucial insights into the morphological and histological architecture of beetle defensive glands, contributing to a deeper understanding of coleopteran defensive mechanisms. The explanation of glandular morphology and secretory processes has relevance for evolutionary biology, especially the beetles' adaptations for defense against predators. Additionally, the defense secretion described here has potential in biosynthetic applications, such as the green synthesis of nanoparticles for antimicrobial and anti-cancer applications. Future studies could investigate the molecular content of such secretions, their interaction with biological systems, and their potential in nanotechnology and medicine. Examining differences between various beetle species may also have a comparative framework for the evolution of defense strategies among Coleoptera.

5.1.2. High-Resolution Liquid Chromatography–Mass Spectrometry (HRLC-MS) in combination with Quadrupole Time-of-Flight (QTOF) mass spectrometry of beetle defense secretion.

Our research corroborates the occurrence of different compounds mainly qualifying as organic acids and amino acid derivatives, with further categorization as

carboxylic acids and purine derivatives for some, with reported occurrences in other insects like Braconid wasp and some species of butterflies (Fukushima *et al.,* 1990; Solazzo *et al.,* 2015). Oleic acid, which occurs in the defense secretion of *L. tristis*, is also found in the rove beetle, *Deleaster dichrous* defensive secretory system (Dettner *et al.,* 1985). Further, the finding of sex pheromone 7-hexadecenal in *L. tristis* defensive gland opens interesting issues about the possible involvement of this compound in intraspecific communication, calling for more experimental confirmation. The same compound is also present in the defensive extract of *D. dichrous,* which has been found as sex pheromone constituents in other insects, indicating shared identity in defensive gland secretions used as pheromones or their precursors (Pfeiffer *et al.,* 2018).

LC-MS-QTOF analysis at high resolution of *L. tristis* glandular extract revealed a number of major metabolites, such as D-gluconic acid, 3-dehydro-L-gulonate, uric acid, citric acid, and 2-pyrrolidone-5-carboxylic acid (Table IV.I.1; Fig. IV.I.3), which are responsible for the biochemical richness and functional bioactivity of the secretion. D-gluconic acid, a glucose oxidation product, has been shown to possess antimicrobial activity (Christakopoulos *et al.,* 2003) and a high electron-donating capability, allowing it to serve both as a reducing and stabilizing agent in the synthesis of green nanoparticles (Lim & Dolzhenko, 2021). Likewise, 3-dehydro-L-gulonate, which participates in oxidative stress responses and carbohydrate metabolism, is characterized by a high redox potential, thus allowing for the reduction of metal ions during nanoparticle synthesis (Blinova *et al.,* 2022; Pal *et al.,* 2016). Uric acid, another dominant component, is a strong antioxidant (Allen *et al.,* 2004) and reducing agent and has been effectively utilized in nanomaterial synthesis because of its redox-active imidazole and hydroxyl groups (Pawar *et al.,* 2022). Citric acid, a key intermediate in cellular respiration, imparts metabolic function and serves as a reducing and capping agent in nanoparticle synthesis, providing electrostatic stabilization through its hydroxyl and carboxyl groups (Krebs & Johnson, 1980; Kumari *et al.,* 2024). 2-pyrrolidone-5-carboxylic acid detection, linked with protein folding and stress responses (Yang *et al.,* 1997), implies a function to ensure the stability of bioactive proteins in the secretion. Such

organic acids play a crucial role in nanoparticle synthesis by stabilizing metal ion intermediates (Dahl *et al.,* 2007).

The LC–MS QTOF profile of *L. tristis* defensive gland secretion indicated metabolites D-gluconic acid, 3-dehydro-L-gulonate, uric acid, citric acid, and 2-pyrrolidone-5-carboxylic acid, all with direct relevance to nanoparticle synthesis, stability, and functionality. They act as both reducing agents and capping/stabilizing agents, which are imperative for controlled nanoparticle formation.

5.1. 3. Biological activities of Beetle Defensive Secretions: Environmental hazard testing, Antibacterial and Cytotoxic Activities

The methanolic extract of *L. tristis* defensive glands showed considerable bioactivity. Chromosomal aberrations, indicative of possible mutagenicity, were revealed by *Allium cepa* assays, consistent with earlier findings on insect-derived genotoxic compounds (Surender *et al.,* 2015). Antioxidant activity was significant and was likely contributed by phenolic and quinonoid compounds, whose redox activity is well documented (Hong *et al.,* 2005; Hwang *et al.,* 2019; Liu *et al.,* 2012; Tang *et al.,* 2018). Quinones are said to have wide biological activities such as antimicrobial, antifungal, antiviral, and anticancer activities (Beheshti *et al.,* 2012).

The secretion also displayed antibacterial activity against *S. aureus* and *E. coli*, akin to observations in other arthropods like *Pachyiulus hungaricus*, whose defense secretions include benzoquinones and hydroquinones (Hoback *et al.,* 2004; Stanković *et al.,* 2016). Cytotoxicity assessed by Trypan blue exclusion assay demonstrated anticancer activity, similar to effects recorded in other carabid beetles and woodland caterpillar hunters (Crespo *et al.,* 2011; Nenadić *et al.,* 2016). These findings validate the pharmacological significance of *L. tristis* secretions, which exhibited considerable antioxidant (Fig. IV.I.5, Table IV.I.3), antimicrobial (Fig. IV.I.6, Table IV.I.4), and anticancer activity (Fig. IV.I.7, Table IV.I.5), together with a low environmental hazard profile (Table IV.I.2, Fig. IV.I.4). It is expected that the bioactivity is due to the secretion's distinctive chemical profile, particularly phenolics and quinones, suggesting intense exploration into their cellular mechanisms and biosynthetic pathways.

5.2. Biosynthesis of Nickel Nanoparticles using Beetle Defensive Gland Extract for Multifunctional Applications.

In the current investigation, NiNPs (LNiNPs) were synthesized through the reduction of a nickel chloride solution using an extract derived from the defensive gland of the insect *L. tristis*. Following the chemical characterization through techniques including UV-Vis spectroscopy, Fourier-transform infrared spectroscopy (FTIR), Scanning electron microscopy (SEM), Transmission electron microscopy (TEM), and measurement of Zeta potential, their biochemical applications were assessed, encompassing glucose sensing, antibacterial analysis, antioxidant activity, antimitotic activity, and anticancer activity. The probable mechanism of the LNiNPs formation shows the scheme given below,

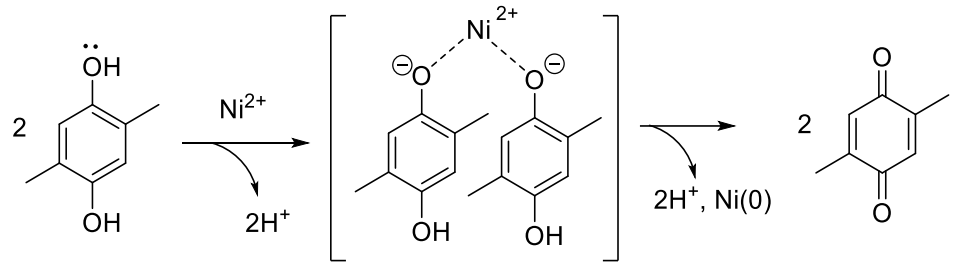

Scheme 1. Mechanistic overview of the Ni (II)-mediated oxidation of hydroquinone.

Several compounds, including 2,5-dimethyl hydroquinone, 1,3-dihydroxy-2-methyl benzene, and 2,3-dimethyl-1,4-benzoquinone, are present in the defensive gland secretion of *L. tristis* (Sabira *et al.,* 2022). From these phenolic molecules most probably hydroquinone undergoes oxidation by nickel (Scheme 1). A mechanistic overview of the oxidation of dimethyl hydroquinone to the corresponding p-quinone may be advanced as depicted in Scheme 1. As the conversion is observed in the presence of a Ni (II) salt, it may be assumed that the latter is involved in the oxidation directly. The oxidation may be initiated via ligand exchange on Ni by the phenol units. This may be followed by loss of H^+ and the transfer of electrons to nickel. Dimethyl-p-quinone is generated in the process with concomitant reduction of nickel. It may be noted that this is a speculative

mechanism at this stage as Ni (II) is not generally considered as a common oxidizing agent.

5.2.1. Optical Characterization of LNiNPs Using UV-Vis Spectroscopy

The UV-Vis spectroscopy analysis revealed a broad peak indicative of polydispersity in the synthesized nanoparticles, with the λmax around 200–300 nm (Figure IV. II. 1**)**. This observation aligns with prior studies. The visible colour change of the reaction mixture from purple to reddish brown is shown in Figure IV. II. 1. Following microwave irradiation within 15 minutes, the first indicator of the formation of LNiNPs. This was followed by UV-Vis spectroscopy, LNiNPs showed a maximum absorption peak at the wavelength (λ_{max}) 204 nm, which was due to the surface plasmon resonance phenomenon, which provides a convenient indication of the formation of LNiNPs. The considerable broadening of the UV-Visible peak revealed that the particles are extremely polydispersed, and this clearly demonstrated the interaction between the metal nickel and the biomolecules present in the gland extract. Helen and Rani synthesized NiNPs in a similar manner using an aqueous nickel sulphate solution and an elephant yam root tuber extract as a capping and reducing agent. The colour of the solution shifted from blue to yellow as NiNP developed, with a UV absorption at 207 nm (Helen & Rani, 2015). The λ_{max} is consistent with other previous research, similar peaks within the range of 200-300 were obtained for NiNP synthesized from the plants *Camellia sinensis* and *Piper longum* (Chandra *et al.,* 2014 ; Bibi *et al.,* 2017 ; Jamila *et al.,* 2020)

5.2.2. FTIR Spectroscopy of LNiNPs: Unraveling Structural Signatures

FTIR analysis established the involvement of phenolic and carboxylic groups in LNiNPs reduction and stabilization (Table IV. II. 1; Fig. IV. II. 2). O–H and C=O stretching characteristic peaks provided evidence of interaction between nickel ions and functional groups of the bioorganic matrix. Phenolics identified, such as hydroquinone and 2,5-dimethyl hydroquinone, were most probably reducing agents, whereas carboxylic acids like citric and uric acid stabilized the nanoparticles via coordination bonding. These observations are consistent with earlier reports of hydrogen bonding and electrostatic forces in the green synthesis of nanoparticles

using plants (Chandra *et al.,* 2014; Patra & Baek, 2014; Shankar & Rhim, 2015; Tomar *et al.,* 2015). The spectral profile was almost identical to the previously reported plant-mediated LNiNPs (Yuan *et al.,* 2022), indicating the role of bioorganic compounds in *L. tristis* nanoparticle formation.

5.2.3. Characterization of LNiNPs via SEM, TEM, and Zeta Potential Analysis

The current study revealed that the biosynthesis of LNiNPs using the defensive gland secretion of *L. tristis* produces diverse nanoparticle shapes, including spherical, irregular polygonal, and cylindrical forms (Figure IV. II. 3), consistent with prior reports (Duan & Li, 2004; Rajakumar *et al.,* 2013; Bibi *et al.,* 2017). These morphological variations can be attributed to magnetic interactions and polymer adhesion between particles, as previously documented. Notably, our findings align with earlier studies indicating size-controlled LNiNPs ranging from 3 to 11 nm (Hou *et al.,* 2005). The produced LNiNPs displayed remarkable stability, supported by zeta potential measurements (Figure IV. II. 4), which are known to influence nanoparticle interactions with biological membranes (Elango *et al.,* 2016; Honary & Zahir, 2013; Liao *et al.,* 2009; V. Sharma *et al.,* 2017). Higher surface charges enhance nanoparticle adhesion to cell membranes, enabling uptake through mechanisms such as phagocytosis, endocytosis, and pinocytosis (Honary & Zahir, 2013). The negative zeta potential of LNiNPs synthesized using the defensive secretion of *L. tristis* arises from the adsorption of negatively charged functional groups and molecules onto the nanoparticle surface, driven by the diverse chemical profile of the secretion. Substances like D-Gluconic acid ($C_6H_{12}O_7$) and 3-Dehydro-L-gulonate ($C_6H_{10}O_7$), with their carboxy and hydroxyl groups, help in this way by donating protons in biological conditions, with remaining negatively charged carboxy groups stabilizing the nanoparticle surface (Pal *et al.,* 2016). Uric acid ($C_5H_4N_4O_3$), a weak acid, increases the charge by losing protons from its oxygen- and nitrogen-containing groups, especially in its keto-enol form (Yadav *et al.,* 2024). Likewise, citric acid ($C_6H_8O_7$), which is a good chelating agent with three carboxy groups, gets deprotonated in aqueous solutions and provides strong negative charges while adhering strongly to the metal surface, stabilizing the nanoparticles

even more (Kumari *et al.,* 2024). Also, 2-Pyrrolidone-5-carboxylic acid ($C_5H_7NO_3$) provides the negative charge through its carboxylic group, particularly in neutral or basic pH conditions. Phenolic and quinonoid compounds like 2,5-dimethyl hydroquinone, 1,3-dihydroxy-2-methylbenzene, and 2,3-dimethyl-1,4-benzoquinone bind to the nanoparticle surface through hydroxyl or carbonyl functional groups. Proton loss from phenolic and charge-transfer with quinonoid compounds leaves other negative charges on the surface (Ghodake *et al.,* 2010). Together, these compounds provide a high concentration of negatively charged functional groups on the surface of the nanoparticle, conferring a high negative zeta potential and promoting colloidal stability by avoiding particle agglomeration by electrostatic repulsion. Current investigation highlights the crucial contribution of the biochemical content of *L. tristis* gland secretions in biosynthesizing biologically active and stable LNiNPs, providing a promising green nanosynthesis method for nanomaterials with improved functional characteristics.

5.2.4. Antibacterial, Antioxidant, and Electrochemical Properties of LNiNPs

Antimicrobial activity of biosynthesized LNiNPs is explained by nickel ion release, membrane disruption, and generation of reactive oxygen species (ROS), in accordance with earlier research on green-synthesized NiNPs (Adwin Jose *et al.,* 2018; Jeyaraj Pandian *et al.,* 2016; Zarenezhad *et al.,* 2022; Gomaji Chaudhary *et al.,* 2015; Helen & Rani, 2015). Functional metabolites like D-gluconic acid and 3-dehydro-L-gulonate in *L. tristis* secretions contribute to nanoparticle stability and improve antibacterial effects by redox activity. Since LNiNPs showed no activity against *E. coli*, which was used only as a general Gram-negative model, *K. pneumoniae,* a clinically significant multidrug-resistant pathogen, was chosen for antibacterial screening to assess the therapeutic relevance of the nanoparticles. Antioxidant activity was established through concentration-dependent DPPH scavenging of radicals due to uric acid and citric acid, which stabilize the particles and inhibit aggregation (Jeyaraj Pandian *et al.,* 2016). The molecules reduce damage due to ROS, enhancing the antioxidative role of LNiNPs. In electrochemical glucose sensing, capping molecules from *L. tristis* that contain redox-active groups promote

signal transduction and sensor stability. 2-pyrrolidone-5-carboxylic acid and benzoquinone derivatives facilitate dispersion and electron transfer efficiency (Mislovirová *et al.,* 2007) for sensitive detection of glucose. This supports the need for accurate glucose monitoring of diabetic complications (Coster *et al.,* 2000; Steiner *et al.,* 2011).

The multifunctionality of LNiNPs across antibacterial, antioxidant, and electrochemical applications is prompted by their distinct biogenic surface chemistry (Figure IV. II. 5, IV. II. 6 & IV. II.7). Novelty, compared to earlier studies (Adwin Jose *et al.,* 2018; Jeyaraj Pandian *et al.,* 2016), is in the employment of *L. tristis* secretions, which provide increased activity and stability. Subsequent investigations should confirm such effects in vivo, examine prolonged cytotoxicity, and evaluate sensor operation within complicated biological media. Additionally, batch homogeneity and synthesis scale-up continue as key hurdles towards translational utilization.

5.2.5. Ecological and Anticancer Assessment of LNiNPs

Biosynthesized LNiNPs caused slight chromosomal aberrations in *Allium cepa* root meristems through ROS generation due to surface adhesion and intracellular penetration. These redox disturbances resulted in genotoxic and mito-depressive effects (Ajaykumar *et al.,* 2023; De *et al.,* 2016; Liman *et al.,* 2022; Wang *et al.,* 2013). But the toxicity registered was notably smaller compared to chemically produced metal nanoparticles, implying their environmentally safer nature (Figure IV.II.8). Their intrinsic phytotoxicity can also allow their employment in agricultural biocontrol, e.g., tumour and gall inhibition.

The augmented bioactivity of LNiNPs is strongly related to the phytochemical capping agents obtained from the secretions of *L. tristis*. Chemicals like D-gluconic acid and 3-dehydro-L-gulonate stabilize and reduce nickel ions, while uric acid and citric acid have antioxidant and chelating capacities, ensuring particle stability as well as ROS neutralization. 2-pyrrolidone-5-carboxylic acid stabilizes dispersion and colloidal integrity. Phenolic and quinonoid derivatives (e.g., 2,5-dimethylhydroquinone, 1,3-dihydroxy-2-methylbenzene, 2,3-dimethyl-1,4-

benzoquinone) are redox-active, which is essential for minimizing oxidative stress and possibly antitumor activity.

DLA cell using cytotoxicity assays showed dose-dependent anticancer action of LNiNPs (Figure IV. II. 9; Table IV. II. 4) due to ROS scavenging and redox-mediated action by the capping agents (Barnes *et al.,* 2010; Guo *et al.,* 2009). This is consistent with earlier reports confirming antitumor efficacy of NiNPs (Rameshthangam & Chitra, 2018), but uniquely highlighting the facilitating role of biogenic ligands in enhancing therapeutic action. This research highlights the dual biomedical and environmental potential of green-synthesized LNiNPs. They have better biocompatibility compared to standard metal NPs, lower ecological footprint, and promising anticancer properties, especially owing to their functional surface chemistry. Although with encouraging results, existing findings are mostly *in vitro*-based, thus constraining immediate translational significance. Long-term toxicological profiles and *in vivo* validations are essential next steps. Also, other challenges including scalability of process, reproducibility, and stability between batches need to be overcome for industrial or clinical deployment to become possible. Unlike previous research (e.g., Adwin Jose *et al.,* 2018; Jeyaraj Pandian *et al.,* 2016), this study specifically emphasizes the multifunctional improvement imparted by *L. tristis*-derived phytochemicals. Future studies need to investigate more extensive biomedical uses, such as wound healing and targeted delivery, while determining mechanistic understanding and safety profiles *in vivo*.

5.2.6. Investigating the Antiangiogenic Potential of LNiNPs via the CAM Assay

The results of this study demonstrate a clear inhibitory effect of LNiNPs on angiogenesis in 48-hour chick embryos, as shown by the marked differences between the control (PBS-treated) and experimental groups (Figure IV. II. 10). In the control group, normal angiogenesis was observed, with a gradual increase in vessel area, junctions, and length, peaking around 7–8 hours, which aligns with typical embryonic blood vessel development. However, embryos treated with 2 µg of LNiNPs exhibited a distinct pattern of reduced angiogenic activity. While there was an initial increase in vessel area, junctions, and length, all parameters began to

decline sharply after 4 hours. This decline became more pronounced between 6 to 8 hours, ultimately leading to the degeneration and death of blood vessels by the 8-hour mark.

The antiangiogenic activity of LNiNPs was demonstrated in the CAM assay on 48-hour chick embryos, highlighting their potential as inhibitors of neovascularization. The antiangiogenic potency of LNiNPs is largely due to the biofunctional surface imparted by the capping agents of *L. tristis*. D-Gluconic acid ($C_6H_{12}O_7$) and 3-Dehydro-L-gulonate ($C_6H_{10}O_7$) are involved in nanoparticle reduction and colloidal stability but also lead to ROS induction that interrupts endothelial proliferation and migration (Santos *et al.,* 2022). Uric acid ($C_5H_4N_4O_3$) regulates the level of ROS, preventing overoxidation via excessive oxidative stress. Citric acid ($C_6H_8O_7$) stabilizes the nanoparticles and inhibits matrix metalloproteinase activity important for angiogenesis. 2-Pyrrolidone-5-carboxylic acid ($C_5H_7NO_3$) improves the nanoparticle's dispersibility and compatibility with the angiogenic environment. Phenolic and quinonoid compounds also downregulate VEGF-mediated signaling, which inhibits capillary formation. Together, these metabolites improve the LNiNPs' stability and bioactivity, enabling them to be used as antiangiogenic agents in neovascular ocular diseases and cancer (Santos *et al.,* 2021). The very significant reduction in vessel junctions, which are responsible for the construction of vascular networks, along with the reduction in vessel length, indicates that LNiNPs disrupt the formation as well as maintenance of the vascular structure. The drastic reduction in vessel area provides strong support in favor of the argument that LNiNPs not only inhibit the formation of new vessels but also induce regression of established vessels (Figure IV. II.11). The above findings indicate that LNiNPs may be an extremely potent anti-angiogenic agent and therefore leave a few questions regarding their potential cytotoxic effect on other biological systems and suggest the necessity to investigate their modes of action.

When compared with previous studies showing anti-angiogenic role of metal nanoparticles, such as those by Baharara *et al.,* (2014), which also highlight the anti-angiogenic effects of metal nanoparticles, the results of this study reinforce

the promising potential of nanoparticles for inhibiting angiogenesis (Baharara *et al.,* 2014; Gurunathan *et al.,* 2009; Zarharan *et al.,* 2023).

5.3. Bio-synthesis of Copper Oxide Nanoparticles Using Beetle Defensive Gland Extract: Exploring Diverse Applications

Utilizing extracts from plants, fungi, algae, or bacteria, copper oxide nanoparticles (CuONPs) are biosynthesized under careful control of variables such as temperature, pH, and precursor concentration. These parameters play a substantial role in determining the nature of copper particles generated during the eco-friendly synthesis process (Chakraborty *et al.,* 2022; Letchumanan *et al.,* 2021). During the present process, biomolecules present in the defensive gland extract of the insect *L. tristis*, especially hydroquinones, reduce Cu^{2+} ions to the Cu^{0} state while simultaneously oxidizing them to form copper oxide nanoparticles. Specific biomolecules within the sample extract act as an agent for capping and contribute towards the stabilisation of the resulting nanoparticles.

5.3.1. Optical Confirmation by UV- Vis spectroscopic analysis of LCuONPs

Production of LCuONPs was first confirmed visually by means of UV-visible spectroscopy, exhibited a prominent absorption peak at a λ_{max} of 218 nm, attributed to the surface plasmon resonance phenomenon (Figure IV. III. 1). The noteworthy broadening of the peak indicated a high degree of polydispersity among the particles, highlighting the evident interaction between the metallic copper and the biomolecules inherent to the gland extract. Researchers who have successfully biosynthesized cost-effective and more stable copper oxide nanoparticles from the leaves of *Ormocarpum cochinchinense* have verified the surface plasmon resonances of these NPs by noting peak absorbance at 200 nm (Gnanavel *et al.,* 2017).

5.3.2. FTIR Spectroscopy analysis of LCuONPs

FTIR investigation affirmed that phenolic compounds assume a crucial part in stabilizing LCuONPs and exhibit enhanced affinity for interaction with them (Figure IV. III. 2). Prior studies have hypothesised that specific bioactive

constituents, including polyphenols, enzymes, and reducing sugars present in defensive gland extracts, might support the bio-reduction copper oxide nanoparticles from copper ions, in addition to the stabilization and encapsulation of metallic ions. Present work recorded the following peaks at 2361(C-H stretch), 1829 (Carbonyl groups), 1324 (O-H in-plane bend), 902 (C-H stretch), 827(C-H stretch), 764 (aromatic out of plane ring bends) and 587 (C-H) bend. According to research by Sharma and coworkers, the development of CuO nanoparticles is indicated by the presence of discrete infrared absorption bands in the 400–600 cm^{-1} range (Sharma *et al.,* 2015). The use of polyphenols in green synthesis adheres to environmentally friendly practices by avoiding harmful chemicals and producing nanoparticles with remarkable catalytic and antimicrobial properties (Sadani *et al.,* 2021).

5.3.3. Ultrastructural Characterization of LCuONPs by Scanning and Transmission Electron Microscopy

Uniform dispersion and crystalline nature of the biosynthesized LCuONPs were identified through Scanning electron microscopy (SEM) and transmission electron microscopy (TEM) images in Figure IV. III. 3 (A, B, C). The analysis indicated that the nanoparticles possessed an average diameter of approximately 15 nm. These are consistent with previous research in the field (Ahamed *et al.,* 2014; Nasrollahzadeh *et al.,* 2015). CuONPs from *Sterculia urens* Roxb. and *Aloe barbadensis* have a size consistent with our study (Gunalan *et al.,* 2012; Padil & Černík, 2013).

5.3.4. ZETA potential stability analysis of LCuONPs

The LCuONPs we prepared showed excellent stability, consistent with previous research in the context of zeta potential (Figure IV. III. 4). The negative reading of zeta potential further confirms the stability, enabling uptake through electrostatic attraction between the cationic nanoparticles and the cationic membrane. The high absolute value of zeta potential confirms high repulsion among the particles and hence effectively prevents their aggregation (Lin *et al.,* 2008; Sankar *et al.,* 2013).

5.3.5. Electrochemical Hydrogen peroxide detection of LCuONPs by Differential Pulse Voltammetry

Hydrogen peroxide (H_2O_2) is a common intermediate in the majority of biological processes and a significant parameter for monitoring these bioprocesses; therefore, it has attracted more attention in the determination of H_2O_2 (Karyakin *et al.,* 2000; Ping *et al.,* 2010). It has previously been established that electrochemical methods are effective and cost-effective in the determination of H_2O_2 (Ricci & Palleschi, 2005). The interaction between the molecules of hydrogen peroxide and surface-functionalized LCuONPs may lead to alterations of electrical conductivity or redox processes, which can be detected and related to hydrogen peroxide concentration. A hydrogen peroxide sensor that is based on a polyalizarin nanocomposite and LCuONPs, using differential pulse voltammetry (DPV), has an LOD of 0.03 μM (Amini *et al.,* 2021). An electrochemical sensor for the determination of hydrogen peroxide based on copper-doped copper oxide nanoparticles has been developed, with a detection limit of 0.23 μM (Haiyan Song, 2015). It should be appreciated that biosynthesized copper oxide nanoparticles could be more biocompatible than their chemically synthesized counterparts, and therefore, they have attracted a lot of interest due to their ability to enhance the sensitivity and specificity of hydrogen peroxide sensors. The present work is consistent with previous work, therefore contributing to the body of evidence in this research area. While this study demonstrates the potential of biosynthesized copper oxide nanoparticles (LCuONPs) in hydrogen peroxide detection, several limitations must be acknowledged (Figure IV. III. 5 (A, B). First, the stability and reproducibility of the sensor in diverse environmental conditions remain unexplored, which may impact its practical applicability. Second, the biocompatibility and environmental impact of LCuONPs, although promising, require further evaluation in real biological systems. Third, the specificity of the sensor toward hydrogen peroxide in the presence of other reactive oxygen species (ROS) or interfering agents was not fully addressed, which could affect its performance in complex matrices. Future studies should focus on optimizing the synthesis process to achieve greater consistency in nanoparticle properties and on integrating these sensors into

portable or wearable devices for real-time applications. Moreover, exploring the use of LCuONPs in tandem with other nanomaterials could potentially enhance their sensitivity and broaden their applicability in biosensing, particularly in medical diagnostics, environmental monitoring, and industrial processes.

5.3.6. Antibacterial Activity of LCuONPs

Biosynthesized LCuONPs were found to have dose-dependent antibacterial activity with increased inhibition zones at increased concentrations (Figure IV.III.6; Table IV.III.1). This can be credited to their nanoscale size, high surface area, and ROS production that harms bacterial membranes and causes cytotoxicity. Of interest, *S. aureus* was found to be more sensitive compared to *K. pneumoniae*, in accordance with earlier observations (Applerot *et al.,* 2012).

Capping agents from *L. tristis*, i.e., D-Gluconic acid and 3-Dehydro-L-gulonate, were used as bioreductants during synthesis. Uric and citric acids increased antimicrobial activity through enhanced membrane interaction and nanoparticle stabilization. Additionally, 2-Pyrrolidone-5-carboxylic acid enabled dispersion, increasing bactericidal action against pathogens like *P. aeruginosa*, *E. coli*, and *C. difficile*. These findings are consistent with earlier research on CuONPs synthesized using plant extracts (Naika *et al.,* 2015; Sutradhar *et al.,* 2014).

5.3.7. Antioxidant Activity by DPPH Assay

The antioxidant activity of LCuONPs, determined by DPPH radical scavenging, followed concentration dependence (Figure IV. III. 7). Metabolites in *L. tristis* secretions, D-Gluconic acid, 3-Dehydro-L-gulonate, and Citric acid, bought electrons to scavenge DPPH radicals, indicated by decreased absorbance at 515 nm.

These results are consistent with earlier reports on CuONPs from *Spinacia oleracea, S. alternifolium, and T. terrestris* (Palani *et al.,* 2024; Thandapani *et al.,* 2023; Yugandhar *et al.,* 2017). Similar IC_{50} values were found with extracts from *Galeopsidis herba* (4.12 µg/mL) and *M. domestica* leaves (24.73 µg/mL) (Dobrucka, 2018; Jadhav *et al.,* 2018), indicating the redox-active character of *L. tristis* metabolites.

5.3.8. Environmental Toxicity Assessed via *Allium cepa* Bioassay

LCuONPs genotoxicity was evaluated using the *A. cepa* assay. Defensive gland metabolites such as hydroquinones and carboxylic acids played a role as stabilizers and reductants, altering nanoparticle bioactivity. Results indicated concentration-dependent reduction in mitotic index (MI) to a minimum of 3.54% at 500 µg/mL and corresponding increase in chromosomal abnormalities (Figure IV. III. 8; Table IV. III. 2). ROS produced by nanoparticle interaction with root tissues most likely perturbed redox balance, as reported by Nagaonkar et *al.,* (2015) and Ahmed *et al.,* (2018). Abnormalities seen chromosomal bridges, stickiness, and laggards verified LCuONPs' genotoxicity, possibly through DNA interaction and oxidative stress (Nagaonkar *et al.,* 2015 ; Ahmed *et al.,* 2018) .

5.3.9. Anticancer Activity of LCuONPs

LCuONPs prepared from the secretions of *L. tristis* were tested for cytotoxicity against Dalton's lymphoma ascites (DLA) cells (Figure IV. III. 9; Table IV. III. 3). Redox-modulating bioactive metabolites (e.g., 2,5-dimethyl hydroquinone, D-Gluconic acid, uric acid) augmented ROS production, causing selective cancer cell apoptosis without affecting normal cells. These findings are in agreement with Pramanik *et al.,* (2018) and Maliki *et al.,* (2022), validating CuONPs' anti-oxidative stress role in the induction of cancer cell death. Optimization of selectivity and minimizing toxicity should be further developed (Pramanik *et al.,* 2018; Maliki *et al.,* 2022).

5.3.10. Antiangiogenic Activity in CAM Assay

LCuONPs had great inhibition against angiogenesis in chick chorioallantoic membrane (CAM) models, which is reflected in decreased vessel length, junctions, and area upon 48 h exposure (Figure IV. III.10 – 11). This is due to disruption of endothelial proliferation and migration, possibly through VEGF downregulation and oxidative stress. These results are consistent with previous research showing copper nanoparticles' antiangiogenic properties in zebrafish and mammalian models (Chang *et al.,* 2015; Kamble *et al.,* 2016; Raj Preeth *et al.,* 2019; Song *et al.,* 2014; Saeed *et*

al., 2019). Limitations, however, are the lack of mechanistic specificity (e.g., VEGF/ROS pathways) and the simplicity of embryonic models. In addition, cytotoxicity against non-target tissues is yet to be investigated.

5.4. Harnessing *Luprops tristis* defensive secretion for Gold Nanoparticle Synthesis and Its Biological Uses

In this study, gold nanoparticles (referred to as LAuNPs) were synthesized by reducing a solution of auric chloride ($AuCl_4$) using an extract derived from the defensive gland of the insect *L. tristis*. Subsequently, the synthesized nanoparticles underwent thorough chemical characterization utilizing techniques such as UV-Vis spectroscopy, FTIR, SEM, TEM, and Zeta potential analysis. Following this characterization, the investigation proceeded to explore the electrochemical and biological functionalities of these nanoparticles. This included assessing their capabilities in glucose sensing, antibacterial activity, antioxidant properties, antimitotic effects, and anticancer potential.

5.4.1. UV-Vis Spectroscopic Profiling of LAuNPs

The surface plasmon resonance phenomenon was the cause of the LAuNPs' apparent absorption peak at 563 nm (Figure IV. IV. 1). This occurrence serves as a trustworthy predictor of LAuNPs synthesis. By demonstrating a large level of polydispersity among the particles, the peak's notable broadening emphasized the apparent interaction between the biomolecules in the gland extract and the metallic gold (Philip, 2008). The UV-Vis spectra of gold nanoparticles showed a clear surface plasmon band centered at 563 nm. This band occurs because noble metal gold, strongly absorb light in the visible region, typically peaking between 500 and 600 nm, due to the surface plasmon resonance (SPR) phenomenon. SPR happens when the free conduction electrons in metallic nanoparticles oscillate collectively in response to an electromagnetic field (Noruzi *et al.,* 2011). Likewise, gold nanoparticles synthesized from sugar beetroot pulp and *Stoechospermum marginatum* (kützing) exhibited a UV-Vis absorption peak at 560 nm (Arockiya Aarthi Rajathi *et al.,* 2012; Castro *et al.,* 2010).

5.4.2. FTIR Fingerprint Analysis of LAuNPs: Decoding Functional Groups and Surface Chemistry

FTIR analysis confirmed the significant role of phenolic compounds in stabilising LAuNPs and their likelihood of interaction with them (Figure IV. IV. 2**)**, consistent with previous research suggesting the involvement of bioactive components like polyphenols, enzymes, and reducing sugars in the bioreduction and stabilisation of metallic ions. Huang *et al.,* (2007) highlighted the detection of strong absorption bands in the 1,000–1,800 cm^{-1} range, revealing the functional role of these chemicals (Huang *et al.,* 2007). Moreover, functional groups like N-H and O-H were observed between 3,200 and 3,500 cm^{-1}. For instance, absorption bands corresponding to C=C, C=O, C–N, C–O, and O–H were identified respectively, in the IR spectrum of *Mangifera indica*-mediated gold nanoparticles (Philip, 2010).

5.4.3. Structural Characterization of LAuNPs: SEM and TEM Imaging for Nano-Morphology Assessment

Scanning electron microscopy was employed to examine the morphology of the nanoparticles. These techniques, including scanning electron microscopy (SEM) and transmission electron microscopy (TEM), are used to characterize the structure and morphology of the synthesized nanoparticles (Figure IV. IV. 3). TEM provides superior resolution and magnification compared to SEM. Hence, when analysing the shape and size of NPs, TEM is preferred. Additionally, TEM, through the selected area electron diffraction (SAED) method, enables the distinction between crystalline and amorphous entities, offering another advantage over SEM (Kasthuri *et al.,* 2009). The SEM and TEM analyzes revealed that LAuNPs synthesized using the extract from *L. tristis* exhibited dense, predominantly spherical structures with a rough surface texture, showing a uniform dispersion at approximately 17 nm in size. These NPs tended to aggregate into larger clusters. The synthesis of LAuNPs from *L. tristis* was attributed to the presence of hydrogen bonds and electrostatic interactions between bio-organic molecules. The spherical structure of LAuNPs was confirmed by previous findings using *Macrotyloma uniflorum, Chenopodium album*

and persimmon leaf extract (Aromal *et al.,* 2012; Dwivedi & Gopal, 2010; Reddy *et al.,* 2013; Song & Kim, 2008).

5.4.4. Zeta Potential Evaluation of LAuNPs: Unraveling Surface Charge and Stability

The results indicated notable stability, with a Zeta Potential of -21.4 mV observed for the LAuNPs (Figure. V. IV. 4). The LAuNPs synthesized in this study demonstrated excellent stability, consistent with previous research findings on zeta potential. Our study confirms that gold nanoparticles have a negative surface charge, influenced by solution pH (Dubey *et al.,* 2010) as per the zeta potential difference between the stationary fluid layer and the dispersion medium (Delgado *et al.,* 2007).

5.4.5. Electrochemical Performance of LAuNPs through Differential Pulse Voltammetry

Electrochemical glucose sensing by biosynthesized LAuNPs was tested through Differential Pulse Voltammetry (DPV), where a linear response between current and glucose content was achieved with a detection limit (LOD) of 7 mM (Figure IV.IV.5). The surface functional chemistry of LAuNPs allows redox interactions with glucose, changing conductivity and allowing quantification. In comparison to chemically synthesized counterparts, biosynthesized LAuNPs present improved biocompatibility and promise for higher sensor specificity. This is in concordance with previous works, wherein enzyme-free sensors comprised of gold alloy nanoparticles on activated carbon had a LOD of 0.41 μM (Arikan *et al.,* 2022), and bi-element CuO-Au nanoparticle sensors quantified methylglyoxal at 2.35 nM (Rajpurohit *et al.,* 2019). *Yuan et al.,* (2010) also recorded 0.1 nM LOD with AuNPs-decorated graphene, while *Sehit et al.,* (2020) constructed a molecularly imprinted AuNP-based sensor with 1.25 nM LOD and 95% stability for 40 days (*Yuan et al.,* 2010; *Sehit et al.,* 2020). These results place biosynthesized LAuNPs as viable contenders for incorporation into future-generation, nonenzymatic glucose sensing platforms.

5.4.6. Antibacterial Potency of LAuNPs: Investigating Inhibitory Effects Against Pathogenic Strains

The research employed a disc diffusion experiment to evaluate the bactericidal activity of LAuNPs against *Staphylococcus aureus* and *Klebsiella pneumoniae*. The zone of inhibition (ZOI) was concentration-dependent, with diameters ranging from 7 mm to 13 mm at 5µg of LAuNPs. A continuous increase in the diameter of the inhibitory zone with a rise in the concentration of LAuNPs, as observed in Figure IV. IV. 6 & Table IV. IV. 1. A rise in LAuNPs concentration leads to a better antimicrobial effect, particularly against *K. pneumoniae* and *S. aureus*. The antibacterial activity of LAuNPs is dose-dependent. Earlier research findings highlight the bactericidal action of AuNPs. Similarly, Ahmed and colleagues investigated the impact of gold nanoparticle conjugation with chlorhexidine (Au–CHX) on *K. pneumoniae* isolates (Ahmed *et al.,* 2016). *Bacillus subtilis, S. aureus, K. pneumonia* and *E. coli* are some of the enteric bacterial human pathogens that Shahzadi Shamaila investigated the bactericidal action of gold nanoparticles (Shamaila *et al.,* 2016). In a recent work by Saima Hameed *et al.,* the antibacterial activity of AuNPs was reported to be shape-dependent. The study tested the impact of nanospheres (AuNSps), nanostars (AuNSts), and nanocubes (AuNCs) at reduced concentrations against various bacteria (Hameed *et al.,* 2020).

5.4.6. Antioxidant Capacity of LAuNPs: DPPH Assay for Radical Scavenging Activity

DPPH test examines antioxidant potential based on the determination of nanoparticles' free radical-scavenging ability. Here, LAuNPs of different concentrations were tested with DPPH, ascorbic acid, and distilled water. UV spectroscopy indicated maximum DPPH free radical absorption to be at 517 nm. The EC_{50} value was found to be 39 µg/mL. Interestingly, antioxidant activity qualitatively perceived by the color of the DPPH solution shifted from dark violet to pale-yellow colour. UV spectroscopic examination confirms LAuNPs enhanced antioxidant activity at higher doses (Figure. IV. IV. 7).

These findings align well with previous studies on the green synthesis of gold nanoparticles (AuNPs) using plant-derived biomolecules. Shabestarian *et al.,* (2016) reported the successful synthesis of AuNPs via a rapid, environmentally benign method employing aqueous sumac extract, which functioned both as a reducing and capping agent. Their study also demonstrated a dose-dependent antioxidant activity of the biosynthesized AuNPs *in vitro* (Shabestarian *et al.,* 2016). Similarly, Milanezi *et al.,* (2019) synthesized quercetin-capped gold nanoparticles (AuNPs-Qct) and confirmed their potent antioxidant potential (Milanezi *et al.,* 2019). Furthermore, Rajan *et al.,* (2015) evaluated the free radical scavenging ability of phytosynthesized AuNPs using the DPPH assay, revealing a significant antioxidant response (Rajan *et al.,* 2015). Collectively, these studies support the antioxidant efficacy of bio-inspired AuNPs and highlight the potential of phytochemicals as dual-functioning agents in green nanoparticle synthesis.

5. 4. 7. Ecotoxicological Assessment of LAuNPs' Environmental Impact

LAuNPs had dose-dependent genotoxic effects in *Allium cepa* as manifested by decreased mitotic index and increased chromosomal aberrations like stickiness, clumping, and breakages with maximum abnormalities at 500 µg/mL (Figure IV.IV.8; Table IV.IV.3). These results show that although LAuNPs interact with root tissues and cause mito-depressive effects, the resulting toxicity is still within acceptable phytotoxicity limits at smaller concentrations. The findings agree with earlier research indicating that gold nanoparticles, including vanillin-capped ones, cause significant cytogenetic alterations in *A. cepa* root meristem cells (Debnath *et al.,* 2018; Arya *et al.,* 2022). Genotoxic effects mirror the capability of particles to access plant tissues and interfere with chromosomal integrity. The research supports emerging evidence that biosynthesized AuNPs can affect plant genome stability, making them pertinent to environmental toxicology.

5.4.2 Anticancer Activity of LAuNPs

LAuNPs exhibited dose-dependent cytotoxicity against DLA cells (Figure IV. IV. 9; Table IV. IV. 4), corroborating earlier research on biosynthesized AuNPs having tremendous anticancer efficacy. The mounting cell death across time

indicates generation of ROS and interference with intracellular redox homeostasis as possible modes of action. Considering the imperative role of antioxidants in regulating oxidative stress and eliminating carcinogenesis, the capping agents of *L. tristis* are perhaps synergistically helping to achieve the same. Similar efficacy has been reported by comparative studies. Munawer *et al.*, (2020) indicated high cytotoxicity of biologically prepared AuNPs. Rajeshkumar (2016) established the efficacy of AuNPs prepared with Enterococcus sp. against HepG2 and A549 cancer cells, whereas Khalaf *et al.,* (2021) revealed superior anticancer activity of chemically prepared AuNPs with various stabilizers against hepatic cancer cells (Munawer *et al.,* 2020; Rajeshkumar, 2016; Khalaf *et al.,* 2021).

These results support the promise of LAuNPs as environmentally friendly and biologically active anticancer drugs. Mechanistic validation, *in vivo* efficacy, and biosafety profiling should be pursued in further studies to enable clinical translation.

5.5. Biosynthesis of zinc oxide nanoparticles from *Luprops tristis* and their diverse applications

The synthesis of zinc oxide nanoparticles (ZnONPs) employs biological entities such as bacteria, fungi, plants, or their extracts to reduce and stabilize zinc ions (Zn^{2+}) from precursor solutions, resulting in the generation of nanoparticles. The green process provides a number of benefits over conventional chemical methods such as decreased toxicity, cost savings, and sustainability. The synthesis begins with the synthesis of a precursor solution made of zinc salts, which is mixed with a biological agent like the defense secretion of *L. tristis*. The biological agent is a reducing and capping mediator. The biological agents have a range of biomolecules such as enzymes, proteins, phenolic compounds, or polysaccharides that are used as reducing and stabilizing agents. These biomolecules play a role in interacting with zinc ions, initiating nucleation and subsequent formation of ZnONPs. Biosynthesis of ZnONPs can be studied by different methodologies, for example, UV-Vis spectroscopy, FTIR, SEM, TEM, and XRD. This green and sustainable method has the potential to be used in biomedicine applications as well

as in environmental remediation. Present research aimed at the utilization of defensive secretion of *L. tristis* for syntheses of LZnONPs.

5.5.1. UV–Vis Spectral Characterization of LZnONPs

Visible color change from reddish brown to purple indicated microwave-assisted synthesis of LZnONPs. UV–Vis spectroscopy validated nanoparticle formation by exhibiting a characteristic peak at 378 nm that is correlated with Zn biomolecule interactions of *L. tristis* gland extract (Figure IV.V.1). This peak, indicating high polydispersity, is consistent with earlier reports with *Ixora coccinea* (Yedurkar *et al.,* 2016), *Cuminum cyminum* (Zare *et al.,* 2017), *Plectranthus amboinicus,* and *Mangifera indica* (Rajeshkumar *et al.,* 2018), which revealed ZnONPs peaks between 340–376 nm.

5.5.2. FTIR Spectroscopy: Functional Groups Involved in ZnONPs Formation

FTIR spectra (4000 – 400 cm^{-1}) indicated characteristic bands for O–H, C–H, and N–H stretching, establishing the role of bioactive groups in nanoparticle synthesis (Figure IV.V. 2). Peaks associated with phenols, amines, and carboxyls validate their contribution to zinc ion reduction and nanoparticle stabilization, agreeing with earlier research (Bhuyan *et al.,* 2015). The findings establish the contribution of polyphenols, enzymes, and reducing sugars to bioreduction and capping of Zn^{2+} ions.

5.5.3. Morphological Analysis through SEM and TEM

SEM indicated predominantly spherical and aggregated ZnONPs, possibly due to interparticle densification based on the reducing agents present in *L. tristis* extract (Figure IV. V. 3A). Particle diameters were between 5–40 nm, consistent with Singh *et al.,* (2011). TEM analysis revealed spherical nanoparticles with a mean size of 26 ± 2 nm (Figure IV. V. 3 B, C), consistent with previous reports using *Parthenium hysterophorus* and *Pichia kudriavzevii* (Moghaddam *et al.,* 2017; Rajiv *et al.,* 2013; Singh *et al.,* 2011 ; Jayaseelan *et al.,* 2012; Pillai *et al.,* 2020) .

5.5.4. Zeta Potential and Stability Evaluation

Zeta potential analysis provided a value of −11.9 mV (Figure IV.V.4), establishing moderate stability of LZnONPs, in keeping with the literature (Nithya & Kalyanasundharam, 2019). Negative surface charge enables electrostatic stabilization and biological membrane interaction potential (Fatehah *et al.,* 2014; Sarkar *et al.,* 2014).

5.5.5. Electrochemical Investigation of LZnONPs: Differential Pulse Voltammetry (DPV) for Sensing Applications

The limit of detection (LOD) for glucose was determined as 15 mM, which confirms the sensitivity of the DPV technique in determining low levels of glucose (Figure IV.V. 5). The results show similarity to past research, showing a detection limit of 0.7 nM obtained through nanoparticles of copper-doped zinc oxide (Mahmoud *et al.,* 2021). LZnONPs prepared in the context of this current research have potential for integration into electrochemical glucose monitoring devices. Interaction of glucose molecules with functionalized LZnONPs can bring about noticeable alterations in electrical conductivity or redox activity, which could be correlated to glucose concentration. Interestingly, biosynthesised LZnONPs could be found to be more biocompatible than chemically synthesised ones, worth significant attention towards their capability of enhancing the sensitivity and specificity of glucose sensors. The proposed sensor exhibited very good selectivity towards glucose among other interfering compounds (Kavitha *et al.,* 2012).

5.5.6. Antibacterial Activity of LZnONPs: Exploring Pathogen Inhibition

The research explored the antibacterial activity of LZnONPs, that is, their effect on the growth of Gram positive and negative bacterias (*S. aureus* and *K. pneumonia*). The zone of inhibition (ZOI) both strains were increased with concentration of LZnONPs, indicating a gradual enlargement of the ZOI diameter according to concentrations hike. The results suggest that LZnONPs may have antibacterial properties (Figure IV.V. 6 & Table IV. V. 1).

The antibacterial effectiveness of LZnONPs has a dose-dependent characteristic; an increase in LZnONPs concentration leads to an enhanced antimicrobial impact, especially when compared to *K. pneumoniae* and *S. aureus.* ZnONPs shows antibacterial activity as demonstrated in earlier research works (Chemingui *et al.,* 2024; Droepenu *et al.,* 2024; Kermanshahi & Akhbari, 2024; Shakal *et al.,* 2024). The observed dose-dependent increase in the zone of inhibition (ZOI) emphasizes the efficacy of LZnONPs in combating microbial growth, aligning with existing literature on the antibacterial properties of ZnONPs. This work is particularly relevant given the growing concern over antibiotic resistance, offering a promising alternative or complementary approach to traditional antibiotics. Future applications could extend to the development of antibacterial coatings, wound dressings, and water purification systems. However, limitations such as the need for detailed cytotoxicity assessments, understanding long-term environmental implications, and scaling up the production of LZnONPs for industrial applications must be addressed. Further studies focusing on the mechanism of action and enhancing the specificity of LZnONPs are essential for their practical deployment in biomedical and environmental fields.

5.5.7. Antioxidant Capacity of LZnONPs: DPPH Assay for Radical Scavenging Activity

The DPPH test is widely used to assess antioxidant potential in nanoparticles. In this study, LZnONPs concentrations were combined with DPPH to create solutions, with ascorbic acid as the standard. UV spectroscopy revealed maximum DPPH free radical electron absorption at 517 nm. The findings thoroughly detail the scavenging activity that varies with concentration of LZnONPs. The EC_{50} value was found to be 26 µg/mL from the calibration curve (Figure IV.V. 7). Notably, the colour of the DPPH solution changed from a deep violet hue to a pale-yellow tint with an increase in the concentration of LZnONPs. LZnOPs enhanced antioxidant activity at increasing concentrations was confirmed by UV spectroscopic investigation, as shown in Figure IV.V.7. The current results

affirm the increasing evidence for the antioxidant activity of green-synthesized zinc oxide nanoparticles (LZnONPs), which are relevant in nanomedicine, food storage, and cosmetics. The free radical scavenging activity, as confirmed by UV spectrophotometry and EC_{50} analysis, concurs with earlier research (Chandra *et al.,* 2019; García-López *et al.,* 2018; Nagajyothi *et al.,* 2015; Rehana *et al.,* 2017). The focus on green synthesis mitigates concerns related to sustainability while providing a sustainable alternative to traditional routes. Potential uses involve therapeutic antioxidants, food packaging shelf-life extension, and inclusion in dermatological products. Still, there are issues of long-term stability, biocompatibility, and cytotoxicity associated with LZnONPs, which need to be explored more *in vivo* for translational feasibility.

5.5.8. Environmental Impact of LZnONPs: Comprehensive Toxicity Testing for Ecosystem Safety

By using biosynthesized LZnONPs in chromosomal aberration tests, it was possible to demonstrate conclusively that phytotoxicity can induce chromosomal aberrations. Conspicuous data showing a dose-dependent modification in the development of root cells after being exposed to various concentrations of LZnONPs ranging from 100 µg/mL to 500 µg/mL, supported this observation (Table IV. V. 2 & Figure IV.V. 8). Chromosomal abnormalities including chromosome bridges, vagrant chromosomes, and lag chromosomes, anaphase stickiness and shattered chromosomes, were discovered by the current investigation. The percentage of LZnONP's genotoxic potential in comparison to control and experiment conditions was calculated. According to data analysis, the control group's Mitotic Index (MI) stayed within the expected range (Figure IV. V. 8); in contrast, the experimental group's percentage of chromosomal anomalies showed a progressive increase, accompanied with a decreasing percentage MI. It is noteworthy that the lowest MI of 12.84 was found at 500 µg/mL and coincided with the largest aberration percentage as the LZnONPs concentration increased. Even though it causes abnormalities but below a 50% so we can use it as an eco friendly

agent and doesn't cause any serious harm to plants when released to nature. The current study suggests that onion bulbs exposed to different nanoparticle concentrations may have contained nanoparticles that, upon adhering to onion roots and infiltrating tissues, induced the generation of ROS, which disturbed the redox balance and led to genotoxic and mitochondrial depressive effects (Ahmed *et al.,* 2018; Fadoju *et al.,* 2020; Kumari *et al.,* 2011; Shaymurat *et al.,* 2012; Sun *et al.,* 2019; Youssef & Elamawi, 2020).

5.5.9. Anticancer Potential of LZnONPs: Evaluating Cytotoxicity and Therapeutic Activity

Numerous nanoparticles have pharmacological and biochemical traits, such as anti-inflammatory and antioxidant activities, which may help explain their anticarcinogenic and antimutagenic properties. Currently, biologically created nanoparticles are essential for diseases, like cancer. The current work, which uses Dalton's lymphoma ascites (DLA) cell lines, demonstrate the efficacy of biologically generated Zinc oxide nanoparticles as an anticancer drug. The cytotoxicity of the Zinc oxide nanoparticles against DLA cells is dose-dependent. The test shows that cellular death escalates over time in proportion to the concentration of biosynthesized zinc oxide nanoparticles (Figure IV.V. 9 & Table IV. V. 3). As was already mentioned, antioxidants are essential for the prevention and treatment of cancer as well as for preventing diseases brought on by the effects of free radicals. Antioxidants are made up of a wide variety of molecular substances that interact with free radicals to neutralize them. Antioxidants have the power to prevent and treat cancer by eradicating free radicals. Thus, the present study supports that LZnONPs prepared by biological synthesis possess broad anticancer activity. This anticancer activity of LZnONPs, demonstrated in several previous research studies, is in line with the findings of the present work (Abdelhakim *et al.,* 2020; Bisht & Rayamajhi, 2016; Chabattula *et al.,* 2021; Ravichandran *et al.,* 2022; Vidhya *et al.,* 2020).

5.6. Comparative analysis

5.6.1. Comparative TEM Study of Metal Nanoparticles Produced by Luprops tristis Defensive Secretion

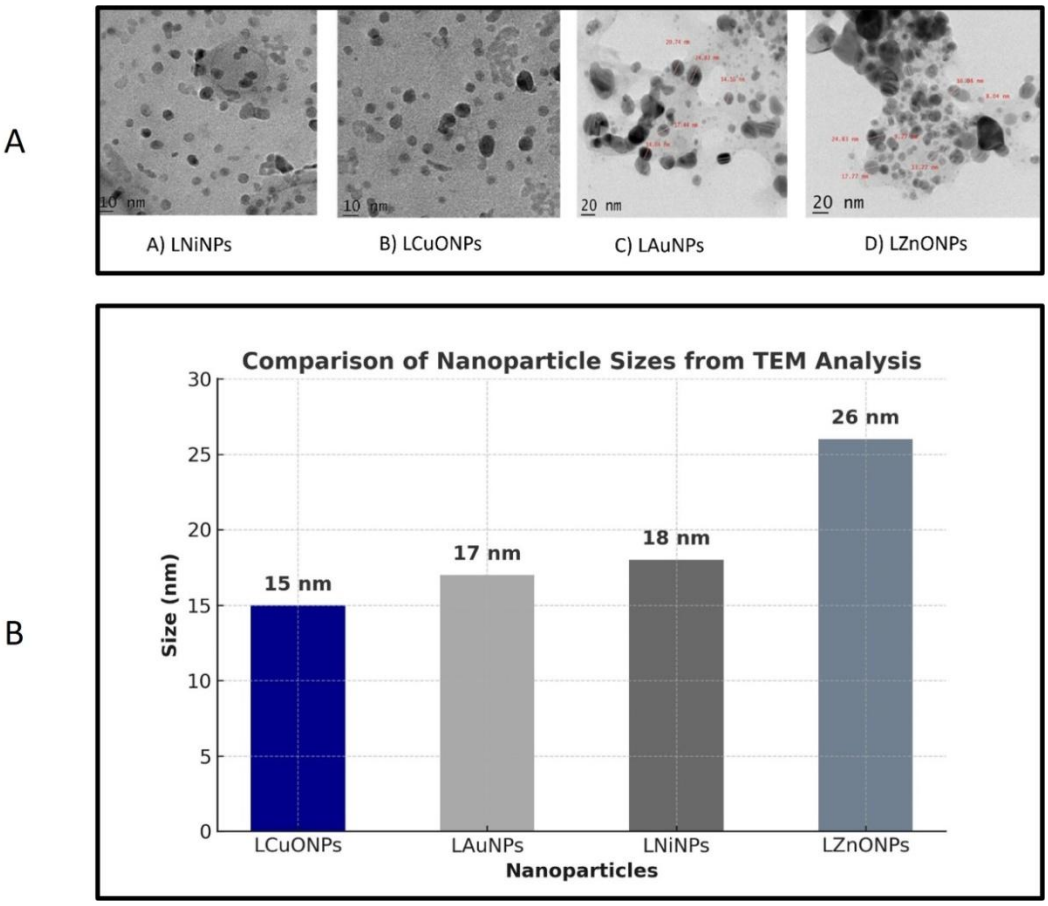

Figure V.VI. 1: Comparison of nanoparticle sizes (A, B)

Transmission electron microscopy (TEM) showed clear morphological variations between metal nanoparticles produced by *L. tristis* defensive secretions (Fig. V.VI.1). The nanoparticles LNiNPs, LCuONPs, LAuNPs, and LZnONPs showed size differences governed by both the biochemical composition of the secretion and microwave-assisted synthesis. The resultant size differences are ascribed to the occurrence of organic acids, polyphenols, and hydrocarbons in the secretion that regulate nucleation and growth upon synthesis (Alegria *et al.,* 2018). Reducing agents like D-gluconic acid, uric acid, and citric acid facilitate the reduction and stabilization of metal ions, whereas polyphenolic agents like 2,3-

dimethyl-1,4-benzoquinone and 2,5-dimethyl hydroquinone facilitate smaller particle formation by controlled growth and restricted aggregation.

LCuONPs had the smallest mean size (~15 nm), followed by LAuNPs (17 nm) and LNiNPs (18 nm), presumably as a result of effective reduction kinetics catalyzed by these compounds. By contrast, LZnONPs (~26 ± 2 nm) had larger sizes, possibly as a result of hydrocarbon-mediated agglomeration (e.g., tetracosane, hexacosane) (Amini & Akbari, 2019). Microwave irradiation (15 min, 350 W) also had an effect on synthesis by speeding up reaction rates, increasing nucleation, and constraining uncontrolled growth, thus improving particle uniformity (Rao *et al.,* 2002; Grassian, 2008). These results demonstrate the interplay between biochemical capping agents and physical factors in controlling nanoparticle size and their resulting biomedical and nanotechnological value.

5.6.2. Comparative Study of Four Nanoparticles in Various Applications

5.6.2.1. Comparative Study of Electrochemical Sensing

A

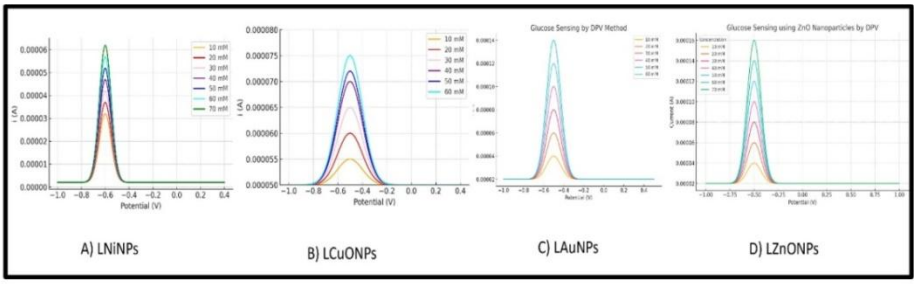

B

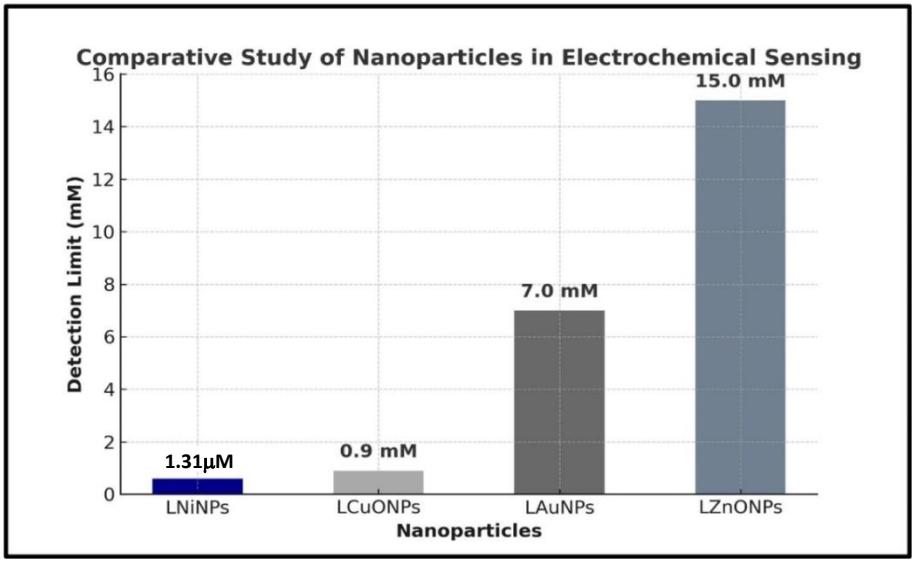

Figure V.VI. 2: Comparison of Electrochemical sensing (A & B)

Nickel (LNiNPs), copper oxide (LCuONPs), gold (LAuNPs), and zinc oxide (LZnONPs) nanoparticles, which are prepared with *L. tristis* secretions, possess different physicochemical properties that impact their electrochemical performance (Fig. V.VI.2). LNiNPs (~18 nm, −16.5 mV zeta potential) displayed the highest sensitivity as a non-enzymatic glucose sensor with a detection limit of 0.6 mM. Their relatively moderate surface charge and nanoscale dimension improved electron transfer and stable glucose interaction. In comparison, LCuONPs (~15 nm, −22 mV) were better in detecting hydrogen peroxide (H_2O_2) with a detection limit of 0.9 mM due to higher surface reactivity and charge stabilization. The higher surface charge of LCuONPs promoted stronger interactions with H_2O_2, enhancing sensor sensitivity and linear response. LAuNPs of 17 nm diameter and -21.4 mV zeta potential were also tested for glucose sensing and showed a detection limit of 7 mM. The biocompatibility and strong redox-active character of LAuNPs enabled good electron transfer during glucose oxidation, albeit with slightly reduced sensitivity compared with LNiNPs. LZnONPs, the biggest of the four at 26 ± 2 nm with a zeta potential of -11.9 mV, exhibited enzyme-free glucose sensing with a detection limit of 15 mM. Even with their bigger size and lower surface charge, LZnONPs retained high catalytic activity, allowing glucose oxidation at various concentrations. The comparative analysis illustrates that even though all the nanoparticles hold electrochemical sensing potential, LNiNPs are the most glucose-sensitive, LCuONPs are optimized for H_2O_2 detection, and LAuNPs and LZnONPs offer secondary choices with moderate efficiency. The variation in particle size, surface charge, and catalytic behavior affects their individual performance, underpinning the need for nanoparticle selection optimized for individual biosensing applications.

5.6.2.2. Comparative analysis of Antibacterial analysis

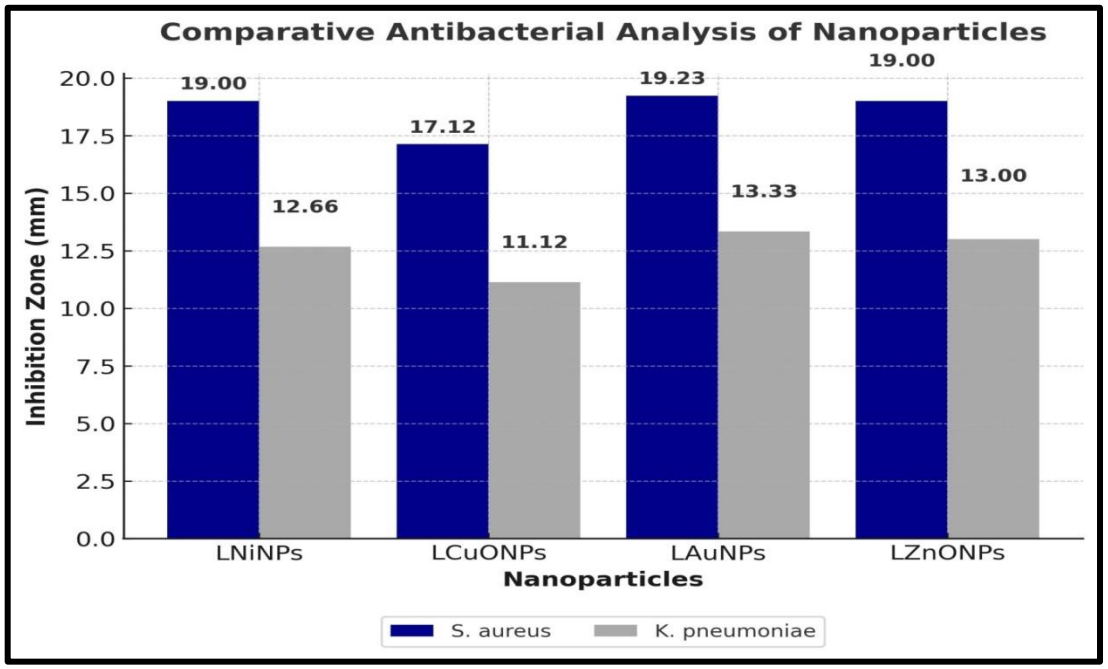

Figure V.VI. 3: Comparison of Antibacterial activity.

The antibacterial activity of LNiNPs, LCuONPs, LAuNPs, and LZnONPs is highly dependent on particle size, surface charge, and metal-specific attributes (Fig. V.VI.3). LNiNPs (size - 18 nm, Zeta potential - −16.5 mV) exhibited strong inhibitory activity against *S. aureus* (ZOI - 19.00 ± 0.58 mm) and *K. pneumoniae* (12.66 ± 0.57 mm) at 20 µg/mL. Their action is due to the release of Ni^{2+} ions, ROS generation, and disruption of membranes (Kovacic & Somanathan, 2013). LCuONPs (15 nm, −22 mV) had improved, dose-dependent action, particularly against *S. aureus* (10.76–17.12 mm), with *K. pneumoniae* being less affected (max 11.12 mm). Their improved activity is associated with their reduced size, augmented surface interactions, and induction of oxidative stress. LAuNPs (17 nm, −21.4 mV) produced notable inhibition zones for *S. aureus* (13.23–19.23 mm) and moderate inhibition for *K. pneumoniae* (7.33–13.33 mm). Their activity is attributed to membrane penetration and redox-mediated cytotoxicity. LZnONPs, though larger in size (26 ± 2 nm, −11.9 mV), were very effective, especially against *S. aureus* (13–19 mm). Their ability to produce ROS compensates for size, favoring direct membrane damage.

Overall, LCuONPs and LNiNPs exhibited better antibacterial activity owing to reduced size and greater zeta potential, resulting in improved cellular interaction and ROS-dependent killing. LZnONPs, although being larger, maintain activity through intrinsic oxidative processes, whereas LAuNPs provide balanced activity, especially against Gram-positive bacteria (Kovacic & Somanathan, 2013).

5.6.2.3. Comparative analysis of Antioxidant activity

A

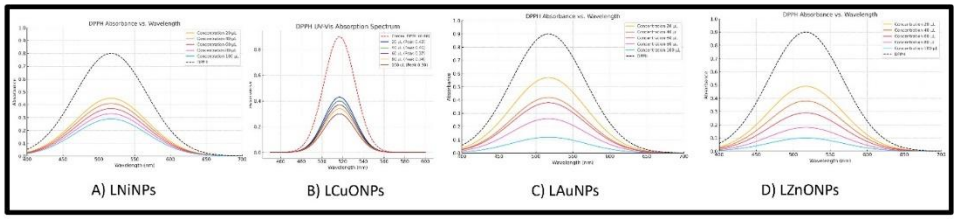

B

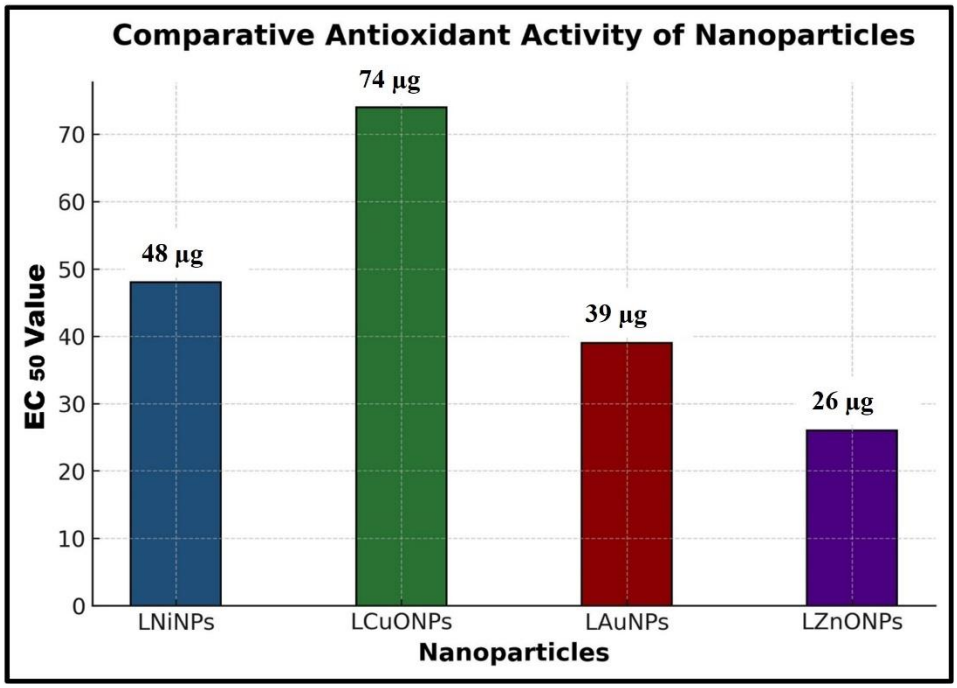

Figure V.VI. 4: Comparison of Antioxidant activity (A, B)

The antioxidant activity of LNiNPs, LCuONPs, LAuNPs, and LZnONPs was assessed through DPPH radical scavenging assay, indicating concentration-dependent activity (Fig. V.VI.4). LZnONPs showed maximum activity (EC_{50} = 26 µg/mL), followed by LAuNPs (39 µg/mL), LNiNPs (48 µg/mL), and LCuONPs (74 µg/mL). The enhanced performance of LZnONPs is due to higher surface area and more efficient electron transfer, with resultant stronger radical interactions. LAuNPs

also exhibited considerable activity based on their natural stability and biocompatibility. LNiNPs had moderate activity, which increased with concentration, as verified spectrophotometrically. LCuONPs, despite their nanoscale size (~15 nm), had the lowest activity, confirming that antioxidant activity is not only based on size but also surface chemistry and charge (Flieger *et al.,* 2021). LZnONPs, at a size of ~26 ± 2 nm, had the best properties for radical neutralization. These results highlight the potential of LZnONPs for applications requiring high antioxidant demand, whereas LAuNPs and LNiNPs are still promising options (Bedlovičová *et al.,* 2020).

5.6.2.4. Comparative Anticancer activity

A

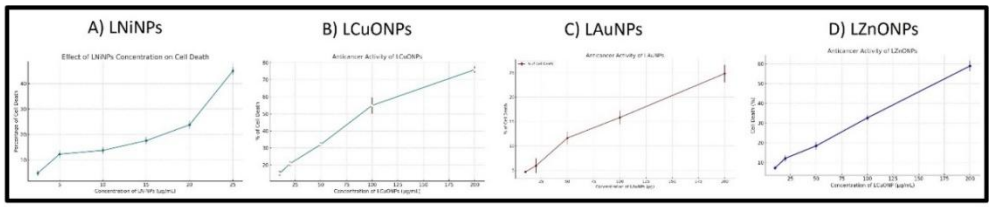

B

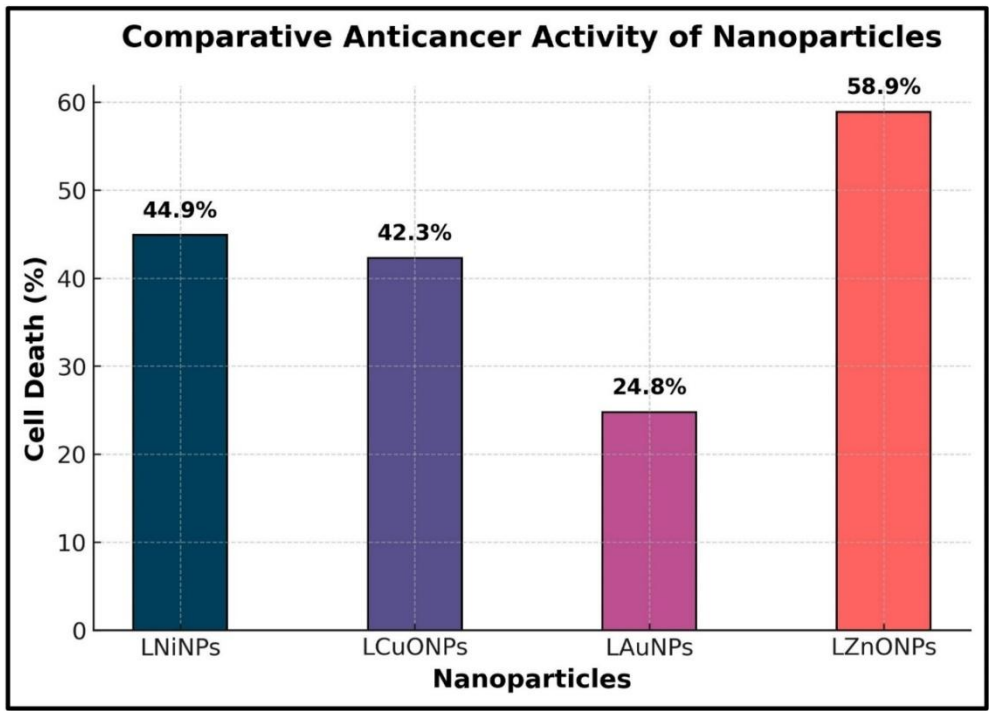

Figure V.VI. 5: Comparison of Anticancer activity (A & B).

The biosynthesized metal nanoparticles Nickel (LNiNPs), Copper Oxide (LCuONPs), Gold (LAuNPs), and Zinc Oxide (LZnONPs) have specific physicochemical properties that govern their anticancer potential (Fig. V.VI.5). LNiNPs with 18 nm size and zeta potential -16.5 mV were found to cause dose-dependent cytotoxicity towards DLA cells, where the cell death progressed from 4.9% at 2.5 µg/mL to 44.9% at 25 µg/mL. The strong anticancer activity is due to their ROS-neutralizing and oxidative stress-modulating activitiesn (Adhikari *et al.,* 2021). For comparison, LCuONPs of a lower size of 15 nm with a highly negative zeta potential value of -22 mV also showed significant anticancer activity through apoptosis induction and oxidative stress generation, consistent with their capacity for disturbing redox homeostasis of cancer cells. The biosynthesis process included major metabolites like D-Gluconic acid and citric acid, which improved stability as well as biocompatibility. LAuNPs, with dimensions of 17 nm and -21.4 mV zeta potential, exhibited moderate cytotoxicity, ranging from 4.67% at 10 µg/mL to 24.8% at 200 µg/mL, that suggests ROS-mediated cellular interference. Yet, their anticancer effectiveness is lower than that of LNiNPs and LZnONPs at similar concentrations, and may indicate potential differences in the uptake or interaction of nanoparticles with cancer cells. LZnONPs, which were the largest of the four (26 ± 2 nm), had the strongest anticancer activity, and cell death increased from 7.22% at 10 µg/mL to 58.9% at 200 µg/mL. The higher cytotoxicity of LZnONPs indicates a higher ability for ROS production and oxidative stress-mediated killing of cancer cells (Dash *et al.,* 2014). Of the four nanoparticles, the variations in size, zeta potential, and bioactive capping agents are the key determinants of their anticancer activity. The negative zeta potential of LCuONPs and LAuNPs indicate greater stability and increased cellular uptake, while that of the comparatively lower zeta potential of LNiNPs could affect interaction with cell membranes. The observed high anticancer activity of LZnONPs, in contrast to their relatively larger size, indicates that the special physicochemical characteristics play an important role in their therapeutic efficacy. Overall, though all four nanoparticles have good anticancer potential, LZnONPs are the most cytotoxic, followed by LNiNPs, LCuONPs, and LAuNPs, and hence show promise as potent therapeutic agents.

Therefore, though these nanoparticles show antioxidant activity in normal cells owing to their capping molecules, their metal ion nature and oxidative stress induction take precedence in cancer cells and cause ROS-mediated cytotoxicity as shown in V.VI. 7A. This bimodal character renders them selectively toxic to cancer cells but nontoxic to normal cells, and hence they are of interest for anticancer use.

5.6.2.5. Comparative study of Antiangiogenic activity - CAM assay

A

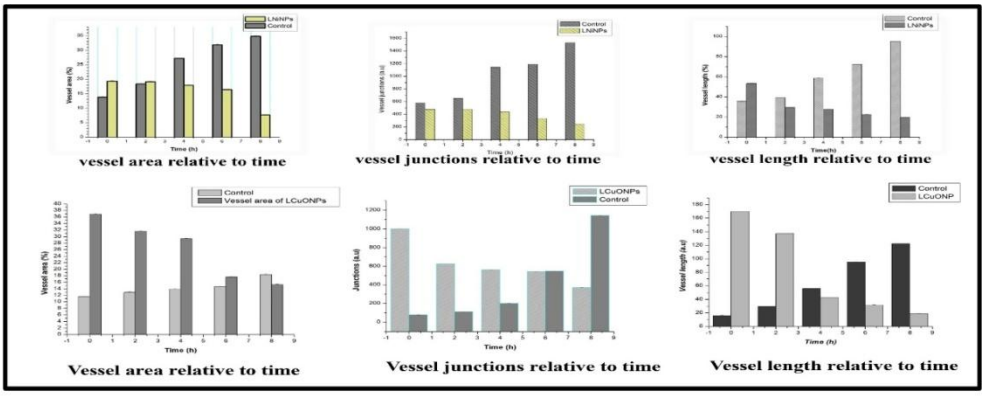

B

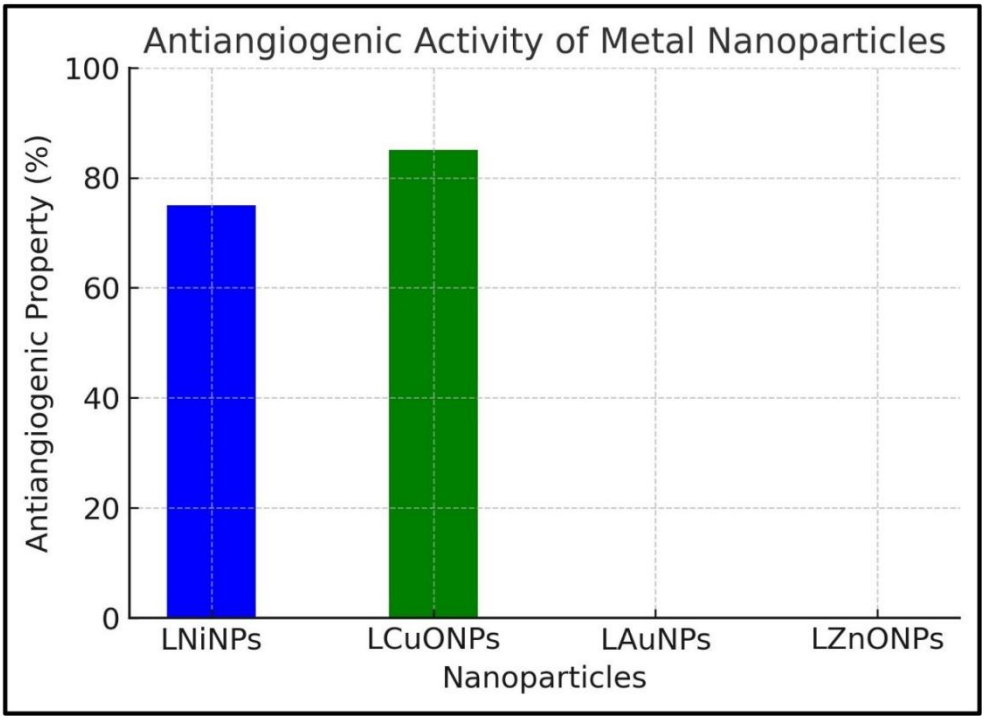

Figure V.VI. 6: Comparison of Antiangiogenic activity (A, B)

Both LNiNPs and LCuONPs have profound antiangiogenic activities (Fig. V.VI.6), but their mode and efficacy differ. LNiNPs show a progressive and

continuous decline in vascular parameters, while LCuONPs first induce vessel enlargement followed by an abrupt decrease in angiogenesis. This would indicate that CuONPs would exert a slower but effective influence on vascular regression than NiNPs. Mechanistically, LNiNPs act by ROS generation, endothelial dysfunction, and ECM disruption, whereas LCuONPs mainly act by VEGF inhibition and endothelial apoptosis. Biofunctionalization of LNiNPs with molecules from beetles provides a distinct advantage, increasing their stability and specificity towards endothelial cells. LCuONPs, however, have shown that they can destabilize established vasculature and are thus effective in later stages of angiogenesis (Barui *et al.,* 2019).

Although both nanoparticles show potential as cancer therapy and diseases dependent on angiogenesis agents, more work is needed to maximize their dosage, biocompatibility, and targeting efficacy. Their long-term safety assessments on non-target tissues are needed to support their use in the clinic. Considering combination therapies in which NiNPs and CuONPs are used in combination may increase their therapeutic effects through summation of their complementary modes. Gold nanoparticles (AuNPs) and zinc oxide nanoparticles (ZnONPs) can have negative outcomes in anti-angiogenic assays because of their special physicochemical properties, biological interactions, and modes of action, which are quite distinct compared to nickel (NiNPs) and copper oxide nanoparticles (CuONPs). Although NiNPs and CuONPs exhibit significant anti-angiogenic activities because of their ROS-mediated cytotoxicity and VEGF inhibition, AuNPs and ZnONPs can either enhance or exert a neutral effect on angiogenesis. Their biocompatibility, minimal ROS generation, and cross-talk with VEGF signaling pathways are responsible for their failure to display pronounced anti-angiogenic activities in the CAM assay shown in V.VI. 7B. More research is warranted to evaluate their activity in various concentrations and surface modifications to ascertain their complete angiogenic capacity (Abdalla *et al.,* 2018; Mukherjee & Patra, 2016). The results highlight the therapeutic potential of metal-based nanoparticles in inhibiting angiogenesis. Both LNiNPs and LCuONPs are efficient at interfering with vascular formation, although their different mechanisms, duration of action, and molecular interactions provide

distinct applications in antiangiogenic therapy. By optimizing synthesis and delivery, these nanoparticles have the potential to be major players in nanomedicine, especially for cancer and vascular disease. Nonetheless, rigorous research in systemic toxicity, dosage, and molecular mechanisms is imperative to enable further clinical translation (Hashemi Goradel *et al.,* 2018).

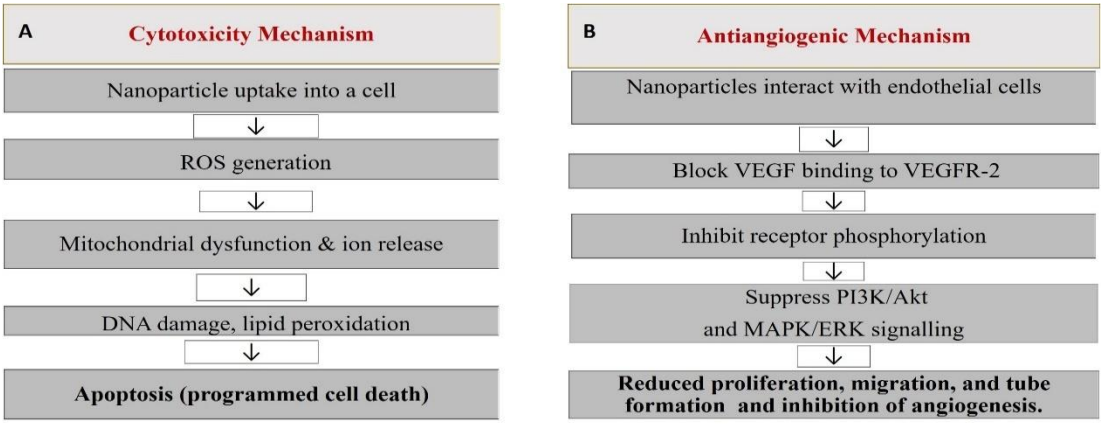

Figure V.VI. 7(A&B): M**echanism of action of NPs on cytotoxicity and angiogenesis**

We initially used a standard concentration for all assays, but as the results were negligible, we optimized each assay by testing higher concentrations to achieve reliable outcomes. Among the metal nanoparticles (MNPs) evaluated, biosynthesized *L. tristis*-mediated LCuONPs exhibited the most promising potential for biomedical applications, particularly in oncology. This was evidenced by their pronounced cytotoxicity and robust anti-angiogenic activity, suggesting a strong therapeutic efficacy against cancer cells. In contrast, LAuNPs, despite demonstrating relatively low cytotoxicity, showed excellent biocompatibility and colloidal stability, making them highly suitable candidates for targeted drug delivery systems. LNiNPs displayed an intermediate biological profile, with moderate cytotoxicity, indicating their potential utility in scenarios requiring controlled therapeutic action. LZnONPs, which exhibited the lowest cytotoxic and anti-angiogenic effects among the tested MNPs, may be more appropriate for applications in regenerative medicine rather than oncology. Collectively, these findings highlight LCuONPs as the most potent candidates for further exploration in cancer therapeutics, meriting continued investigation for their potential translation into clinical practice.

CHAPTER VI

SUMMARY AND CONCLUSION

SUMMARY

This study provides a comprehensive investigation into the chemical composition and biological potential of the defensive gland secretion of *L. tristis*, which was effectively utilized in the green synthesis of various metal nanoparticles (Ni, CuO, Au, and ZnO) with promising biomedical applications. The secretion demonstrated significant antioxidant, antibacterial, cytotoxic, and genotoxic properties, emphasizing its potential as a natural bioresource for nanoparticle synthesis. Microwave-assisted synthesis of nickel nanoparticles (LNiNPs) yielded nanostructures with excellent physicochemical stability and pronounced antioxidant, antibacterial, cytotoxic, and anti-angiogenic activities, affirming their applicability in cancer therapy and biosensing platforms. Similarly, copper oxide nanoparticles (LCuONPs) exhibited potent biological effects, including reactive oxygen species (ROS)-mediated cytotoxicity, anti-mitotic, anti-angiogenic, and antibacterial activities, positioning them as strong candidates for oncological applications. Gold nanoparticles (LAuNPs) demonstrated superior biocompatibility and colloidal stability, making them ideal for targeted drug delivery systems, alongside their established antioxidant and antibacterial efficacy. In contrast, zinc oxide nanoparticles (LZnONPs), though exhibiting moderate cytotoxic and anti-mitotic responses, displayed notable antioxidant and antimicrobial activities, suggesting their potential for regenerative medicine and environmental applications. Overall, the findings highlight the remarkable functional versatility of *L. tristis* defensive gland secretion as a renewable, eco-friendly platform for the synthesis of multifunctional metal nanoparticles, with CuONPs emerging as the most promising candidates for anticancer applications due to their high cytotoxicity, ROS generation, and anti-angiogenic effects.

CONCLUSION

The defensive gland secretion of *L. tristis* offers a unique biochemical environment conducive to the green synthesis of metal nanoparticles with diverse biomedical and environmental utilities. LC-MS analysis of the methanolic extract revealed a complex matrix of bioactive secondary metabolites, including D-gluconic acid, 3-dehydro-L-gulonate, uric acid, citric acid, and 2-pyrrolidone-5-carboxylic acid. These compounds served as effective reducing, capping, and stabilizing agents, influencing key physicochemical parameters such as particle size, morphology, and surface charge. Citric acid and uric acid contributed significantly to nanoparticle stabilization, as supported by zeta potential and FTIR analyses, while 3-dehydro-L-gulonate and D-gluconic acid enhanced antioxidant and redox properties. The resulting synthesis protocol is both environmentally sustainable and capable of producing nanoparticles with consistent bioactivity and colloidal stability. The biosynthesized nanoparticles LNiNPs, LCuONPs, LAuNPs, and LZnONPs exhibited multifunctional biological properties, including antimicrobial, antioxidant, biosensing, genotoxic, and anticancer activities. Notably, LAuNPs displayed superior antibacterial activity against *Staphylococcus aureus*, while LNiNPs and LZnONPs were effective as glucose sensors. Genotoxicity assays revealed minimal chromosomal aberrations, indicating safe application potential in agricultural systems under regulated conditions. Crucially, LCuONPs demonstrated the most potent anticancer and anti-angiogenic effects, highlighting their promise in oncology-directed nanomedicine. This research not only establishes *L. tristis* as a valuable, previously underutilized biological resource but also advances a cost-effective and sustainable strategy for fabricating bioactive nanomaterials. The findings pave the way for future innovations in nanomedicine, biosensing, agriculture, and antimicrobial technologies, positioning insect-derived secretions as transformative tools in green nanotechnology.

CHAPTER VII

RECOMMENDATIONS

Although the present study highlights the significant biomedical potential of metal nanoparticles (MNPs) synthesized using the defensive secretion of *L. tristis*, the experimental outcomes are predominantly based on *in vitro* assessments. To enhance their translational applicability, future investigations should be directed toward systematic *in vivo* studies. Such studies are essential to comprehensively evaluate the toxicological profiles, pharmacokinetics, biodistribution, and therapeutic efficacy of these nanoparticles within relevant animal models. This will provide crucial insights into their behavior within complex biological systems and serve as a foundation for their progression toward clinical implementation and environmental applications. Nevertheless, the low natural abundance and labor-intensive extraction of the insect's defensive secretion present substantial barriers to the large-scale production of these bioengineered nanoparticles. To overcome these limitations, future research should emphasize the elucidation, isolation, and synthetic or semi-synthetic replication of the principal bioactive molecules involved in nanoparticle synthesis. Special attention should be directed toward compounds such as organic acids (e.g., D-gluconic acid, citric acid, uric acid), amino acid derivatives, and quinonoid constituents. Quinones, in particular, owing to their potent redox potential and inherent antimicrobial activity, are hypothesized to play a pivotal role in metal ion reduction and the enhancement of nanoparticle biofunctionality. The synthetic reproduction of these key biomolecules, through environmentally benign chemical synthesis or biotechnological approaches, would enable the scalable and sustainable fabrication of biofunctional nanoparticles without compromising the unique properties conferred by the natural secretion. This approach not only ensures reproducibility and cost-effectiveness but also addresses ethical and environmental concerns associated with insect-derived biomaterials. Ultimately, such strategies will pave the way for the broader application of these nanomaterials in biomedicine, agriculture, and environmental science.

REFERENCES

Abboud, Y., Saffaj, T., Chagraoui, A., El Bouari, A., Brouzi, K., Tanane, O., & Ihssane, B. (2014). Biosynthesis, characterization and antimicrobial activity of copper oxide nanoparticles (CONPs) produced using brown alga extract (*Bifurcaria bifurcata*). *Applied Nanoscience*, *4*(5), 571–576. https://doi.org/10.1007/s13204-013-0233-x

Abdalla, A. M. E., Xiao, L., Ullah, M. W., Yu, M., Ouyang, C., & Yang, G. (2018). Current Challenges of Cancer Anti-angiogenic Therapy and the Promise of Nanotherapeutics. *Theranostics*, *8*(2), 533–548. https://doi.org/10.7150/thno.21674

Abdel Fattah, A. R., Majdi, T., Abdalla, A. M., Ghosh, S., & Puri, I. K. (2016). Nickel Nanoparticles Entangled in Carbon Nanotubes: Novel Ink for Nanotube Printing. *ACS Applied Materials & Interfaces*, *8*(3), 1589–1593. https://doi.org/10.1021/acsami.5b11700

Abdelhakim, H. K., El-Sayed, E. R., & Rashidi, F. B. (2020). Biosynthesis of zinc oxide nanoparticles with antimicrobial, anticancer, antioxidant and photocatalytic activities by the endophytic *Alternaria tenuissima. Journal of Applied Microbiology*, *128*(6), 1634–1646. https://doi.org/10.1111/jam.14581

Abhitha, P., Vinod, K. V., & Sabu, T. K. (2010). Defensive Glands in the Adult and Larval Stages of the Darkling Beetle, *Luprops tristis*. *Journal of Insect Science*, *10*(7), 1–5. https://doi.org/10.1673/031.010.0701

Abrori, S. A., Septiani, N. L. W., Nugraha, Anshori, I., Suyatman, Suendo, V., & Yuliarto, B. (2020). Metal-Organic-Framework FeBDC-Derived Fe3O4 for Non-Enzymatic Electrochemical Detection of Glucose. *Sensors*, *20*(17), Article 17. https://doi.org/10.3390/s20174891

Adachi, M., Tsukui, S., & Okuyama, K. (2003). Nanoparticle Synthesis by Ionizing Source Gas in Chemical Vapor Deposition. *Japanese Journal of Applied Physics*, *42*(1A), L77. https://doi.org/10.1143/JJAP.42.L77

Adhikari, A., Mondal, S., Das, M., Ghosh, R., Biswas, P., Darbar, S., Singh, S., Das, A. K., Bhattacharya, S. S., Pal, D., Mallick, A. K., & Pal, S. K. (2021). Redox Buffering Capacity of Nanomaterials as an Index of ROS-Based Therapeutics and Toxicity: A Preclinical Animal Study. *ACS Biomaterials Science & Engineering*, *7*(6), 2475–2484. https://doi.org/10.1021/acsbiomaterials.1c00402

Adhikary, J., Chakraborty, P., Das, B., Datta, A., Kumar Dash, S., Roy, S., Chen, J.-W., & Chattopadhyay, T. (2015). Preparation and characterization of ferromagnetic nickel oxide nanoparticles from three different precursors: Application in drug delivery. *RSC Advances*, *5*(45), 35917–35928. https://doi.org/10.1039/C5RA00642B

Adwin Jose, P., Dhaveethu Raja, J., Sankarganesh, M., & Rajesh, J. (2018). Evaluation of antioxidant, DNA targeting, antimicrobial and cytotoxic studies of imine capped copper and nickel nanoparticles. *Journal of Photochemistry and Photobiology B: Biology*, *178*(1), 143–151. https://doi.org/10.1016/j.jphotobiol.2017.11.005

Ahamed, M., Alhadlaq, H. A., Khan, M. A. M., Karuppiah, P., & Al-Dhabi, N. A. (2014). Synthesis, Characterization, and Antimicrobial Activity of Copper Oxide Nanoparticles. *Journal of Nanomaterials*, *2014*(1), 637858. https://doi.org/10.1155/2014/637858

Ahmad, A., Mukherjee, P., Mandal, D., Senapati, S., Khan, M. I., Kumar, R., & Sastry, M. (2002). Enzyme Mediated Extracellular Synthesis of CdS Nanoparticles by the Fungus, *Fusarium oxysporum. Journal of the American Chemical Society*, *124*(41), 12108–12109. https://doi.org/10.1021/ja027296o

Ahmar Rauf, M., Owais, M., Rajpoot, R., Ahmad, F., Khan, N., & Zubair, S. (2017). Biomimetically synthesized ZnO nanoparticles attain potent antibacterial activity against less susceptible *S. aureus* skin infection in experimental animals. *RSC Advances*, *7*(58), 36361–36373. https://doi.org/10.1039/C7RA05040B

Ahmed, A., Khan, A. K., Anwar, A., Ali, S. A., & Shah, M. R. (2016). Biofilm inhibitory effect of chlorhexidine conjugated gold nanoparticles against *Klebsiella pneumoniae. Microbial Pathogenesis*, *98*, 50–56. https://doi.org/10.1016/j.micpath.2016.06.016

Ahmed, B., Shahid, M., Khan, M. S., & Musarrat, J. (2018a). Chromosomal aberrations, cell suppression and oxidative stress generation induced by metal oxide nanoparticles in onion (*Allium cepa*) bulb†. *Metallomics*, *10*(9), 1315–1327. https://doi.org/10.1039/c8mt00093j

Ajaykumar, A. P., Sabira, O., Binitha, V. S., Varma, S. R., Mathew, A., Jayaraj, K. N., Janish, P. A., Zeena, K. V., Sheena, P., Venugopal, V., Palakkapparambil, P., & Aswathi. (2023). Bio-Fabricated Silver Nanoparticles from the Leaf Extract of the Poisonous Plant, *Holigarna arnottiana*: Assessment of Antimicrobial, Antimitotic, Anticancer, and Radical-Scavenging Properties. *Pharmaceutics*, *15*(10), Article 10. https://doi.org/10.3390/pharmaceutics15102468

Ajaykumar, A. P., Sabira, O., Sebastian, M., Varma, S. R., Roy, K. B., Binitha, V. S., Rasheed, V. A., Jayaraj, K. N., & Vignesh, A. R. (2023). A novel approach for the biosynthesis of silver nanoparticles using the defensive gland extracts of the beetle, *Luprops tristis* Fabricius. *Scientific Reports*, *13*(1), 10186. https://doi.org/10.1038/s41598-023-37175-0

Akintelu, S. A., Folorunso, A. S., Folorunso, F. A., & Oyebamiji, A. K. (2020). Green synthesis of copper oxide nanoparticles for biomedical application and environmental remediation. *Heliyon*, *6*(7), e04508. https://doi.org/10.1016/j.heliyon.2020.e04508

Alegria, E. C. B. A., Ribeiro, A. P. C., Mendes, M., Ferraria, A. M., Do Rego, A. M. B., & Pombeiro, A. J. L. (2018). Effect of Phenolic Compounds on the Synthesis of Gold Nanoparticles and its Catalytic Activity in the Reduction of Nitro Compounds. *Nanomaterials*, *8*(5), Article 5. https://doi.org/10.3390/nano8050320

Ali, T., Warsi, M., Zulfiqar, S., Sami, A., Ullah, S., Rasheed, A., Alsafari, I., Agboola, P., Shakir, I., & Mahmood, M. (2021). Green nickel/nickel oxide nanoparticles for prospective antibacterial and environmental remediation applications. *Ceramics International*, *48*. https://doi.org/10.1016/j.ceramint.2021.12.039

Allen, R. N., Shukla, M. K., & Leszczynski, J. (2004). A theoretical study of the structure and properties of uric acid: A potent antioxidant. *International Journal of Quantum Chemistry*, *100*(5), 801–809. https://doi.org/10.1002/qua.20246

Alonso, F., Riente, P., & Yus, M. (2008). Hydrogen-transfer reduction of carbonyl compounds promoted by nickel nanoparticles. *Tetrahedron*, *64*(8), 1847–1852. https://doi.org/10.1016/j.tet.2007.11.093

Alonso, F., Riente, P., & Yus, M. (2009). Wittig-Type Olefination of Alcohols Promoted by Nickel Nanoparticles: Synthesis of Polymethoxylated and Polyhydroxylated Stilbenes. *European Journal of Organic Chemistry*, *2009*(34), 6034–6042. https://doi.org/10.1002/ejoc.200900951

Alsamhary, K., Ameen, F., & Kha, M. (2024). Biosynthesis cobalt-doped nickel nanoparticles and their toxicity against disease. *Microscopy Research and Technique*, *87*(2), 272–278. https://doi.org/10.1002/jemt.24430

Ameen, F., AlYahya, S., Govarthanan, M., ALjahdali, N., Al-Enazi, N., Alsamhary, K., Alshehri, W. A., Alwakeel, S. S., & Alharbi, S. A. (2020). Soil bacteria *Cupriavidus sp.* Mediates the extracellular synthesis of antibacterial silver nanoparticles. *Journal of Molecular Structure*, *1202*(127233), 127233. https://doi.org/10.1016/ j.molstruc.2019.127233

Amendola, V., & Meneghetti, M. (2009). Laser ablation synthesis in solution and size manipulation of noble metal nanoparticles. *Physical Chemistry Chemical Physics*, *11*(20), 3805–3821. https://doi.org/10.1039/B900654K

Amini, N., Rashidzadeh, B., Amanollahi, N., Maleki, A., Yang, J.-K., & Lee, S.-M. (2021). Application of an electrochemical sensor using copper oxide nanoparticles/polyalizarin yellow R nanocomposite for hydrogen peroxide. *Environmental Science and Pollution Research*, *28*(29), 38809–38816. https://doi.org/10.1007/s11356-021-13299-6

Amini, S. M., & Akbari, A. (2019). Metal nanoparticles synthesis through natural phenolic acids. *IET Nanobiotechnology*, *13*(8), 771–777. https://doi.org/10.1049/iet-nbt.2018.5386

Amreen Nisa, S., Govindaraju, K., Vasantharaja, R., Kannan, M., & Karthickeyan, D. (2023). Biosynthesis of gold nanoparticles using jellyfish nematocyst venom protein and evaluation of their anticancer activity against breast cancer cells: *In-vitro* study. *Chemical Physics Letters*, *823*(1), 140523. https://doi.org/10.1016/ j.cplett.2023. 140523

Ananthi, V., Siva Prakash, G., Mohan Rasu, K., Gangadevi, K., Boobalan, T., Raja, R., Anand, K., Sudhakar, M., Chuturgoon, A., & Arun, A. (2018). Comparison of integrated sustainable biodiesel and antibacterial nano silver production by microalgal and yeast isolates. *Journal of Photochemistry and Photobiology B: Biology*, *186*(1), 232–242. https://doi.org/10.1016/j.jphotobiol.2018.07.021

Anbuvannan, M., Ramesh, M., Viruthagiri, G., Shanmugam, N., & Kannadasan, N. (2015). Synthesis, characterization and photocatalytic activity of ZnO nanoparticles prepared by biological method. *Spectrochimica Acta Part A: Molecular and Biomolecular Spectroscopy*, *143*(1), 304–308. https://doi.org/10.1016/j.saa. 2015.01.124

Ancona, A., Dumontel, B., Garino, N., Demarco, B., Chatzitheodoridou, D., Fazzini, W., Engelke, H., & Cauda, V. (2018). Lipid-Coated Zinc Oxide Nanoparticles as

Innovative ROS-Generators for Photodynamic Therapy in Cancer Cells. *Nanomaterials*, *8*(3), Article 3. https://doi.org/10.3390/nano8030143

Angeline Mary, A. P., Thaminum Ansari, A., & Subramanian, R. (2019). Sugarcane juice mediated synthesis of copper oxide nanoparticles, characterization and their antibacterial activity. *Journal of King Saud University - Science*, *31*(4), 1103–1114. https://doi.org/10.1016/j.jksus.2019.03.003

Applerot, G., Lellouche, J., Lipovsky, A., Nitzan, Y., Lubart, R., Gedanken, A., & Banin, E. (2012). Understanding the Antibacterial Mechanism of CuO Nanoparticles: Revealing the Route of Induced Oxidative Stress. *Small*, *8*(21), 3326–3337. https://doi.org/10.1002/smll.201200772

Argueta-Figueroa, L., Morales-Luckie, R. A., Scougall-Vilchis, R. J., & Olea-Mejía, O. F. (2014). Synthesis, characterization and antibacterial activity of copper, nickel and bimetallic Cu–Ni nanoparticles for potential use in dental materials. *Progress in Natural Science: Materials International*, *24*(4), 321–328. https://doi.org/10.1016/j.pnsc.2014.07.002

Arikan, K., Burhan, H., Sahin, E., & Sen, F. (2022). A sensitive, fast, selective, and reusable enzyme-free glucose sensor based on monodisperse AuNi alloy nanoparticles on activated carbon support. *Chemosphere*, *291*(1), 132718. https://doi.org/10.1016/j.chemosphere.2021.132718

Arockiya Aarthi Rajathi, F., Parthiban, C., Ganesh Kumar, V., & Anantharaman, P. (2012). Biosynthesis of antibacterial gold nanoparticles using brown alga, *Stoechospermum marginatum* (kützing). *Spectrochimica Acta Part A: Molecular and Biomolecular Spectroscopy*, *99*(1), 166–173. https://doi.org/10.1016/j.saa.2012.08.081

Aromal, S. A., Vidhu, V. K., & Philip, D. (2012). Green synthesis of well-dispersed gold nanoparticles using *Macrotyloma uniflorum*. *Spectrochimica Acta Part A: Molecular and Biomolecular Spectroscopy*, *85*(1), 99–104. https://doi.org/10.1016/j.saa.2011.09.035

Aromal, S., & Philip, D. (2012). *Benincasa hispida* seed mediated green synthesis of gold nanoparticles and its optical nonlinearity. *Physica E: Low-Dimensional Systems and Nanostructures*, *44*, 1329–1334. https://doi.org/10.1016/j.physe.2012.02.013

Arunraj, C., Vineesh, J. P., & Sabu, T. K. (2017). Darkling beetles (Coleoptera: Tenebrionidae) of forest sites and agricultural fields in the south Western Ghats (South India). *Journal of Insect Biodiversity*, *5(3)*(3), 1–12. https://doi.org/10.12976/jib/2017.5.3

Arya, S. S., Rookes, J. E., Cahill, D. M., & Lenka, S. K. (2022). Reduced Genotoxicity of Gold Nanoparticles With Protein Corona in *Allium cepa*. *Frontiers in Bioengineering and Biotechnology*, *10*(1). https://doi.org/10.3389/fbioe.2022.849464

Astefanei, A., Núñez, O., & Galceran, M. T. (2015). Characterisation and determination of fullerenes: A critical review. *Analytica Chimica Acta*, *882*, 1–21. https://doi.org/10.1016/j.aca.2015.03.025

Aydin Sevinç, B., & Hanley, L. (2010). Antibacterial activity of dental composites containing zinc oxide nanoparticles. *Journal of Biomedical Materials Research Part B: Applied Biomaterials*, *94B*(1), 22–31. https://doi.org/10.1002/jbm.b.31620

Azam, A., Ahmed, A. S., Oves, M., Khan, M., & Memic, A. (2012). Size-dependent antimicrobial properties of CuO nanoparticles against Gram-positive and -negative bacterial strains. *International Journal of Nanomedicine*, *7*(1), 3527–3535. https://doi.org/10.2147/IJN.S29020

Baharara, J., Namvar, F., Mousavi, M., Ramezani, T., & Mohamad, R. (2014). Anti-Angiogenesis Effect of Biogenic Silver Nanoparticles Synthesized Using *Saliva officinalis* on Chick Chorioalantoic Membrane (CAM). *Molecules*, *19*(9), Article 9. https://doi.org/10.3390/molecules190913498

Bai, K.-J., Chuang, K.-J., Ma, C.-M., Chang, T.-Y., & Chuang, H.-C. (2017). Human lung adenocarcinoma cells with an EGFR mutation are sensitive to non-autophagic cell death induced by zinc oxide and aluminium-doped zinc oxide nanoparticles. *The Journal of Toxicological Sciences*, *42*(4), 437–444. https://doi.org/10.2131/jts.42.437

Ban, I., Stergar, J., & Maver, U. (2018). NiCu magnetic nanoparticles: Review of synthesis methods, surface functionalization approaches, and biomedical applications. *Nanotechnology Reviews*, *7*(2), 187–207. https://doi.org/10.1515/ntrev-2017-0193

Bankar, A., Joshi, B., Ravi Kumar, A., & Zinjarde, S. (2010). Banana peel extract mediated synthesis of gold nanoparticles. *Colloids and Surfaces B: Biointerfaces*, *80*(1), 45–50. https://doi.org/10.1016/j.colsurfb.2010.05.029

Bansal, P., Duhan, J. S., & Gahlawat, S. K. (2014). Biogenesis of nanoparticles: A review. *African Journal of Biotechnology*, *13*(28), Article 28. https://doi.org/10.5897/AJB2013.13458

Bao, Q.-Y., Geng, D.-D., Xue, J.-W., Zhou, G., Gu, S.-Y., Ding, Y., & Zhang, C. (2013). Glutathione-mediated drug release from Tiopronin-conjugated gold nanoparticles for acute liver injury therapy. *International Journal of Pharmaceutics*, *446*(1), 112–118. https://doi.org/10.1016/j.ijpharm.2013.01.073

Barnes, K. M., Gennard, D. E., & Dixon, R. A. (2010). An assessment of the antibacterial activity in larval excretion/secretion of four species of insects recorded in association with corpses, using *Lucilia sericata* Meigen as the marker species. *Bulletin of Entomological Research*, *100*(6), 635–640. https://doi.org/10.1017/S000748530999071X

Barsan, M. M., Enache, T. A., Preda, N., Stan, G., Apostol, N. G., Matei, E., Kuncser, A., & Diculescu, V. C. (2019). Direct Immobilization of Biomolecules through Magnetic Forces on Ni Electrodes via Ni Nanoparticles: Applications in Electrochemical Biosensors. *ACS Applied Materials & Interfaces*, *11*(22), 19867–19877. https://doi.org/10.1021/acsami.9b04990

Barui, A. K., Nethi, S. K., Haque, S., Basuthakur, P., & Patra, C. R. (2019). Recent Development of Metal Nanoparticles for Angiogenesis Study and Their Therapeutic Applications. *ACS Applied Bio Materials*, *2*(12), 5492–5511. https://doi.org/10.1021/acsabm.9b00587

Bauer, A. W., Kirby, W. M., Sherris, J. C., & Turck, M. (1966). Antibiotic susceptibility testing by a standardized single disk method. *American Journal of Clinical Pathology*, *45*(4), 493–496.

Becker, E. M., Nissen, L. R., & Skibsted, L. H. (2004). Antioxidant evaluation protocols: Food quality or health effects. *European Food Research and Technology*, *219*(6), 561–571. https://doi.org/10.1007/s00217-004-1012-4

Bedlovičová, Z., Strapáč, I., Baláž, M., & Salayová, A. (2020). A Brief Overview on Antioxidant Activity Determination of Silver Nanoparticles. *Molecules*, *25*(14), Article 14. https://doi.org/10.3390/molecules25143191

Beheshti, A., Norouzi, P., & Ganjali, M. R. (2012). A Simple and Robust Model for Predicting the Reduction Potential of Quinones Family; Electrophilicity Index Effect. *Int. J. Electrochem. Sci.*, *7*, 11.

Behzad, F., Naghib, S. M., kouhbanani, M. A. J., Tabatabaei, S. N., Zare, Y., & Rhee, K. Y. (2021). An overview of the plant-mediated green synthesis of noble metal nanoparticles for antibacterial applications. *Journal of Industrial and Engineering Chemistry*, *94*(1), 92–104. https://doi.org/10.1016/j.jiec.2020.12.005

Bhattacharya, P., Swarnakar, S., Ghosh, S., Majumdar, S., & Banerjee, S. (2019). Disinfection of drinking water via algae mediated green synthesized copper oxide nanoparticles and its toxicity evaluation. *Journal of Environmental Chemical Engineering*, *7*(1), 102867. https://doi.org/10.1016/j.jece.2018.102867

Bhattacharya, R., Patra, C. R., Verma, R., Kumar, S., Greipp, P. R., & Mukherjee, P. (2007). Gold Nanoparticles Inhibit the Proliferation of Multiple Myeloma Cells. *Advanced Materials*, *19*(5), 711–716. https://doi.org/10.1002/adma.200602098

Bhaviripudi, S., Mile, E., Steiner, S. A., Zare, A. T., Dresselhaus, M. S., Belcher, A. M., & Kong, J. (2007). CVD synthesis of single-walled carbon nanotubes from gold nanoparticle catalysts. *Journal of the American Chemical Society*, *129*(6), 1516–1517. https://doi.org/10.1021/ja0673332

Bhumkar, D. R., Joshi, H. M., Sastry, M., & Pokharkar, V. B. (2007). Chitosan Reduced Gold Nanoparticles as Novel Carriers for Transmucosal Delivery of Insulin. *Pharmaceutical Research*, *24*(8), 1415–1426. https://doi.org/10.1007/s11095-007-9257-9

Bhuyan, T., Mishra, K., Khanuja, M., Prasad, R., & Varma, A. (2015). Biosynthesis of zinc oxide nanoparticles from *Azadirachta indica* for antibacterial and photocatalytic applications. *Materials Science in Semiconductor Processing*, *32*, 55–61. https://doi.org/10.1016/j.mssp.2014.12.053

Bian, Z., Das, S., Wai, M. H., Hongmanorom, P., & Kawi, S. (2017). A Review on Bimetallic Nickel-Based Catalysts for CO_2 Reforming of Methane. *ChemPhysChem*, *18*(22), 3117–3134. https://doi.org/10.1002/cphc.201700529

Bibi, I., Kamal, S., Ahmed, A., Iqbal, M., Nouren, S., Jilani, K., Nazar, N., Amir, M., Abbas, A., Ata, S., & Majid, F. (2017). Nickel nanoparticle synthesis using *Camellia Sinensis* as reducing and capping agent: Growth mechanism and photo-catalytic activity evaluation. *International Journal of Biological Macromolecules*, *103*(1), 783–790. https://doi.org/10.1016/j.ijbiomac.2017.05.023

Bindhu, M. R., Vijaya Rekha, P., Umamaheswari, T., & Umadevi, M. (2014). Antibacterial activities of *Hibiscus cannabinus* stem-assisted silver and gold nanoparticles. *Materials Letters*, *131*(1), 194–197. https://doi.org/10.1016/j.matlet.2014.05.172

Binupriya, A. R., Sathishkumar, M., & Yun, S.I. (2010). Biocrystallization of silver and gold ions by inactive cell filtrate of *Rhizopus stolonifer*. *Colloids and Surfaces B: Biointerfaces*, *79*(2), 531–534. https://doi.org/10.1016/j.colsurfb.2010.05.021

Bisht, G., & Rayamajhi, S. (2016). ZnO Nanoparticles: A Promising Anticancer Agent. *Nanobiomedicine*, *3*(1), 9. https://doi.org/10.5772/63437

Blinova, E., Turovsky, E., Eliseikina, E., Igrunkova, A., Semeleva, E., Golodnev, G., Termulaeva, R., Vasilkina, O., Skachilova, S., Mazov, Y., Zhandarov, K., Simakina, E., Belanov, K., Zalogin, S., & Blinov, D. (2022). Novel Hydroxypyridine Compound Protects Brain Cells against Ischemic Damage In Vitro and In Vivo. *International Journal of Molecular Sciences*, *23*(21), Article 21. https://doi.org/10.3390/ijms232112953

Blois, M. S. (1958). Antioxidant Determinations by the Use of a Stable Free Radical. *Nature*, *181*(4617), 1199–1200. https://doi.org/10.1038/1811199a0

Blum, M. S., Crewe, R. M., & Pasteels, J. M. (1971). Defensive Secretion of *Lomechusa strumosa*, a Myrmecophilous Beetle. *Annals of the Entomological Society of America*, *64*(4), 975–976. https://doi.org/10.1093/aesa/64.4.975

Bonciu, E., Firbas, P., Fontanetti, C. S., Wusheng, J., Karaismailoğlu, M. C., Liu, D., Menicucci, F., Pesnya, D. S., Popescu, A., Romanovsky, A. V., Schiff, S., Ślusarczyk, J., de Souza, C. P., Srivastava, A., Sutan, A., & Papini, A. (2018). An evaluation for the standardization of the *Allium cepa* test as cytotoxicity and genotoxicity assay. *Caryologia*, *71*(3), 191–209. https://doi.org/10.1080/00087114.2018.1503496

Boroumand Moghaddam, A., Moniri, M., Azizi, S., Abdul Rahim, R., Bin Ariff, A., Navaderi, M., & Mohamad, R. (2017). Eco-Friendly Formulated Zinc Oxide Nanoparticles: Induction of Cell Cycle Arrest and Apoptosis in the MCF-7 Cancer Cell Line. *Genes*, *8*(10), Article 10. https://doi.org/10.3390/genes8100281

Brock, S. L. (2004). Nanostructures and Nanomaterials: Synthesis, Properties and Applications . *Journal of the American Chemical Society*, *126*(44), 14679–14679. https://doi.org/10.1021/ja0409457

Buszewski, B., Railean-Plugaru, V., Pomastowski, P., Rafińska, K., Szultka-Mlynska, M., Golinska, P., Wypij, M., Laskowski, D., & Dahm, H. (2018). Antimicrobial activity of biosilver nanoparticles produced by a novel *Streptacidiphilus durhamensis* strain. *Journal of Microbiology, Immunology and Infection*, *51*(1), 45–54. https://doi.org/10.1016/j.jmii.2016.03.002

Cai, W., & Chen, X. (2007). Nanoplatforms for Targeted Molecular Imaging in Living Subjects. *Small*, *3*(11), 1840–1854. https://doi.org/10.1002/smll.200700351

Carvalho, J. J. V. de, Boaventura, F. G., Silva, A. de C. R. da, Ximenes, R. L., Rodrigues, L. K. C., Nunes, D. A. de A., & Souza, V. K. G. de. (2021). Mult resistant bacteria and their impacts on public health: A social responsibility. *Research, Society and Development*, *10*(6), Article 6. https://doi.org/10.33448/rsd-v10i6.16303

Castro, L., Blázquez, M. L., González, F., Muñoz, J. A., & Ballester, A. (2010). Extracellular biosynthesis of gold nanoparticles using sugar beet pulp. *Chemical Engineering Journal*, *164*(1), 92–97. https://doi.org/10.1016/j.cej.2010.08.034

Chabattula, S. C., Gupta, P. K., Tripathi, S. K., Gahtori, R., Padhi, P., Mahapatra, S., Biswal, B. K., Singh, S. K., Dua, K., Ruokolainen, J., Mishra, Y. K., Jha, N. K., Bishi, D. K., & Kesari, K. K. (2021). Anticancer therapeutic efficacy of biogenic *Am*-ZnO nanoparticles on 2D and 3D tumor models. *Materials Today Chemistry*, *22*(1), 100618. https://doi.org/10.1016/j.mtchem.2021.100618

Chakraborty, N., Banerjee, J., Chakraborty, P., Banerjee, A., Chanda, S., Ray, K., Acharya, K., & Sarkar, J. (2022). Green synthesis of copper/copper oxide nanoparticles and their applications: A review. *Green Chemistry Letters and Reviews*, *15*(1), 187–215. https://doi.org/10.1080/17518253.2022.2025916

Chand, K., Abro, M. I., Aftab, U., Shah, A. H., Lakhan, M. N., Cao, D., Mehdi, G., & Ali Mohamed, A. M. (2019). Green synthesis characterization and antimicrobial activity against *Staphylococcus aureus* of silver nanoparticles using extracts of neem, onion and tomato. *RSC Advances*, *9*(30), 17002–17015. https://doi.org/10.1039/C9RA01407A

Chandra, H., Patel, D., Kumari, P., Jangwan, J. S., & Yadav, S. (2019). Phyto-mediated synthesis of zinc oxide nanoparticles of *Berberis aristata*: Characterization, antioxidant activity and antibacterial activity with special reference to urinary tract pathogens. *Materials Science and Engineering: C*, *102*(1), 212–220. https://doi.org/10.1016/j.msec.2019.04.035

Chandra, S., Kumar, A., & Tomar, P. K. (2014). Synthesis of Ni nanoparticles and their characterizations. *Journal of Saudi Chemical Society*, *18*(5), 437–442. https://doi.org/10.1016/j.jscs.2011.09.008

Chandrasekaran, M., & Pandurangan, M. (2016). In Vitro Selective Anti-Proliferative Effect of Zinc Oxide Nanoparticles Against Co-Cultured C2C12 Myoblastoma Cancer and 3T3-L1 Normal Cells. *Biological Trace Element Research*, *172*(1), 148–154. https://doi.org/10.1007/s12011-015-0562-6

Chang, J., Ichihara, G., Shimada, Y., Tada-Oikawa, S., Kuroyanagi, J., Zhang, B., Suzuki, Y., Sehsah, R., Kato, M., Tanaka, T., & Ichihara, S. (2015). Copper Oxide Nanoparticles Reduce Vasculogenesis in Transgenic Zebrafish Through Down-Regulation of Vascular Endothelial Growth Factor Expression and Induction of Apoptosis. *Journal of Nanoscience and Nanotechnology*, *15*(3), 2140–2147. https://doi.org/10.1166/jnn.2015.9762

Chatterjee, A., & Deopura, B. L. (2002). Carbon nanotubes and nanofibre: An overview. *Fibers and Polymers*, *3*(4), 134–139. https://doi.org/10.1007/BF02912657

Chatterjee, T., Chakraborti, S., Joshi, P., Singh, S. P., Gupta, V., & Chakrabarti, P. (2010). The effect of zinc oxide nanoparticles on the structure of the periplasmic domain of the *Vibrio cholerae* ToxR protein. *The FEBS Journal*, *277*(20), 4184–4194. https://doi.org/10.1111/j.1742-4658.2010.07807.x

Chemingui, H., Moulahi, A., Missaoui, T., Al-Marri, A. H., & Hafiane, A. (2024). A novel green preparation of zinc oxide nanoparticles with *Hibiscus sabdariffa* L.:

Photocatalytic performance, evaluation of antioxidant and antibacterial activity. *Environmental Technology*, *45*(5), 926–944. https://doi.org/10.1080/09593330.2022.2130108

Chen, H., Wang, J., Huang, D., Chen, X., Zhu, J., Sun, D., Huang, J., & Li, Q. (2014). Plant-mediated synthesis of size-controllable Ni nanoparticles with *alfalfa* extract. *Materials Letters*, *122*(1), 166–169. https://doi.org/10.1016/j.matlet.2014.02.028

Cheng, Y., Doane, T. L., Chuang, C.-H., Ziady, A., & Burda, C. (2014). Near Infrared Light-Triggered Drug Generation and Release from Gold Nanoparticle Carriers for Photodynamic Therapy. *Small*, *10*(9), 1799–1804. https://doi.org/10.1002/smll.201303329

Cheng, Y., Guo, M., Zhai, M., Yu, Y., & Hu, J. (2020). Nickel Nanoparticles Anchored onto Ni Foam for Supercapacitors with High Specific Capacitance. *Journal of Nanoscience and Nanotechnology*, *20*(4), 2402–2407. https://doi.org/10.1166/jnn.2020.17377

Christakopoulos, P., Katapodis, P., Kalogeris, E., Kekos, D., Macris, B. J., Stamatis, H., & Skaltsa, H. (2003). Antimicrobial activity of acidic xylo-oligosaccharides produced by family 10 and 11 endoxylanases. *International Journal of Biological Macromolecules*, *31*(4), 171–175. https://doi.org/10.1016/S0141-8130(02)00079-X

Chung, I.-M., Rahuman, A. A., Marimuthu, S., Kirthi, A. V., Anbarasan, K., & Rajakumar, G. (2015). An Investigation of the Cytotoxicity and Caspase-Mediated Apoptotic Effect of Green Synthesized Zinc Oxide Nanoparticles Using *Eclipta prostrata* on Human Liver Carcinoma Cells. *Nanomaterials*, *5*(3), Article 3. https://doi.org/10.3390/nano5031317

Clogston, J. D., & Patri, A. K. (2011). Zeta Potential Measurement. In S. E. McNeil (Ed.), *Characterization of Nanoparticles Intended for Drug Delivery* (1st ed., Vol. 697, pp. 63–70). Humana Press. https://doi.org/10.1007/978-1-60327-198-1_6

Colin, J. A., Pech-Pech, I. E., Oviedo, M., Águila, S. A., Romo-Herrera, J. M., & Contreras, O. E. (2018). Gold nanoparticles synthesis assisted by marine algae extract: Biomolecules shells from a green chemistry approach. *Chemical Physics Letters*, *708*(1), 210–215. https://doi.org/10.1016/j.cplett.2018.08.022

Coster, S., Gulliford, M. C., Seed, P. T., Powrie, J. K., & Swaminathan, R. (2000). Monitoring blood glucose control in diabetes mellitus: A systematic review. *Health Technology Assessment (Winchester, England)*, *4*(12), i–iv, 1–93.

Crespo, R., Villaverde, M. L., Girotti, J. R., Güerci, A., Juárez, M. P., & de Bravo, M. G. (2011). Cytotoxic and genotoxic effects of defence secretion of *Ulomoides dermestoides* on A549 cells. *Journal of Ethnopharmacology*, *136*(1), 204–209. https://doi.org/10.1016/j.jep.2011.04.056

Dahl, J. A., Maddux, B. L. S., & Hutchison, J. E. (2007). Toward Greener Nanosynthesis. *Chemical Reviews*, *107*(6), 2228–2269. https://doi.org/10.1021/cr050943k

Das, S. K., Das, A. R., & Guha, A. K. (2009). Gold Nanoparticles: Microbial Synthesis and Application in Water Hygiene Management. *Langmuir*, *25*(14), 8192–8199. https://doi.org/10.1021/la900585p

Dash, S. K., Ghosh, T., Roy, S., Chattopadhyay, S., & Das, D. (2014). Zinc sulfide nanoparticles selectively induce cytotoxic and genotoxic effects on leukemic cells: Involvement of reactive oxygen species and tumor necrosis factor alpha. *Journal of Applied Toxicology*, *34*(11), 1130–1144. https://doi.org/10.1002/jat.2976

De, A., Chakrabarti, M., Ghosh, I., & Mukherjee, A. (2016). Evaluation of genotoxicity and oxidative stress of aluminium oxide nanoparticles and its bulk form in *Allium cepa. The Nucleus*, *59*(3), 219–225. https://doi.org/10.1007/s13237-016-0179-y

Debnath, P., Mondal, A., Hajra, A., Das, C., & Mondal, N. K. (2018). Cytogenetic effects of silver and gold nanoparticles on *Allium cepa* roots. *Journal of Genetic Engineering and Biotechnology*, *16*(2), 519–526. https://doi.org/10.1016/j.jgeb.2018.07.007

Delgado, A. V., González-Caballero, F., Hunter, R. J., Koopal, L. K., & Lyklema, J. (2007). Measurement and interpretation of electrokinetic phenomena. *Journal of Colloid and Interface Science*, *309*(2), 194–224. https://doi.org/10.1016/j.jcis.2006.12.075

Demenev, V. A., Shchinova, M. A., Ivanov, L. I., Vorob'eva, R. N., Zdanovskaia, N. I., & Nebaĭkina, N. V. (1996). [Perfection of methodical approaches to designing vaccines against tick-borne encephalitis]. *Voprosy virusologii*, *41*(3), 107–110.

Desai, M. P., Sangaokar, G. M., & Pawar, K. D. (2018). Kokum fruit mediated biogenic gold nanoparticles with photoluminescent, photocatalytic and antioxidant activities. *Process Biochemistry*, *70*(1), 188–197. https://doi.org/10.1016/ j.procbio. 2018. 03.027

Dettner, K., Schwinger, G., & Wunderle, P. (1985). Sticky secretion from two pairs of defensive glands of rove beetle *Deleaster dichrous* (Grav.) (Coleoptera: Staphylinidae): Gland morphology, chemical constituents, defensive functions, and chemotaxonomy. *Journal of Chemical Ecology*, *11*(7), 859–883. https://doi.org/ 10.1007/BF01012074

Devi, R., Yadav, S., & Pundir, C. S. (2012). Amperometric determination of xanthine in fish meat by zinc oxide nanoparticle/chitosan/multiwalled carbon nanotube/polyaniline composite film bound xanthine oxidase. *Analyst*, *137*(3), 754–759. https://doi.org/ 10.1039/C1AN15838D

Dhakshinamoorthy, A., & Pitchumani, K. (2008). Clay entrapped nickel nanoparticles as efficient and recyclable catalysts for hydrogenation of olefins. *Tetrahedron Letters*, *49*(11), 1818–1823. https://doi.org/10.1016/j.tetlet.2008.01.061

Dhar, S., Daniel, W. L., Giljohann, D. A., Mirkin, C. A., & Lippard, S. J. (2009). Polyvalent Oligonucleotide Gold Nanoparticle Conjugates as Delivery Vehicles for Platinum(IV) Warheads. *Journal of the American Chemical Society*, *131*(41), 14652–14653. https://doi.org/10.1021/ja9071282

Dhayalan, M., Denison, M. I. J., Ayyar, M., Gandhi, N. N., Krishnan, K., & Abdulhadi, B. (2018). Biogenic synthesis, characterization of gold and silver nanoparticles from *Coleus forskohlii* and their clinical importance. *Journal of Photochemistry and Photobiology B: Biology*, *183*(1), 251–257. https://doi.org/10.1016/ j.jphotobiol. 2018.04.042

Di Giulio, A., Muzzi, M., & Romani, R. (2015). Functional anatomy of the explosive defensive system of bombardier beetles (Coleoptera, Carabidae, Brachininae).

Arthropod Structure & Development, *44*(5), 468–490. https://doi.org/10.1016/j.asd.2015.08.013

Dimitrov, D. S. (2006). Interactions of antibody-conjugated nanoparticles with biological surfaces. *Colloids and Surfaces A: Physicochemical and Engineering Aspects*, *Complete*(282–283), 8–10. https://doi.org/10.1016/j.colsurfa.2005.11.001

Divakaran, D., Lakkakula, J. R., Thakur, M., Kumawat, M. K., & Srivastava, R. (2019). Dragon fruit extract capped gold nanoparticles: Synthesis and their differential cytotoxicity effect on breast cancer cells. *Materials Letters*, *236*(1), 498–502. https://doi.org/10.1016/j.matlet.2018.10.156

Dobrucka, R. (2018). Antioxidant and Catalytic Activity of Biosynthesized CuO Nanoparticles Using Extract of *Galeopsidis herba*. *Journal of Inorganic and Organometallic Polymers and Materials*, *28*(3), 812–819. https://doi.org/10.1007/s10904-017-0750-2

Doostmohammadi, A., Monshi, A., Salehi, R., Fathi, M. H., Golniya, Z., & Daniels, Alma. U. (2011). Bioactive glass nanoparticles with negative zeta potential. *Ceramics International*, *37*(7), 2311–2316. https://doi.org/10.1016/j.ceramint.2011.03.026

Dos Santos, M. S., Antunes Filho, S., & Backx, B. P. (2023). Bionanotechnology in Agriculture: A One Health Approach. *Life*, *13*(2), Article 2. https://doi.org/10.3390/life13020509

Doubrovsky, V. A., Yanina, I. Y., & Tuchin, V. V. (2011). Inhomogeneity of photo-induced fat cell lipolysis. *Saratov Fall Meeting 2010: Optical Technologies in Biophysics and Medicine XII*, *7999*, 145–153. https://doi.org/10.1117/12.889326

Droepenu, E. K., Amenyogbe, E., Boatemaa, M. A., & Opoku, E. (2024). Study of the antimicrobial activity of zinc oxide nanostructures mediated by two morphological structures of leaf extracts of *Eucalyptus robusta* . *Heliyon*, *10*(4), e25590. https://doi.org/10.1016/j.heliyon.2024.e25590

Du, L., Jiang, H., Liu, X., & Wang, E. (2007). Biosynthesis of gold nanoparticles assisted by *Escherichia coli* DH5 And its application on direct electrochemistry of haemoglobin. *Electrochemistry Communications*, *9*(5), 1165–1170. https://doi.org/10.1016/j.elecom.2007.01.007

Duan, Y., & Li, J. (2004). Structure study of nickel nanoparticles. *Materials Chemistry and Physics*, *87*(2–3), 452–454. https://doi.org/10.1016/j.matchemphys.2004.06.034

Dubey, S. P., Lahtinen, M., & Sillanpää, M. (2010). Tansy fruit mediated greener synthesis of silver and gold nanoparticles. *Process Biochemistry*, *45*(7), 1065–1071. https://doi.org/10.1016/j.procbio.2010.03.024

Dutta, P. P., Bordoloi, M., Gogoi, K., Roy, S., Narzary, B., Bhattacharyya, D. R., Mohapatra, P. K., & Mazumder, B. (2017). Antimalarial silver and gold nanoparticles: Green synthesis, characterization and in vitro study. *Biomedicine & Pharmacotherapy*, *91*(1), 567–580. https://doi.org/10.1016/j.biopha.2017.04.032

Dutta, R., Nenavathu, B., & Gangishetty, M. (2013). Antibacterial effect of chronic exposure of low concentration ZnO nanoparticles on *E. coli. Journal of Environmental Science and Health. Part A, Toxic/Hazardous Substances &*

Environmental Engineering, *48*(1), 871–878. https://doi.org/10.1080/10934529.2013.761489

Dwivedi, A. D., & Gopal, K. (2010). Biosynthesis of silver and gold nanoparticles using *Chenopodium album* leaf extract. *Colloids and Surfaces A: Physicochemical and Engineering Aspects*, *369*(1), 27–33. https://doi.org/10.1016/j.colsurfa.2010.07.020

Elango, G., Roopan, S. M., Dhamodaran, K. I., Elumalai, K., Al-Dhabi, N. A., & Arasu, M. V. (2016). Spectroscopic investigation of biosynthesized nickel nanoparticles and its larvicidal, pesticidal activities. *Journal of Photochemistry and Photobiology B: Biology*, *162*(1), 162–167. https://doi.org/10.1016/j.jphotobiol.2016.06.045

El-Batal, A. I., El-Sayyad, G. S., Mosallam, F. M., & Fathy, R. M. (2020). *Penicillium chrysogenum*-Mediated Mycogenic Synthesis of Copper Oxide Nanoparticles Using Gamma Rays for In Vitro Antimicrobial Activity Against Some Plant Pathogens. *Journal of Cluster Science*, *31*(1), 79–90. https://doi.org/10.1007/s10876-019-01619-3

Elmegdar, S., Elkheloui, R., Laktib, A., Mimouni, R., & Hamadi, F. (2024). Antibiofilm and Anti-quorum Sensing Activities of Biological Nanoparticles. *Current applied science and technology*, *2*, e0257479–e0257479. https://doi.org/10.55003/cast.2023.257479

Eltarahony, M., Zaki, S., & Abd-El-Haleem, D. (2018). Concurrent Synthesis of Zero- and One-Dimensional, Spherical, Rod-, Needle-, and Wire-Shaped CuO Nanoparticles by *Proteus mirabilis* 10B. *Journal of Nanomaterials*, *2018*(1), e1849616. https://doi.org/10.1155/2018/1849616

Fadoju, O. M., Osinowo, O. A., Ogunsuyi, O. I., Oyeyemi, I. T., Alabi, O. A., Alimba, C. G., & Bakare, A. A. (2020). Interaction of titanium dioxide and zinc oxide nanoparticles induced cytogenotoxicity in *Allium cepa*. *The Nucleus*, *63*(2), 159–166. https://doi.org/10.1007/s13237-020-00308-1

Fang, L., Huang, K., Zhang, B., Liu, B., Liu, Y., & Zhang, Q. (2014). Nanosheet-based 3D hierarchical ZnO structure decorated with Au nanoparticles for enhanced electrochemical detection of dopamine. *RSC Advances*, *4*(90), 48986–48993. https://doi.org/10.1039/C4RA06090C

Fatehah, M. O., Aziz, H. A., & Stoll, S. (2014). Stability of ZnO Nanoparticles in Solution. Influence of pH, Dissolution, Aggregation and Disaggregation Effects. *Journal of Colloid Science and Biotechnology*, *3*(1), 75–84. https://doi.org/10.1166/jcsb.2014.1072

Fernández, J. G., Fernández-Baldo, M. A., Berni, E., Camí, G., Durán, N., Raba, J., & Sanz, M. I. (2016). Production of silver nanoparticles using yeasts and evaluation of their antifungal activity against phytopathogenic fungi. *Process Biochemistry*, *51*(9), 1306–1313. https://doi.org/10.1016/j.procbio.2016.05.021

Feynman, R. P. (1960). There's Plenty of Room at the Bottom. *Engineering and Science*, *23*(5), Article 5. https://resolver.caltech.edu/CaltechES:23.5.1960Bottom

Filip, G. A., Moldovan, B., Baldea, I., Olteanu, D., Suharoschi, R., Decea, N., Cismaru, C. M., Gal, E., Cenariu, M., Clichici, S., & David, L. (2019). UV-light mediated green synthesis of silver and gold nanoparticles using Cornelian cherry fruit extract and

their comparative effects in experimental inflammation. *Journal of Photochemistry and Photobiology B: Biology*, *191*(1), 26–37. https://doi.org/10.1016/j.jphotobiol.2018.12.006

Fiskesjö, G. (1985). The Allium test as a standard in environmental monitoring. *Hereditas*, *102*(1), 99–112. https://doi.org/10.1111/j.1601-5223.1985.tb00471.x

Flieger, J., Flieger, W., Baj, J., & Maciejewski, R. (2021). Antioxidants: Classification, Natural Sources, Activity/Capacity Measurements, and Usefulness for the Synthesis of Nanoparticles. *Materials*, *14*(15), Article 15. https://doi.org/10.3390/ma14154135

Fukushima, J., Kuwahara, Y., Yamada, A., & Suzuki, T. (1990). New Non-cyclic Homo-diterpene from the Sting Glands of *Bracon hebetor* Say (Hymenoptera: *Braconidae*). *Agricultural and Biological Chemistry*, *54*(3), 809–810. https://doi.org/10.1080/00021369.1990.10869987

Ganesan, V., Hariram, M., Vivekanandhan, S., & Muthuramkumar, S. (2020). *Periconium* sp. (Endophytic fungi) extract mediated sol-gel synthesis of ZnO nanoparticles for antimicrobial and antioxidant applications. *Materials Science in Semiconductor Processing*, *105*(104739), 1–12. https://doi.org/10.1016/j.mssp.2019.104739

Ganeshkumar, M., Sathishkumar, M., Ponrasu, T., Dinesh, M. G., & Suguna, L. (2013). Spontaneous ultra fast synthesis of gold nanoparticles using *Punica granatum* for cancer targeted drug delivery. *Colloids and Surfaces B: Biointerfaces*, *106*(1), 208–216. https://doi.org/10.1016/j.colsurfb.2013.01.035

García-López, J. I., Zavala-García, F., Olivares-Sáenz, E., Lira-Saldívar, R. H., Díaz Barriga-Castro, E., Ruiz-Torres, N. A., Ramos-Cortez, E., Vázquez-Alvarado, R., & Niño-Medina, G. (2018). Zinc Oxide Nanoparticles Boosts Phenolic Compounds and Antioxidant Activity of *Capsicum annuum* L. during Germination. *Agronomy*, *8*(10), Article 10. https://doi.org/10.3390/agronomy8100215

Gautam, S., Misra, P., Shukla, P., & Ramteke, P. (2016). Effect of Copper Oxide Nanoparticle on the Germination, Growth and Chlorophyll in Soybean (G*lycine max (L.). Vegetos- An International Journal of Plant Research*, *29*, 157. https://doi.org/10.5958/2229-4473.2016.00050.1

Geim, A. K. (2009). Graphene: Status and Prospects. *Science*, *324*(5934), 1530–1534. https://doi.org/10.1126/science.1158877

Ghaedi, M., Pakniat, M., Mahmoudi, Z., Hajati, S., Sahraei, R., & Daneshfar, A. (2014). Synthesis of nickel sulfide nanoparticles loaded on activated carbon as a novel adsorbent for the competitive removal of Methylene blue and Safranin-O. *Spectrochimica Acta Part A: Molecular and Biomolecular Spectroscopy*, *123*(1), 402–409. https://doi.org/10.1016/j.saa.2013.12.083

Ghasemi, F., & Jalal, R. (2016). Antimicrobial action of zinc oxide nanoparticles in combination with ciprofloxacin and ceftazidime against multidrug-resistant *Acinetobacter baumannii. Journal of Global Antimicrobial Resistance*, *6*(1), 118–122. https://doi.org/10.1016/j.jgar.2016.04.007

Ghodake, G., Eom, C.-Y., Kim, S.-W., & Jin, E.-S. (2010). Biogenic Nano-Synthesis; towards the Efficient Production of the Biocompatible Gold Nanoparticles. *Bulletin*

of the Korean Chemical Society, *31*(10), 2771–2775. https://doi.org/10.5012/bkcs.2010.31.10.2771

Gnanavel, V., Palanichamy, V., & Roopan, S. M. (2017). Biosynthesis and characterization of copper oxide nanoparticles and its anticancer activity on human colon cancer cell lines (HCT-116). *Journal of Photochemistry and Photobiology B: Biology*, *171*, 133–138. https://doi.org/10.1016/j.jphotobiol.2017.05.001

Gomaji Chaudhary, R., A. Tanna, J., V. Gandhare, N., R. Rai, A., & D. Juneja, H. (2015). Synthesis Of Nickel Nanoparticles: Microscopic Investigation, An Efficient Catalyst And Effective Antibacterial Activity. *Advanced Materials Letters*, *6*(11), 990–998. https://doi.org/10.5185/amlett.2015.5901

Gómez-Hernández, R., Panecatl-Bernal, Y., & Méndez-Rojas, M. Á. (2019). High yield and simple one-step production of carbon black nanoparticles from waste tires. *Heliyon*, *5*(7), e02139. https://doi.org/10.1016/j.heliyon.2019.e02139

Gong, N., Shao, K., Feng, W., Lin, Z., Liang, C., & Sun, Y. (2011). Biotoxicity of nickel oxide nanoparticles and bio-remediation by microalgae *Chlorella vulgaris*. *Chemosphere*, *83*(4), 510–516. https://doi.org/10.1016/j.chemosphere.2010.12.059

González-Ballesteros, N., Prado-López, S., Rodríguez-González, J. B., Lastra, M., & Rodríguez-Argüelles, M. C. (2017). Green synthesis of gold nanoparticles using brown algae *Cystoseira baccata:* Its activity in colon cancer cells. *Colloids and Surfaces B: Biointerfaces*, *153*(2017), 190–198. https://doi.org/10.1016/j.colsurfb.2017.02.020

Gopinath, V., Priyadarshini, S., R. Al-Maleki, A., Alagiri, M., Yahya, R., Saravanan, S., & Vadivelu, J. (2016). In vitro toxicity, apoptosis and antimicrobial effects of phyto-mediated copper oxide nanoparticles. *RSC Advances*, *6*(112), 110986–110995. https://doi.org/10.1039/C6RA13871C

Gorgizadeh, M., Azarpira, N., Lotfi, M., Daneshvar, F., Salehi, F., & Sattarahmady, N. (2019). Sonodynamic cancer therapy by a nickel ferrite/carbon nanocomposite on melanoma tumor: In vitro and in vivo studies. *Photodiagnosis and Photodynamic Therapy*, *27*(1), 27–33. https://doi.org/10.1016/j.pdpdt.2019.05.023

Goswami, U., Dutta, A., Raza, A., Kandimalla, R., Kalita, S., Ghosh, S. S., & Chattopadhyay, A. (2018). Transferrin–Copper Nanocluster–Doxorubicin Nanoparticles as Targeted Theranostic Cancer Nanodrug. *ACS Applied Materials & Interfaces*, *10*(4), 3282–3294. https://doi.org/10.1021/acsami.7b15165

Grassian, V. H. (2008). When Size Really Matters: Size-Dependent Properties and Surface Chemistry of Metal and Metal Oxide Nanoparticles in Gas and Liquid Phase Environments. *The Journal of Physical Chemistry C*, *112*(47), 18303–18313. https://doi.org/10.1021/jp806073t

Gross, J., Podsiadlowski, L., & Hilker, M. (2002). Antimicrobial Activity of Exocrine Glandular Secretion of *Chrysomela* Larvae. *Journal of Chemical Ecology*, *28*(2), 317–331. https://doi.org/10.1023/A:1017934124650

Grubisha, D. S., Lipert, R. J., Park, H.-Y., Driskell, J., & Porter, M. D. (2003). Femtomolar Detection of Prostate-Specific Antigen: An Immunoassay Based on Surface-

Enhanced Raman Scattering and Immunogold Labels. *Analytical Chemistry*, *75*(21), 5936–5943. https://doi.org/10.1021/ac034356f

Gubitosa, J., Rizzi, V., Lopedota, A., Fini, P., Laurenzana, A., Fibbi, G., Fanelli, F., Petrella, A., Laquintana, V., Denora, N., Comparelli, R., & Cosma, P. (2018). One pot environmental friendly synthesis of gold nanoparticles using *Punica Granatum* Juice: A novel antioxidant agent for future dermatological and cosmetic applications. *Journal of Colloid and Interface Science*, *521*(1), 50–61. https://doi.org/10.1016/j.jcis.2018.02.069

Gulcin, İ., & Alwasel, S. H. (2023). DPPH Radical Scavenging Assay. *Processes*, *11*(8), Article 8. https://doi.org/10.3390/pr11082248

Gunalan, S., Sivaraj, R., & Venckatesh, R. (2012). *Aloe barbadensis Miller* mediated green synthesis of mono-disperse copper oxide nanoparticles: Optical properties. *Spectrochimica Acta Part A: Molecular and Biomolecular Spectroscopy*, *97*, 1140–1144. https://doi.org/10.1016/j.saa.2012.07.096

Guo, D., Wu, C., Li, J., Guo, A., Li, Q., Jiang, H., Chen, B., & Wang, X. (2009). Synergistic Effect of Functionalized Nickel Nanoparticles and Quercetin on Inhibition of the SMMC-7721 Cells Proliferation. *Nanoscale Research Letters*, *4*(12), 1395. https://doi.org/10.1007/s11671-009-9411-x

Guo, D., Wu, C., Li, X., Jiang, H., Wang, X., & Chen, B. (2008). In Vitro Cellular Uptake and Cytotoxic Effect of Functionalized Nickel Nanoparticles on Leukemia Cancer Cells. *Journal of Nanoscience and Nanotechnology*, *8*(5), 2301–2307. https://doi.org/10.1166/jnn.2008.18272

Gurunathan, S., Lee, K.-J., Kalishwaralal, K., Sheikpranbabu, S., Vaidyanathan, R., & Eom, S. H. (2009). Antiangiogenic properties of silver nanoparticles. *Biomaterials*, *30*(31), 6341–6350. https://doi.org/10.1016/j.biomaterials.2009.08.008

Haiyan Song. (2015). A novel electrochemical sensor based on the copper-doped copper oxide nano-particles for the analysis of hydrogen peroxide. *Colloids and Surfaces A: Physicochemical and Engineering Aspects*, *465*, 153–158. https://doi.org/10.1016/j.colsurfa.2014.10.047

Hameed, S., Wang, Y., Zhao, L., Xie, L., & Ying, Y. (2020). Shape-dependent significant physical mutilation and antibacterial mechanisms of gold nanoparticles against foodborne bacterial pathogens (*Escherichia coli, Pseudomonas aeruginosa* and *Staphylococcus aureus*) at lower concentrations. *Materials Science and Engineering: C*, *108*(1), 110338. https://doi.org/10.1016/j.msec.2019.110338

Hamelian, M., Hemmati, S., Varmira, K., & Veisi, H. (2018). Green synthesis, antibacterial, antioxidant and cytotoxic effect of gold nanoparticles using *Pistacia Atlantica* extract. *Journal of the Taiwan Institute of Chemical Engineers*, *93*(1), 21–30. https://doi.org/10.1016/j.jtice.2018.07.018

Han, Z., Wang, X., Heng, C., Han, Q., Cai, S., Li, J., Qi, C., Liang, W., Yang, R., & Wang, C. (2015). Synergistically enhanced photocatalytic and chemotherapeutic effects of aptamer-functionalized ZnO nanoparticles towards cancer cells. *Physical Chemistry Chemical Physics*, *17*(33), 21576–21582. https://doi.org/10.1039/C5CP02139A

Hanley, C., Layne, J., Punnoose, A., Reddy, K. M., Coombs, I., Coombs, A., Feris, K., & Wingett, D. (2008). Preferential killing of cancer cells and activated human T cells using ZnO nanoparticles. *Nanotechnology*, *19*(29), 295103. https://doi.org/10.1088/0957-4484/19/29/295103

Hasan, S. (2015). A Review on Nanoparticles: Their Synthesis and Types. *Research Journal of Recent Sciences*, *4*(ISC-2014), 9–11.

Hashem, A. H., Al Abboud, M. A., Alawlaqi, M. M., Abdelghany, T. M., & Hasanin, M. (2022). Synthesis of Nanocapsules Based on Biosynthesized Nickel Nanoparticles and Potato Starch: Antimicrobial, Antioxidant, and Anticancer Activity. *Starch - Stärke*, *74*(1–2), 2100165. https://doi.org/10.1002/star.202100165

Hashemi Goradel, N., Ghiyami-Hour, F., Jahangiri, S., Negahdari, B., Sahebkar, A., Masoudifar, A., & Mirzaei, H. (2018). Nanoparticles as new tools for inhibition of cancer angiogenesis. *Journal of Cellular Physiology*, *233*(4), 2902–2910. https://doi.org/10.1002/jcp.26029

Hassan, S. E.-D., Fouda, A., Radwan, A. A., Salem, S. S., Barghoth, M. G., Awad, M. A., Abdo, A. M., & El-Gamal, M. S. (2019). Endophytic actinomycetes *Streptomyces spp* mediated biosynthesis of copper oxide nanoparticles as a promising tool for biotechnological applications. *JBIC Journal of Biological Inorganic Chemistry*, *24*(3), 377–393. https://doi.org/10.1007/s00775-019-01654-5

Helan, V., Prince, J. J., Al-Dhabi, N. A., Arasu, M. V., Ayeshamariam, A., Madhumitha, G., Roopan, S. M., & Jayachandran, M. (2016). Neem leaves mediated preparation of NiO nanoparticles and its magnetization, coercivity and antibacterial analysis. *Results in Physics*, *6*, 712–718. https://doi.org/10.1016/j.rinp.2016.10.005

Helen, S. M., & Rani, M. H. E. (2015). Characterization and antimicrobial study of nickel nanoparticles synthesized from *dioscorea* (Elephant Yam) by green route. *International Journal of Science and Research*, *4*(11), 216–219.

Hernández-Sierra, J. F., Ruiz, F., Cruz Pena, D. C., Martínez-Gutiérrez, F., Martínez, A. E., de Jesús Pozos Guillén, A., Tapia-Pérez, H., & Martínez Castañón, G. (2008). The antimicrobial sensitivity of *Streptococcus mutans* to nanoparticles of silver, zinc oxide, and gold. *Nanomedicine: Nanotechnology, Biology and Medicine*, *4*(3), 237–240. https://doi.org/10.1016/j.nano.2008.04.005

Hewitson, T. D., Wigg, B., & Becker, G. J. (2010). Tissue Preparation for Histochemistry: Fixation, Embedding, and Antigen Retrieval for Light Microscopy. In T. D. Hewitson & I. A. Darby (Eds.), *Histology Protocols* (Vol. 299, pp. 3–18). Humana Press. https://doi.org/10.1007/978-1-60327-345-9_1

Hill, D., Barron, A. R., & Alexander, S. (2019). Comparison of hydrophobicity and durability of functionalized aluminium oxide nanoparticle coatings with magnetite nanoparticles–links between morphology and wettability. *Journal of Colloid and Interface Science*, *555*, 323–330. https://doi.org/10.1016/j.jcis.2019.07.080

Hischier, R., & Walser, T. (2012). Life cycle assessment of engineered nanomaterials: State of the art and strategies to overcome existing gaps. *Science of The Total Environment*, *425*(1), 271–282. https://doi.org/10.1016/j.scitotenv.2012.03.001

Hoback, W. W., Bishop, A. A., Kroemer, J., Scalzitti, J., & Shaffer, J. J. (2004). Differences Among Antimicrobial Properties of Carrion Beetle Secretions Reflect Phylogeny and Ecology. *Journal of Chemical Ecology*, *30*(4), 719–729. https://doi.org/10.1023/B:JOEC.0000028427.53141.41

Honary, S., & Zahir, F. (2013). Effect of Zeta Potential on the Properties of Nano-Drug Delivery Systems—A Review (Part 1). *Tropical Journal of Pharmaceutical Research*, *12*(2), 255–264. https://doi.org/10.4314/tjpr.v12i2.19

Hong, F., Yang, F., Liu, C., Gao, Q., Wan, Z., Gu, F., Wu, C., Ma, Z., Zhou, J., & Yang, P. (2005). Influences of Nano-TiO2 on the chloroplast aging of spinach under light. *Biological Trace Element Research*, *104*(3), 249–260. https://doi.org/10.1385/BTER:104:3:249

Hoque, S. M., Tariq, M., Liba, S. I., Salehin, F., Mahmood, Z. H., Khan, M. N. I., Chattopadhayay, K., Islam, R., & Akhter, S. (2016). Thermo-therapeutic applications of chitosan- and PEG-coated NiFe2O4 nanoparticles. *Nanotechnology*, *27*(28), 285702. https://doi.org/10.1088/0957-4484/27/28/285702

Horváth, Gy., Bencsik, T., Ács, K., & Kocsis, B. (2016). Chapter 12—Sensitivity of ESBL-Producing Gram-Negative Bacteria to Essential Oils, Plant Extracts, and Their Isolated Compounds. In K. Kon & M. Rai (Eds.), *Antibiotic Resistance* (pp. 239–269). Academic Press. https://doi.org/10.1016/B978-0-12-803642-6.00012-5

Hoshyar, R., Khayati, G. R., Poorgholami, M., & Kaykhaii, M. (2016). A novel green one-step synthesis of gold nanoparticles using crocin and their anti-cancer activities. *Journal of Photochemistry and Photobiology B: Biology*, *159*(1), 237–242. https://doi.org/10.1016/j.jphotobiol.2016.03.056

Hou, Y., Kondoh, H., Ohta, T., & Gao, S. (2005). Size-controlled synthesis of nickel nanoparticles. *Applied Surface Science*, *241*(1–2), 218–222. https://doi.org/10.1016/j.apsusc.2004.09.045

Hu, G., Guo, M., Xu, J., Wu, F., Fan, J., Huang, Q., Yang, G., Lv, Z., Wang, X., & Jin, Y. (2019). Nanoparticles Targeting Macrophages as Potential Clinical Therapeutic Agents Against Cancer and Inflammation. *Frontiers in Immunology*, *10*. https://doi.org/10.3389/fimmu.2019.01998

Huang, J., Li, Q., Sun, D., Lu, Y., Su, Y., Yang, X., Wang, H., Wang, Y., Shao, W., He, N., Hong, J., & Chen, C. (2007). Biosynthesis of silver and gold nanoparticles by novel sundried *Cinnamomum camphora l*eaf. *Nanotechnology*, *18*(10), 105104. https://doi.org/10.1088/0957-4484/18/10/105104

Huang, X., El-Sayed, I. H., Qian, W., & El-Sayed, M. A. (2007). Cancer Cells Assemble and Align Gold Nanorods Conjugated to Antibodies to Produce Highly Enhanced, Sharp, and Polarized Surface Raman Spectra: A Potential Cancer Diagnostic Marker. *Nano Letters*, *7*(6), 1591–1597. https://doi.org/10.1021/nl070472c

Hulteen, J. C., Treichel, D. A., Smith, M. T., Duval, M. L., Jensen, T. R., & Van Duyne, R. P. (1999). Nanosphere lithography: Size-tunable silver nanoparticle and surface cluster arrays. *Journal of Physical Chemistry B*, *103*(19), 3854–3863. https://doi.org/10.1021/jp9904771

Huo, Y., Singh, P., Kim, Y. J., Soshnikova, V., Kang, J., Markus, J., Ahn, S., Castro-Aceituno, V., Mathiyalagan, R., Chokkalingam, M., Bae, K.-S., & Yang, D. C. (2018). Biological synthesis of gold and silver chloride nanoparticles by *Glycyrrhiza uralensis* and in vitro applications. *Artificial Cells, Nanomedicine, and Biotechnology*, *46*(2), 303–312. https://doi.org/10.1080/21691401.2017.1307213

Hussain, S., Ali Muazzam, M., Ahmed, M., Ahmad, M., Mustafa, Z., Murtaza, S., Ali, J., Ibrar, M., Shahid, M., & Imran, M. (2023). Green synthesis of nickel oxide nanoparticles using *Acacia nilotica* leaf extracts and investigation of their electrochemical and biological properties. *Journal of Taibah University for Science*, *17*(1), 2170162. https://doi.org/10.1080/16583655.2023.2170162

Hwa, K.-Y., & Subramani, B. (2014). Synthesis of zinc oxide nanoparticles on graphene–carbon nanotube hybrid for glucose biosensor applications. *Biosensors and Bioelectronics*, *62*, 127–133. https://doi.org/10.1016/j.bios.2014.06.023

Hwang, B. B., Chang, M. H., Lee, J. H., Heo, W., Kim, J. K., Pan, J. H., Kim, Y. J., & Kim, J. H. (2019). The Edible Insect *Gryllus bimaculatus* Protects against Gut-Derived Inflammatory Responses and Liver Damage in Mice after Acute Alcohol Exposure. *Nutrients*, *11*(4), Article 4. https://doi.org/10.3390/nu11040857

Ijaz, F., Shahid, S., Khan, S. A., Ahmad, W., & Zaman, S. (2017). Green synthesis of copper oxide nanoparticles using *Abutilon indicum* leaf extract: Antimicrobial, antioxidant and photocatalytic dye degradation activitie. *Tropical Journal of Pharmaceutical Research*, *16*(4), Article 4. https://doi.org/10.4314/tjpr.v16i4.2

Inbakandan, D., Venkatesan, R., & Ajmal Khan, S. (2010). Biosynthesis of gold nanoparticles utilizing marine sponge *Acanthella elongata* (Dendy, 1905). *Colloids and Surfaces B: Biointerfaces*, *81*(2), 634–639. https://doi.org/10.1016/j.colsurfb.2010.08.016

Ingle, A., Gade, A., Pierrat, S., Sonnichsen, C., & Rai, M. (2008). Mycosynthesis of Silver Nanoparticles Using the Fungus *Fusarium acuminatum* and its Activity Against Some Human Pathogenic Bacteria. *Current Nanoscience*, *4*(2), 141–144. https://doi.org/10.2174/157341308784340804

Iravani, S. (2011). Green synthesis of metal nanoparticles using plants. *Green Chemistry*, *13*(10), 2638–2650. https://doi.org/10.1039/C1GC15386B

Iravani, S., Korbekandi, H., Mirmohammadi, S. V., & Zolfaghari, B. (2014). Synthesis of silver nanoparticles: Chemical, physical and biological methods. *Research in Pharmaceutical Sciences*, *9*(6), 385–406. https://www.ncbi.nlm.nih.gov/pmc/articles/PMC4326978/

Ishwarya, R., Vaseeharan, B., Kalyani, S., Banumathi, B., Govindarajan, M., Alharbi, N. S., Kadaikunnan, S., Al-Anbr, M. N., Khaled, J. M., & Benelli, G. (2018). Facile green synthesis of zinc oxide nanoparticles using *Ulva lactuca* seaweed extract and evaluation of their photocatalytic, antibiofilm and insecticidal activity. *Journal of Photochemistry and Photobiology. B, Biology*, *178*(1), 249–258. https://doi.org/10.1016/j.jphotobiol.2017.11.006

Ivanov, M. S., Khomchenko, V. A., Salimian, M., Nikitin, T., Kopyl, S., Buryakov, A. M., Mishina, E. D., Salehli, F., Marques, P. A. A. P., Goncalves, G., Fausto, R., Paixão,

J. A., & Kholkin, A. L. (2018). Self-assembled diphenylalanine peptide microtubes covered by reduced graphene oxide/spiky nickel nanocomposite: An integrated nanobiomaterial for multifunctional applications. *Materials & Design*, *142*(1), 149–157. https://doi.org/10.1016/j.matdes.2018.01.018

Jadoun, S., Arif, R., Jangid, N. K., & Meena, R. K. (2021). Green synthesis of nanoparticles using plant extracts: A review. *Environmental Chemistry Letters*, *19*(1), 355–374. https://doi.org/10.1007/s10311-020-01074-x

Jafari, A. R., Mosavi, T., Mosavari, N., Majid, A., Movahedzade, F., Tebyaniyan, M., Kamalzadeh, M., Dehgan, M., Jafari, S., & Arastoo, S. (2016). Mixed metal oxide nanoparticles inhibit growth of *Mycobacterium tuberculosis* into THP-1 cells. *International Journal of Mycobacteriology*, *5 Suppl 1*, S181–S183. https://doi.org/10.1016/j.ijmyco.2016.09.011

Jaji, N.-D., Lee, H. L., Hussin, M. H., Akil, H. M., Zakaria, M. R., & Othman, M. B. H. (2020). Advanced nickel nanoparticles technology: From synthesis to applications. *Nanotechnology Reviews*, *9*(1), 1456–1480. https://doi.org/10.1515/ntrev-2020-0109

Jamila, N., Khan, N., Bibi, A., Haider, A., Noor Khan, S., Atlas, A., Nishan, U., Minhaz, A., Javed, F., & Bibi, A. (2020). *Piper longum* catkin extract mediated synthesis of Ag, Cu, and Ni nanoparticles and their applications as biological and environmental remediation agents. *Arabian Journal of Chemistry*, *13*(8), 6425–6436. https://doi.org/10.1016/j.arabjc.2020.06.001

Jayabalan, J., Mani, G., Krishnan, N., Pernabas, J., Devadoss, J. M., & Jang, H. T. (2019). Green biogenic synthesis of zinc oxide nanoparticles using *Pseudomonas putida* culture and its In vitro antibacterial and anti-biofilm activity. *Biocatalysis and Agricultural Biotechnology*, *21*(2019), 101327. https://doi.org/10.1016/j.bcab.2019.101327

Jayaseelan, C., Rahuman, A. A., Kirthi, A. V., Marimuthu, S., Santhoshkumar, T., Bagavan, A., Gaurav, K., Karthik, L., & Rao, K. V. B. (2012). Novel microbial route to synthesize ZnO nanoparticles using *Aeromonas hydrophila* and their activity against pathogenic bacteria and fungi. *Spectrochimica Acta Part A: Molecular and Biomolecular Spectroscopy*, *90*(1), 78–84. https://doi.org/10.1016/j.saa.2012.01.006

Jayaseelan, C., Ramkumar, R., Rahuman, A. A., & Perumal, P. (2013). Green synthesis of gold nanoparticles using seed aqueous extract of *Abelmoschus esculentus* and its antifungal activity. *Industrial Crops and Products*, *45*(1), 423–429. https://doi.org/10.1016/j.indcrop.2012.12.019

Jeronsia, J. E., Raj, D. J. V., Joseph, L. A., Rubini, K., & Das, S. J. (2016). In Vitro Antibacterial and Anticancer Activity of Copper Oxide Nanostructures in Human Breast Cancer Michigan Cancer Foundation-7 Cells. *Journal of Medical Sciences*, *36*(4), 145. https://doi.org/10.4103/1011-4564.188899

Jeyaraj Pandian, C., Palanivel, R., & Dhanasekaran, S. (2016). Screening Antimicrobial Activity of Nickel Nanoparticles Synthesized Using *Ocimum sanctum* Leaf Extract. *Journal of Nanoparticles*, *2016*, 1–13. https://doi.org/10.1155/2016/4694367

Jiao, M., Yao, Y., Pastel, G., Li, T., Liang, Z., Xie, H., Kong, W., Liu, B., Song, J., & Hu, L. (2019). Fly-through synthesis of nanoparticles on textile and paper substrates. *Nanoscale*, *11*(13), 6174–6181. https://doi.org/10.1039/C8NR10137J

Joshi, A., Rastedt, W., Faber, K., Schultz, A. G., Bulcke, F., & Dringen, R. (2016). Uptake and Toxicity of Copper Oxide Nanoparticles in C6 Glioma Cells. *Neurochemical Research*, *41*(11), 3004–3019. https://doi.org/10.1007/s11064-016-2020-z

Kah, J. C. Y., Kho, K. W., Lee, C. G. L., Richard, C. J., Sheppard, Shen, Z. X., Soo, K. C., & Olivo, M. C. (2007). Early diagnosis of oral cancer based on the surface plasmon resonance of gold nanoparticles. *International Journal of Nanomedicine*, *2*(4), 785–798. https://doi.org/10.2147/IJN.S2.4.785

Kamble, S., Utage, B., Mogle, P., Kamble, R., Hese, S., Dawane, B., & Gacche, R. (2016). Evaluation of Curcumin Capped Copper Nanoparticles as Possible Inhibitors of Human Breast Cancer Cells and Angiogenesis: A Comparative Study with Native Curcumin. *AAPS PharmSciTech*, *17*(5), 1030–1041. https://doi.org/10.1208/s12249-015-0435-5

Kammler, H., Mädler, L., & Pratsinis, S. (2001). Flame Synthesis of Nanoparticles. *Chemical Engineering & Technology*, *24*(6), 583–596. https://doi.org/10.1002/1521-4125(200106)24:6<583::AID-CEAT583>3.0.CO;2-H

Kanehisa, K. (1978). Comparative study of the abdominal defensive systems in tenebrionid beetles. *Berichte Des Ohara Instituts Für Landwirtschaftliche Biologie, Okayama Universität*, *17*(2), 47–55.

Kareem, M., Babu, H., & Lakshmi, G. V. (2022). The study of the antioxidative and catalytic activities of ni nanoparticles synthesized from *Terminalia chebula* extract. *Journal of Advanced Scientific Research*, *13*(06), Article 06. https://doi.org/10.55218/JASR.202213604

Karyakin, A. A., Karyakina, E. E., & Gorton, L. (2000). Amperometric Biosensor for Glutamate Using Prussian Blue-Based "Artificial Peroxidase" as a Transducer for Hydrogen Peroxide. *Analytical Chemistry*, *72*(7), 1720–1723. https://doi.org/10.1021/ac990801o

Kasana, R. C., Panwar, N. R., Kaul, R. K., & Kumar, P. (2016). Copper Nanoparticles in Agriculture: Biological Synthesis and Antimicrobial Activity, *Nanoscience in Food and Agriculture 3* (Vol. 23, pp. 129–143). Springer International Publishing. https://doi.org/10.1007/978-3-319-48009-1_5

Kasthuri, J., Kathiravan, K., & Rajendiran, N. (2009). Phyllanthin-assisted biosynthesis of silver and gold nanoparticles: A novel biological approach. *Journal of Nanoparticle Research*, *11*(5), 1075–1085. https://doi.org/10.1007/s11051-008-9494-9

Kaur, P., Thakur, R., & Chaudhury, A. (2016). Biogenesis of copper nanoparticles using peel extract of *Punica granatum* and their antimicrobial activity against opportunistic pathogens. *Green Chemistry Letters and Reviews*, *9*(1), 33–38. https://doi.org/10.1080/17518253.2016.1141238

Kavitha, T., Gopalan, A. I., Lee, K.-P., & Park, S.-Y. (2012). Glucose sensing, photocatalytic and antibacterial properties of graphene–ZnO nanoparticle hybrids. *Carbon*, *50*(8), 2994–3000. https://doi.org/10.1016/j.carbon.2012.02.082

Kedare, S. B., & Singh, R. P. (2011). Genesis and development of DPPH method of antioxidant assay. *Journal of Food Science and Technology*, *48*(4), 412–422. https://doi.org/10.1007/s13197-011-0251-1

Kendall, D. A. (1974). The structure of defence glands in some Tenebrionidae and Nilionidae (Coleoptera). *Transactions of the Royal Entomological Society of London*, *125*(4), 437–487. https://doi.org/10.1111/j.1365-2311.1974.tb02308.x

Kermanshahi, P. K., & Akhbari, K. (2024). The antibacterial activity of three zeolitic-imidazolate frameworks and zinc oxide nanoparticles derived from them. *RSC Advances*, *14*(8), 5601–5608. https://doi.org/10.1039/D4RA00447G

Kesmati, M., & Torabi, M. (2014). Interaction between Analgesic Effect of Nano and Conventional size of Zinc Oxide and Opioidergic System Activity in Animal Model of Acute Pain. *Basic and Clinical Neuroscience*, *5*(1), 80–87. https://www.ncbi.nlm.nih.gov/pmc/articles/PMC4202607/

Khalaf, M. M., Abd El-Lateef, H. M., Mohamed, I. M. A., Zaki, M. E. A., & Toghan, A. (2021). Facile synthesis of gold-nanoparticles by different capping agents and their anticancer performance against liver cancer cells. *Colloid and Interface Science Communications*, *44*(1), 100482. https://doi.org/10.1016/j.colcom.2021.100482

Khani, R., Roostaei, B., Bagherzade, G., & Moudi, M. (2018). Green synthesis of copper nanoparticles by fruit extract of *Ziziphus spina-christi* (L.) Willd.: Application for adsorption of triphenylmethane dye and antibacterial assay. *Journal of Molecular Liquids*, *255*(1), 541–549. https://doi.org/10.1016/j.molliq.2018.02.010

Kim, G. J., & Nie, S. (2005). Targeted cancer nanotherapy. *Materials Today*, *8*(8, Supplement), 28–33. https://doi.org/10.1016/S1369-7021(05)71034-8

Kiran, S., Rafique, M. A., Iqbal, S., Nosheen, S., Naz, S., & Rasheed, A. (2020). Synthesis of nickel nanoparticles using *Citrullus colocynthis* stem extract for remediation of Reactive Yellow 160 dye. *Environmental Science and Pollution Research*, *27*(26), 32998–33007. https://doi.org/10.1007/s11356-020-09510-9

Kneipp, K., Haka, A. S., Kneipp, H., Badizadegan, K., Yoshizawa, N., Boone, C., Shafer-Peltier, K. E., Motz, J. T., Dasari, R. R., & Feld, M. S. (2002). Surface-Enhanced Raman Spectroscopy in Single Living Cells Using Gold Nanoparticles. *Applied Spectroscopy*, *56*(2), 150–154. https://doi.org/10.1366/0003702021954557

Kobashigawa, J. M., Robles, C. A., Martínez Ricci, M. L., & Carmarán, C. C. (2019). Influence of strong bases on the synthesis of silver nanoparticles (AgNPs) using the ligninolytic fungi *Trametes trogii. Saudi Journal of Biological Sciences*, *26*(7), 1331–1337. https://doi.org/10.1016/j.sjbs.2018.09.006

Korbekandi, H., Iravani, S., & Abbasi, S. (2012). Optimization of biological synthesis of silver nanoparticles using *Lactobacillus casei* subsp. Casei. *Journal of Chemical Technology & Biotechnology*, *87*(7), 932–937. https://doi.org/10.1002/jctb.3702

Kouhkan, M., Ahangar, P., Babaganjeh, L. A., & Allahyari-Devin, M. (2020). Biosynthesis of Copper Oxide Nanoparticles Using *Lactobacillus casei* Subsp. Casei and its Anticancer and Antibacterial Activities. *Current Nanoscience*, *16*(1), 101–111. https://doi.org/10.2174/1573413715666190318155801

Kourmouli, A., Valenti, M., van Rijn, E., Beaumont, H. J. E., Kalantzi, O.-I., Schmidt-Ott, A., & Biskos, G. (2018). Can disc diffusion susceptibility tests assess the antimicrobial activity of engineered nanoparticles, *Journal of Nanoparticle Research*, *20*(3), 62. https://doi.org/10.1007/s11051-018-4152-3

Kovacic, P., & Somanathan, R. (2013). Nanoparticles: Toxicity, Radicals, Electron Transfer, and Antioxidants. In D. Armstrong & D. J. Bharali (Eds.), *Oxidative Stress and Nanotechnology: Methods and Protocols* (pp. 15–35). Humana Press. https://doi.org/10.1007/978-1-62703-475-3_2

Krebs, H. a., & Johnson, W. a. (1980). The role of citric acid in intermediate metabolism in animal tissues. *FEBS Letters*, *117*(S1), K2–K10. https://doi.org/10.1016/0014-5793(80)80564-3

Kreuter, J. (2007). Nanoparticles—A historical perspective. *International Journal of Pharmaceutics*, *331*(1), 1–10. https://doi.org/10.1016/j.ijpharm.2006.10.021

Król, A., Railean-Plugaru, V., Pomastowski, P., & Buszewski, B. (2019). Phytochemical investigation of *Medicago sativa* L. extract and its potential as a safe source for the synthesis of ZnO nanoparticles: The proposed mechanism of formation and antimicrobial activity. *Phytochemistry Letters*, *31*, 170–180. https://doi.org/10.1016/j.phytol.2019.04.009

Kumar, P. P. N. V., Shameem, U., Kollu, P., Kalyani, R. L., & Pammi, S. V. N. (2015). Green Synthesis of Copper Oxide Nanoparticles Using *Aloe vera* Leaf Extract and Its Antibacterial Activity Against Fish Bacterial Pathogens. *BioNanoScience*, *5*(3), 135–139. https://doi.org/10.1007/s12668-015-0171-z

Kumari, M., Khan, S. S., Pakrashi, S., Mukherjee, A., & Chandrasekaran, N. (2011). Cytogenetic and genotoxic effects of zinc oxide nanoparticles on root cells of *Allium cepa*. *Journal of Hazardous Materials*, *190*(1), 613–621. https://doi.org/10.1016/j.jhazmat.2011.03.095

Kumari, N., Sarita, Anchal, Priya, Palsaniya, K. K., Beniwal, R. K., Choudhary, S. R., Rulaniya, M. S., Saini, P. M., Dolia, S. N., Alvi, P. A., & Choudhary, B. L. (2024). The role of citric acid for formation of nanocrystalline MnFe2O4 ferrite. *Applied Physics A*, *130*(4), 266. https://doi.org/10.1007/s00339-024-07423-9

Kumari, S., kumari, P., Panda, P. K., Pramanik, N., Verma, S. K., & Mallick, M. A. (2019). Molecular aspect of phyto fabrication of gold nanoparticle from *Andrographis peniculata* photosystem II and their *in vivo* biological effect on embryonic zebrafish (*Danio rerio*). *Environmental Nanotechnology, Monitoring & Management*, *11*(1), 100201. https://doi.org/10.1016/j.enmm.2018.100201

Kundu, D., Hazra, C., Chatterjee, A., Chaudhari, A., & Mishra, S. (2014). Extracellular biosynthesis of zinc oxide nanoparticles using *Rhodococcus pyridinivorans* NT2: Multifunctional textile finishing, biosafety evaluation and *in vitro* drug delivery in colon carcinoma. *Journal of Photochemistry and Photobiology B: Biology*, *140*(1), 194–204. https://doi.org/10.1016/j.jphotobiol.2014.08.001

Lebeau, P. F., Chen, J., Byun, J. H., Platko, K., & Austin, R. C. (2019). The trypan blue cellular debris assay: A novel low-cost method for the rapid quantification of cell death. *MethodsX*, *6*, 1174–1180. https://doi.org/10.1016/j.mex.2019.05.010

Lečić, S., Ćurčić, S., Vujisić, L., Ćurčić, B., Curcic, N., Nikolić, Z., Anđelković, B., Milosavljević, S., Tešević, V., & Makarov, S. (2014). Defensive Secretions in three ground beetle species (Insecta: Coleoptera: Carabidae). *Annales Zoologici Fennici*, *51*, 285–300. https://doi.org/10.5735/086.051.0301

Lee, H.-J., Song, J. Y., & Kim, B. S. (2013). Biological synthesis of copper nanoparticles using *Magnolia kobus l*eaf extract and their antibacterial activity. *Journal of Chemical Technology & Biotechnology*, *88*(11), 1971–1977. https://doi.org/10.1002/jctb.4052

Letchumanan, D., Sok, S. P. M., Ibrahim, S., Nagoor, N. H., & Arshad, N. M. (2021). Plant-Based Biosynthesis of Copper/Copper Oxide Nanoparticles: An Update on Their Applications in Biomedicine, Mechanisms, and Toxicity. *Biomolecules*, *11*(4), Article 4. https://doi.org/10.3390/biom11040564

Li, X., Xu, H., Chen, Z.-S., & Chen, G. (2011). Biosynthesis of Nanoparticles by Microorganisms and Their Applications. *Journal of Nanomaterials*, *2011*(270974), e270974. https://doi.org/10.1155/2011/270974

Li, X.-K., Ji, W.-J., Zhao, J., Wang, S.-J., & Au, C.-T. (2005). Ammonia decomposition over Ru and Ni catalysts supported on fumed SiO2, MCM-41, and SBA-15. *Journal of Catalysis*, *236*(2), 181–189. https://doi.org/10.1016/j.jcat.2005.09.030

Li, Y., Duan, X., Qian, Y., Yang, L., & Liao, H. (1999). Nanocrystalline Silver Particles: Synthesis, Agglomeration, and Sputtering Induced by Electron Beam. *Journal of Colloid and Interface Science*, *209*(2), 347–349. https://doi.org/10.1006/jcis.1998.5879

Li, Y., Zhang, B., Xie, X., Liu, J., Xu, Y., & Shen, W. (2006). Novel Ni catalysts for methane decomposition to hydrogen and carbon nanofibers. *Journal of Catalysis*, *238*(2), 412–424. https://doi.org/10.1016/j.jcat.2005.12.027

Liao, D. L., Wu, G. S., & Liao, B. Q. (2009). Zeta potential of shape-controlled TiO_2 nanoparticles with surfactants. *Colloids and Surfaces A: Physicochemical and Engineering Aspects*, *348*(1), 270–275. https://doi.org/10.1016/j.colsurfa.2009.07.036

Lim, H. Y., & Dolzhenko, A. V. (2021). Gluconic acid aqueous solution: A bio-based catalytic medium for organic synthesis. *Sustainable Chemistry and Pharmacy*, *21*, 100443. https://doi.org/10.1016/j.scp.2021.100443

Liman, R., Ali, M. M., Istifli, E. S., Ciğerci, İ. H., & Bonciu, E. (2022). Genotoxic and cytotoxic effects of pethoxamid herbicide on *Allium cepa* cells and its molecular docking studies to unravel genotoxicity mechanism. *Environmental Science and Pollution Research*, *29*(42), 63127–63140. https://doi.org/10.1007/s11356-022-20166-5

Limbach, L. K., Wick, P., Manser, P., Grass, R. N., Bruinink, A., & Stark, W. J. (2007). Exposure of engineered nanoparticles to human lung epithelial cells: Influence of chemical composition and catalytic activity on oxidative stress. *Environmental Science & Technology*, *41*(11), 4158–4163. https://doi.org/10.1021/es062629t

Lin, L., Qiu, P., Cao, X., & Jin, L. (2008). Colloidal silver nanoparticles modified electrode and its application to the electroanalysis of Cytochrome c. *Electrochimica Acta*, *53*(16), 5368–5372. https://doi.org/10.1016/j.electacta.2008.02.080

Lingaraju, K., Raja Naika, H., Nagabhushana, H., Jayanna, K., Devaraja, S., & Nagaraju, G. (2020). Biosynthesis of Nickel oxide Nanoparticles from *Euphorbia heterophylla* (L.) and their biological application. *Arabian Journal of Chemistry*, *13*(3), 4712–4719. https://doi.org/10.1016/j.arabjc.2019.11.003

Liu, J., Ma, X., Jin, S., Xue, X., Zhang, C., Wei, T., Guo, W., & Liang, X.-J. (2016). Zinc Oxide Nanoparticles as Adjuvant to Facilitate Doxorubicin Intracellular Accumulation and Visualize pH-Responsive Release for Overcoming Drug Resistance. *Molecular Pharmaceutics*, *13*(5), 1723–1730. https://doi.org/10.1021/acs.molpharmaceut.6b00311

Liu, S., Sun, J., Yu, L., Zhang, C., Bi, J., Zhu, F., Qu, M., & Yang, Q. (2012). Antioxidant activity and phenolic compounds of *Holotrichia parallela* Motschulsky extracts. *Food Chemistry*, *134*(4), 1885–1891. https://doi.org/10.1016/j.foodchem.2012.03.091

Liu, Z., Kiessling, F., & Gätjens, J. (2010). Advanced Nanomaterials in Multimodal Imaging: Design, Functionalization, and Biomedical Applications. *Journal of Nanomaterials*, *2010*, e894303. https://doi.org/10.1155/2010/894303

Lokman, N. A., Elder, A. S. F., Ricciardelli, C., & Oehler, M. K. (2012). Chick chorioallantoic membrane (CAM) assay as an in vivo model to study the effect of newly identified molecules on ovarian cancer invasion and metastasis. *International Journal of Molecular Sciences*, *13*(8), Article 8. https://doi.org/10.3390/ijms13089959

Lugscheider, E., Bärwulf, S., Barimani, C., Riester, M., & Hilgers, H. (1998). Magnetron-sputtered hard material coatings on thermoplastic polymers for clean room applications. *Surface and Coatings Technology*, *108–109*, 398–402. https://doi.org/10.1016/S0257-8972(98)00627-6

Machado, S., Pacheco, J. G., Nouws, H. P. A., Albergaria, J. T., & Delerue-Matos, C. (2015). Characterization of green zero-valent iron nanoparticles produced with tree leaf extracts. *The Science of the Total Environment*, *533*, 76–81. https://doi.org/10.1016/j.scitotenv.2015.06.091

Machado, T. de B., Leal, I. C. R., Amaral, A. C. F., Santos, K. R. N. dos, Silva, M. G. da, & Kuster, R. M. (2002). Antimicrobial Ellagitannin of *Punica granatum* Fruits. *Journal of the Brazilian Chemical Society*, *13*, 606–610. https://doi.org/10.1590/S0103-50532002000500010

Madhusudhan, A., Reddy, G. B., Venkatesham, M., Veerabhadram, G., Kumar, D. A., Natarajan, S., Yang, M.-Y., Hu, A., & Singh, S. S. (2014). Efficient pH Dependent Drug Delivery to Target Cancer Cells by Gold Nanoparticles Capped with Carboxymethyl Chitosan. *International Journal of Molecular Sciences*, *15*(5), Article 5. https://doi.org/10.3390/ijms15058216

Magaye, R., Gu, Y., Wang, Y., Su, H., Zhou, Q., Mao, G., Shi, H., Yue, X., Zou, B., Xu, J., & Zhao, J. (2016). In vitro and in vivo evaluation of the toxicities induced by

metallic nickel nano and fine particles. *Journal of Molecular Histology*, *47*(3), 273–286. https://doi.org/10.1007/s10735-016-9671-6

Mahmoud, A., Echabaane, M., Omri, K., Boudon, J., Saviot, L., Millot, N., & Chaabane, R. B. (2021). Cu-Doped ZnO Nanoparticles for Non-Enzymatic Glucose Sensing. *Molecules*, *26*(4), Article 4. https://doi.org/10.3390/molecules26040929

Maliki, M., Ifijen, I. H., Ikhuoria, E. U., Jonathan, E. M., Onaiwu, G. E., Archibong, U. D., & Ighodaro, A. (2022). Copper nanoparticles and their oxides: Optical, anticancer and antibacterial properties. *International Nano Letters*, *12*(4), 379–398. https://doi.org/10.1007/s40089-022-00380-2

Manzoor, U., Siddique, S., Ahmed, R., Noreen, Z., Bokhari, H., & Ahmad, I. (2016). Antibacterial, Structural and Optical Characterization of Mechano-Chemically Prepared ZnO Nanoparticles. *PLOS ONE*, *11*(5), e0154704. https://doi.org/10.1371/journal.pone.0154704

Mariam, A., Kashif, M., Selvaraj, A., Bououdina, M., Sankaracharyulu, M., Muthurulandi, & Hashim, U. (2014). Bio-synthesis of NiO and Ni nanoparticles and their characterization. *Digest Journal of Nanomaterials and Biostructures*, *9*, 1007–1019.

Markarian, H., Florentine, G. J., & Pratt, J. J. (1978). Quinone production of some species of Tribolium. *Journal of Insect Physiology*, *24*(12), 785–790. https://doi.org/10.1016/0022-1910(78)90096-3

Markus, J., Wang, D., Kim, Y.-J., Ahn, S., Mathiyalagan, R., Wang, C., & Yang, D. C. (2017). Biosynthesis, Characterization, and Bioactivities Evaluation of Silver and Gold Nanoparticles Mediated by the Roots of Chinese Herbal *Angelica pubescens* Maxim. *Nanoscale Research Letters*, *12*(1), 46. https://doi.org/10.1186/s11671-017-1833-2

Martínez-Carmona, M., Gun'ko, Y., & Vallet-Regí, M. (2018). ZnO Nanostructures for Drug Delivery and Theranostic Applications. *Nanomaterials*, *8*(4), Article 4. https://doi.org/10.3390/nano8040268

Milanezi, F. G., Meireles, L. M., de Christo Scherer, M. M., de Oliveira, J. P., da Silva, A. R., de Araujo, M. L., Endringer, D. C., Fronza, M., Guimarães, M. C. C., & Scherer, R. (2019). Antioxidant, antimicrobial and cytotoxic activities of gold nanoparticles capped with quercetin. *Saudi Pharmaceutical Journal*, *27*(7), 968–974. https://doi.org/10.1016/j.jsps.2019.07.005

Mishra, A., Kumari, M., Pandey, S., Chaudhry, V., Gupta, K. C., & Nautiyal, C. S. (2014). Biocatalytic and antimicrobial activities of gold nanoparticles synthesized by *Trichoderma* sp. *Bioresource Technology*, *166*(1), 235–242. https://doi.org/10.1016/j.biortech.2014.04.085

Mishra, P., Ray, S., Sinha, S., Das, B., Khan, Md. I., Behera, S. K., Yun, S.-I., Tripathy, S. K., & Mishra, A. (2016). Facile bio-synthesis of gold nanoparticles by using extract of *Hibiscus sabdariffa* and evaluation of its cytotoxicity against U87 glioblastoma cells under hyperglycemic condition. *Biochemical Engineering Journal*, *105*, 264–272. https://doi.org/10.1016/j.bej.2015.09.021

Mislovičová, D., Michálková, E., & Vikartovská, A. (2007). Immobilized glucose oxidase on different supports for biotransformation removal of glucose from oligosaccharide

mixtures. *Process Biochemistry*, *42*(4), 704–709. https://doi.org/10.1016/j.procbio.2006.11.001

Moghaddam, A. B., Moniri, M., Azizi, S., Rahim, R. A., Ariff, A. B., Saad, W. Z., Namvar, F., Navaderi, M., & Mohamad, R. (2017). Biosynthesis of ZnO Nanoparticles by a New *Pichia kudriavzevii* Yeast Strain and Evaluation of Their Antimicrobial and Antioxidant Activities. *Molecules*, *22*(6), Article 6. https://doi.org/10.3390/molecules22060872

Mohammadi, S., Harvey, A., & Boodhoo, K. (2014). Synthesis of TiO2 nanoparticles in a spinning disc reactor. *Chemical Engineering Journal*, *258*, 171–184. https://doi.org/10.1016/j.cej.2014.07.042

Mohammadpourdounighi, N., Behfar, A., Ezabadi, A., Zolfagharian, H., & Heydari, M. (2010). Preparation of chitosan nanoparticles containing *Naja naja oxiana* snake venom. *Nanomedicine: Nanotechnology, Biology and Medicine*, *6*(1), 137–143. https://doi.org/10.1016/j.nano.2009.06.002

Mohan Kumar, K., Mandal, B. K., Sinha, M., & Krishnakumar, V. (2012). *Terminalia chebula* mediated green and rapid synthesis of gold nanoparticles. *Spectrochimica Acta Part A: Molecular and Biomolecular Spectroscopy*, *86*(1), 490–494. https://doi.org/10.1016/j.saa.2011.11.001

Mohanpuria, P., Rana, N. K., & Yadav, S. K. (2008). Biosynthesis of nanoparticles: Technological concepts and future applications. *Journal of Nanoparticle Research*, *10*(3), 507–517. https://doi.org/10.1007/s11051-007-9275-x

Muhammad, F., Guo, M., Qi, W., Sun, F., Wang, A., Guo, Y., & Zhu, G. (2011). pH-Triggered Controlled Drug Release from Mesoporous Silica Nanoparticles via Intracelluar Dissolution of ZnO Nanolids. *Journal of the American Chemical Society*, *133*(23), 8778–8781. https://doi.org/10.1021/ja200328s

Mukherjee, P., Ahmad, A., Mandal, D., Senapati, S., Sainkar, S. R., Khan, M. I., Parishcha, R., Ajaykumar, P. V., Alam, M., Kumar, R., & Sastry, M. (2001). Fungus-Mediated Synthesis of Silver Nanoparticles and Their Immobilization in the Mycelial Matrix: A Novel Biological Approach to Nanoparticle Synthesis. *Nano Letters*, *1*(10), 515–519. https://doi.org/10.1021/nl0155274

Mukherjee, S., & Patra, C. R. (2016). Therapeutic application of anti-angiogenic nanomaterials in cancers. *Nanoscale*, *8*(25), 12444–12470. https://doi.org/10.1039/C5NR07887C

Munawer, U., Raghavendra, V. B., Ningaraju, S., Krishna, K. L., Ghosh, A. R., Melappa, G., & Pugazhendhi, A. (2020). Biofabrication of gold nanoparticles mediated by the endophytic *Cladosporium* species: Photodegradation, *in vitro* anticancer activity and *in vivo* antitumor studies. *International Journal of Pharmaceutics*, *588*, 119729. https://doi.org/10.1016/j.ijpharm.2020.119729

Murthy, S. K. (2007). Nanoparticles in modern medicine: State of the art and future challenges. *International Journal of Nanomedicine*, *2*(2), 129–141. https://www.ncbi.nlm.nih.gov/pmc/articles/PMC2673971/

Mustafa, S., Mahmood, F., Shafqat, U., Hussain, S., Shahid, M., Batool, F., Elnour, R. O., Hashem, M., Asseri, T. A. Y., & Shahzad, T. (2023). The Biosynthesis of Nickel

Oxide Nanoparticles: An Eco-Friendly Approach for Azo Dye Decolorization and Industrial Wastewater Treatment. *Sustainability*, *15*(20), Article 20. https://doi.org/10.3390/su152014965

Nagajyothi, P. C., Cha, S. J., Yang, I. J., Sreekanth, T. V. M., Kim, K. J., & Shin, H. M. (2015). Antioxidant and anti-inflammatory activities of zinc oxide nanoparticles synthesized using *Polygala tenuifolia* root extract. *Journal of Photochemistry and Photobiology B: Biology*, *146*(1), 10–17. https://doi.org/10.1016/j.jphotobiol.2015.02.008

Nagajyothi, P. C., Muthuraman, P., Sreekanth, T. V. M., Kim, D. H., & Shim, J. (2017). Green synthesis: *In-vitro* anticancer activity of copper oxide nanoparticles against human cervical carcinoma cells. *Arabian Journal of Chemistry*, *10*(2), 215–225. https://doi.org/10.1016/j.arabjc.2016.01.011

Nagaonkar, D., Shende, S., & Rai, M. (2015). Biosynthesis of copper nanoparticles and its effect on actively dividing cells of mitosis in Allium cepa. *Biotechnology Progress*, *31*(2), 557–565. https://doi.org/10.1002/btpr.2040

Naika, H. R., Lingaraju, K., Manjunath, K., Kumar, D., Nagaraju, G., Suresh, D., & Nagabhushana, H. (2015). Green synthesis of CuO nanoparticles using *Gloriosa superba* L. extract and their antibacterial activity. *Journal of Taibah University for Science*, *9*(1), 7–12. https://doi.org/10.1016/j.jtusci.2014.04.006

Naimi-Shamel, N., Pourali, P., & Dolatabadi, S. (2019). Green synthesis of gold nanoparticles using *Fusarium oxysporum* and antibacterial activity of its tetracycline conjugant. *Journal de Mycologie Médicale*, *29*(1), 7–13. https://doi.org/10.1016/j.mycmed.2019.01.005

Namvar, F., Azizi, S., Rahman, H. S., Mohamad, R., Rasedee, A., Soltani, M., & Rahim, R. A. (2016). Green synthesis, characterization, and anticancer activity of hyaluronan/zinc oxide nanocomposite. *OncoTargets and Therapy*, *9*(1), 4549–4559. https://doi.org/10.2147/OTT.S95962

Nasrollahzadeh, M., Maham, M., & Mohammad Sajadi, S. (2015). Green synthesis of CuO nanoparticles by aqueous extract of *Gundelia tournefortii* and evaluation of their catalytic activity for the synthesis of N-monosubstituted ureas and reduction of 4-nitrophenol. *Journal of Colloid and Interface Science*, *455*, 245–253. https://doi.org/10.1016/j.jcis.2015.05.045

Naz, S., Siddiqi, R., Ahmad, S., Rasool, S. a., & Sayeed, S. a. (2007). Antibacterial Activity Directed Isolation of Compounds from *Punica granatum. Journal of Food Science*, *72*(9), M341–M345. https://doi.org/10.1111/j.1750-3841.2007.00533.x

Nazaripour, E., Mosazadeh, F., Rahimi, S. S., Alijani, H. Q., Isaei, E., Borhani, F., Iravani, S., Ghasemi, M., Akbarizadeh, M. R., Azizi, E., Sharifi, F., Haghighat, M., Hadizadeh, S., Moghadam, M. D., Abdollahpour-Alitappeh, M., & Khatami, M. (2022). Ferromagnetic nickel (II) oxide (NiO) nanoparticles: Biosynthesis, characterization and their antibacterial activities. *Rendiconti Lincei. Scienze Fisiche e Naturali*, *33*(1), 127–134. https://doi.org/10.1007/s12210-021-01042-9

Neiva, E. G. C., Bergamini, M. F., Oliveira, M. M., Marcolino, L. H., & Zarbin, A. J. G. (2014). PVP-capped nickel nanoparticles: Synthesis, characterization and utilization

as a glycerol electrosensor. *Sensors and Actuators B: Chemical*, *196*(1), 574–581. https://doi.org/10.1016/j.snb.2014.02.041

Nenadić, M., Soković, M., Glamočlija, J., Ćirić, A., Perić-Mataruga, V., Tešević, V., Vujisić, L., Todosijević, M., Vesović, N., & Ćurčić, S. (2016). Antimicrobial activity of the pygidial gland secretion of the troglophilic ground beetle *Laemostenus (Pristonychus) punctatus (*Dejean, 1828) (Insecta: Coleoptera: Carabidae). *Bulletin of Entomological Research*, *106*(4), 474–480. https://doi.org/10.1017/S0007485316000109

Neng, J., Harpster, M. H., Zhang, H., Mecham, J. O., Wilson, W. C., & Johnson, P. A. (2010). A versatile SERS-based immunoassay for immunoglobulin detection using antigen-coated gold nanoparticles and malachite green-conjugated protein A/G. *Biosensors and Bioelectronics*, *26*(3), 1009–1015. https://doi.org/10.1016/j.bios.2010.08.015

Ni, H., Zhu, J., Wang, Z., Lv, H., Su, Y., & Zhang, X. (2019). A brief overview on grain growth of bulk electrodeposited nanocrystalline nickel and nickel-iron alloys. *Reviews on advanced materials science*, *58*(1), 98–106. https://doi.org/10.1515/rams-2019-0011

Nisa, A., Govindaraju, K., Raguraman, V., Kannan, M., & Kalimuthu, R. (2023). Jellyfish *Acromitus flagellatus* (Maas) nematocyst venom-mediated biogenic synthesis of gold nanoparticles and its anti-proliferative effects. *Aquaculture International*, *31*(1), 1–10. https://doi.org/10.1007/s10499-023-01081-z

Nithya, K., & Kalyanasundharam, S. (2019). Effect of chemically synthesis compared to biosynthesized ZnO nanoparticles using aqueous extract of *C. halicacabum* and their antibacterial activity. *OpenNano*, *4*(1), 100024. https://doi.org/10.1016/j.onano.2018.10.001

Noruzi, M., Zare, D., Khoshnevisan, K., & Davoodi, D. (2011). Rapid green synthesis of gold nanoparticles using *Rosa hybrida* petal extract at room temperature. *Spectrochimica Acta Part A: Molecular and Biomolecular Spectroscopy*, *79*(5), 1461–1465. https://doi.org/10.1016/j.saa.2011.05.001

Oh, K. H., Soshnikova, V., Markus, J., Kim, Y. J., Lee, S. C., Singh, P., Castro-Aceituno, V., Ahn, S., Kim, D. H., Shim, Y. J., Kim, Y. J., & Yang, D. C. (2018). Biosynthesized gold and silver nanoparticles by aqueous fruit extract of *Chaenomeles sinensis* and screening of their biomedical activities. *Artificial Cells, Nanomedicine, and Biotechnology*, *46*(3), 599–606. https://doi.org/10.1080/21691401.2017.1332636

Ohira, T., & Yamamoto, O. (2012). Correlation between antibacterial activity and crystallite size on ceramics. *Chemical Engineering Science*, *68*(1), 355–361. https://doi.org/10.1016/j.ces.2011.09.043

Onitsuka, S., Hamada, T., & Okamura, H. (2019). Preparation of antimicrobial gold and silver nanoparticles from tea leaf extracts. *Colloids and Surfaces B: Biointerfaces*, *173*(1), 242–248. https://doi.org/10.1016/j.colsurfb.2018.09.055

Paciotti, G. F., Kingston, D. G. I., & Tamarkin, L. (2006). Colloidal gold nanoparticles: A novel nanoparticle platform for developing multifunctional tumor-targeted drug

delivery vectors. *Drug Development Research*, *67*(1), 47–54. https://doi.org/10.1002/ddr.20066

Paciotti, G. F., Myer, L., Weinreich, D., Goia, D., Pavel, N., McLaughlin, R. E., & Tamarkin, L. (2004). Colloidal Gold: A Novel Nanoparticle Vector for Tumor-Directed Drug Delivery. *Drug Delivery*, *11*(3), 169–183. https://doi.org/10.1080/10717540490433895

Padalia, H., & Chanda, S. (2017). Characterization, antifungal and cytotoxic evaluation of green synthesized zinc oxide nanoparticles using *Ziziphus nummularia l*eaf extract. *Artificial Cells, Nanomedicine, and Biotechnology*, *45*(8), 1751–1761. https://doi.org/10.1080/21691401.2017.1282868

Padil, V. V. T., & Černík, M. (2013). Green synthesis of copper oxide nanoparticles using *Gum karaya* as a biotemplate and their antibacterial application. *International Journal of Nanomedicine*, *8*, 889–898. https://doi.org/10.2147/IJN.S40599

Pal, G., Rai, P., & Pandey, A. (2019). Green synthesis of nanoparticles: A greener approach for a cleaner future. In A. K. Shukla & S. Iravani (Eds.), *Green Synthesis, Characterization and Applications of Nanoparticles* (Vol. 2019, pp. 1–26). Elsevier. https://doi.org/10.1016/B978-0-08-102579-6.00001-0

Pal, P., Kumar, R., & Banerjee, S. (2016). Manufacture of gluconic acid: A review towards process intensification for green production. *Chemical Engineering and Processing: Process Intensification*, *104*, 160–171. https://doi.org/10.1016/j.cep.2016.03.009

Palani, M., Kalaiselvan, S., Martin Mark, J. A., Chandran, K., & Ekhambaram, V. (2024). Green synthesis of CuO nanoparticles: A promising role of antioxidant and antimicrobial activity by using *Tribulus terrestris* L. *Aspects of Molecular Medicine*, *4*, 100049. https://doi.org/10.1016/j.amolm.2024.100049

Parthasarathy, R., Jayabaskaran, C., Manikandan, A., & Anusuya, S. (2023). Synthesis of Nickel-Chitosan Nanoparticles for Controlling Blast Diseases in Asian Rice. *Applied Biochemistry and Biotechnology*, *195*(3), 2134–2148. https://doi.org/10.1007/s12010-022-04198-8

Parveen, K., Banse, V., & Ledwani, L. (2016). Green synthesis of nanoparticles: Their advantages and disadvantages. *AIP Conference Proceedings*, *1724*(1), 020048. https://doi.org/10.1063/1.4945168

Patra, J. K., & Baek, K.-H. (2014). Green Nanobiotechnology: Factors Affecting Synthesis and Characterization Techniques. *Journal of Nanomaterials*, *2014*(1), 1–12. https://doi.org/10.1155/2014/417305

Pawar, C. A., Sharma, A. K., Prasad, N. R., Suryawanshi, S. S., Nazeruddin, G. M., Shaikh, V. S., Kulkarni, A. N., Al-Sehemi, A. G., & Shaikh, Y. I. (2022). A comparative study on anti-microbial efficacies of biologically synthesized nano gold using *Bos taurus indicus* urine with pharmaceutical drug sample. *Current Research in Green and Sustainable Chemistry*, *5*, 100311. https://doi.org/10.1016/j.crgsc.2022.100311

Peschke, K., & Eisner, T. (1987). Defensive secretion of the tenebrionid beetle,*Blaps mucronata*: Physical and chemical determinants of effectiveness. *Journal of Comparative Physiology A*, *161*(3), 377–388. https://doi.org/10.1007/BF00603963

Pfeiffer, L., Ruther, J., Hofferberth, J., & Stökl, J. (2018). Interference of chemical defence and sexual communication can shape the evolution of chemical signals. *Scientific Reports*, *8*(1), Article 1. https://doi.org/10.1038/s41598-017-18376-w

Philip, D. (2008). Synthesis and spectroscopic characterization of gold nanoparticles. *Spectrochimica Acta Part A: Molecular and Biomolecular Spectroscopy*, *71*(1), 80–85. https://doi.org/10.1016/j.saa.2007.11.012

Philip, D. (2010). Rapid green synthesis of spherical gold nanoparticles using *Mangifera indica* leaf. *Spectrochimica Acta Part A: Molecular and Biomolecular Spectroscopy*, *77*(4), 807–810. https://doi.org/10.1016/j.saa.2010.08.008

Pietruska, J. R., Liu, X., Smith, A., McNeil, K., Weston, P., Zhitkovich, A., Hurt, R., & Kane, A. B. (2011). Bioavailability, Intracellular Mobilization of Nickel, and HIF-1α Activation in Human Lung Epithelial Cells Exposed to Metallic Nickel and Nickel Oxide Nanoparticles. *Toxicological Sciences*, *124*(1), 138–148. https://doi.org/10.1093/toxsci/kfr206

Pillai, A. M., Sivasankarapillai, V. S., Rahdar, A., Joseph, J., Sadeghfar, F., Anuf A, R., Rajesh, K., & Kyzas, G. Z. (2020). Green synthesis and characterization of zinc oxide nanoparticles with antibacterial and antifungal activity. *Journal of Molecular Structure*, *1211*(1), 128107. https://doi.org/10.1016/j.molstruc.2020.128107

Pimpin, A., & Srituravanich, W. (2012). Review on Micro- and Nanolithography Techniques and Their Applications. *Engineering Journal*, *16*(1), 37–56. https://doi.org/10.4186/ej.2012.16.1.37

Pimprikar, P. S., Joshi, S. S., Kumar, A. R., Zinjarde, S. S., & Kulkarni, S. K. (2009). Influence of biomass and gold salt concentration on nanoparticle synthesis by the tropical marine yeast *Yarrowia lipolytica* NCIM 3589. *Colloids and Surfaces B: Biointerfaces*, *74*(1), 309–316. https://doi.org/10.1016/j.colsurfb.2009.07.040

Ping, J., Mao, X., Fan, K., Li, D., Ru, S., Wu, J., & Ying, Y. (2010). A Prussian blue-based amperometric sensor for the determination of hydrogen peroxide residues in milk. *Ionics*, *16*(6), 523–527. https://doi.org/10.1007/s11581-010-0418-1

Pramanik, A., Datta, A. K., Das, D., Kumbhakar, D. V., Ghosh, B., Mandal, A., Gupta, S., Saha, A., & Sengupta, S. (2018). Assessment of Nanotoxicity (Cadmium Sulphide and Copper Oxide) Using Cytogenetical Parameters in *Coriandrum sativum* L. (Apiaceae). *Cytology and Genetics*, *52*(4), 299–308. https://doi.org/10.3103/S0095452718040084

Premanathan, M., Karthikeyan, K., Jeyasubramanian, K., & Manivannan, G. (2011). Selective toxicity of ZnO nanoparticles toward Gram-positive bacteria and cancer cells by apoptosis through lipid peroxidation. *Nanomedicine: Nanotechnology, Biology and Medicine*, *7*(2), 184–192. https://doi.org/10.1016/j.nano.2010.10.001

Rahimi Kalateh Shah Mohammad, G., Homayouni-Tabrizi, M., Ghahremanloo, A., & Yazdanbakhsh, N. (2021). Cytotoxic effect, apoptotic activity, hematological and histological alterations induced by green synthesized ZnO nanoparticles applying *Hyssopus officinalis* leaves. *Inorganic and Nano-Metal Chemistry*, *51*(11), 1560–1569. https://doi.org/10.1080/24701556.2020.1849303

Rahman, M., Abd-El-Barr, M., Mack, V., Tkaczyk, T., Sokolov, K., Richards-Kortum, R., & Descour, M. (2005). Optical imaging of cervical pre-cancers with structured illumination: An integrated approach. *Gynecologic Oncology*, *99*(3, Supplement), S112–S115. https://doi.org/10.1016/j.ygyno.2005.07.053

Raj Preeth, D., Shairam, M., Suganya, N., Hootan, R., Kartik, R., Pierre, K., Suvro, C., & Rajalakshmi, S. (2019). Green synthesis of copper oxide nanoparticles using sinapic acid: An underpinning step towards antiangiogenic therapy for breast cancer. *JBIC Journal of Biological Inorganic Chemistry*, *24*(5), 633–645. https://doi.org/10.1007/s00775-019-01676-z

Rajakumar, G., Rahuman, A. A., Velayutham, K., Ramyadevi, J., Jeyasubramanian, K., Marikani, A., Elango, G., Kamaraj, C., Santhoshkumar, T., Marimuthu, S., Zahir, A. A., Bagavan, A., Jayaseelan, C., Kirthi, A. V., Iyappan, M., & Siva, C. (2013). Novel and simple approach using synthesized nickel nanoparticles to control blood-sucking parasites. *Veterinary Parasitology*, *191*(3–4), 332–339. https://doi.org/10.1016/j.vetpar.2012.08.028

Rajan, A., Vilas, V., & Philip, D. (2015). Studies on catalytic, antioxidant, antibacterial and anticancer activities of biogenic gold nanoparticles. *Journal of Molecular Liquids*, *212*(1), 331–339. https://doi.org/10.1016/j.molliq.2015.09.013

Rajasree, S. R., & Suman, T. (2012). Extracellular biosynthesis of gold nanoparticles using a gram negative bacterium *Pseudomonas fluorescens*. *Asian Pacific Journal of Tropical Disease*, *2*(1), S796–S799. https://doi.org/10.1016/S2222-1808(12)60267-9

Rajesh, K. M., Ajitha, B., Reddy, Y. A. K., Suneetha, Y., & Reddy, P. S. (2018). Assisted green synthesis of copper nanoparticles using *Syzygium aromaticum* bud extract: Physical, optical and antimicrobial properties. *Optik*, *154*(1), 593–600. https://doi.org/10.1016/j.ijleo.2017.10.074

Rajeshkumar, S. (2016). Anticancer activity of eco-friendly gold nanoparticles against lung and liver cancer cells. *Journal of Genetic Engineering and Biotechnology*, *14*(1), 195–202. https://doi.org/10.1016/j.jgeb.2016.05.007

Rajeshkumar, S., Kumar, S. V., Ramaiah, A., Agarwal, H., Lakshmi, T., & Roopan, S. M. (2018). Biosynthesis of zinc oxide nanoparticles using *Mangifera indica* leaves and evaluation of their antioxidant and cytotoxic properties in lung cancer (A549) cells. *Enzyme and Microbial Technology*, *117*(1), 91–95. https://doi.org/10.1016/j.enzmictec.2018.06.009

Rajiv, P., Rajeshwari, S., & Venckatesh, R. (2013). Bio-Fabrication of zinc oxide nanoparticles using leaf extract of *Parthenium hysterophorus* L. and its size-dependent antifungal activity against plant fungal pathogens. *Spectrochimica Acta Part A: Molecular and Biomolecular Spectroscopy*, *112*(1), 384–387. https://doi.org/10.1016/j.saa.2013.04.072

Rajpurohit, A. S., Punde, N. S., & Srivastava, A. K. (2019). An electrochemical sensor with a copper oxide/gold nanoparticle-modified electrode for the simultaneous detection of the potential diabetic biomarkers methylglyoxal and its detoxification enzyme glyoxalase. *New Journal of Chemistry*, *43*(42), 16572–16582. https://doi.org/10.1039/C9NJ03553B

Ramaswamy, S. V. P., Narendhran, S., & Sivaraj, R. (2016). Potentiating effect of ecofriendly synthesis of copper oxide nanoparticles using brown alga: Antimicrobial and anticancer activities. *Bulletin of Materials Science*, *39*(2), 361–364. https://doi.org/10.1007/s12034-016-1173-3

Ramesh, M., Anbuvannan, M., & Viruthagiri, G. (2015). Green synthesis of ZnO nanoparticles using *Solanum nigrum* leaf extract and their antibacterial activity. *Spectrochimica Acta Part A: Molecular and Biomolecular Spectroscopy*, *136*, 864–870. https://doi.org/10.1016/j.saa.2014.09.105

Rameshthangam, P., & Chitra, J. P. (2018). Synergistic anticancer effect of green synthesized nickel nanoparticles and quercetin extracted from *Ocimum sanctum* leaf extract. *Journal of Materials Science & Technology*, *34*(3), 508–522. https://doi.org/10.1016/j.jmst.2017.01.004

Rao, C. N. R., Kulkarni, G. U., Thomas, P. J., & Edwards, P. P. (2002). Size-Dependent Chemistry: Properties of Nanocrystals. *Chemistry – A European Journal*, *8*(1), 28–35. https://doi.org/10.1002/1521-3765.

Ravichandran, S., Radhakrishnan, J., Sengodan, P., Rajendran, R., Ramalingam, R., & Arunachalam, K. D. (2022). Bio synthesis of Zinc oxide nanoparticles using *Clerodendrum phlomidis* extract for antibacterial, anticancer, antioxidant and photocatalytic studies. *Journal of Materials Science: Materials in Electronics*, *33*(14), 11455–11466. https://doi.org/10.1007/s10854-022-08118-8

Reddy, K. M., Feris, K., Bell, J., Wingett, D. G., Hanley, C., & Punnoose, A. (2007). Selective toxicity of zinc oxide nanoparticles to prokaryotic and eukaryotic systems. *Applied Physics Letters*, *90*(213902), 213902-1-213902–213903. https://doi.org/10.1063/1.2742324

Reddy, V., Torati, R. S., Oh, S., & Kim, C. (2013). Biosynthesis of Gold Nanoparticles Assisted by *Sapindus mukorossi* Gaertn. Fruit Pericarp and Its Catalytic Application for the Reduction of p-Nitroaniline. *Industrial & Engineering Chemistry Research*, *52*(2), 556–564. https://doi.org/10.1021/ie302037c

Regier, N., Cosio, C., von Moos, N., & Slaveykova, V. I. (2015). Effects of copper-oxide nanoparticles, dissolved copper, and ultraviolet radiation on copper bioaccumulation, photosynthesis, and oxidative stress in the aquatic macrophyte *Elodea nuttallii*. *Chemosphere*, *128*(1), 56–61. https://doi.org/10.1016/j.chemosphere.2014.12.078

Rehana, D., Mahendiran, D., Kumar, R. S., & Rahiman, A. K. (2017). In vitro antioxidant and antidiabetic activities of zinc oxide nanoparticles synthesized using different plant extracts. *Bioprocess and Biosystems Engineering*, *40*(6), 943–957. https://doi.org/10.1007/s00449-017-1758-2

Ricci, F., & Palleschi, G. (2005). Sensor and biosensor preparation, optimisation and applications of Prussian Blue modified electrodes. *Biosensors and Bioelectronics*, *21*(3), 389–407. https://doi.org/10.1016/j.bios.2004.12.001

Roselina, N. R. N., & Azizan, A. (2012). Ni nanoparticles: Study of Particles Formation and Agglomeration. *Procedia Engineering*, *41*(1), 1620–1626. https://doi.org/10.1016/j.proeng.2012.07.359

Rubab, M., Chelliah, R., & Oh, D.-H. (2022). Screening for Antioxidant Activity: Diphenyl picrylhydrazine (DPPH) Assay , *Methods in Actinobacteriology* (Vol. 1, pp. 453–454). Springer US. https://doi.org/10.1007/978-1-0716-1728-1_61

S, M., Ravi, A. K., Muthukrishnan, S., Shanmugam, V., Arumugam, V. A., & Muthukrishnan, A. (2022a). *Synthesis and Characterization of Nickel Nanoparticles of Gloriosa Superba and Its Anti-Angiogenic Activity in Cervical Cancer*. Research Square. https://doi.org/10.21203/rs.3.rs-1456787/v1

Sabeen, M., Mahmood, Q., Ahmad Bhatti, Z., Faridullah, Irshad, M., Bilal, M., Hayat, M. T., Irshad, U., Ali Akbar, T., Arslan, M., & Shahid, N. (2020). *Allium cepa* assay based comparative study of selected vegetables and the chromosomal aberrations due to heavy metal accumulation. *Saudi Journal of Biological Sciences*, *27*(5), 1368–1374. https://doi.org/10.1016/j.sjbs.2019.12.011

Sabira, O., Vignesh, A. R., Ajaykumar, A. P., Varma, S. R., Jayaraj, K. N., Sebastin, M., Nikhila, K., Babu, A., Rasheed, V. A., Binitha, V. S., Vasu, Z. koldath, & Sujith, M. S. (2022). The Chemical Composition and Antimitotic, Antioxidant, Antibacterial and Cytotoxic Properties of the Defensive Gland Extract of the Beetle, Luprops tristis Fabricius. *Molecules*, *27*(21), Article 21. https://doi.org/10.3390/molecules27217476

Sabu, T. K., & Vinod, K. V. (2009). Food Preferences of the Rubber Plantation Litter Beetle, *Luprops tristis* , a Nuisance Pest in Rubber Tree Plantations. *Journal of Insect Science*, *9*(72), 1–5. https://doi.org/10.1673/031.009.7201

Sabu, T. K., Vinod, K. V., & Jobi, M. C. (2008). Life history, aggregation and dormancy of the rubber plantation litter beetle, *Luprops tristis*, from the rubber plantations of moist south Western Ghats. *Journal of Insect Science*, *8*(1), 1. https://doi.org/10.1673/031.008.0101

Sadani, K., Nag, P., Pisharody, L., Thian, X. Y., Bajaj, G., Natu, G., Mukherji, S., & Mukherji, S. (2021). Polyphenol stabilized copper nanoparticle formulations for rapid disinfection of bacteria and virus on diverse surfaces. *Nanotechnology*, *33*(3), 035701. https://doi.org/10.1088/1361-6528/ac2e77

Sadhasivam, S., Shanmugam, M., Umamaheswaran, P. D., Venkattappan, A., & Shanmugam, A. (2021). Zinc Oxide Nanoparticles: Green Synthesis and Biomedical Applications. *Journal of Cluster Science*, *32*(6), 1441–1455. https://doi.org/10.1007/s10876-020-01918-0

Saeed, B. A., Lim, V., Yusof, N. A., Khor, K. Z., Rahman, H. S., & Abdul Samad, N. (2019). Antiangiogenic properties of nanoparticles: A systematic review. *International Journal of Nanomedicine*, *14*, 5135–5146. https://doi.org/10.2147/IJN.S199974

Saeed, K., & Khan, I. (2013). Carbon nanotubes–properties and applications: A review. *Carbon Letters*, *14*(3), 131–144. https://doi.org/10.5714/CL.2013.14.3.131-

Saif, S., Tahir, A., Asim, T., & Chen, Y. (2016). Plant Mediated Green Synthesis of CuO Nanoparticles: Comparison of Toxicity of Engineered and Plant Mediated CuO Nanoparticles towards *Daphnia magna*. *Nanomaterials*, *6*(11), Article 11. https://doi.org/10.3390/nano6110205

Salata, O. (2004). Applications of nanoparticles in biology and medicine. *Journal of Nanobiotechnology*, *2*(1), 3. https://doi.org/10.1186/1477-3155-2-3

Salavati-Niasari, M., Davar, F., & Mir, N. (2008). Synthesis and characterization of metallic copper nanoparticles via thermal decomposition. *Polyhedron*, *27*(17), 3514–3518. https://doi.org/10.1016/j.poly.2008.08.020

Salieri, B., Turner, D. A., Nowack, B., & Hischier, R. (2018). Life cycle assessment of manufactured nanomaterials: Where are we? *Nano Impact*, *10*(1), 108–120. https://doi.org/10.1016/j.impact.2017.12.003

Sandana Mala, J. G., & Rose, C. (2014). Facile production of ZnS quantum dot nanoparticles by *Saccharomyces cerevisiae* MTCC 2918. *Journal of Biotechnology*, *170*(2014), 73–78. https://doi.org/10.1016/j.jbiotec.2013.11.017

Sankar, R., Karthik, A., Prabu, A., Karthik, S., Shivashangari, K. S., & Ravikumar, V. (2013). *Origanum vulgare* mediated biosynthesis of silver nanoparticles for its antibacterial and anticancer activity. *Colloids and Surfaces B: Biointerfaces*, *108*, 80–84. https://doi.org/10.1016/j.colsurfb.2013.02.033

Santos, J. G., Lopes, H., Moreno, H., Ramirez, M. A., Garcia, F. G., & Simões, A. Z. (2021). Towards anti-angiogenic activity of NiFe2O4 nanoparticles. *Ceramics International*, *47*(11), 16152–16161. https://doi.org/10.1016/j.ceramint.2021.02.191

Saratale, R. G., Karuppusamy, I., Saratale, G. D., Pugazhendhi, A., Kumar, G., Park, Y., Ghodake, G. S., Bharagava, R. N., Banu, J. R., & Shin, H. S. (2018). A comprehensive review on green nanomaterials using biological systems: Recent perception and their future applications. *Colloids and Surfaces. B, Biointerfaces*, *170*(1), 20–35. https://doi.org/10.1016/j.colsurfb.2018.05.045

Saravanakumar, K., Shanmugam, S., Varukattu, N. B., MubarakAli, D., Kathiresan, K., & Wang, M.-H. (2019). Biosynthesis and characterization of copper oxide nanoparticles from indigenous fungi and its effect of photothermolysis on human lung carcinoma. *Journal of Photochemistry and Photobiology B: Biology*, *190*(1), 103–109. https://doi.org/10.1016/j.jphotobiol.2018.11.017

Sarkar, J., Ghosh, M., Mukherjee, A., Chattopadhyay, D., & Acharya, K. (2014). Biosynthesis and safety evaluation of ZnO nanoparticles. *Bioprocess and Biosystems Engineering*, *37*(2), 165–171. https://doi.org/10.1007/s00449-013-0982-7

Sarwar, S., Chakraborti, S., Bera, S., Sheikh, I. A., Hoque, K. M., & Chakrabarti, P. (2016). The antimicrobial activity of ZnO nanoparticles against *Vibrio cholerae:* Variation in response depends on biotype. *Nanomedicine: Nanotechnology, Biology, and Medicine*, *12*(6), 1499–1509. https://doi.org/10.1016/j.nano.2016.02.006

Saxena, A., Tripathi, R., Zafar, F., & Singh, P. (2012). Green synthesis of silver nanoparticles using aqueous solution of *Ficus benghalensis* leaf extract and characterization of their antibacterial activity. *Materials Letters*, *67*, 91–94. https://doi.org/10.1016/j.matlet.2011.09.038

Schäffler, M., Sousa, F., Wenk, A., Sitia, L., Hirn, S., Schleh, C., Haberl, N., Violatto, M., Canovi, M., Andreozzi, P., Salmona, M., Bigini, P., Kreyling, W. G., & Krol, S. (2014). Blood protein coating of gold nanoparticles as potential tool for organ

targeting. *Biomaterials*, *35*(10), 3455–3466. https://doi.org/10.1016/j.biomaterials.2013.12.100

Sehit, E., Drzazgowska, J., Buchenau, D., Yesildag, C., Lensen, M., & Altintas, Z. (2020). Ultrasensitive nonenzymatic electrochemical glucose sensor based on gold nanoparticles and molecularly imprinted polymers. *Biosensors and Bioelectronics*, *165*, 112432. https://doi.org/10.1016/j.bios.2020.112432

Seigneuric, R., Markey, L., S.A. Nuyten, D., Dubernet, C., T.A. Evelo, C., Finot, E., & Garrido, C. (2010). From Nanotechnology to Nanomedicine: Applications to Cancer Research. *Current Molecular Medicine*, *10*(7), 640–652.

Seil, J. T., & Webster, T. J. (2008). Decreased astroglial cell adhesion and proliferation on zinc oxide nanoparticle polyurethane composites. *International Journal of Nanomedicine*, *3*(4), 523–531. https://doi.org/10.2147/ijn.s4346

Senapati, S., Syed, A., Moeez, S., Kumar, A., & Ahmad, A. (2012). Intracellular synthesis of gold nanoparticles using alga *Tetraselmis kochinensis*. *Materials Letters*, *79*(2012), 116–118. https://doi.org/10.1016/j.matlet.2012.04.009

Seregina, T., Chernikova, O., Mazhaysky, Y., & Ampleeva, L. (2020). *Features of the influence of copper nanoparticles and copper oxide on the formation of barley crop*. *18*(1), 1–9. https://doi.org/10.15159/ar.20.025

Shabestarian, H., Homayouni-Tabrizi, M., Soltani, M., Namvar, F., Azizi, S., Mohamad, R., & Shabestarian, H. (2016). Green Synthesis of Gold Nanoparticles Using *Sumac* Aqueous Extract and Their Antioxidant Activity. *Materials Research*, *20*(1), 264–270. https://doi.org/10.1590/1980-5373-MR-2015-0694

Shah, P., & Gavrin, A. (2006). Synthesis of nanoparticles using high-pressure sputtering for magnetic domain imaging. *Journal of Magnetism and Magnetic Materials*, *301*(1), 118–123. https://doi.org/10.1016/j.jmmm.2005.06.023

Shakal, M., Youssef, F. S., Mohamed, G. G., Ismail, S. H., & Salem, H. M. (2024). Evaluation of antibacterial activity of zinc oxide nanoparticles against avian mycoplasmosis with assessment of its impact on broiler chickensâ€™ performance and health. *Journal of Advanced Veterinary Research*, *14*(1), Article 1. https://www.advetresearch.com/index.php/AVR/article/view/1573

Shamaila, S., Zafar, N., Riaz, S., Sharif, R., Nazir, J., & Naseem, S. (2016). Gold Nanoparticles: An Efficient Antimicrobial Agent against Enteric Bacterial Human Pathogen. *Nanomaterials*, *6*(4), Article 4. https://doi.org/10.3390/nano6040071

Shankar, S., & Rhim, J.-W. (2015). Amino acid mediated synthesis of silver nanoparticles and preparation of antimicrobial agar/silver nanoparticles composite films. *Carbohydrate Polymers*, *130*(1), 353–363. https://doi.org/10.1016/j.carbpol.2015.05.018

Sharma, J. K., Akhtar, M. S., Ameen, S., Srivastava, P., & Singh, G. (2015). Green synthesis of CuO nanoparticles with leaf extract of *Calotropis gigantea* and its dye-sensitized solar cells applications. *Journal of Alloys and Compounds*, *632*, 321–325. https://doi.org/10.1016/j.jallcom.2015.01.172

Sharma, T. S. K., Selvakumar, K., Hwa, K. Y., Sami, P., & Kumaresan, M. (2019). Biogenic fabrication of gold nanoparticles using *Camellia japonica* L. leaf extract and its biological evaluation. *Journal of Materials Research and Technology*, *8*(1), 1412–1418. https://doi.org/10.1016/j.jmrt.2018.10.006

Sharma, V., Anderson, D., & Dhawan, A. (2012). Zinc oxide nanoparticles induce oxidative DNA damage and ROS-triggered mitochondria mediated apoptosis in human liver cells (HepG2). *Apoptosis*, *17*(8), 852–870. https://doi.org/10.1007/s10495-012-0705-6

Sharma, V., Chotia, C., Tarachand, Ganesan, V., & Okram, G. S. (2017). Influence of particle size and dielectric environment on the dispersion behaviour and surface plasmon in nickel nanoparticles. *Physical Chemistry Chemical Physics*, *19*(21), 14096–14106. https://doi.org/10.1039/C7CP01769C

Shaymurat, T., Gu, J., Xu, C., Yang, Z., Zhao, Q., Liu, Y., & Liu, Y. (2012). Phytotoxic and genotoxic effects of ZnO nanoparticles on garlic (*Allium sativum* L.): A morphological study. *Nanotoxicology*, *6*(3), 241–248. https://doi.org/10.3109/17435390.2011.570462

Shende, S., Ingle, A. P., Gade, A., & Rai, M. (2015). Green synthesis of copper nanoparticles by *Citrus medica* Linn. (Idilimbu) juice and its antimicrobial activity. *World Journal of Microbiology and Biotechnology*, *31*(6), 865–873. https://doi.org/10.1007/s11274-015-1840-3

Siddiqui, M. A., Alhadlaq, H. A., Ahmad, J., Al-Khedhairy, A. A., Musarrat, J., & Ahamed, M. (2013). Copper Oxide Nanoparticles Induced Mitochondria Mediated Apoptosis in Human Hepatocarcinoma Cells. *PLOS ONE*, *8*(8), e69534. https://doi.org/10.1371/journal.pone.0069534

Silva-Zacarin, E. C., Chauzat, M.-P., Zeggane, M. P. S., Drajnudel, P., Schurr, F., Faucon, J. P., Malaspina, O., & Engler, J. A. (2012). Protocol for optimization of histological, histochemical and immunohistochemical analyses of larval tissues: Application to histopathology of honey bee. *Curr. Micro. Contri. Adv. Sci. Tech.*, *1*, 696–703.

Singh, P., Pandit, S., Garnæs, J., Tunjic, S., Mokkapati, V. R., Sultan, A., Thygesen, A., Mackevica, A., Mateiu, R. V., Daugaard, A. E., Baun, A., & Mijakovic, I. (2018). Green synthesis of gold and silver nanoparticles from *Cannabis sativa* (industrial hemp) and their capacity for biofilm inhibition. *International Journal of Nanomedicine*, *13*(1), 3571–3591. https://doi.org/10.2147/IJN.S157958

Singh, R., Sadasivam, M., & Rakkiyappan, C. (2011). *Ginger (Zingiber officinale) root extract: a source of silver nanoparticles and their application*. *2*(3), 75–80.

Sirelkhatim, A., Mahmud, S., Seeni, A., Kaus, N. H. M., Ann, L. C., Bakhori, S. K. M., Hasan, H., & Mohamad, D. (2015). Review on Zinc Oxide Nanoparticles: Antibacterial Activity and Toxicity Mechanism. *Nano-Micro Letters*, *7*(3), 219–242. https://doi.org/10.1007/s40820-015-0040-x

Siva Kumar, K., Kumar, G., Prokhorov, E., Luna-Bárcenas, G., Buitron, G., Khanna, V. G., & Sanchez, I. C. (2014). Exploitation of anaerobic enriched mixed bacteria (AEMB) for the silver and gold nanoparticles synthesis. *Colloids and Surfaces A:*

Physicochemical and Engineering Aspects, *462*(1), 264–270. https://doi.org/10.1016/j.colsurfa.2014.09.021

Sivasamy, R. (2013). Sol-Gel Synthesis and Characterization of Nanoparticles. *Journal of Nanoscience*, *2013*. https://doi.org/10.1155/2013/929321

S. Jadhav, M., Kulkarni, S., Raikar, P., A. Barretto, D., Kumar Vootla, S., & S. Raikar, U. (2018). Green biosynthesis of CuO & Ag–CuO nanoparticles from *Malus domestica* leaf extract and evaluation of antibacterial, antioxidant and DNA cleavage activities. *New Journal of Chemistry*, *42*(1), 204–213. https://doi.org/10.1039/C7NJ02977B

Solazzo, G., Seidelmann, K., Moritz, R. F. A., & Settele, J. (2015). Tetracosane on the cuticle of the parasitic butterfly *Phengaris (Maculinea) nausithous* triggers the first contact in the adoption process by *Myrmica rubra* foragers. *Physiological Entomology*, *40*(1), 10–17. https://doi.org/10.1111/phen.12083

Soliman, H., Elsayed, A., & Dyaa, A. (2018). Antimicrobial activity of silver nanoparticles biosynthesised by *Rhodotorula* sp . strain ATL72. *Egyptian Journal of Basic and Applied Sciences*, *5*(3), 228–233. https://doi.org/10.1016/j.ejbas.2018.05.005

Song, H., Wang, W., Zhao, P., Qi, Z., & Zhao, S. (2014). Cuprous oxide nanoparticles inhibit angiogenesis via down regulation of VEGFR2 expression. *Nanoscale*, *6*(6), 3206–3216. https://doi.org/10.1039/C3NR04363K

Song, H., Xu, Q., Zhu, Y., Zhu, S., Tang, H., Wang, Y., Ren, H., Zhao, P., Qi, Z., & Zhao, S. (2015). Serum adsorption, cellular internalization and consequent impact of cuprous oxide nanoparticles on uveal melanoma cells: Implications for cancer therapy. *Nanomedicine*, *10*(24), 3547–3562. https://doi.org/10.2217/nnm.15.178

Song, J. Y., & Kim, B. S. (2008). Biological synthesis of bimetallic Au/Ag nanoparticles using Persimmon (*Diospyros kaki*) leaf extract. *Korean Journal of Chemical Engineering*, *25*(4), 808–811. https://doi.org/10.1007/s11814-008-0133-z

Song, W., Zhao, C., & Lercher, J. A. (2013). Importance of Size and Distribution of Ni Nanoparticles for the Hydrodeoxygenation of Microalgae Oil. *Chemistry – A European Journal*, *19*(30), 9833–9842. https://doi.org/10.1002/chem.201301005

Southam, G., & Beveridge, T. J. (1994). The in vitro formation of placer gold by bacteria. *Geochimica et Cosmochimica Acta*, *58*(20), 4527. https://www.academia.edu/16063683/The_in_vitro_formation_of_placer_gold_by_bacteria

Sperling, R. A., Gil, P. R., Zhang, F., Zanella, M., & Parak, W. J. (2008). Biological applications of gold nanoparticles. *Chemical Society Reviews*, *37*(9), 1896–1908. https://doi.org/10.1039/B712170A

Stanković, S., Dimkić, I., Vujisić, L., Pavković-Lučić, S., Jovanović, Z., Stević, T., Sofrenić, I., Mitić, B., & Tomić, V. (2016). Chemical Defence in a Millipede: Evaluation and Characterization of Antimicrobial Activity of the Defensive Secretion from *Pachyiulus hungaricus* (Karsch, 1881) (Diplopoda, Julida, Julidae). *PLOS ONE*, *11*(12), e0167249. https://doi.org/10.1371/journal.pone.0167249

Steiner, M.-S., Duerkop, A., & Wolfbeis, O. S. (2011). Optical methods for sensing glucose. *Chemical Society Reviews*, *40*(9), 4805–4839. https://doi.org/10.1039/C1CS15063D

Strober, W. (1997). Trypan Blue Exclusion Test of Cell Viability. *Current Protocols in Immunology*, *21*(1), A.3B.1-A.3B.2. https://doi.org/10.1002/0471142735.ima03bs21

Strober, W. (2015). Trypan Blue Exclusion Test of Cell Viability. *Current Protocols in Immunology*, *111*, A3.B.1-A3.B.3. https://doi.org/10.1002/0471142735.ima03bs111

Sudhasree, S., Shakila Banu, A., Brindha, P., & Kurian, G. A. (2014). Synthesis of nickel nanoparticles by chemical and green route and their comparison in respect to biological effect and toxicity. *Toxicological & Environmental Chemistry*, *96*(5), 743–754. https://doi.org/10.1080/02772248.2014.923148

Sun, Z., Xiong, T., Zhang, T., Wang, N., Chen, D., & Li, S. (2019). Influences of zinc oxide nanoparticles on *Allium cepa* root cells and the primary cause of phytotoxicity. *Ecotoxicology*, *28*(2), 175–188. https://doi.org/10.1007/s10646-018-2010-9

Sunderam, V., Thiyagarajan, D., Lawrence, A. V., Mohammed, S. S. S., & Selvaraj, A. (2019). *In-vitro* antimicrobial and anticancer properties of green synthesized gold nanoparticles using *Anacardium occidentale* leaves extract. *Saudi Journal of Biological Sciences*, *26*(3), 455–459. https://doi.org/10.1016/j.sjbs.2018.12.001

Sunkar, S., & Nachiyar, C. V. (2012). Biogenesis of antibacterial silver nanoparticles using the endophytic bacterium *Bacillus cereus* isolated from *Garcinia xanthochymus*. *Asian Pacific Journal of Tropical Biomedicine*, *2*(12), 953–959. https://doi.org/10.1016/S2221-1691(13)60006-4

Surender, P., Mogili, T., Thirupathi, D., Janaiah, C., & Vidyavati (Eds.). (n.d.). Effect of scent components on somatic cells of *Allium sativum* L. *CURRENT SCIENCE*.

Suresh, D., Nethravathi, P. C., Udayabhanu, Pavan Kumar, M. A., Raja Naika, H., Nagabhushana, H., & Sharma, S. C. (2015). *Chironji* mediated facile green synthesis of ZnO nanoparticles and their photoluminescence, photodegradative, antimicrobial and antioxidant activities. *Materials Science in Semiconductor Processing*, *40*(1), 759–765. https://doi.org/10.1016/j.mssp.2015.06.088

Sutradhar, P., Saha, M., & Maiti, D. (2014). Microwave synthesis of copper oxide nanoparticles using tea leaf and coffee powder extracts and its antibacterial activity. *Journal of Nanostructure in Chemistry*, *4*(1), 86. https://doi.org/10.1007/s40097-014-0086-1

Szymański, P., Frączek, T., Markowicz, M., & Mikiciuk-Olasik, E. (2012). Development of copper based drugs, radiopharmaceuticals and medical materials. *BioMetals*, *25*(6), 1089–1112. https://doi.org/10.1007/s10534-012-9578-y

Tai, C., Tai, C.-T., Chang, M.-H., & Liu, H.-S. (2007). Synthesis of Magnesium Hydroxide and Oxide Nanoparticles Using a Spinning Disk Reactor. *Ind. Eng. Chem. Res*, *46*(1), 5536–5541. https://doi.org/10.1021/ie060869b

Tang, Y., Debnath, T., Choi, E.-J., Kim, Y. W., Ryu, J. P., Jang, S., Chung, S. U., Choi, Y.-J., & Kim, E.-K. (2018). Changes in the amino acid profiles and free radical scavenging activities of *Tenebrio molitor* larvae following enzymatic hydrolysis. *PLOS ONE*, *13*(5), e0196218. https://doi.org/10.1371/journal.pone.0196218

Thandapani, G., K., A., P., P., J. John, J., C., V., V., R., K., S., & Sekar, V. (2023). Green synthesis of copper oxide nanoparticles using *Spinacia oleracea* leaf extract and evaluation of biological applications: Antioxidant, antibacterial, larvicidal and biosafety assay. *Materials Today Communications*, *34*, 105248. https://doi.org/10.1016/j.mtcomm.2022.105248

Thangaraj, P. (2016). In Vitro Antioxidant Assays. In T. Parimelazhagan (Ed.), *Pharmacological Assays of Plant-Based Natural Products* (pp. 57–72). Springer International Publishing. https://doi.org/10.1007/978-3-319-26811-8_9

Thiruvengadam, M., Chung, I.-M., Gomathi, T., Ansari, M. A., Gopiesh Khanna, V., Babu, V., & Rajakumar, G. (2019). Synthesis, characterization and pharmacological potential of green synthesized copper nanoparticles. *Bioprocess and Biosystems Engineering*, *42*(11), 1769–1777. https://doi.org/10.1007/s00449-019-02173-y

Tiwari, D., Behari, J., & Sen, P. (2008). Application of Nanoparticles in Waste Water Treatment. *World Applied Sciences Journal*, *3*(3), 417–433.

Tomar, R. S., Chauhan, P., & Shrivastava, V. (2015). A critical review on nanoparticle synthesis: Physicochemical V/s biological approach. *World Journal of Pharmaceutical Research*, *4*(1), 595–620.

Torabi, M., Kesmati, M., Harooni, H. E., & Varzi, H. N. (2013). Effects of nano and conventional Zinc Oxide on anxiety-like behavior in male rats. *Indian Journal of Pharmacology*, *45*(5), 508–512. https://doi.org/10.4103/0253-7613.117784

Tschinkel, W. R. (1975). A comparative study of the chemical defensive system of tenebrionid beetles III. Morphology of the glands. *Journal of Morphology*, *145*(3), 355–370. https://doi.org/10.1002/jmor.1051450308

Vahedi, M., Hosseini-Jazani, N., Yousefi, S., & Ghahremani, M. (2017). Evaluation of anti-bacterial effects of nickel nanoparticles on biofilm production by *Staphylococcus epidermidis. Iranian Journal of Microbiology*, *9*(3), 160–168. https://www.ncbi.nlm.nih.gov/pmc/articles/PMC5719510/

Vaidehi, D., Bhuvaneshwari, V., Bharathi, D., & Sheetal, B. P. (2018). Antibacterial and photocatalytic activity of copper oxide nanoparticles synthesized using *Solanum lycopersicum* leaf extract. *Materials Research Express*, *5*(8), 085403. https://doi.org/10.1088/2053-1591/aad426

Vanathi, P., Rajiv, P., & Sivaraj, R. (2016). Synthesis and characterization of *Eichhornia*-mediated copper oxide nanoparticles and assessing their antifungal activity against plant pathogens. *Bulletin of Materials Science*, *39*(5), 1165–1170. https://doi.org/10.1007/s12034-016-1276-x

Verma, V., & Kaushik, D. (2020). Mupirocin-Mounted Copper Nanoparticle Offered Augmented Drug Delivery against Resistant Bacteria. *Indian Journal of Pharmaceutical Education and Research*, *54*(3), 637–646. https://doi.org/10.5530/ijper.54.3.113

Vesović, N., Vujisić, L., Perić-Mataruga, V., Krstić, G., Nenadić, M., Cvetković, M., Ilijin, L., Stanković, J., & Ćurčić, S. (2017). Chemical secretion and morpho-histology of the pygidial glands in two Palaearctic predatory ground beetle species: *Carabus* (*Tomocarabus*) *convexus* and *C* . (*Procrustes*) *coriaceus* (Coleoptera: Carabidae).

Journal of Natural History, *51*(9–10), 545–560. https://doi.org/10.1080/00222933.2017.1293183

Vidhya, E., Vijayakumar, S., Prathipkumar, S., & Praseetha, P. K. (2020). Green way biosynthesis: Characterization, antimicrobial and anticancer activity of ZnO nanoparticles. *Gene Reports*, *20*(1), 100688. https://doi.org/10.1016/j.genrep.2020.100688

Vijaya Kumar, P., Mary Jelastin Kala, S., & Prakash, K. S. (2019). Green synthesis of gold nanoparticles using *Croton Caudatus Geisel* leaf extract and their biological studies. *Materials Letters*, *236*(1), 19–22. https://doi.org/10.1016/j.matlet.2018.10.025

Vimalraj, S., Ashokkumar, T., & Saravanan, S. (2018). Biogenic gold nanoparticles synthesis mediated by *Mangifera indica* seed aqueous extracts exhibits antibacterial, anticancer and anti-angiogenic properties. *Biomedicine & Pharmacotherapy*, *105*(1), 440–448. https://doi.org/10.1016/j.biopha.2018.05.151

Wageh, S., Maize, M., Donia, A. M., Al-Ghamdi, A. A., & Umar, A. (2015). Synthesis and Characterization of Mercaptoacetic Acid Capped Cadmium Sulphide Quantum Dots. *Journal of Nanoscience and Nanotechnology*, *15*(12), 9861–9867. https://doi.org/10.1166/jnn.2015.10346

Wahab, R., Kaushik, N. K., Kaushik, N., Choi, E. H., Umar, A., Dwivedi, S., Musarrat, J., & Al-Khedhairy, A. A. (2013). ZnO Nanoparticles Induces Cell Death in Malignant Human T98G Gliomas, KB and Non-Malignant HEK Cells. *Journal of Biomedical Nanotechnology*, *9*(7), 1181–1189. https://doi.org/10.1166/jbn.2013.1652

Wanarska, E., & Maliszewska, I. (2019). The possible mechanism of the formation of silver nanoparticles by *Penicillium cyclopium. Bioorganic Chemistry*, *93*(102803), 1–9. https://doi.org/10.1016/j.bioorg.2019.02.028

Wang, D., Markus, J., Wang, C., Kim, Y.-J., Mathiyalagan, R., Aceituno, V. C., Ahn, S., & Yang, D. C. (2017). Green synthesis of gold and silver nanoparticles using aqueous extract of *Cibotium barometz* root. *Artificial Cells, Nanomedicine, and Biotechnology*, *45*(8), 1548–1555. https://doi.org/10.1080/21691401.2016.1260580

Wang, G., Tan, X., Zhou, Q., Liu, Y., Wang, M., & Yang, L. (2014). Synthesis of highly dispersed zinc oxide nanoparticles on carboxylic graphene for development a sensitive acetylcholinesterase biosensor. *Sensors and Actuators B: Chemical*, *190*, 730–736. https://doi.org/10.1016/j.snb.2013.09.042

Wang, J., Zhu, G., You, M., Song, E., Shukoor, M. I., Zhang, K., Altman, M. B., Chen, Y., Zhu, Z., Huang, C. Z., & Tan, W. (2012). Assembly of aptamer switch probes and photosensitizer on gold nanorods for targeted photothermal and photodynamic cancer therapy. *ACS Nano*, *6*(6), 5070–5077. https://doi.org/10.1021/nn300694v

Wang, Q., Ebbs, S. D., Chen, Y., & Ma, X. (2013). Trans-generational impact of cerium oxide nanoparticles on tomato plants. *Metallomics*, *5*(6), 753. https://doi.org/10.1039/c3mt00033h

Wang, Y., Yang, Q.-W., Yang, Q., Zhou, T., Shi, M.-F., Sun, C.-X., Gao, X.-X., Cheng, Y.-Q., Cui, X.-G., & Sun, Y.-H. (2017). Cuprous oxide nanoparticles inhibit prostate cancer by attenuating the stemness of cancer cells via inhibition of the Wnt

signaling pathway. *International Journal of Nanomedicine*, *12*(1), 2569–2579. https://doi.org/10.2147/IJN.S130537

Watt, J. C. (1974). A revised subfamily classification of Tenebrionidae (Coleoptera). *New Zealand Journal of Zoology*, *1*(4), 381–452. https://doi.org/10.1080/03014223.1974.9517846

Wei, Z., Abbaspour, S., & Tayebee, R. (2023). Nickel Nanoparticles Originated from Cressa Leaf Extract in the Preparation of a Novel Melem@Ni-HPA Photocatalyst for the Synthesis of Some Chromenes and a Preliminary MTT Assay on the Anticancer Activity of the Nanocomposite. *Polycyclic Aromatic Compounds*, *43*(1), 552–571. https://doi.org/10.1080/10406638.2021.2019063

Wu, Y. L., Fu, S., Tok, A. I. Y., Zeng, X. T., Lim, C. S., Kwek, L. C., & Boey, F. C. Y. (2008). A dual-colored bio-marker made of doped ZnO nanocrystals. *Nanotechnology*, *19*(34), 345605. https://doi.org/10.1088/0957-4484/19/34/345605

Xu, C., Yang, C., Gu, B., & Fang, S. (2013). Nanostructured ZnO for biosensing applications. *Chinese Science Bulletin*, *21*(58), 2563–2566. https://doi.org/10.1007/s11434-013-5714-5

Xue, Y., Yu, G., Shan, Z., & Li, Z. (2018). Phyto-mediated synthesized multifunctional Zn/CuO NPs hybrid nanoparticles for enhanced activity for kidney cancer therapy: A complete physical and biological analysis. *Journal of Photochemistry and Photobiology B: Biology*, *186*(1), 131–136. https://doi.org/10.1016/j.jphotobiol.2018.07.004

Yadav, A., Ghune, M., & Jain, D. K. (2011). Nano-medicine based drug delivery system. *Journal of Advanced Pharmacy Education & Research*, *1*(4), 2249–3379.

Yadav, S., Nadar, T., Lakkakula, J., & Wagh, N. S. (2024). Biogenic Synthesis of Nanomaterials: Bioactive Compounds as Reducing, and Capping Agents. In M. P. Shah, N. Bharadvaja, & L. Kumar (Eds.), *Biogenic Nanomaterials for Environmental Sustainability: Principles, Practices, and Opportunities* (pp. 147–188). Springer International Publishing. https://doi.org/10.1007/978-3-031-45956-6_6

Yadav, T., Yadav, R. M., & Singh, D. (2012). Mechanical Milling: A Top Down Approach for the Synthesis of Nanomaterials and Nanocomposites. *Nanoscience and Nanotechnology*, *2*(3), 22–48. https://doi.org/10.5923/j.nn.20120203.01

Yang, Q., Wang, Y., Yang, Q., Gao, Y., Duan, X., Fu, Q., Chu, C., Pan, X., Cui, X., & Sun, Y. (2017). Cuprous oxide nanoparticles trigger ER stress-induced apoptosis by regulating copper trafficking and overcoming resistance to sunitinib therapy in renal cancer. *Biomaterials*, *146*(1), 72–85. https://doi.org/10.1016/j.biomaterials.2017.09.008

Yang, Z., Suomalainen, T., Mäyrä-Mäkinen, A., & Huttunen, E. (1997). Antimicrobial Activity of 2-Pyrrolidone-5-Carboxylic Acid Produced by Lactic Acid Bacteria. *Journal of Food Protection*, *60*(7), 786–790. https://doi.org/10.4315/0362-028X-60.7.786

Yedurkar, S., Maurya, C., & Mahanwar, P. (2016). Biosynthesis of Zinc Oxide Nanoparticles Using *Ixora Coccinea* Leaf Extract—A Green Approach. *Open*

Journal of Synthesis Theory and Applications, *5*(1), Article 1. https://doi.org/10.4236/ojsta.2016.51001

Yılmaz Öztürk, B., Yenice Gürsu, B., & Dağ, İ. (2020). Antibiofilm and antimicrobial activities of green synthesized silver nanoparticles using marine red algae *Gelidium corneum*. *Process Biochemistry*, *89*(1), 208–219. https://doi.org/10.1016/j.procbio.2019.10.027

Youssef, M. S., & Elamawi, R. M. (2020). Evaluation of phytotoxicity, cytotoxicity, and genotoxicity of ZnO nanoparticles in *Vicia faba*. *Environmental Science and Pollution Research*, *27*(16), 18972–18984. https://doi.org/10.1007/s11356-018-3250-1

Yu, Chang, S.-S., Lee, C.-L., & Wang, C. R. C. (1997). Gold Nanorods: Electrochemical Synthesis and Optical Properties. *The Journal of Physical Chemistry B*, *101*(34), 6661–6664. https://doi.org/10.1021/jp971656q

Yuan, C., Jiang, B., Xu, X., Wan, Y., Wang, L., & Chen, J. (2022). Anti-human ovarian cancer and cytotoxicity effects of nickel nanoparticles green-synthesized by *Alhagi maurorum* leaf aqueous extract. *Journal of Experimental Nanoscience*, *17*(1), 113–125. https://doi.org/10.1080/17458080.2021.2011860

Yuan, Q., Hein, S., & Misra, R. D. K. (2010). New generation of chitosan-encapsulated ZnO quantum dots loaded with drug: Synthesis, characterization and in vitro drug delivery response. *Acta Biomaterialia*, *6*(7), 2732–2739. https://doi.org/10.1016/j.actbio.2010.01.025

Yuan, Q., Hein, S., & Misra, R. D. K. (2010b). New generation of chitosan-encapsulated ZnO quantum dots loaded with drug: Synthesis, characterization and in vitro drug delivery response. *Acta Biomaterialia*, *6*(7), 2732–2739. https://doi.org/10.1016/j.actbio.2010.01.025

Yugandhar, P., Vasavi, T., Uma Maheswari Devi, P., & Savithramma, N. (2017). Bioinspired green synthesis of copper oxide nanoparticles from *Syzygium alternifolium* (Wt.) Walp: Characterization and evaluation of its synergistic antimicrobial and anticancer activity. *Applied Nanoscience*, *7*(7), 417–427. https://doi.org/10.1007/s13204-017-0584-9

Zare, E., Pourseyedi, S., Khatami, M., & Darezereshki, E. (2017). Simple biosynthesis of zinc oxide nanoparticles using nature's source, and it's in vitro bio-activity. *Journal of Molecular Structure*, *1146*(1), 96–103. https://doi.org/10.1016/j.molstruc.2017.05.118

Zarenezhad, E., Abdulabbas, H. T., Marzi, M., Ghazy, E., Ekrahi, M., Pezeshki, B., Ghasemian, A., & Moawad, A. A. (2022). Nickel Nanoparticles: Applications and Antimicrobial Role against Methicillin-Resistant Staphylococcus aureus Infections. *Antibiotics*, *11*(9), 1208. https://doi.org/10.3390/antibiotics11091208

Zarharan, H., Bagherian, M., Shah Rokhi, A., Ramezani Bajgiran, R., Yousefi, E., Heravian, P., Niazi Khazrabig, M., Es-haghi, A., & Taghavizadeh Yazdi, M. E. (2023). The anti-angiogenesis and antioxidant activity of chitosan-mediated synthesized selenium-gold nanostructure. *Arabian Journal of Chemistry*, *16*(7), 104806. https://doi.org/10.1016/j.arabjc.2023.104806

Zent, C. S., Call, T. G., Hogan, W. J., Shanafelt, T. D., & Kay, N. E. (2006). Update on risk-stratified management for chronic lymphocytic leukemia. *Leukemia & Lymphoma*, *47*(9), 1738–1746. https://doi.org/10.1080/10428190600634036

Zhang, P., & Liu, W. (2010). ZnO QD@PMAA-co-PDMAEMA nonviral vector for plasmid DNA delivery and bioimaging. *Biomaterials*, *31*(11), 3087–3094. https://doi.org/10.1016/j.biomaterials.2010.01.007

Zvereva, E. L., & Kozlov, M. V. (2016). The costs and effectiveness of chemical defenses in herbivorous insects: A meta-analysis. *Ecological Monographs*, *86*(1), 107–124. https://doi.org/10.1890/15-0911.1

Appendices

Appendix A1: Protocol for the Synthesis of Nickel Nanoparticles (NiNPs)
Materials Required:

- Nickel (II) chloride hexahydrate ($NiCl_2 \cdot 6H_2O$) – NICE Chemicals Pvt. Ltd.
- *Luprops tristis* gland extract (from 30 beetles)
- Distilled water
- Deionized water
- Microwave oven (LG MS2042DB, South Korea)
- Centrifuge
- Lyophilizer

Procedure:

1. **Preparation of Gland Extract:**
   Crush the defensive glands from 30 *L. tristis* beetles and mix with distilled water to obtain a concentration of 300 µg/mL.
2. **Preparation of Nickel Solution (0.01 M):**
   Dissolve 0.01 moles of $NiCl_2 \cdot 6H_2O$ in 1 L of deionized water.
3. **Reaction Mixture Preparation:**
   Mix the gland extract (300 µg/mL) with the 0.01 M nickel solution at a ratio to achieve a final concentration of 600 µg/mL metal precursor.
4. **Microwave-Assisted Synthesis:**
   Heat the mixture in a microwave oven at 350 W for 15 minutes. Monitor for a visible change in colour indicating nanoparticle formation.
5. **Post-Synthesis Processing:**
   Centrifuge the solution to collect the nanoparticles.
   Lyophilize the pellet for subsequent characterization and applications.

Appendix A2: Protocol for the Synthesis of Copper Oxide Nanoparticles (CuONPs)
Materials Required:

- Copper (II) sulfate pentahydrate ($CuSO_4 \cdot 5H_2O$) – NICE Chemicals Pvt. Ltd.
- *Luprops tristis* gland extract (from 30 beetles)
- Distilled water
- Deionized water
- Microwave oven (LG MS2042DB, South Korea)
- Centrifuge
- Lyophilizer

Procedure:

1. **Preparation of Gland Extract:**
   Prepare the gland extract as above, ensuring a concentration of 300 µg/mL.
2. **Preparation of Copper Solution (0.01 M):**
   Dissolve 0.01 moles of $CuSO_4 \cdot 5H_2O$ in 1 L of deionized water.
3. **Reaction Mixture Preparation:**
   Combine the gland extract (300 µg/mL) with the copper solution to achieve a final metal concentration of 600 µg/mL.
4. **Microwave-Assisted Synthesis:**
   Expose the mixture to microwave irradiation at 350 W for 15 minutes. Observe for a colour change.
5. **Post-Synthesis Processing:**
   Centrifuge the mixture, collect the nanoparticle pellet, and lyophilize it.

Appendix A3: Protocol for the Synthesis of Zinc Oxide Nanoparticles (ZnONPs)
Materials Required:

- Zinc acetate ($Zn(CH_3CO_2)_2$) – NICE Chemicals Pvt. Ltd.
- *Luprops tristis* gland extract (from 30 beetles)

- Distilled water
- Deionized water
- Microwave oven (LG MS2042DB, South Korea)
- Centrifuge
- Lyophilizer

Procedure:

1. **Preparation of Gland Extract:**
   Obtain a gland extract of 300 µg/mL from 30 *L. tristis* beetles.
2. **Preparation of Zinc Solution (0.01 M):**
   Dissolve 0.01 moles of zinc acetate in 1 L of deionized water.
3. **Reaction Mixture Preparation:**
   Mix the gland extract with the zinc solution to achieve 600 µg/mL metal concentration.
4. **Microwave-Assisted Synthesis:**
   Heat the solution in the microwave at 350 W for 15 minutes. Note any colour changes.
5. **Post-Synthesis Processing:**
   Centrifuge and lyophilize the nanoparticles for further use.

Appendix A4: Protocol for the Synthesis of Gold Nanoparticles (AuNPs)
Materials Required:

- Auric chloride ($AuCl_3 \cdot H_2O$) – NICE Chemicals Pvt. Ltd.
- *Luprops tristis* gland extract (from 30 beetles)
- Distilled water
- Deionized water
- Microwave oven (LG MS2042DB, South Korea)
- Centrifuge
- Lyophilizer

Procedure:

1. **Preparation of Gland Extract:**
   Extract defensive glands from 30 beetles and dilute to 300 µg/mL with distilled water.
2. **Preparation of Gold Solution (0.01 M):**
   Dissolve 0.01 moles of $AuCl_3 \cdot H_2O$ in 1 L of deionized water.
3. **Reaction Mixture Preparation:**
   Combine the gland extract and gold solution, ensuring a final metal concentration of 600 µg/mL.
4. **Microwave-Assisted Synthesis:**
   Microwave the solution at 350 W for 15 minutes. A colour change confirms nanoparticle synthesis.
5. **Post-Synthesis Processing:**
   Centrifuge and lyophilize the gold nanoparticles for storage and characterization

---

Appendix B: Protocol for Electrochemical Sensing Studies
B1. Materials and Equipment

- Electrochemical workstation (e.g., CH Instruments, Autolab, or equivalent)
- Three-electrode electrochemical cell (10 mL capacity)
- Phosphate-buffered saline (PBS), pH 7.4
- Platinum foil (counter electrode)
- Ag/AgCl reference electrode
- Working electrode (modified with synthesized nanomaterial)
- Target analyte solutions (e.g., glucose, hydrogen peroxide)
- Micropipettes and tips
- Analytical balance
- Volumetric flasks and beakers

B2. Experimental Procedure

1. **Electrochemical Cell Setup:**

- Fill the electrochemical cell with 10 mL of phosphate-buffered saline (PBS).
- Assemble the three-electrode system:
    - **Working electrode**: Modified with the synthesized metal nanoparticle sensing material.
    - **Reference electrode**: Ag/AgCl.
    - **Counter electrode**: Platinum foil.
- Connect all electrodes to the electrochemical workstation.

2. **Parameter Configuration:**
    - Program the electrochemical workstation to run **Differential Pulse Voltammetry (DPV)**.
    - Set the potential window to sweep from **+1.000 V to -1.000 V**.
3. **Analyte Addition and Measurement:**
    - Prepare standard solutions of the target analytes (e.g., glucose, H_2O_2) in PBS at varying concentrations.
    - Sequentially add known volumes of each analyte to the electrochemical cell.
    - After each addition, record the DPV response.
    - Rinse and stabilize electrodes between runs if necessary.
4. **Data Collection and Analysis:**
    - Record current outputs for each analyte concentration.
    - Plot a **calibration curve** of current (µA) versus analyte concentration (mM or µM).
    - Determine the **slope** of the linear range of the curve.
5. **Limit of Detection (LOD) Calculation:**
    - Measure the standard deviation (SD) of blank (analyte-free) runs.
    - Calculate LOD using the formula: LOD = 3 × SD / Slope.

Appendix C: Protocol for Dose-Dependent Antibacterial Activity Assay Using Disc Diffusion Method

C1. Materials and Equipment

- *Escherichia coli* (Gram-negative) and *Staphylococcus aureus* (Gram-positive) bacterial strains
- Muller Hinton Agar (MHA) powder (4 g per 100 mL)
- Nutrient agar plates
- Sterile Petri dishes (autoclaved)
- Distilled water
- Defensive gland extract from *Luprops tristis*
- Tetracycline (positive control)
- Sterile filter paper discs (5 mm diameter)
- Micropipettes and tips
- Forceps
- Sterile cotton swabs
- Shaking incubator (e.g., LABLINE)
- Ruler or digital caliper (for measuring inhibition zones)

C2. Preparation of Culture Media and Plates

1. **Muller Hinton Agar Preparation:**
    - Dissolve **4 g of MHA powder** in **100 mL distilled water**.
    - Autoclave the solution to sterilize.
    - Pour the sterile MHA into **4 well-autoclaved Petri dishes** under aseptic conditions.
    - Allow the media to solidify.
2. **Microbial Inoculation:**
    - Sub-culture pure colonies of *E. coli* and *S. aureus* on nutrient agar.
    - Using sterile cotton swabs, **uniformly swab** the entire surface of the MHA plates with bacterial suspensions (separate plates for each bacterium).

C3. Disc Diffusion Assay

1. **Preparation of Test Discs:**
    - Prepare gland extract solutions at **5 µg/mL** and **10 µg/mL** concentrations.

- Soak sterile **5 mm filter paper discs** in each solution.
- Allow the discs to air-dry under sterile conditions.

2. **Placement of Discs:**
   - Using sterile forceps, place the dried, extract-impregnated discs onto the inoculated MHA plates.
   - Place a disc soaked with **Tetracycline** as the **positive control**.
   - Ensure discs are spaced sufficiently to avoid overlapping zones of inhibition.
3. **Incubation:**
   - Incubate the plates in a **shaking incubator** at **35 ± 1 °C** for **16 hours**.

C4. Measurement and Analysis

1. **Observation:**
   - After incubation, examine the plates for **zones of inhibition** around each disc.
2. **Measurement:**
   - Measure the **diameter (in mm)** of the clear zone around each disc using a ruler or digital caliper.
3. **Interpretation:**
   - Larger zones of inhibition indicate stronger antibacterial activity.
   - Compare results between extract concentrations and against the positive control.

Appendix D: Protocol for DPPH Free Radical Scavenging Assay of Defensive Secretion

D1. Materials and Equipment

- DPPH (2,2-diphenyl-1-picrylhydrazyl)
- Defensive secretion extract
- Ascorbic acid (reference standard)
- Distilled water
- UV-Visible spectrophotometer (PerkinElmer UV-WinLab or equivalent)
- Quartz cuvettes
- Micropipettes and tips
- Amber tubes or aluminum foil (for dark incubation)

D2. Preparation of Solutions

1. **DPPH Solution:**
   - Prepare a fresh 0.1 mM DPPH solution in methanol or ethanol.
2. **Sample Solutions:**
   - Prepare defensive secretion extract at **five concentrations**:
     20 µg/mL, **40 µg/mL**, **60 µg/mL**, **80 µg/mL**, and **100 µg/mL**, using distilled water or suitable solvent.
3. **Standard Solution:**
   - Prepare **ascorbic acid** solution in distilled water at equivalent concentrations for comparison.

D3. Assay Procedure

1. In labeled tubes or cuvettes, **mix 2 mL of DPPH solution** with **1 mL of each sample concentration**.
2. Prepare a **control** by mixing 2 mL of DPPH with 1 mL of distilled water (no sample).
3. **Incubate the mixtures in the dark** for **30 minutes** at room temperature to prevent photodegradation.
4. After incubation, observe the **colour change** from deep violet to pale yellow, indicating free radical scavenging.
5. Measure the **absorbance at 517 nm** using a UV-Visible spectrophotometer.

D4. Data Analysis

1. **Calculate Scavenging Activity (S%)** using the equation:S% = [(Absorbance of control – Absorbance of sample) / Absorbance of control] x 100
2. Plot **S% vs. sample concentration** to obtain a dose-response curve.

3. Use **linear regression** to calculate the **IC_{50} value**, which represents the concentration required to achieve 50% radical scavenging activity

---

Appendix E: Protocol for Environmental Toxicity Testing of Defensive Gland Secretion Using Allium Test

E1. Objective

To evaluate the cytotoxic and genotoxic potential of biosynthesized nanoparticles (NPs) derived from *Luprops tristis* defensive gland secretion by examining their effects on *Allium cepa* root meristematic cells.

E2. Materials and Equipment

- *Allium cepa* bulbs (equal-sized, healthy)
- Biosynthesized nanoparticle solutions (100, 200, 300, 400, 500 µg/mL)
- Distilled water (negative control)
- Hydrogen peroxide (positive control)
- Glass jars or test tubes for incubation
- Scalpel or sharp blade
- Acetocarmine stain
- Methylene blue stain
- Microscope slides and cover slips
- LEICA ICC50E compound microscope or equivalent
- Forceps, dropper, filter paper
- Water bath or flame for slide preparation

E3. Experimental Procedure

1. **Bulb Preparation:**
    - Select healthy *Allium cepa* bulbs of equal size.
    - Remove dry outer scales without damaging the root primordia.
2. **Sample Exposure:**
    - Place bulbs in test tubes or jars containing sample NP solutions at concentrations of:
        - **100 µg/mL**, **200 µg/mL**, **300 µg/mL**, **400 µg/mL**, **500 µg/mL**
    - Use **distilled water** as the **negative control** and **hydrogen peroxide** as the **positive control**.
    - Incubate the bulbs for **48–72 hours** at room temperature.
3. **Root Collection:**
    - When roots reach **2–3 cm**, select **3–5 root tips** per bulb for analysis.
4. **Slide Preparation (Squash Technique):**
    - Cut the root tips (~1–2 mm from the tip).
    - Stain root tips with **acetocarmine** or **methylene blue**.
    - Warm gently to enhance staining if necessary.
    - Place the stained tip on a microscope slide, add a drop of stain if required.
    - Cover with a cover slip and squash gently using filter paper or blunt object to spread the cells.
5. **Microscopic Analysis:**
    - Observe under a **compound microscope (LEICA ICC50E)**.
    - Identify and count a minimum of **1500 cells** from the **three best preparations**.
    - Record mitotic stages and chromosomal aberrations (e.g., stickiness, bridges, laggards, micronuclei).

E4. Data Analysis

1. **Calculate frequency of chromosomal aberrations** per treatment group.
2. Present data as **mean ± standard deviation**.
3. Compare values against negative and positive controls to assess cytogenotoxic effects.

Appendix F: Protocol for Anticancer Cytotoxicity Assay of Defensive Gland Secretion Using Trypan Blue Exclusion Method

F1. Objective

To assess the **cytotoxic effect** of *Luprops tristis* defensive gland secretion on **Dalton's lymphoma ascites (DLA) cells** using the **Trypan Blue Exclusion Assay** as described by Strober (1997).

F2. Materials and Equipment

- Dalton's lymphoma ascites (DLA) cells (from tumor-bearing mice)
- Defensive gland secretion samples
- Phosphate-buffered saline (PBS)
- Normal saline (0.9% NaCl)
- Trypan blue dye (1% solution)
- Hemocytometer (Neubauer chamber)
- Light microscope
- Microcentrifuge tubes or sterile test tubes
- Incubator set at 37 °C
- Micropipettes and sterile tips

F3. Cell Preparation

1. **Cell Harvesting:**
    - Collect ascitic fluid from DLA tumor-bearing mice under aseptic conditions.
    - Wash the collected DLA cells **three times** with sterile **normal saline** by centrifugation.
    - Resuspend cells in PBS to achieve a uniform, viable cell suspension.

F4. Treatment with Defensive Secretion

1. **Preparation of Treatment Groups:**
    - Dispense equal volumes of cell suspension into sterile tubes.
    - Add gland secretion samples to achieve final concentrations of:
        - **2.5 µg/mL**, **5 µg/mL**, **10 µg/mL**, **15 µg/mL**, **20 µg/mL**, **25 µg/mL**
2. **Control Setup:**
    - Include a **PBS-only control** with DLA cells (negative control).
    - Maintain volume at **1 mL** in each tube using PBS.
3. **Incubation:**
    - Incubate the tubes at **37 °C** for **3 hours**.

F5. Trypan Blue Staining and Cell Counting

1. **Staining Procedure:**
    - After incubation, add **0.1 mL of 1% Trypan blue solution** to each sample tube.
    - Mix gently and allow to stand for **3 minutes**.
2. **Viability Assessment:**
    - Load a small volume onto a **hemocytometer**.
    - Observe under a **light microscope**.
3. **Interpretation:**
    - **Dead cells** will appear **blue** due to membrane permeability.
    - **Live cells** will **exclude the dye** and remain clear.

F6. Data Analysis

1. **Cell Viability (%)** is calculated using:Cell Viability (%) =Number of viable (unstained) cells}/{Total number of cells}* 100
2. **Cytotoxicity (%)** is then derived as:Cytotoxicity (%) = 100 - Cell Viability (%)
3. Plot the cytotoxicity (%) against different secretion concentrations to observe dose-dependent activity.

Appendix G: Protocol for LNiNPs-Mediated Anti-Angiogenesis Assay Using 48-Hour Chick Embryo Model

G1. Objective
To investigate the anti-angiogenic effect of *Luprops tristis*-derived nickel nanoparticles (LNiNPs) on developing vasculature using the **chick embryo chorioallantoic membrane (CAM)** model at 48 hours of incubation.

G2. Materials and Equipment

- Freshly fertilized **Leghorn chicken eggs**
- 70% ethanol (for surface sterilization)
- LNiNPs solution (2 µg per disc)
- Phosphate-buffered saline (PBS) (control)
- Sterile filter paper (Whatman or equivalent)
- Sterile forceps, scissors, and hole punch (5 mm)
- Sterile Petri dishes
- Incubator (37.5°C, 60% humidity)
- Parafilm (for resealing eggs)
- **Leica ICC50E** microscope with digital camera
- **AngioGen 0.5** software (for image analysis)

G3. Embryo Preparation and Treatment

1. **Egg Incubation:**
    - Clean fertilized eggs using **70% ethanol** to remove surface contaminants.
    - Incubate eggs at **37.5°C** and **60% relative humidity** for **48 hours** in a humidified incubator.
2. **Embryo Exposure:**
    - After 48 hours, carefully crack open the blunt end of the egg using **sterile forceps** in a **laminar airflow chamber**.
    - Gently expose the developing embryo with minimal disturbance.
3. **PBS Irrigation:**
    - Rinse the exposed embryo with **sterile PBS** to remove residual albumin and enhance visibility.

G4. Nanoparticle Treatment

1. **Disc Preparation:**
    - Use a sterile hole punch to prepare **5 mm filter paper discs**.
    - Impregnate discs with **2 µg of LNiNPs** in a sterile environment.
    - For the control group, use discs soaked in **sterile PBS**.
2. **Application:**
    - Place one treated disc **near the developing blood vessels** of each embryo (not directly on the heart or head).
    - Take care not to damage the delicate embryonic tissues.
3. **Sealing and Incubation:**
    - Reseal the opened egg with **sterile parafilm** to maintain humidity and sterility.
    - Return the eggs to the incubator and maintain the same conditions (37.5°C, 60% RH).

G5. Monitoring and Imaging

1. **Imaging Schedule:** Monitor and photograph the embryos **every 2 hours**, for a total of **8 hours post-treatment**.
2. **Microscopy:** Capture high-resolution images using the **LEICA ICC50E** digital microscope.

G6. Image Analysis

1. **Software:** Analyze the vascular networks using **AngioGen 0.5** software.
2. **Parameters Measured: Vessel area**, **Number of junctions, Total vessel length**
3. **Comparative Analysis:**
    - Compare LNiNP-treated embryos with PBS-treated controls to evaluate anti-angiogenic effect.

PUBLICATIONS

1. Sabira, O., Ajaykumar, A.P., Varma, S.R. *et al.* **Nepenthes pitcher fluid for the green synthesis of silver nanoparticles with biofilm inhibition, anticancer and antioxidant properties.** *Sci Rep* **15**, 5349 (2025). https://doi.org/10.1038/s41598-025-89212-9
2. Sabira O, Vignesh AR, Ajaykumar AP, Varma SR, Jayaraj KN, Sebastin M, Nikhila K, Babu A, Rasheed VA, Binitha VS, et al. **The Chemical Composition and Antimitotic, Antioxidant, Antibacterial and Cytotoxic Properties of the Defensive Gland Extract of the Beetle, *Luprops tristis* Fabricius.** ***Molecules***. 2022; 27(21):7476. https://doi.org/10.3390/molecules27217476
3. Ajaykumar, A.P., Sabira, O., Sebastian, M. *et al.* **A novel approach for the biosynthesis of silver nanoparticles using the defensive gland extracts of the beetle, *Luprops tristis* Fabricius**. ***Sci Rep* 13**, 10186 (2023). https://doi.org/10.1038/s41598-023-37175-0
4. Ajaykumar, A. P., Nikhila, K., Sabira, O., Jayaraj, K. N., Varma, S. R., Rasheed, V. A., ... & Babu, A. (2024). **A bio-inspired approach for the synthesis of few-layer graphene using beetle defensive gland extract.** ***RSC advances***, 14(9), 5729-5739.
5. Ajaykumar AP, Mathew A, Chandni AP, Varma SR, Jayaraj KN, Sabira O, Rasheed VA, Binitha VS, Swaminathan TR, Basheer VS, et al. **Green Synthesis of Silver Nanoparticles Using the Leaf Extract of the Medicinal Plant, *Uvaria narum* and Its Antibacterial, Antiangiogenic, Anticancer and Catalytic Properties**. ***Antibiotics***. 2023; 12(3):564. https://doi.org/10.3390/antibiotics12030564
6. Mathew, A., Ravindran, R. A., Vazhanthodi, A. R., Sivadasan, B. V., Ovungal, S., Subrahmanian, S. M., & Parambil, A. A. (2022). **Microwave-assisted greener synthesis of silver nanoparticles using Entada rheedii leaf extract and investigation of its anticancer and antimicrobial properties.** ***International Journal of Nano Dimension***, *13*(3), 329-334.
7. Ajaykumar, A.P.; Sabira, O.; Binitha, V.S.; Varma, S.R.; Mathew, A.; Jayaraj, K.N.; Janish, P.A.; Zeena, K.V.; Sheena, P.; Venugopal, V.; et al. **Bio-Fabricated Silver Nanoparticles from the Leaf Extract of the Poisonous Plant, *Holigarna arnottiana*: Assessment of Antimicrobial, Antimitotic, Anticancer, and Radical-Scavenging Properties.** ***Pharmaceutics*** 2023, 15, 2468. https://doi.org/10.3390/pharmaceutics15102468
8. Sabira, O.; Anthyalam Parambil, A. **Bio-Synthesis of Copper Oxide Nanoparticles Using Beetle Defensive Gland Extract: Exploring Diverse Applications**. International Journal of Nano Dimension (Int. J. Nano Dimens.) 2024, doi:10.57647/j.ijnd.2024.1503.21.
9. Sabira, O., Drisya, N., Ajaykumar, A. P., Mathew, A., Narayanan Jayaraj, K., Binitha, V. S.,& Viswanathan, K. P. (2024). **From *Ficus recemosa* Leaf Galls to Therapeutic Silver Nanoparticles: Antibacterial and Anticancer Applications**. *Pharmaceutics*, *16*(8), 1025.

10. Sabira, O., Ajaykumar, A. P., Roy, K. B., Janish, P. A., & Viswanathan, K. P. (2024). **Microwave assisted biosynthesis of nickel nanoparticles from beetle Luprops tristis defensive gland secretion: Structural characterization, multifunctional bioactivities, and glucose sensing applications.** *International Journal of Nano Dimension*.
11. Anugraha SN, Sabira, O. et al. **Biocompatible carbon dots from fermented and non-fermented coconut water: Evaluation of antioxidant, antimitotic, antibacterial, and cytotoxic activities.** Bioresource Technology Reports, 30, 102176 (2025)

12. Palakkaparambil, P., Venugopal, V., Vijayan, G., Alsaegh, M. A., Thachan Kundil, V., Gangadharan, A. K., Sabira, O., Aswathi, Raghu, A. V., Narayanan Jayaraj, K., & Ajaykumar, A. P. (2025). **Exploring the Hemolymph of the Pill Millipede *Arthrosphaera lutescens* (Butler, 1872): Chemical Composition, Bioactive Properties, and Computational Studies**. *Current issues in molecular biology*, *47*(6), 434. https://doi.org/10.3390/cimb47060434

WORK PRESENTATIONS

- **PAPER PRESENTATION** on "**Biomedical application of biosynthesised ZnO nanoparticles**" at Govt. Of Kerala Directorate of collegiate education sponsored **NATIONAL WORK SHOP ON ADVANCED TECHNIQUES IN BIOLOGICAL RESEARCH** organized by KKTM Govt. college Thrissur on November 22-23
- **POSTER PRESENTATION** on "**Bio synthesis of nickel nanoparticles from defensive secretion of the beetle *Luprops tristis* Fabricius. and its biochemical properties**" at 35th Kerala Science Congress organized by Kerala State Council for Science Technology and Environment.
- **PAPER PRESENTATION** on **Green Synthesis of Silver Nanoparticles Using the Leaf Extract of the Medicinal Plant, Uvaria narum and Its Antibacterial, Antiangiogenic, Anticancer and Catalytic Properties.** In National seminar on "CHEMISTRY: PAST, PRESENT AND FUTURE", in 2019 Organised by SNGS College, Pattambi, Palakkad: sponsored by the Directorate of Collegiate Education, Thiruvanthapuram.
- **ORAL PRESENTATION on "Novel Synthesis of CDOT from defensive secretion of beetle *Luprops tristis* characterizations and antimicrobial studies" at** ICAMGT Amrita School of Engineering, Coimbatore.

TRAININGS

- **Hands on training on small laboratory animal handling and experimentation** at Amala cancer research centre, thrissur, Kerala, 2024.
- **Hands on training on the synthesis of Nanoparticles and its Antibacterial and anti fungal activity** at JSPC, Malappuram, 2024.
- **Tools& techniques in proteomic studies**, SNGSC, Palakkad, Kerala, 2024.
- **Hands on training** on **"Basic Molecular Genetic Techniques and Bioinformatics Tools For Life Science Research"** at KVASU, 2025.